

# INVESTIGATION OF HEAT TRANSFER CHARACTERISTICS OF KEROSENE BASED NANOFUIDS

A thesis submitted  
in partial fulfilment for the degree of  
**Doctorate of Philosophy**

By

**DEEPAK KUMAR AGARWAL**



DEPARTMENT OF AEROSPACE ENGINEERING  
INDIAN INSTITUTE OF SPACE SCIENCE AND TECHNOLOGY  
THIRUVANANTHPURAM-695547

AUGUST 2016

## CERTIFICATE

This is to certify that the thesis titled **Investigation of Heat Transfer Characteristics of Kerosene based Nanofluids**, submitted by **Deepak Kumar Agarwal** to the Indian Institute of Space Science and Technology, Thiruvananthapuram, in partial fulfillment for the award of the degree of **Doctor of Philosophy**, is a bonafide record of the research work done by him under our supervision. The contents of the thesis, in full or in part, have not been submitted to any other Institute or University for the award of any degree or diploma.

Dr. Aravind Vaidyanathan (Supervisor)

Associate Professor

Department of Aerospace Engg.

IIST, Trivandrum, 695 547

Dr. S Sunil Kumar (Co- Supervisor)

Deputy Director

Propulsion Research and Studies

LPSC, ISRO, Trivandrum, 695 547

Counter Signature of HOD with Seal

Place: Thiruvananthapuram

August 2016

## DECLARATION

I declare that the thesis titled **Investigation of Heat Transfer Characteristics of Kerosene based Nanofluids**, submitted in fulfilment of the Degree of **Doctor of Philosophy**, is a record of original work carried out by me under the supervision of **Dr. Aravind Vaidyanathan and Dr. S Sunil Kumar**, and has not formed the basis for the award of any degree, diploma, associateship, fellowship or other titles in this or any other Institution or University of higher learning. In keeping with the ethical practice in reporting scientific information, due acknowledgment have been made wherever the finding of others have been cited.

Deepak Kumar Agarwal

SC10D001

Place: Thiruvananthapuram

August 2016

## ACKNOWLEDGMENTS

*“A hundred times every day I remind myself that my inner and outer lives depend on the labours of other men”* Albert Einstein (1879 – 1955)

The completion of this dissertation would not have been possible without the help of several people who were in and around me to motivate and guide. First, I acknowledge the Supreme Power for providing the companionship of such a people.

Further and most important, I would like to express my sincere gratitude to my research supervisor, Dr. S Sunil Kumar, Deputy Director, LPSC; who has supported me throughout my Ph.D. with his profound knowledge, kindness and personality. He was not only my mentor, but also an ethical guide and a supportive person during difficult times. Without his genuine and constant supervision and help, this dissertation would never have been possible.

Dr. Aravind Vaidyanathan, my adviser from IIST has been a motivating person throughout my research work. His insightful suggestions and constructive inputs have helped me in shaping this work. His continuing guidance and support is greatly appreciated.

I would also like to thank the Director, LPSC for providing me an opportunity to carry out research work in the field of nanofluids as a part of my PhD at IIST.

I am deeply indebted to my doctoral committee members Prof. T Sundararajan, IITM, Prof. K Kurian Issac, IIST, Prof. C. S. Narayanamurthy, IIST, Prof. U. Bhandarkar, IITB and Prof. A Salih, IIST. Their reviews and comments made my research work focused and streamlined. I was fortunate to have these members in my doctoral committee.

I would like to express my special thanks to Prof. T. Sundarajan for his vision and expertise in the field of nanofluids. His guidance and treating me like his own PhD student made my life easy during the tough times.

I also wish to thank Prof. Gautam Biswas, Director, IIT Guwahati, who was my supervisor for M. Tech thesis, Shri. N. K Gupta, former Deputy Director, LPSC and Prof. P. S Ghoshastidar, IIT Kanpur for always encouraging me to pursue PhD.

I would like to express special thanks to all my friends and office colleagues, especially, Mr. Jophy peter, Mr. Neeraj Naithani, Mr. Abhishek Sharma and Ms. Sharmistha Choubey. Jophy assisted me for setting up the experimental facility for the research work and Neeraj in particle size measurement at VSSC facility. I had many fruitful discussions with Abhishek and Sharmistha. Special thanks to Pranav Nath for reading the earlier version of manuscript and making suggestions to improve it.

Last but not the least; I would also like to acknowledge my family for all their encouragement and support throughout my research work. Special thanks to my wife, Payal whose love helped me to accomplish my goal successfully. My angelic daughters; Deepanshi and Devisha, always wanted to see me getting a Doctorate degree. Heartfelt thanks to both of them for their love and patience during my late working hours in this regard.

Other than those I have mentioned by name, there are many more people to thank, but like stars, some shine bright for all to see and others fade in the background aiding in the beauty of the night sky. Thank you all very much.

Deepak Kumar Agarwal

## ABSTRACT

The study intends to explore the potential application of employing kerosene based nanofluids in regenerative cooling channels of semi-cryogenic rocket engine for augmenting the heat transfer. Alumina nanoparticles and Graphene Nano Platelets (GNP) are dispersed in kerosene to prepare kerosene based nanofluids. Thermo-physical properties of the nanofluids are estimated and their convective heat transfer characteristics are investigated in turbulent flow regime using simulated experiments to evaluate the augmentation in heat transfer in coolant channels. Various combinations at different particle concentrations are analyzed to ascertain the relative effectiveness of nanofluids for nozzle cooling application. The study also brings out appropriate surfactants and its optimized quantity in conjunction with the effective techniques for mixing for the preparation of a highly stable nanofluid.

In the current study, kerosene-alumina nanofluid is prepared and characterized with varying particle loadings of 0.05vol% to 1.0vol%, in steps, for two different catalogue particle sizes of 13 nm and 50 nm. Oleic acid, as a surfactant, is found to be suitable to stabilize kerosene-alumina nanofluid and an optimum surfactant to particle volume ratio is determined for enhanced stability of nanofluid. Particle size measurement using Dynamic Light Scattering (DLS) technique and thermal conductivity measurement using Transient Hot Wire (THW) method is used to determine the stability of nanofluid with time. Subsequently, heat transfer studies show significant increase in thermal conductivity and viscosity of kerosene-alumina nanofluid with particle loading. Maximum enhancement of 33% in thermal conductivity and 22% in viscosity is observed for 13 nm particle size nanofluid at 1.0vol% particle concentration at room temperature. Higher thermal conductivity and viscosity of nanofluid at elevated temperature for nanofluids with smaller size nanoparticles, indicates significant role of particle Brownian motion in nanofluid.

Experimental investigation of turbulent convective heat transfer behaviour of nanofluid is determined using horizontal circular test section configuration in a closed loop test setup. The effects of particle size, volume fraction and Reynolds number on convective heat transfer performance and pressure drop are determined using a uniformly heated test section. Heat transfer performance of the nanofluid is evaluated based on identical Reynolds number, Peclet number, velocity and constant pressure drop conditions. The experimental results reveal that the heat transfer properties of kerosene-alumina nanofluid are significantly high as compared to pure kerosene. Higher heat transfer coefficient is noticed for larger particle size nanofluid as compared to smaller size though the measured thermal conductivity is higher for lower particle size nanofluid. The observed trend is corroborated with the hypothesis of boundary layer disruption caused by bigger sized particle during flow of nanofluids. The experiments also highlight the significant role of Prandtl number in convective heat transfer of nanofluids. A homogeneous fluid correlation which accurately predicts heat transfer coefficient and pressure drop for nanofluids is also presented in the work.

Further in the study, stable kerosene-GNP nanofluids at 0.005, 0.02, 0.05, 0.1, 0.2 weight percentage (wt %) and specific surface area (SSA) values of 300, 500, 750 mm<sup>2</sup>/g are prepared using ultrasonication and steric stabilization technique. Oleylamine is found to be the suitable surfactant for the maximum stability of nanofluid. Similar to the kerosene-alumina nanofluid, augmentation in thermo-physical properties are found for higher SSA kerosene-GNP nanofluid. 23% enhancement in thermal conductivity and 8% increase in viscosity at room temperature are observed for 750 SSA, 0.2 wt% kerosene-GNP nanofluids. The study shows only marginal effect of temperature on the thermal conductivity of kerosene-GNP nanofluid as compared to kerosene-alumina nanofluid. The behaviour observed is attributed to the percolation mechanism related heat transfer phenomenon in

kerosene-GNP nanofluid. Experimental study on convective heat transfer performance of the nanofluids at turbulent flow regime show significant improvement in heat transfer performance of kerosene-GNP nanofluid as compared to pure kerosene. Higher enhancement convective heat transfer coefficient is observed for higher SSA nanofluid. Correlations for friction factor and Nusselt number are determined using experimental data. Merit number which is used to determine the total heat transfer performance shows the utility of these nanofluids as heat transfer fluids.

The current study clearly brings out the method of synthesis of stable kerosene-alumina and kerosene-GNP nanofluid and their augmentation in enhanced thermo-physical properties. Detailed experiments carried out to understated the influence of various parameters on thermal performance of kerosene based nanofluid gives immense scope and advantage for the potential use of these nanofluids as a coolant in the regenerative channels of semi-cryogenic engine thrust chamber which could lead to significant payload advantage.

# TABLE OF CONTENTS

CERTIFICATE.....	v
DECLARATION .....	vii
ACKNOWLEDGEMENTS.....	ix
ABSTRACT.....	xi
TABLE OF CONTENTS.....	xv
LIST OF TABLES .....	xxi
LIST OF FIGURES .....	xxiii
ABBREVIATIONS .....	xxxii
NOTATION.....	xxxiii
CHAPTER 1 .....	1
1 INTRODUCTION.....	1
1.1 Background and Motivation .....	1
1.2 Concept of Nanofluids .....	5
1.3 Advantages of Nanofluids.....	7
1.4 Synthesis of Nanofluids .....	8
1.4.1 Preparation methods.....	12

1.4.2	Stability of nanofluids .....	13
1.5	Thesis Organization .....	16
CHAPTER 2 .....		17
2	LITERATURE SURVEY .....	17
2.1	Introduction.....	17
2.2	Preparation and Characterization of Nanofluids.....	17
2.3	Measurement of Thermal Conductivity .....	20
2.3.1	Effect of particle concentration .....	20
2.3.2	Effect of Particle Size.....	21
2.3.3	Effect of fluid temperature .....	23
2.4	Measurement of Dynamic Viscosity.....	24
2.5	Convective Heat Transfer .....	26
2.5.1	Effect of particle concentration and comparison methods .....	26
2.5.2	Effect of particle size.....	30
2.6	Studies on Graphene based Nanofluid.....	31
2.6.1	Effect of particle concentration .....	32
2.6.2	Effect of fluid temperature .....	33
2.7	Potential Mechanisms of Heat transport .....	35

2.7.1	Brownian motion and micro convection .....	36
2.7.2	Aggregation of nanoparticles (Clustering).....	37
2.7.3	Liquid layering at liquid - particle interface.....	39
2.7.4	Ballistic heat transport in nanoparticles .....	41
2.8	Summary of the Literature Survey.....	43
2.9	Scope and Objective of the Present Study .....	44
CHAPTER 3 .....		47
3	EXPERIMENTAL METHOD .....	47
3.1	Materials .....	47
3.1.1	Base fluid.....	47
3.2	Synthesis .....	49
3.2.1	Ultrasonication method: .....	49
3.2.2	Stabilization method:.....	52
3.3	Characterization .....	52
3.3.1	Particle surface area measurement .....	52
3.3.2	Particle size measurement .....	54
3.3.3	Thermal conductivity measurements .....	57
3.3.4	Dynamic viscosity measurement.....	62

3.4	Convective Heat Transfer Setup .....	64
3.4.1	Experimental setup description .....	64
3.4.2	Experimental procedure .....	67
3.5	Data Reduction.....	68
3.6	Uncertainty Analysis.....	72
3.6.1	Absolute error.....	72
3.6.2	Random experimental uncertainty .....	75
CHAPTER 4 .....		77
4	RESULTS AND DISCUSSION.....	77
4.1	Kerosene-Alumina Nanofluid.....	77
4.1.1	Synthesis.....	78
4.1.2	Particle size measurement .....	82
4.1.3	Thermal conductivity .....	86
4.1.4	Dynamic viscosity .....	95
4.1.5	Measurement for stability.....	100
4.1.6	Convective heat transfer.....	104
4.2	Kerosene-GNP Nanofluid.....	127
4.2.1	Synthesis.....	127

4.2.2	Particle size measurement .....	129
4.2.3	Thermal conductivity .....	132
4.2.4	Dynamic viscosity .....	141
4.2.5	Stability of nanofluids .....	143
4.2.6	Convective heat transfer performance.....	145
CHAPTER 5 .....		159
5	CONCLUSION .....	159
5.1	Synthesis of Nanofluids .....	159
5.2	Thermal Conductivity and Dynamic Viscosity.....	160
5.3	Convective Heat transfer Performance .....	162
5.4	Future Scope .....	165
6	REFERENCES .....	169
7	LIST OF PUBLICATIONS .....	191

## LIST OF TABLES

<b>Table 1.1:</b> Thermal conductivity of various Materials .....	5
<b>Table 1.2:</b> HLB range with dispensability in water .....	15
<b>Table 3.1:</b> Thermodynamic properties of rocket grade kerosene .....	48
<b>Table 3.2:</b> Size and surface area of alumina powder.....	48
<b>Table 3.3:</b> Nano material properties .....	49
<b>Table 3.4:</b> Type of ultrasonication methods.....	50
<b>Table 3.5:</b> Surfactants used for preparation of kerosene based nanofluids .....	52
<b>Table 3.6:</b> Accuracy of various instruments used in the study.....	66
<b>Table 3.7:</b> Maximum uncertainty in various measured parameters .....	74
<b>Table 3.8:</b> Uncertainty in various derived parameters .....	75
<b>Table 3.9:</b> Maximum uncertainty in various derived parameters for kerosene-aluminium nanofluid .....	76
<b>Table 3.10:</b> Maximum uncertainty in various derived parameters for kerosene-GNP nanofluid .....	76
<b>Table 4.1:</b> Matrix of Experimental study .....	78
<b>Table 4.2:</b> Minimum and average particle size measured for kerosene-alumina nanofluid ...	84
<b>Table 4.3:</b> Convective heat transfer enhancement ratio for kerosene-alumina nanofluid.....	118

**Table 4.4** : List of various surfactants used to stabilized kerosene-GNP nanofluids..... 128

# LIST OF FIGURES

<b>Figure 1.1:</b> Schematic of gas generator cycle liquid rocket engine .....	1
<b>Figure 1.2:</b> Wall heat flux profile for typical rocket thrust chamber .....	3
<b>Figure 1.3:</b> Regenerative cooling technique in rocket thrust chamber .....	3
<b>Figure 1.4:</b> Electric double layer formation in nanoparticle .....	10
<b>Figure 1.5:</b> Potential Energy variation with distance between the charged particles .....	11
<b>Figure 1.6:</b> (a) Electrostatic stabilization (b) Steric Stabilization.....	14
<b>Figure 2.1:</b> Structure of clustered particles in nanofluid.....	38
<b>Figure 2.2:</b> Presence of liquid layer around nanoparticle in nanofluid.....	40
<b>Figure 3.1:</b> Ultrasonic disruptor and bath (25KHz 500W) .....	51
<b>Figure 3.2:</b> Ultrasonic disruptor with flow cell.....	51
<b>Figure 3.3:</b> Instrument for particle specific surface area measurement .....	54
<b>Figure 3.4:</b> Schematic of DLS measurement techniques .....	55
<b>Figure 3.5:</b> Zetasizer-Nano for particle size measurement using DLS technique .....	57
<b>Figure 3.6:</b> THW Setup for nanofluid thermal conductivity measurements.....	59
<b>Figure 3.7:</b> TPS System used for thermal conductivity measurement.....	62
<b>Figure 3.8:</b> Brookfield LVDV-II for viscosity measurments.....	63

<b>Figure 3.9:</b> Schematic of closed loop setup for convective heat transfer experiments.....	65
<b>Figure 3.10:</b> Convective heat transfer setup.....	67
<b>Figure 4.1:</b> Kerosene-alumina nanofluid prepared using various particle concentrations.....	80
<b>Figure 4.2:</b> Kerosene-alumina nanofluid sample - a) after 1 hour of ultrasonication b) after 2 hours of ultrasonication.....	81
<b>Figure 4.3:</b> Particle size distribution of the kerosene-alumina nanofluid at different particle volume concentration for 50 nm nanofluid sample .....	83
<b>Figure 4.4:</b> Particle size distribution for two sample sizes of alumina nanoparticle at 0.2vol% .....	84
<b>Figure 4.5:</b> Particle size distribution of 50 nm nanofluid sample with time for 0.2vol% particle concentration.....	85
<b>Figure 4.6:</b> Thermal conductivity of 13nm kerosene-alumina nanofluid sample at various particle volume concentrations at 25 °C .....	87
<b>Figure 4.7:</b> Effect of particle size on thermal conductivity of kerosene-alumina nanofluid at various particle volume concentrations at 25 °C.....	88
<b>Figure 4.8:</b> Relative increase in thermal conductivity ratio with particle concentration .....	89
<b>Figure 4.9:</b> Thermal conductivity of 13 nm kerosene- alumina nanofluid sample at various temperatures.....	91
<b>Figure 4.10:</b> Thermal conductivity of 50 nm kerosene- alumina nanofluid sample at various temperatures.....	92

<b>Figure 4.11:</b> Effect of temperature on thermal conductivity ratio of 13 nm and 50 nm kerosene-alumina nanofluid samples .....	93
<b>Figure 4.12:</b> Comparison of measured thermal conductivity of kerosene-alumina nanofluid with literature data .....	94
<b>Figure 4.13:</b> Effect of particle size on dynamic viscosity of kerosene-alumina nanofluid samples at various particle volume concentrations at 25 °C.....	96
<b>Figure 4.14:</b> Comparison of measured dynamic viscosity of kerosene-alumina nanofluid with literature data and various theoretical models .....	97
<b>Figure 4.15:</b> Dynamic Viscosity of 13 nm kerosene- alumina nanofluid sample at various fluid temperatures .....	98
<b>Figure 4.16:</b> Dynamic Viscosity of 50 nm kerosene- alumina nanofluid at various temperatures.....	99
<b>Figure 4.17:</b> Effect of temperature on viscosity ratio for 13 and 50 nm nanofluid samples at $\phi = 0.2\text{vol}\%$ .....	100
<b>Figure 4.18:</b> Variation in thermal conductivity of kerosene-alumina nanofluid with time at $\phi = 0.2\text{vol}\%$ , $0.5\text{vol}\%$ .....	101
<b>Figure 4.19:</b> Thermal conductivity of 13 nm and 50 nm kerosene-alumina nanofluid samples with time at $\phi = 0.2\text{vol}\%$ .....	102
<b>Figure 4.20:</b> Estimated percentage particle settling of kerosene-alumina nanofluid with time .....	104
<b>Figure 4.21:</b> Nusselt numbers vrs Reynolds numbers for pure kerosene.....	105

<b>Figure 4.22:</b> Pressure drop characteristic of pure kerosene .....	106
<b>Figure 4.23:</b> Mouromtseff number for kerosene- alumina nanofluid .....	107
<b>Figure 4.24:</b> Surface temperature along the test section at various X/D locations .....	109
<b>Figure 4.25:</b> Heat transfer coefficient for 13nm, 0.5vol% kerosene-alumina nanofluid sample at various X/D locations.....	109
<b>Figure 4.26:</b> Heat transfer coefficient vrs Reynolds number for kerosene-alumina nanofluid .....	110
<b>Figure 4.27:</b> Comparison of convective heat transfer coefficient with Sonawane et al. [109] .....	112
<b>Figure 4.28:</b> Heat transfer coefficient vrs fluid velocity for kerosene-alumina nanofluid ...	113
<b>Figure 4.29:</b> Heat transfer coefficient vrs Peclet number for kerosene-alumina nanofluid..	114
<b>Figure 4.30:</b> Ratio of heat transfer coefficient of kerosene-alumina nanofluid to base fluid with Reynolds number (A) 13 nm nanofluid sample, (B) 50 nm nanofluid sample.....	115
<b>Figure 4.31:</b> Ratio of heat transfer coefficient of kerosene-alumina nanofluid to base fluid with fluid velocity (a) 13 nm nanofluid sample, (b) 50 nm nanofluid sample .....	116
<b>Figure 4.32:</b> Ratio of heat transfer coefficient of kerosene-alumina nanofluid to base fluid with Peclet number (a) 13 nm nanofluid sample, (b) 50 nm nanofluid sample.....	117
<b>Figure 4.33:</b> Friction factor with Reynolds number for kerosene-alumina nanofluid .....	119
<b>Figure 4.34:</b> Variation in Merit number with Reynolds number for kerosene-alumina nanofluid (a) 13 nm nanofluid sample, (b) 50 nm nanofluid sample.....	121

<b>Figure 4.35:</b> Variation in Merit number with Peclet number for kerosene-alumina nanofluid (a) 13 nm nanofluid sample, (b) 50 nm nanofluid sample .....	122
<b>Figure 4.36:</b> Variation in Merit number with flow velocity for various particle concentrations of kerosene-alumina nanofluids. (a) 13 nm, (b) 50 nm.....	123
<b>Figure 4.37:</b> Nusselt number with Reynolds number for kerosene-alumina nanofluid .....	125
<b>Figure 4.38:</b> Ratio of Nusselt number of kerosene-alumina nanofluid to pure kerosene at identical velocity condition.....	126
<b>Figure 4.39:</b> Kerosene- GNP nanofluid with (a) Oleylamine (b) Oleic acid (c) Tween-20 .	128
<b>Figure 4.40:</b> Particle size distribution of 750 SSA 0.05 wt% kerosene-GNP nanofluid sample with time (days) .....	131
<b>Figure 4.41:</b> Particle size distribution of 500 SSA 0.05 wt% kerosene- GNP nanofluid sample with time (days).....	131
<b>Figure 4.42:</b> Effect of particle size (SSA) on thermal conductivity of kerosene- GNP nanofluid at various mass concentrations at 30 °C .....	133
<b>Figure 4.43:</b> Effect of measurement techniques on thermal conductivity of kerosene- GNP nanofluids.....	134
<b>Figure 4.44:</b> Comparison of measured thermal conductivity of kerosene-GNP nanofluid with theoretical models .....	136
<b>Figure 4.45:</b> Effect of temperature on thermal conductivity ratio of kerosene-GNP nanofluids to pure kerosene at various particle concentration and sizes .....	138

<b>Figure 4.46:</b> Effect of temperature on thermal conductivity of kerosene based nanofluids .	139
<b>Figure 4.47:</b> Relative increase in thermal conductivity of kerosene-GNP nanofluid to kerosene-Alumina nanofluid over various temperature ranges. ....	140
<b>Figure 4.48:</b> Effect of particle size on dynamic viscosity of kerosene-GNP nanofluid at various particle mass concentrations at 30 <sup>0</sup> C .....	142
<b>Figure 4.49:</b> Effect of temperature on viscosity of kerosene-GNP nanofluid at 0.2wt% .....	143
<b>Figure 4.50:</b> Thermal conductivity of 750 SSA kerosene- GNP nanofluid with time (days) .....	144
<b>Figure 4.51:</b> Dynamic Viscosity of 750 SSA kerosene- GNP nanofluid with time (days)...	144
<b>Figure 4.52:</b> Mouromtseff number for kerosene-GNP nanofluid .....	146
<b>Figure 4.53:</b> Heat transfer coefficient vrs Reynolds number for kerosene-GNP nanofluid .	147
<b>Figure 4.54:</b> Ratio of heat transfer coefficient of nanofluid to base fluid with Reynolds number for kerosene-GNP nanofluid.....	149
<b>Figure 4.55:</b> Ratio of heat transfer coefficient of kerosene-GNP nanofluid to base fluid with flow velocity .....	150
<b>Figure 4.56:</b> Comparison of heat transfer coefficient ratio for kerosene-alumina and kerosene-GNP nanofluid.....	151
<b>Figure 4.57:</b> Friction factor with Reynolds number for kerosene-GNP nanofluid .....	152
<b>Figure 4.58:</b> Nusselt number at various Reynolds number for kerosene-GNP nanofluid ....	154

**Figure 4.59:** Ratio of Nusselt number of kerosene-GNP nanofluid to pure kerosene at various Reynolds number ..... 155

Figure 4.60: Ratio of Nusselt number of kerosene-GNP nanofluid to pure kerosene at various flow velocity conditions..... 156

**Figure 4.61:** Variation in Merit number with Reynolds number for various particle size and concentrations of kerosene-GNP nanofluid ..... 157

**Figure 4.62:** Heat transfer coefficient vrs pressure drop for kerosene-GNP nanofluid. .... 158

## ABBREVIATION

BET	Brunauer–Emmett–Teller Theory
CNT	Carbon Nanotube
DLS	Dynamic Light Scattering
DLVO	Derjaguin and Landau, Verwey and Overbeek Theory
GNP	Graphene Nano Platelets
HLB	Hydrophilic Lipophilic Balance
IEP	Iso Electric Point
LRE	Liquid Rocket Engine
RMSE	Root Mean Square Error
SSA	Specific Surface Area ( $\text{m}^2/\text{g}$ )
THW	Transient Hot Wire Method
TPS	Transient Plane Source Method

# NOTATIONS

## Nomenclature

A	Area
C	BET constant
$C_f$	Thrust coefficient
$C_p$	Specific heat
D	Hydrodynamic diameter
$D_d$	Thermal diffusivity
$D_f$	Diffusion coefficient
$D_i$	Diameter of test section
$D_t$	throat diameter
E	Heat of adsorption
f	Friction factor
F	Thrust
H	Hamaker constant
h	Heat transfer coefficient
$h_e$	Height
I	Current
K	Inverse Debye length
k	Thermal conductivity

$k_b$	Boltzmann constant
$L$	Length of test section
$L_e$	Equivalent length of graphene sheet
$M$	Torque
$N$	Particle count
$n$	Refractive index
$Nu$	Nusselt number
$P$	Pressure
$P_e$	Peclet number
$P_o$	Saturation pressure
$Pr$	Prandtl number
$Q$	Heat energy
$q$	Scaling vector
$r$	Radius
$R$	Resistance
$Re$	Reynolds number
$S$	Separation distance between particles
$T$	Temperature
$U$	Uncertainty
$V$	Voltage
$\tilde{V}$	Volume flow rate

$V_A$	Van der Walls force
$V_R$	Repulsive force
$W$	Electrical power
$X$	Axial distance along the test section
$Z$	Harmonic intensity averaged particle diameter

### **Greek Symbol**

$\Delta$	Difference
$\delta$	Thermal boundary layer thickness
$\varepsilon$	Relative permittivity
$\Gamma$	Intensity decay rate
$\lambda$	Wave length
$\mu$	Dynamic viscosity
$\nu$	Absorbed gas quantity
$\Phi$	Nanoparticle mass concentration (%)
$\varphi$	Nanoparticle volume concentration (%)
$\rho$	Density
$\theta$	Angle

### **Subscripts**

bf	base fluid
c	current value
e	exit

f fluid  
i initial value  
nf nanofluid  
np nanoparticle  
s inner surface  
so outer surface

# CHAPTER 1

## 1 INTRODUCTION

### 1.1 Background and Motivation

Cooling of liquid rocket engine (LRE) is an important and challenging area of research in rocket launch vehicle technology development. Figure 1.1 represents the schematic of flow circuit of LRE. Fuel and oxidiser are stored in a tank and pumped to the combustion chamber using high pressure turbo-pumps. Fuel and oxidizer are burnt in the combustion chamber of LRE and the hot gases are exhausted through the nozzle to obtain the desired thrust. The increased payload mass for the launch vehicle necessitates higher thrust for rocket systems.

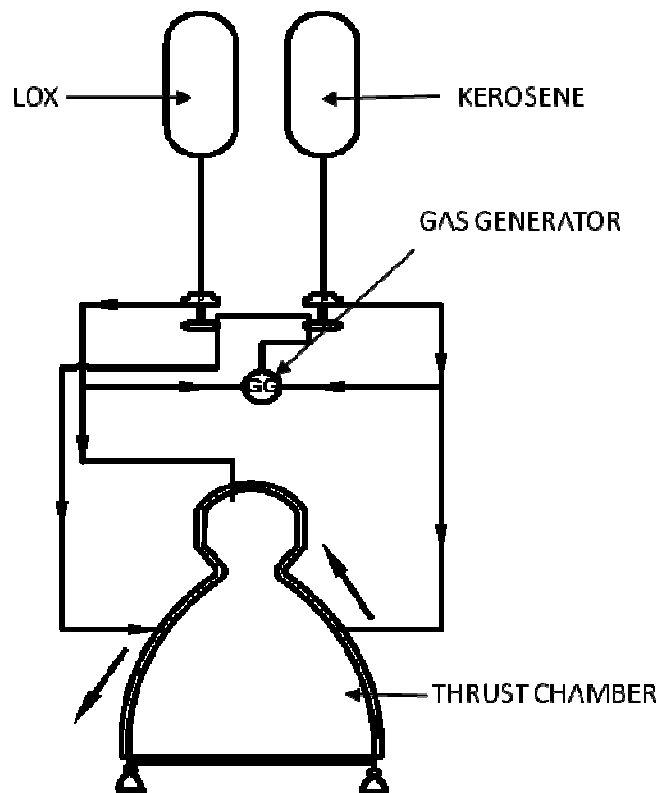


**Figure 1.1:** Schematic of gas generator cycle liquid rocket engine

One of the methods to increase the thrust of rocket engine is to increase its chamber pressure [112] leading to higher combustion gas temperature. Engine thrust is related to chamber pressure as shown in equation 1.1.

$$\text{Thrust, } F = C_f * A_t * P \quad (1.1)$$

here,  $C_f$  =thrust coefficient,  $A_t$  = nozzle throat area and  $P$  =chamber pressure

In general higher chamber pressure results in higher heat flux on the thrust chamber wall and it is evident from the Bartz expression [112] described in equation 1.2:

$$Q = \frac{0.026}{D_t^{0.2}} A(T_{aw} - T_w) \frac{P}{C^*} \frac{D_t}{D} C_p \mu_e^{0.2} \left(\frac{T_e}{T}\right)^{0.8-0.2w} \quad (1.2)$$

From Eq. 1.2 it is observed that the variation of heat flux with chamber pressure is almost linear ( $Q \propto P_c^{0.8}$ ). Thus for high chamber pressure rocket engines, the importance of managing the resultant higher heat flux of the order of 50MW and more, becomes critically important. The chamber and the nozzle wall experience high temperatures and need to be cooled. The thrust chamber wall will be exposed to very high heat fluxes and in the absence of a proper cooling mechanism, could result in the melting of wall material thereby causing total breakdown of the system. Figure 1.2 shows the axial variation of heat flux on the thrust chamber wall of a typical liquid rocket engine. Various types of cooling techniques are being used to protect the thrust chamber walls. In a typical cooling technique as shown in Fig. 1.3, viz; regenerative cooling, one of the propellant is passed through the coolant channels surrounding the wall of the nozzle prior to its entry into the combustion chamber. In such regenerative cooling systems, the rate of heat transfer in the coolant channel can be described as;

$$Q = h A \Delta T \quad (1.3)$$

where 'Q' is the heat transfer rate, 'h' is coolant side heat transfer coefficient, 'A' is the heat transfer area, and  $\Delta T$  is the temperature difference between the wall and the bulk coolant.

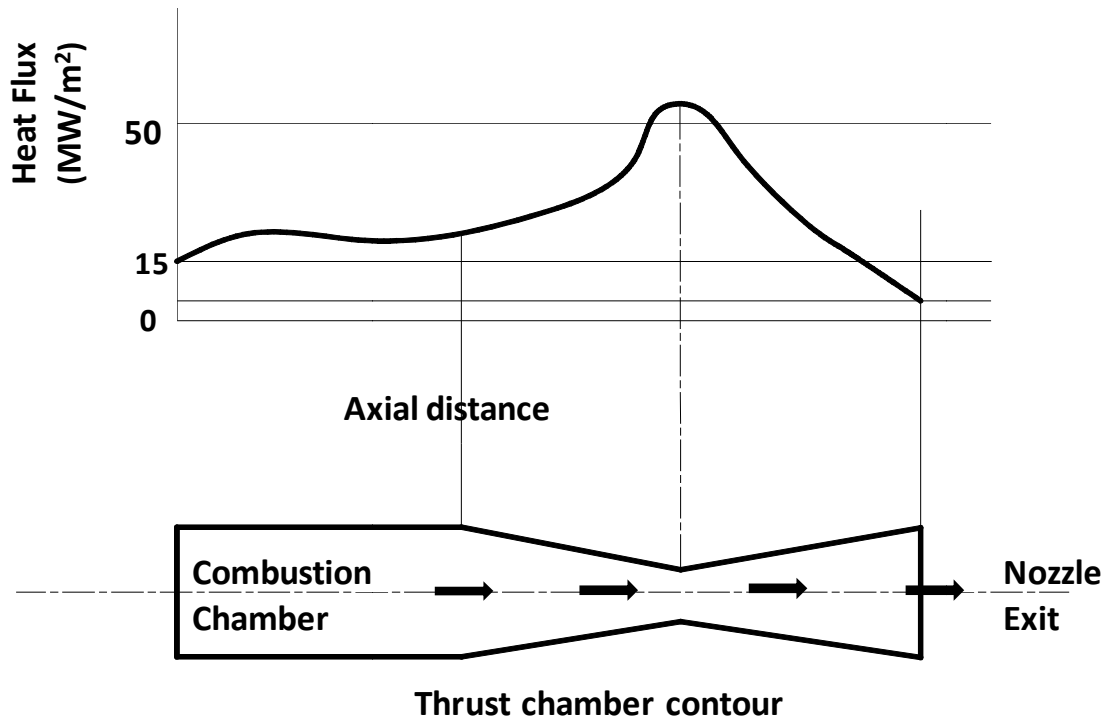


**Figure 1.2:** Wall heat flux profile for typical rocket thrust chamber

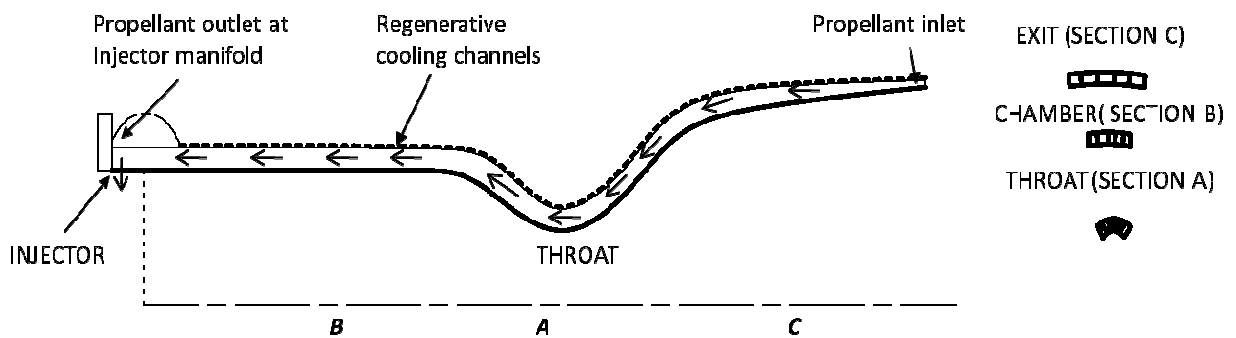


**Figure 1.3:** Regenerative cooling technique in rocket thrust chamber

The cooling efficiency of such a system depends on the rate of heat transfer in the channel and also the associated flow characteristics. The increased heat transfer can be achieved by either increasing the temperature difference ' $\Delta T$ ', surface area ' $A$ ' or by increasing the heat transfer coefficient, ' $h$ '. A higher temperature difference  $\Delta T$  is limited by material constraints and the increase in surface area ' $A$ ' available for heat transfer may not be possible due to various size and weight constraints in thrust chamber design. The other alternative is to increase the heat transfer coefficient ' $h$ '. Thus the major factors controlling the cooling performance are thermo-physical properties of the fluid and the flow velocity. The required pumping power increases significantly with increasing flow velocity due to resultant higher pressure drop in coolant channels. Alternatively, the heat transfer coefficient could be increased by enhancing the properties of the coolant for the particular mode of heat transfer.

In the case of semi-cryogenic rocket engines, kerosene, the fuel, is being used as regenerative coolant. Moreover, though the thermal conductivity of kerosene is relatively low, the temperature should be maintained below the coking limits during its flow through the regenerative passage. The heat transfer performance of this system can be augmented either by improving thermo-physical properties of kerosene or to a marginal extent by optimizing the thrust chamber coolant channel design. In this context, the attention is drawn towards the higher heat transfer performance exhibited by nanofluids over the base fluids. Fluids, referred to as base fluids, dispersed with nanoparticles are known to exhibit significantly enhanced thermal properties as compared to the base fluid [15,20]. The size of the nanoparticles imparts unique characteristics to the base fluids, including greatly enhanced energy, momentum and mass transfer, as well as reduced tendency for sedimentation and erosion of the containing surfaces [20]. Thus, the potential of an innovative cooling system

for semi cryogenic engine could be explored by improving the thermo-physical properties of kerosene, which might enhance the heat transfer characteristics of kerosene.

## 1.2 Concept of Nanofluids

Cooling has become one of the foremost challenges in current technological fields including electronics, lighting, transportation, space exploration and manufacturing. Heat transfer coefficients are limited due to the poor coolant properties in many applications. In energy-efficient heat transfer fluids, the thermal conductivity of the heat transfer fluids plays vital role.

**Table 1.1:** Thermal conductivity of various Materials

	<b>Material</b>	<b>Thermal Conductivity (W/m K)</b>
<b>Metals</b>	Silver	429
	Copper	401
	Aluminum	237
<b>Non-metals</b>	Graphene/Carbon nanotubes	1000-3000
	Silicon carbide	260
	Alumina (Al <sub>2</sub> O <sub>3</sub> )	40
<b>Liquids</b>	Water	0.613
	Ethylene glycol	0.253
	Engine oil	0.145
	Kerosene (Rocket grade)	0.104

Despite considerable research and development efforts on heat transfer enhancement, there is little or no major breakthrough in the thermal management of systems, and cooling capabilities have been largely limited due to the poor thermal conductivity of traditional heat

transfer fluids used [20], such as water, oils, and ethylene glycol. These fluids have inherently, orders-of-magnitude lower thermal conductivities than most of the solids as presented in Table 1.1.

Since solid materials have much higher thermal conductivities than fluids, it is expected that the addition of solid particles could increase the thermal conductivity of the fluids. However, if solid particles in the size range of millimeter or micrometer are added into the base fluids, it can pose other major challenges as given below.

1. Unstable solution leads to particle settling and form a sediment layer at the surface during flow. This will increase the thermal resistance and also impair the heat transfer performance of the fluids.
2. The large size of the particles or the agglomerates of these particles causes severe clogging, especially at low velocity of fluids or in micro channels.
3. Large particles and the agglomerates in fluid flows may carry large momentum and kinetic energy, which may cause damage to the surface of the heat transfer equipment.
4. The erosion of the fluid system by the coarse and hard particles increases as the fluid velocity increases.
5. Noticeable conductivity enhancement is based on high particle concentration, which leads to apparent increase in viscosity. Higher viscosity of the fluids also necessitates high pumping power and thus limits the utility of these fluids.

Fluids with suspensions of higher thermal conductivity nanosize metal and metal oxide particles are being considered as an option for improving thermal performance of heat

transfer systems. By adding high thermal conductivity nanoparticles, the thermal conductivity of the fluid can be enhanced while accommodating for the moderate increase in the fluid viscosity.

### 1.3 Advantages of Nanofluids

Nanofluids are fundamentally characterized by the fact that the Brownian motion due to small size of particles overcomes the particle settling due to gravity. A stable solution is thus possible if the particle size is in the range of nanometers. Nanofluid can be defined as engineering colloidal solution [15] with nanoparticle dispersed in base fluid, having particle size  $<100\text{nm}$  and particle concentration  $<5\text{vol}\%$ . The size of the nanoparticles imparts unique characteristics to the base fluids, including greatly enhanced energy, momentum and mass transfer, as well as reduced tendency for sedimentation and erosion of the containing surfaces. The improved heat transfer property of nanofluids is ascribed to various reasons ranging from an increase in thermal conductivity of fluids to the random Brownian motion of the nanoparticles.

Apart from the above, nanofluids have the following specific advantages as a heat transfer fluid:

1. High specific surface area (SSA) leads to efficient heat transfer in nanofluids.
2. Higher dispersion stability due to smaller size of particles in the base fluid.
3. Reduced particle clogging as compared to conventional slurries, thus promoting system miniaturization.
4. Adjustable properties, including thermal conductivity and surface wettability, through varying particle concentrations to suit different applications.

The aforementioned advantages of nanofluids make them a suitable choice as coolant for various heat transfer applications. Nanofluids have high demand as a coolant in electronic cooling industries, automobile engine cooling application, solar reflectors, nuclear system cooling etc.

#### **1.4 Synthesis of Nanofluids**

Modern fabrication technology provides great opportunities to process nanostructure material. Nanostructure materials are defined as the materials whose structural elements such as clusters, crystallites or molecules have dimension less than 100nm, and exhibit different properties than the conventional solids. The notable property of nano-size materials is attributed to the relatively high surface area/volume ratio, due to the high proportion of constituent atoms residing at the grain boundaries. The thermal, mechanical, optical, magnetic, and electrical properties of nano-size materials are superior to those of conventional materials with coarse grain structures [20].

Preparation of nanofluid basically involves dispersion of nano-size particles into a heat transfer base fluid. Nanoparticle of metals, oxides, carbides and carbon nanotubes can be dispersed into heat transfer fluids, such as water, ethylene glycol, hydrocarbons with or without the addition of stabilizing agents. Synthesis methods for nanoparticles are typically grouped into two categories: 'top-down' and 'bottom-up' approach [40]. The first involves division of a massive solid into smaller portions. This approach involves milling or attrition, chemical methods, and volatilization of a solid followed by condensation of the volatilized components. The second, bottom-up method of nanoparticle fabrication involves condensation of atoms or molecules in the gas phase or in solution.

Long term physical and chemical stability of nanofluids is an important practical aspect because of the aggregation of nanoparticles due to very strong Vander Waals interactions. Dispersion of nanoparticles in the base fluid is intrinsically thermodynamically metastable due to their very high surface area and it also indicates the positive contribution to the free enthalpy of the system. Nanofluids are basically colloidal solutions. The stability mainly depends on the attractive and the repulsive forces that exist between the particles. Researchers [22] have formulated the DLVO (Derjaguin and Landau, Verwey and Overbeek) theory, which proposes the stability of the solution depending upon the total potential energy of the system. DLVO theory suggests that the stability of a particle in a solution is determined by the sum of attractive Vander Waals forces and the electrical double layer repulsive forces that exist between particles as they approach each other due to Brownian motion. If the attractive forces are higher than repulsive forces, the two particles will collide and suspension is not stable; however if the particles have sufficiently high repulsive force, the suspension will be stable.

Figure 1.4 shows the electric double layer near a nanoparticle in a fluid. Electric double layer model [20] is used to visualise the ionic environment when the nanoparticle is present in a charged colloid. Development of a net charge at the surface of a particle affects the distribution of ions in the nearby surrounding region, and increases the concentration of counter charge ions close to the surface. Attraction of negatively charged particles (assumed negative) causes some of the positive ions from the solution to form a firmly attached Stern layer around the surface of colloids. Few more positive ions are still attracted by negative colloid, but they are repelled by the stern layer and results in a diffuse outer layer. The attached counter-ions in the Stern layer and the charged atmosphere in the diffuse layer are generally referred to as the electrical double layer. The thickness of the layer depends upon the type and concentration of ions in solution.

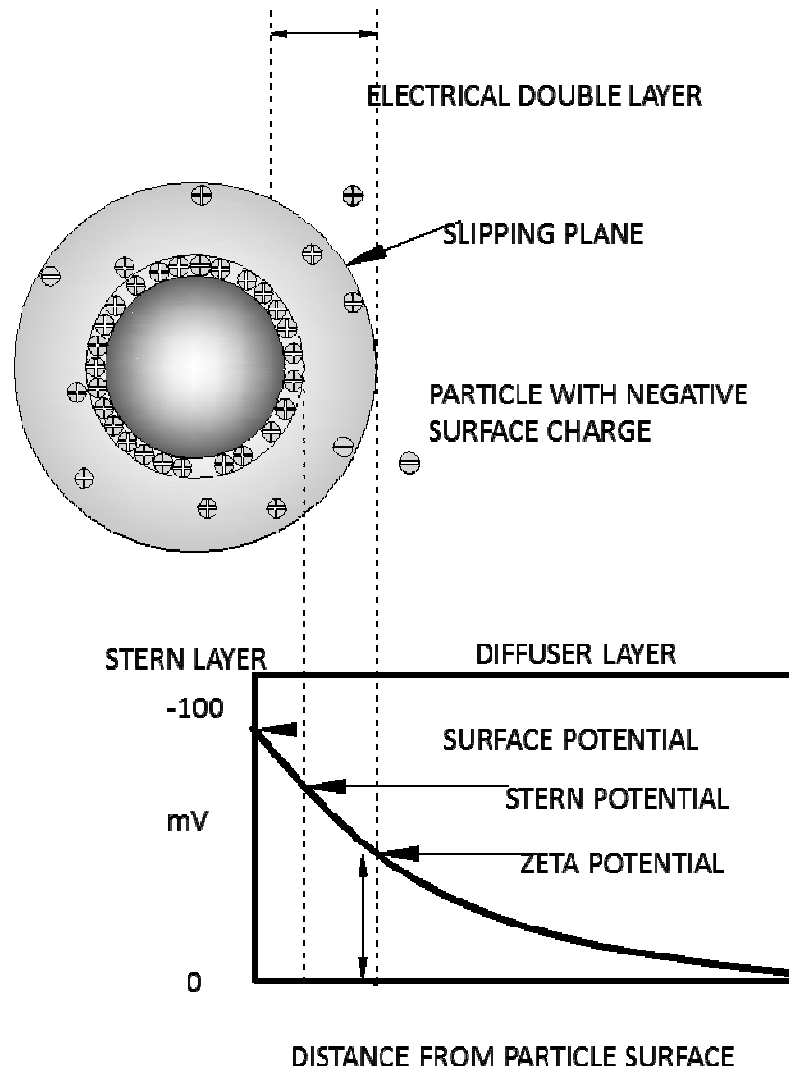


**Figure 1.4:** Electric double layer formation in nanoparticle

Electrostatic repulsion becomes significant when two particles approach each other and their double layers begin to interfere. Hence there is combination of attractive Van der Waal's force ( $V_A$ ) and repulsive force ( $V_R$ ) between the electric double layers.

$$V_A = H D / 12S^2 \quad (1.4)$$

where 'H' the Hamaker constant, 'S' is the surface to surface particle separation distance and 'D' is the particle diameter.

$$V_R = 2\pi\epsilon\epsilon_0 D\phi_0^2 k e^{-kS} \quad (1.5)$$

where,  $\phi_0$  is the surface potential, 'D' is the particle diameter, 'S' is the surface to surface particle separation distance, ' $\epsilon$ ' is the relative permittivity of the base fluid,  $\epsilon_0$  is the relative permittivity of free space and k is the inverse Debye length.

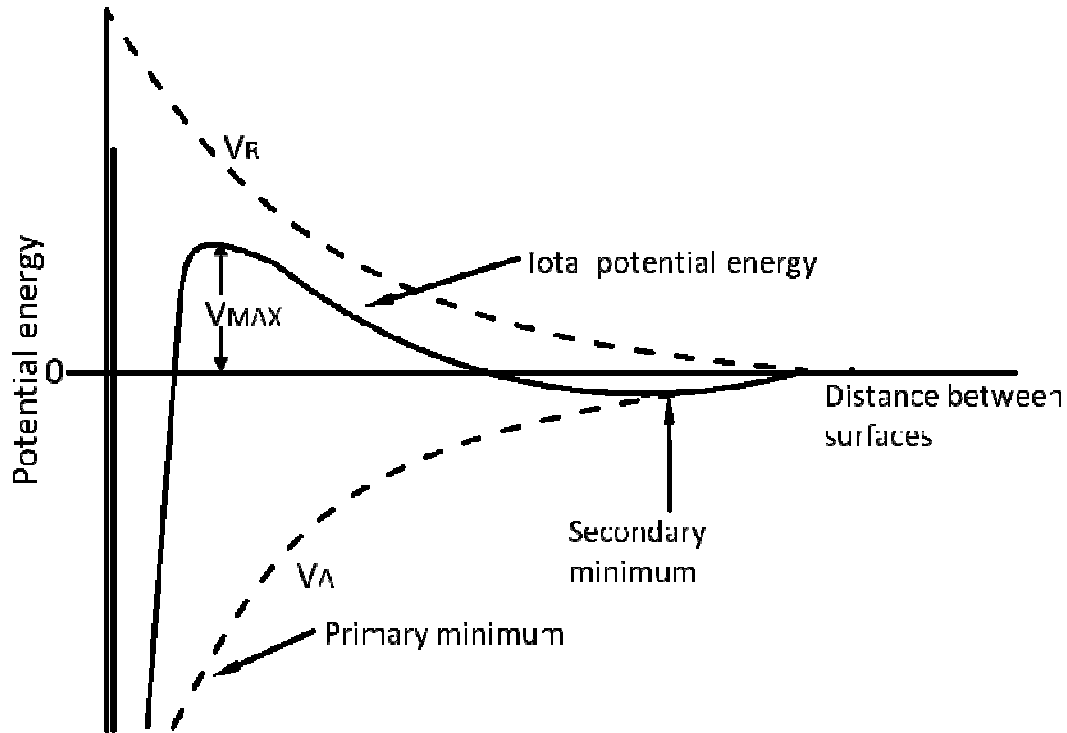


**Figure 1.5:** Potential Energy variation with distance between the charged particles

Figure 1.5 presents the attractive and the repulsive force as a function of distance between the particles. The total potential energy of a particle for a stable configuration is negative. Primary minimum at which the particles are agglomerated is the most stable configuration. However for a stable nanofluid without agglomeration secondary minimum is desirable. It can be also observed that the energy required in overcoming the two repulsive forces as they come closer is notably high. On exceeding this energy barrier, the particles agglomerate, causing the particle size to increase, become heavier and results in

sedimentation. Stability indicates how effectively the particles are dispersed in the fluid and are maintained to be kept apart. The process of preventing nanoparticles from agglomeration is known as stabilization.

#### **1.4.1 Preparation methods**

Preparation of a stable nanofluid is the most important and challenging process in nanofluid heat transfer studies. The agglomeration of solid particles in base liquid can occur if the nanofluids are not prepared properly and may in turn result in poor thermo-physical properties of nanofluids. There are two major techniques [148], which are typically used for nanofluid preparation: two-step method and single step method.

##### **1.4.1.1 Two-step method**

In two-step method, nanoparticles, either produced or procured are dispersed into the base fluid. Various techniques like stirring, ultrasonication and high pressure shearing are employed to disperse the nanoparticles into the base fluid. The two-step process works better for oxide particles than their metallic counterparts [57]. The disadvantage in this method is the agglomeration of nanoparticles due to increased surface interaction of the particles.

##### **1.4.1.2 Single-step method**

The single-step method involves simultaneous production and dispersion of nanoparticles in fluids. The single-step method [40] includes the direct evaporation and condensation method, SANSS (submerged- arc nanoparticle synthesis system), and laser ablation methods, in which metals are vaporized using physical technology and cooled into liquids to obtain nanofluids. Preparation of nanofluid via a single-step method provides some

advantages such as minimizing the agglomeration of nanoparticle. In this method, the steps of nanoparticle drying, storage, transportation and dispersion of particles in the base liquid media are combined and this leads to minimum agglomeration. Nevertheless, scalability of some fabrication methods could be costly and troublesome.

## **1.4.2 Stability of nanofluids**

The agglomeration of nanoparticles results not only in the settling and clogging of micro-channels but also decrease in thermal conductivity of nanofluids. Two types of stabilizing techniques are used to prepare nanofluids.

### **1.4.2.1 Electrostatic stabilization**

The stability of nanofluid is directly influenced by its electro-kinetic properties [148]. Surface charge on nanoparticle dispersed into a base liquid is also an important factor for its stability. Surface charge causes nanoparticles to create an electric field resulting in attraction or repulsion among them. The charge depends on the pH of the suspension. As the pH of the suspension departs from the iso-electric point (IEP) of the particles, the nanofluid becomes more stable. At IEP the charge density at the particle surface equals the charge density of the medium. As the value of pH of the suspension approaches the IEP, nanoparticles tend to agglomerate due to the weak repulsive forces and eventually particles settling take place. Therefore, by adjusting the pH value of suspension, stability of nanofluid can be thoroughly controlled. Optimum value of pH will result in higher stability of the nanofluid.

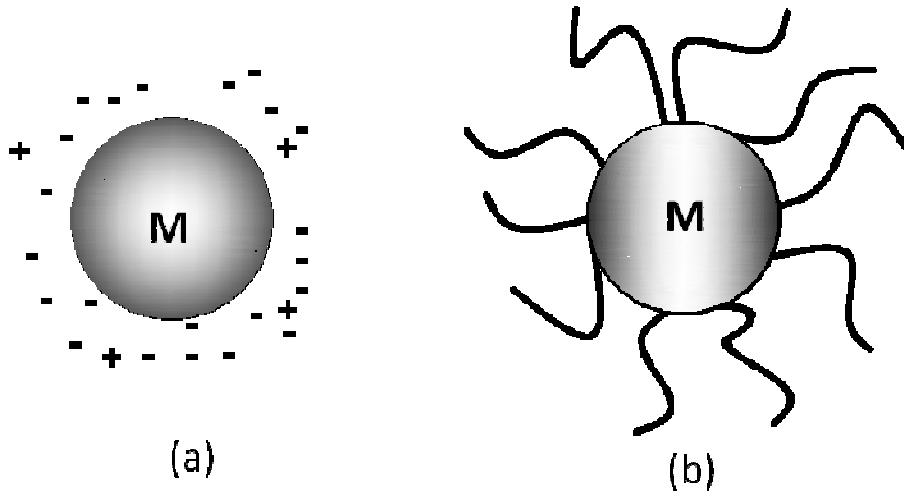


**Figure 1.6:** (a) Electrostatic stabilization (b) Steric Stabilization

#### 1.4.2.2 Steric stabilization

In steric stabilization technique, surfactants are added in the nanofluid to coat the surface of the nanoparticles to prevent the agglomeration. Surfactants consist of a hydrophobic tail portion, usually a long-chain hydrocarbon, and a hydrophilic polar head group [20]. Surfactants are employed to increase the contact of two materials, sometimes known as wettability. Selection of the surfactant depends on both, the type of nanoparticle and the base fluid. The particle surface is modified using the surfactant and results in favorable electrostatic repulsion between the particles. By this method, hydrophilic surfaces of nanostructured materials are modified to become hydrophobic and vice versa.

According to the composition of the head, surfactants are divided into four classes: non-ionic surfactants without charge groups in its head (alcohols, and other polar groups), anionic surfactants with negatively charged head groups (long-chain fatty acids, sulfosuccinates, alkyl sulfates, phosphates, and sulfonates), cationic surfactants with positively charged head groups (long-chain amines and quaternary ammonium compounds),

and amphoteric surfactants with zwitterionic head groups (betaines and lecithins). The selection of suitable dispersants is a key issue. In general, when the base fluid of nanofluids is a polar solvent, the suitable surfactant can be water-soluble or oil soluble. Adequate quantity of surfactant is required in the suspension to overcome Van der Waals attractions.

The solubility of non-ionic surfactants is evaluated through Hydrophilic - Lipophilic Balance (HLB) value [21,42,43]. HLB numbers >10 have an affinity for water (hydrophilic) and those with HLB <10 have an affinity for oil (lipophilic). Ionic surfactants have recently been assigned relative HLB values, allowing the range of numbers to extend to 60. Table 1.2 details the HLB range of various surfactants with their dispersability. It is to be noted that the HLB range for oil is inverse of water. Surfactants with HLB range which are dispersable in water will show no dispersability in oil.

**Table 1.2:** HLB range with dispersability in water

<b>Dispersability</b>	<b>HLB Range</b>
No dispersibility in water	1-4
Poor Dispersion	3-6
Milky Dispersion after vigorous agitation	6-8
Stable milky dispersion	8-10
Translucent to clear dispersion	10-13
Clear solution	13+

## 1.5 Thesis Organization

The thesis comprises of five chapters as follows:

**Chapter 1** presents the concept of nanofluids, its enhanced performance over the base fluid, preparation techniques and their characteristics for heat transfer application. Detailed discussion of various methods is also made for the synthesis of stable nanofluids.

**Chapter 2** discusses the detailed literature survey on synthesis and characterization of nanofluids, thermal conductivity and viscosity measurements, convective heat transfer experiments and possible mechanisms involved in the observed better thermal performance of nanofluids. The objective and scope of the current work is also defined at the end of the chapter 2.

**Chapter 3** presents the experimental techniques used in the present study for synthesis and characterization of nanofluids. Detailed discussion on uncertainty and data reduction process for the experimentation is presented. Details associated with the closed loop convective heat transfer setup are also discussed.

**Chapter 4** reports the results and discussion of the experimental study. Two separate subsections are provided for discussing the results obtained from the study carried out on the kerosene-alumina and kerosene-GNP nanofluids respectively. Detailed discussion is done for the experimental observations and the trends observed in experiments are explained.

**Chapter 5** provides the summary and conclusions of the present work in conjunction with future scope to extend this research activity.

## CHAPTER 2

### 2 LITERATURE SURVEY

#### 2.1 Introduction

Dispersion of solids in fluids to enhance the thermal conductivity is a concept that is proposed more than 100 years ago. Maxwell [83] in the year 1873 presented a theoretical model for predicting the enhanced thermal conductivity of liquids on dispersion of solids in them. However, till around year 1990, particle size was limited to micrometer or millimeter, and the solid particle concentrations used were low to avoid the immediate settlement of the particles upon dispersing them in the fluids.

Pioneering work in dispersing nano-sized particle in a base fluid had been carried out by Choi [15] at the Argonne National Laboratory, Chicago at 1995 and he named this colloidal solution as nanofluid. In the last two decades, several researchers have carried out wide range of heat transfer studies with various oxides, carbon nanotubes, carbide and metal nanoparticles in water or Ethylene Glycol (EG). All these studies reported higher thermal performance for nanofluids as compared to the respective base fluids.

#### 2.2 Preparation and Characterization of Nanofluids

Enhanced heat transfer properties of nanofluids depend upon the stability and the respective method adopted for its preparation as indicated by many reviewers [8,19,27,40,109,126,129,138,148]. Two methods are used for the preparation of nanofluid. Out of the two techniques that are being used for the preparation of nanofluids, a single step

direct evaporation approach for producing nanofluids, referred to as the modified VEROS (Vacuum Evaporation onto a Running Oil Substrate) technique is successfully used by Eastman et al. [26]. The single-step method has been used with success to produce nanofluids containing dispersed high thermal conductivity metal nanoparticles [78,138]. One of the successful methods is called the direct evaporation technique, which is first developed by Yatsuya et al. [144]. During this process, nanoparticles are synthesized and dispersed into the fluid simultaneously. The single-step method can significantly reduce the agglomeration and improve the stability of nanofluids. However, the main limitation is the limited production of nanofluids as compared to the two-step techniques.

In the two step process, first the nanoparticles are either produced or procured. Although there exists a possibility for certain degree of agglomeration to occur during this process of nanoparticle preparation, storage and dispersion, it is well known that these agglomerates require only very little energy to be disbanded into smaller constituents. Thus it is possible that even agglomerated nanocrystalline powders can be successfully dispersed into fluids with the desirable properties.

Several researchers [18,40,57,101,110,111] successfully employed the two-step technique for preparation of the respective nanofluids. The method utilizes nanoparticles, which are initially produced as dry powders via chemical or physical methods. The method is extensively used in synthesizing nanofluids by mixing base fluids with commercially-available nanopowders. Various techniques like stirring, ultrasonication and high pressure shearing are adopted to disperse the nanoparticles into the base fluid. Hwang et al. [57], have made nanofluids using a stirrer, ultrasonic bath, an ultrasonic disruptor and a high pressure homogenizer, and also examined the samples using Dynamic Light Scattering (DLS) and Transmission Electron Microscope (TEM). They observed that the two-step process yielded

better results for oxide particles as compared to the single step method. The only disadvantage in the two step method is the agglomeration of nanoparticles due to the Van der Waals forces.

The stability of nanofluid is a highly desirable property of the nanofluid to be used as a potential fluid for heat transfer applications. Research in the last few years has mainly focused on the preparation of stable nanofluids. The review paper of Ghadimi et al. [40] and Solangi et al. [109] provides an exhaustive commentary on the stability of the nanofluids.

In the past, several researchers have used various surfactants for the preparation of stable nanofluids using steric stabilization technique. Some of the popular surfactants used by the researchers are sodium dodecyl sulfate (SDS) [57,101] sodium dodecyl benzene sulfonate (SDBS) [101,130], oleic acid [57,111,136], cetyltrimethyl ammonium bromide (CTAB) [101] and polyoxyethylene sorbitan monolaurate [Tween 20 LR] [111]. Measurements are carried out to evaluate the particle size distribution with time, assess the visual stability of the nanofluids and also to determine the stability of various nanofluids prepared by different dispersion techniques.

The pH of the nanofluid is changed by adding either acid or base in the solution in the case of electrostatic stabilization. Xie et al. [136] have modified the surface characteristics of water-carbon nanotube (CNT) nanofluid by changing the pH and were able to prepare stable nanofluid. Zhu et al. [155] have determined the dispersion behavior of water-alumina nanofluid by measuring zeta potential of nanofluids under different pH values and SDBS concentrations. They recommended the combined use of steric and electrostatic stabilization for water-alumina nanofluid for improved thermal conductivity. A systematic study was carried out by Raghu et al. [101] in which the effect of surface charge (pH), type of

nanoparticle and dispersion method on thermal conductivity of oxide nanofluids are examined. They concluded that high surface charge (low pH) of nanofluids improves dispersion stability, results in lower viscosity and high thermal conductivity for nanofluids.

## **2.3 Measurement of Thermal Conductivity**

In the past twenty years the nanofluids prepared with water, ethylene glycol (EG) and oil as the base fluids have been of great research interest to heat transfer community due to higher thermal conductivity observed. Choi [15] is the first to theoretically demonstrate the possibility of obtaining exceptionally high thermal conductivity with water-Cu nanofluid as compared to the respective base fluid. Subsequently, many researchers have carried out wide range of experimental studies with various oxides [2,52,111], carbon nanotubes [130,133], carbide [115,134] and metal nanoparticles [78,138] in water or ethylene glycol. All these studies reported higher thermal conductivity for nanofluids as compared to the respective base fluids.

### **2.3.1 Effect of particle concentration**

Eastman et al. [28] measured the thermal conductivity of water based nanofluids, and reported enhancement of 60% and 40% in thermal conductivity for 5vol% CuO and alumina nanofluid respectively. Subsequently, many authors have reported data for wide variety of nanofluids. Choi et al. [17] measured 150% thermal conductivity enhancement of poly ( $\alpha$ -olefin) oil with the addition of multiwalled carbon nanotubes (MWCNT) at 1vol% concentration. Yang et al. [143] reported 200% thermal conductivity enhancement for poly ( $\alpha$ -olefin) oil containing 0.35 vol% MWCNT.

Eastman et al. [29] found 40% thermal conductivity enhancement for 0.3vol% copper nanoparticles dispersed in EG. The authors however added about 1vol% thioglycolic acid as a surfactant in their nanofluid and noted higher thermal conductivity with surfactant as compared to the case without using surfactant. Jana et al. [61] measured the thermal conductivity of a similar nanofluid, with water containing copper nanoparticles. They used laurate salt as the surfactant and observed 70% enhancement in thermal conductivity.

Zhang et al. [153] reported 15% enhancement in thermal conductivity of water-alumina nanofluid at 5vol% whereas Timofeeva et al. [114] reported only 7% enhancement in thermal conductivity of water-alumina nanofluid for the same volume fraction and nanoparticle size. Both these research groups have used the transient hot wire (THW) method for thermal conductivity measurement. In another study by Li and Peterson [77], where the thermal conductivity of nanofluids are measured with steady state method, enhancement of 10-12% is noticed for 6vol% for water-alumina nanofluid. The disagreement between these reported values may be attributed to the different techniques used for realizing the nanoparticles, and also the different methods involved in preparation of the nanofluid. A benchmark study conducted by International Nanofluid Property Benchmark Exercise (INPBE) for thermal conductivity of nanofluids, and presented by Buongiorno et al. [13] also reports an increase in thermal conductivity of nanofluids with particle concentration irrespective of the measurement technique used.

### **2.3.2 Effect of Particle Size**

The effect of particle size on the thermal conductivity of nanofluids is determined by many researchers. Anoop et al. [2] observed higher thermal conductivity for 45 nm alumina particle water nanofluid as compared to the 150 nm case. However, Kim et al. [70] measured

thermal conductivity of nanofluids containing different sizes of  $\text{Al}_2\text{O}_3$ ,  $\text{TiO}_2$ , and  $\text{ZnO}$  in water and in ethylene glycol (EG). They observed higher thermal conductivity for nanofluids containing the smaller nanoparticles. For nanofluids containing 3vol%  $\text{TiO}_2$  in ethylene glycol, the thermal conductivity enhancement for the 10 nm nanoparticle size sample is approximately double as compared with those obtained for the 70 nm sample. The study of Kim et al. [70] with metal-oxide nanofluid shows linear increase in thermal conductivity of nanofluid with decreasing particle size for identical volume concentration. Li and Peterson [77] have determined thermal conductivity of water-alumina nanofluid for two particle sizes at various volume concentrations and temperatures. Though, in most of their studies, higher thermal conductivity of nanofluid with 47 nm nanoparticles is observed, as compared to 36 nm case. However for some combinations of volume concentration and temperature, reverse trend is also observed. Based on this, it is concluded that an optimum particle size and base fluid combination exists, which yields the maximum thermal conductivity; the phenomenon is currently neither predicted nor explainable using theoretical models.

Xie et al. [137,156] measured the thermal conductivity of nanofluids containing different sizes of alumina nanoparticles with diameters between 12nm and 304nm. The thermal conductivity was found to decrease as particle size decreases, except in the case of large sized particles. They concluded that there exists optimal particle size for which the enhancement in thermal conductivity is highest. The experimental study of Beck et al. [10] with varying particle size of 8 to 282 nm for water-alumina nanofluid shows a decreasing trend in thermal conductivity of nanofluid for particle size lower than 50 nm. Timofeeva et al. [115] investigated the effect of particle size on water/ $\alpha$ -SiC nanofluid by varying  $\alpha$ -SiC particle size from 16 to 90 nm, and reported higher thermal conductivity for nanofluids made up of larger particle size as compared to the lower size.

### 2.3.3 Effect of fluid temperature

The effect of temperature on thermal conductivity is first reported by Das et al. [18]. The authors have used temperature oscillation method, and observed 2 to 4 fold increase in thermal conductivity as the temperature is increased from 21°C to 51°C. Subsequently, Wen and Ding [130], Li and Peterson [77] and Mintsa et al. [86] have used different methods viz.; transient hot wire method (THW), steady state "cut bar method" and KD2 pro respectively for the measurement of thermal conductivity. Irrespective of different measurement techniques, all of them observed significant increase in thermal conductivity with increase in temperature. In the recent study of Sonawane et al. [111] with Aviation Turbine Fuel (ATF)-alumina nanofluid the significant effect of temperature on the thermal conductivity of nanofluids is reported. They have used transient hot wire method and observed an increase of 13% to 41% in thermal conductivity of nanofluid at 1% particle volume concentration over a temperature range of 30°C to 50°C.

Though many of the researchers have observed significantly high thermal conductivity for nanofluids at elevated temperature, the experimental study carried out by Ju et al. [63] reported only weak temperature dependence of thermal conductivity for water-alumina nanofluid. Similar finding is reported by Zhang et al. [153] and Timofeeva et al. [114] the thermal conductivity of nanofluids is found to have negligible dependence on fluid temperature. Xie et al. [134] carried out a detailed experimental study with oxide and Cu nanofluids. Eventhough they found a rapid increase in thermal conductivity of ethylene glycol (EG)-Cu nanofluid with temperature, they did not observe any temperature dependency for EG based nanofluids containing MgO, ZnO, SiO and Graphene nanoparticles. These studies indicate that the temperature dependence is largely be influenced by the nanoparticle and base fluid combination.

The other parameters that could also influence the thermal conductivity of nanofluids include pH value, different base fluid materials, shape of nanoparticles and additives. Zhu et al. [155] showed that the pH of the nanofluid strongly affects the thermal conductivity of the suspensions.

Different particle shapes can also influence the thermal conductivity of nanofluids [17,147]. Nanoparticles with high aspect ratio are found to enhance the thermal conductivity. For example, the enhancement in thermal conductivity associated with spherical particles will be relatively low as compared to those associated with nanorods [88].

## 2.4 Measurement of Dynamic Viscosity

Viscosity of nanofluids has been less investigated than thermal conductivity; however, the rheological properties of liquid suspensions have been investigated since the period of Einstein [31]. The viscosity of a liquid suspension of hard spheres can be predicted according to the Einstein [31] as,

$$\mu_{nf} = \mu_{bf} (1 + 2.5\phi) \quad (2.1)$$

where,  $\mu$  is the viscosity of base fluids and  $\phi$  is the volume fraction of solid dispersed particles. This equation is valid only when the interactions between solid particles are negligible, ie; for very dilute suspension ( $\phi < 0.03$ ). With increasing particle concentration, the flow around one particle tends to be affected by other particles in the neighborhood, and assumption of negligible interaction between solid particles could lead to large errors.

Pak and Cho [96] are the first to measure the viscosity of water-alumina nanofluids with particle concentration up to 10 vol% and observed maximum viscosity up to 300%

higher than that of the base fluid. Wang et al. [125] observed only 90% increase in viscosity for water-alumina nanofluids with similar concentrations and particle dimensions.

Lee et al. [75] measured thermal conductivity and viscosity for water-alumina nanofluids at very low concentration (0.01vol% to 0.3vol%) and observed nonlinear enhancement in viscosity with concentration. In the recent works, Li et al. [78] and Sonawane et al. [110,111] have carried out detailed studies respectively with the kerosene and ATF based nanofluids. Li et al. [78] have prepared kerosene-Cu nanofluids by surface modification of nanoparticles and revealed the effect of surface modification on the thermal conductivity and viscosity of nanofluids. In the study of Sonawane et al. [111] with ATF-alumina nanofluid, thermo physical properties and heat transfer coefficient are determined at various volume concentrations.

Wang et al. [125] have prepared water-alumina and EG-alumina nanofluid and measured the dynamic viscosity at various volume fractions. Similar to other research groups, they also observed higher viscosity for nanofluids as compared to base fluid; however the increase in viscosity is relatively low for better dispersed nanofluids. Nguyen et al. [91] have experimentally investigated the effect of temperature and particle concentration on viscosity for water-alumina nanofluids, and reported significant increase in viscosity with particle loading and as expected, there is a decreasing trend with temperature. They also found that the viscosity is altered only on temperatures beyond a certain value of the temperature. Sonawane et al. [111] observed higher percentage increase in viscosity as compared to thermal conductivity, and reported 55% increase in viscosity in comparison with only 17% increase in thermal conductivity for 0.3vol% particle concentration in nanofluid at 50°C. Benchmark study on the measurement of nanofluid viscosity, conducted by INPBE is

compiled in the research paper by Venerus et al. [123]. This study also shows significant increase in viscosity of nanofluids with particle concentration.

## **2.5 Convective Heat Transfer**

Many experimental and theoretical studies carried out in by the researchers clearly indicate higher thermal conductivity and viscosity for nanofluids as compared to the base fluid. Although increase in effective thermal conductivity of fluid is important for its heat transfer performance augmentation, viscosity, specific heat and density are the other factors that affect the heat transfer performance of a fluid in a flowing system.

### **2.5.1 Effect of particle concentration and comparison methods**

Over the last two decades, several researchers have investigated the convective heat transfer performance of nanofluids in turbulent flow regime. Initially researchers have used identical Reynolds number as criteria to compare the convective heat transfer performance of nanofluid with base fluid; subsequently, some researchers [96] have argued that since higher viscosity of nanofluids requires higher velocity to achieve the same Reynolds number, an identical velocity based comparison rather than identical Reynolds number based assessment is more appropriate for determining the heat transfer performance of nanofluids. Peclet number based criterion is also used by many researchers [52,90,138] for the comparison of heat transfer performance of nanofluids. The Peclet number describes the effect of thermal dispersion induced by micro-convection and micro-diffusion of nanoparticles.

The heat transfer performance of water- alumina and water-TiO<sub>2</sub> nanofluid is first experimentally investigated by Pak and Cho [96]. They observed 12% decrease in heat transfer coefficient for 3vol% particle concentration of water- alumina nanofluid as compared

to the performance of pure water at identical velocity condition. Xuan and Li [139] have theoretically shown that the enhanced convective performance of nanofluid results not only from its enhanced thermal conductivity but also from the random movement of particle inside the base fluid and its dispersion effects. Further, Xuan and Li [138] examined the heat transfer performance of water-Cu nanofluid at turbulent flow regime, and observed 40% increase in heat transfer coefficient of nanofluid as compared to the case with water at the same velocity. They suggested that the relatively low heat transfer performance observed by Pak and Cho [96] might be due to the higher viscosity of their nanofluid as compared to water. They measured the pressure drop during convective experiments for various particle volume fractions and showed that the presence of nanoparticles in base fluid does not result in significant pressure drop.

Heris et al. [52] have carried out convective heat transfer experiments using water-alumina nanofluid at laminar flow regime and observed an increase in heat transfer coefficient of nanofluid with Peclet number and nanoparticle concentrations. The convective heat transfer experiments carried out by He et al. [50] on water-  $\text{TiO}_2$  nanofluid with three different particle size showed increased convective heat transfer coefficient with particle concentration in both laminar and turbulent flow regimes. They concluded that the effect of particle concentration is more evident in turbulent flow regime. They did not observe any particle size dependency on convective heat transfer performance. The measured pressure drop of the nanofluid is observed to be very similar to that of the base fluid at a given Reynolds number.

Contrary to many research findings, experimental study of Ko et. al. [71] to evaluate the pressure drop of water-carbon nano-tube nanofluid indicated lower friction factors for nanofluids as compared to pure water for certain ranges of flow rates. Yu et al. [150]

observed 50-60% enhancement in heat transfer coefficient of 3.7% volume concentration water-silicon carbide nanofluid as compared to water for identical Reynolds numbers. However, the heat transfer coefficient of the nanofluid is found to be lower than the base fluid at identical fluid velocity condition. They used Mouromtseff number (Mo) to compare the relative performance of water- SiC and water- alumina nanofluid, and found the convective heat transfer performance of water- SiC nanofluid is higher as compared to water- alumina nanofluid. Experimental study by Williams et al. [131] with water- alumina and water-ZrO<sub>2</sub> nanofluid to evaluate the temperature and loading depended thermo-physical properties indicated that conventional correlation of pure fluids would accurately reproduce heat transfer performance in nanofluids. The authors opined that the nanofluids do not exhibit any additional heat transfer performance enhancement other than those due to thermo physical property in static condition. Rea et al. [102] also observed that the convective heat transfer property and pressure drop characteristics of nanofluids can be correctly predicted by means of the traditional correlations provided the effective nanofluid properties are appropriately incorporated in the calculations.

Even though Hwang et al. [56] found good agreement between nanofluid friction factor calculated through an analytical method, and those obtained through experiments, the experimental convective heat transfer performance of the nanofluid is found to be significantly higher as compared to the one calculated through analytical models. Based on their scaling analysis, the enhanced convection property of nanofluid is not only influenced by the increase in thermal conductivity but also due to the flattening of velocity profile near the surface, which results in large temperature gradient near the wall. The flattening of the velocity profile is due to large gradients in bulk properties like particle concentration, thermal conductivity and viscosity. Based on the experimental study on convective heat transfer using Polyalphaolefin (PAO) - alumina and PAO-Multi Wall Carbon Nano Tube (MWCNT)

nanofluid, Yu et al. [147] showed that for laminar flow regime, the theoretical correlation works very well for nanofluid spherical particles whereas it is not effective for the case with nanofluids containing rod-like nanoparticles.

Experimental investigation carried out by Heyhat et al. [53] at laminar regime revealed that the single phase correlation is not effective in predicting the convective performance and pressure drop characteristics of water-alumina nanofluid and the measured pressure drop is about 5.7 times higher than the pure fluid at 2% volume concentration of nanoparticle. The research article of Haghigghi et al. [46] reported significant enhancement in nanofluid heat transfer at laminar flow regime for identical Reynolds numbers, whereas only marginal improvement in heat transfer is noticed when the same is compared against identical velocity.

Yu et al. [147] have experimentally investigated the heat transfer performance of water based nanofluid and compared the heat transfer coefficient of nanofluid to the base fluid on the basis of identical Reynolds number, velocity and pumping power. Further, based on a theoretical study, Yu et al. [147] concluded that the identical Reynolds number based comparison should not be employed for analyzing the performance of nanofluid as this approach might not represent the true flow physics. Timofeeva et al. [118] used Mouromtseff number for comparing the relative importance of various parameters in nanofluid. Nasiri et al. [90] investigated the heat transfer performance of water based alumina and TiO<sub>2</sub> nanofluids in a square channel and found high heat transfer performance for both the nanofluids at identical Peclet number.

### 2.5.2 Effect of particle size

Timofeeva et al. [115] investigated the effect of particle size on convective heat transfer coefficient of water-SiC nanofluid. The heat transfer coefficient for nanofluids with 16 and 29 nm particle sizes is found to be lower than that of pure water for identical velocity conditions; however for 66 and 90 nm particle nanofluid, the heat transfer coefficient is slightly higher as compared to the case with water. The study also indicated that the heat transfer performance of nanofluid is independent of the inlet fluid temperature. In another study by Timafeeva et al. [116] with SiC in Ethylene glycol + water nanofluid, significant improvement in heat transfer characteristics of nanofluid with particle size and temperature is observed.

Recent study of Sonawane et al. [111] with Aviation Turbine fuel (ATF) - alumina nanofluid also showed increased heat transfer coefficient of nanofluid as compared to the ATF alone. An enhancement of 28% in heat transfer coefficient is observed for nanofluid with 1% alumina particle concentration over the base fluid for the same value of pressure drop in both the fluids. In a further study conducted by Sonawane et al. [110] with ATF based alumina, TiO<sub>2</sub>, CuO nanofluids in turbulent flow regime, it is found that the nanofluids exhibit higher heat transfer performance at elevated temperature. They experimentally analysed the effect of particle size on heat transfer coefficient for ATF- alumina nanofluid and found that the heat transfer performance of nanofluid with 150 nm size alumina particles is higher as compared to the case with 50 nm particle size nanofluid.

Many researchers [8,9,27,64,109,126] have clearly reported higher heat transfer performance for nanofluid as compared to the base fluid alone. The degree of enhancement

depends not only on the nanoparticle size and its combination with base fluid but also on the different methodologies adopted for comparing the performance.

## 2.6 Studies on Graphene based Nanofluid

As already discussed, in past wide range of experimental studies using spherical particles made of oxides, carbide and metal nanoparticles in water or ethylene glycol are carried out by various research groups all over the globe. Most of the studies clearly indicate higher heat transfer performance for nanofluids as compared to the respective base fluid. The enhanced thermal conductivity of nanofluid that consists of non-spherical particles, viz; multiwalled carbon nanotube (MWCNT) is first reported by Choi et al. [17]. An increase of 160% in thermal conductivity for 1 vol% MWCNTs dispersed in poly-( $\alpha$ olefin) oil is noticed. The main reason for the selection of carbon nanotubes (CNT) is due to its very high thermal conductivity. Assael et al. [4] systematically introduced the definition of MWNT, methods to make homogeneous stable CNT suspensions without large agglomerates, and reported the effective thermal conductivities for CNT nanofluids with SDS surfactant. He concluded that the relative variation on the effective thermal conductivity due to the addition SDS is negligible. Again, by using THW method, Liu et al. [82] reported up to 30% enhancement in effective thermal conductivity for CNT nanofluids with different base fluids. Many other studies are carried out using MWCNT [3,17,104] and single walled carbon nanotube SWCNT [16,49,54], and most of the studies reported significantly higher heat transfer properties for these nanofluids in comparison to spherical particle nanofluids.

Graphene, a single atomic layer of graphite has two-dimensional form of carbon and is found to exhibit high crystal quality as it has ballistic electronic transport at room temperature. Graphene attracted much attention since it is discovered by Novoselov et al.

[94] in the year 2004. Graphene has superior thermal conductivity and therefore it is expected to exhibit higher heat transfer performance as a nanofluid. According to Hamilton and Crosser [47], as the particle to liquid thermal conductivity ratio of a suspension is above 100, the particle shape can play substantial role in altering the effective thermal conductivity. More recently Balandin et al. [9] reported very high value of thermal conductivity of 5000 W/mk for single-layer graphene. This has generated increased interest among the scientific community to utilise this novel material as suspension in base fluid to be employed as a heat transfer fluid.

### **2.6.1 Effect of particle concentration**

The first study on graphene based nanofluid is simultaneously reported in the year 2010 by two researcher groups, Yu et al. [152], and Baby and Ramaprabhu [5]. Yu et al. [152] experimentally determined the thermal conductivity of Graphene Oxide based nanofluid and reported 30.2%, 62.3% and 76.8% enhancement in thermal conductivity for 5 vol% Graphene oxide nanosheets in water, propyl glycol and liquid paraffin respectively. Baby and Ramaprabhu [5] used functionalized thermal exfoliated graphene oxide (f-TEG) in Deionized (DI) water and Ethylene glycol (EG) as nanofluid. They found significant increase in thermal conductivity of water based nanofluid as compared to those with EG. The reported value for 0.056vol% f-TEG water nanofluid is 14% at 25<sup>0</sup>C and 64% at 50<sup>0</sup>C. Further, in their study [6], the authors found 76% enhancement in heat transfer coefficient at 0.01 vol% f-TEG water nanofluid for a Reynolds number of 4500. In their subsequent work [7] the thermal performance of Ag/HEG nanofluid are determined and the nanofluid is found to be stable for a period of more than 3 month.

Mehrali et al. [85] prepared water-Graphene Nano Platelets (GNP) nanofluids without using surfactant and observed maximum enhancement of 27.64% in thermal conductivity for 0.1wt% GNP. They determined the rate of sedimentation of GNPs with time and reported the effect of specific surface area (SSA) and concentration of sedimentation rate. They also observed increased viscosity for higher SSA nanofluids.

### **2.6.2 Effect of fluid temperature**

As reported earlier, Das et al. [18] determined the effect of temperature on thermal conductivity on metal oxide based nanofluids. The authors observed 2 to 4 fold increase in thermal conductivity of nanofluid as the temperature is increased from 21<sup>0</sup>C to 51<sup>0</sup>C. Subsequently, many researchers carried out detailed study in this area and some of them reported significant enhancement of thermal conductivities with temperature [58,81,111,128] whereas some have reported no enhancement [63,72,114,152].

Baby and Ramaprabhu [5] observed significant effect of temperature on thermal conductivity for water- graphene nanofluid. Ijam et al. [58] prepared GNP - glycerol + water nanofluids and monitored the stability of nanofluids with time. It is found that their nanofluids are stable for more than 5 months. The study also showed significant effect of temperature on the thermal conductivity of nanofluids. Wang et al. [128] prepared stable graphene based nanofluid in ionic liquid without surfactant and reported 15.5% and 18.6% increase in thermal conductivity at 25 <sup>0</sup>C and 65 <sup>0</sup>C respectively for 0.06 wt% of graphene. They found reduction in viscosity for graphene based nanofluid as compared to the base fluid. Thermal conductivity of nanofluid at very high temperature is measured by Liu et al. [81] for 1-hexyl-3-methylimidazolium tetrafluoroborate [HMIMM] BF<sub>4</sub>- graphene nanofluid.

Increase in thermal conductivity from 15.2% at 20 °C to 22.9% at 200°C for 0.06 wt% GNP nanofluid is observed.

Contrary to above mentioned findings, Yu et al. [152] did not observe any increase in thermal conductivity for graphene oxide nanofluids with temperature. Kole and Dey [72] determined the thermal conductivity and viscosity at various volume fractions of graphene nanosheets in water + EG fluid and also reported the insignificant effect of temperature on thermal conductivity of the nanofluids. The increase in viscosity reported for their nanofluid is up to 100% for 0.395 vol% loading.

Gupta et al. [44] noticed different behaviour of temperature dependency on thermal conductivity of graphene based nanofluids in comparison with spherical particles nanofluid. Based on the experimental observations they proposed a possible mechanism of Brownian motion-percolation hybrid to exist in graphene based nanofluid. The phenomenon of Brownian motion of nanosheets depends upon the fluid temperature whereas the percolation of nanosheet is temperature independent phenomenon. This hybrid mechanism explains the trend in GNP behaviour, and it is observed to exist between the respective trends of metal oxides and carbon nanotubes. Also the role of percolation and sheet dynamics in graphene nanofluid is reported by Dhar et al. [23].

A study carried out by Sabourin et al. [105] on combustion characteristics of graphene based fuels indicates higher combustion performance of graphene based nanofuels. They studied the linear burning rates of nitro-methane in presence of aluminium, silicon oxide and graphene sheets, and reported highest increase in burning rate with graphene sheets. The authors attributed it to the enhanced burning rate of graphene-nitromethane, due to its increased thermal conductivity. Pure aluminium particles are used as additive in solid rocket

motor to enhance combustion characteristics. The handling of pure aluminium is very difficult as it spontaneously gets oxidized in the presence of atmosphere and catches fire. As the heat of combustion of carbon and aluminium is 31.1 kJ/g and 32.8 kJ/g respectively, graphene could be considered as an alternate option to be used as fuel additive in rocket engine. Kerosene is an aviation fuel and is also used as a fuel in semi cryogenic engine. Moreover the use of graphene in fuel will not contribute to any particulate matter of plume “signature”. It will undergo complete combustion and will result in CO<sub>2</sub>.

## 2.7 Potential Mechanisms of Heat transport

Various mechanisms of heat transports in nanofluids are proposed by researchers. Keblinski et al. [66] and Eastman et al. [30] proposed four possible heat conduction mechanisms. They are: Brownian motion of the nanoparticles, molecular level layering of the liquid at the liquid/solid interface, nature of heat transport (diffusive or ballistic), and the influence of nanoparticle aggregation. Lee et al. [74] showed that the particle charge state also influences the thermal conductivity enhancement. Recently, Gao et al. [38] performed thermal measurements and structural analysis of phase reversible materials. From their investigations, it is identified that particle aggregation is mainly responsible for improvement in thermal conductivity. Biercuk et al. [11] suggested the formation of three dimensional percolating networks as the primary reason for the conductivity enhancement from their investigation on CNT composites. Wen and Ding [130] argued that the formation of ordered nano layer was not possible, especially in the case of surfactant-encapsulated CNTs. Due to the large diameter of CNTs they also ruled out the possibility of Brownian motion playing a significant role in heat conduction. However, the authors are not able to explain the conductivity enhancement at higher temperatures. All these mechanisms and the views of various researchers on the mechanisms are discussed in detail in the following sections.

### 2.7.1 Brownian motion and micro convection

Brownian motion is the random motion of the particles suspended in a fluid. In nanofluids the random motion of nanoparticles can directly transport energy from one place to another. In addition, a micro-convection effect, which is due to fluid mixing around the particles, is also proposed to be important. Various researchers have studied the nanofluid behaviour with respect to Brownian motion mechanism. The Brownian motion and micro convection models attempts to rationalize the temperature and size dependency by postulating the mechanism of diffusion dependent thermal conductivity of nanofluids. This theory assumes that the nanofluid thermal conductivity is dependent on the self diffusion coefficient ( $D_f$ ) of the nanoparticle which can be defined using well known Stokes-Einstein relationship as;

$$D_f = \frac{k_b T}{3\pi\eta d} \quad (2.2)$$

where  $k_b$  is the Boltzmann constant,  $T$  is the temperature of the fluid,  $\eta$  is the fluid viscosity and  $d$  is the diameter of the particle.

Tsai et al. [119,120] performed systematic experiments on fluids with different viscosities seeded with  $Fe_3O_4$  particles. From their experiments, they showed that Brownian motion could play an important role in the thermal conductivity enhancement. Koo and Kleinstreuer [73] considered the kinetic energy of nanoparticles due to the Brownian motion in their thermal conductivity model and demonstrated the significant effect of Brownian motion on nanofluid thermal conductivity. However, Keblinski et al. [66] revealed that the contribution of Brownian motion alone in heat transport is insignificant as the effect of thermal diffusion is much higher than the effect due to Brownian motion.

Further, model developed by Jang and Choi [62] showed the significant role of micro convection caused by Brownian motion on thermal conductivity of nanofluids. Parsher et al. [100] compared the effect of translational Brownian motion and convection induced by Brownian motion. By making an-order-of magnitude analysis, they concluded that the convection due to Brownian motion of the particles in the nanofluid is mainly responsible for significantly high thermal conductivity of the nanofluids. A model focusing on the effect of Brownian motion to predict effective thermal conductivity of nanofluids is developed by Shukla and Dhir [107]. It clearly indicated the effect of particle size and fluid temperature on nanofluid thermal conductivity. Further a numerical study conducted by Li and Peterson [80] to understand the effect of mixing due to Brownian motion of nanoparticles on thermal conductivity of nanofluids also indicate significant effect of Brownian motion induced mixing on heat transport in nanofluids. A thermal conductivity model developed by Yang [142] using kinetic theory of particles under relaxation time approximations also reveals the significant role of Brownian motion induced micro convection on nanofluid thermal conductivity.

### **2.7.2 Aggregation of nanoparticles (Clustering)**

Clustering or aggregation is an inherent property of the nanoparticles whether they are in liquid or dry powder form due to Van der Waals force. Clustering of nanoparticles into particular patterns may influence the effective thermal conductivity. Percolating pattern with higher interaction will lower down the thermal resistance in heat flow path. Although large clusters would most likely settle down in the fluid, local clustering is also possible and has been observed experimentally by Eastman et al. [30]. The effective volume of a cluster could be much larger than the physical volume of the particles. Since within such clusters, heat can move very rapidly, the volume fraction of highly-conductive solid phase is larger than the

volume of solid and may significantly increase thermal conductivity. In systems like CNT, graphite and Graphene nanofluids the nanoparticles are more likely to form a percolation network.

Keblinski et al. [66] conceptualized clustering of nanoparticles as a mechanism of enhanced thermal conductivity of nanofluids as shown in Fig.2.1. They demonstrated that the clustered nanoparticles provide local percolation-like path for rapid heat transport and increases the effective nanoparticle volume fraction. They suggested that the dramatic increase of effective thermal conductivity occurs even though the particles are not in physical contact, but just within a specific distance, allowing rapid heat flow between them. Such liquid-mediated clusters exhibit a very low packing fraction. This is a very large effective volume and in principle could be used to explain the unusually large experimentally observed enhancements of effective thermal conductivity of nanofluids.

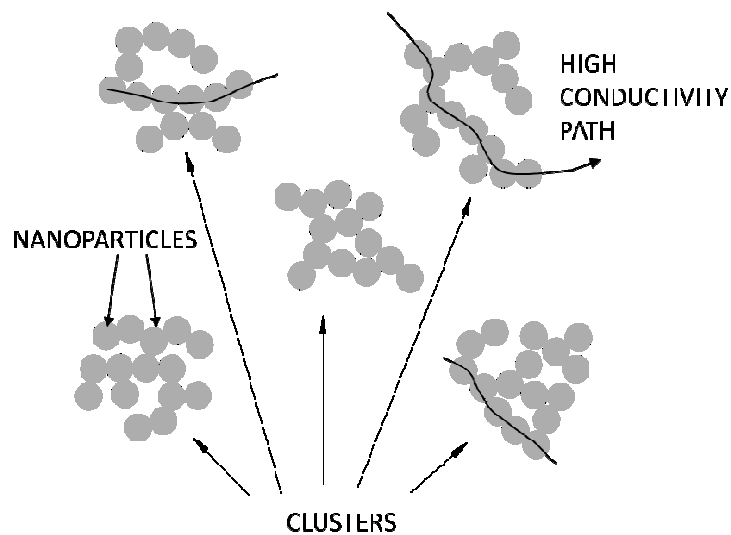


**Figure 2.1:** Structure of clustered particles in nanofluid

Parsher et al. [99] studied the effects of aggregation on the thermal conductivity of nanofluids and reported rapid reduction in aggregation time constant with decreasing nanoparticle size; also the thermal conductivity enhancement increases with increasing level of aggregation and remains constant once the optimum level of aggregation is attained. However, Xuan et al. [139] simulated Brownian motion and aggregation of nanoparticles and reported that the nanoparticles aggregation reduces the thermal conductivity of nanofluid due to their smaller velocity as compared to single nanoparticles.

Evans et al. [33] developed three-level homogenization theory and validated it by Monte Carlo simulation of heat conduction on model fractal aggregates. This was done to understand the role of aggregates on nanofluid thermal conductivity. They have demonstrated the significant enhancement in nanofluid thermal conductivity as a result of aggregation of the nanoparticles. Feng et al. [36] modeled the effect of clustering by accounting for the effect of particle size. They reported improvement in thermal conductivity of nanofluids with cluster and found it more pronounced in nanofluid with smaller nanoparticles. This is due to smaller interparticle distance in the case of smaller size nanofluid that results in increased Van der Waals forces among the particles.

### **2.7.3 Liquid layering at liquid - particle interface**

The atomic structure of the liquid layer at the solid-liquid interface is much more ordered than that of the bulk liquid. It is well known that materials with ordered structure like crystalline solids exhibit much higher thermal conductivity than liquids [66]. The liquid layering at the interface is therefore expected to result in higher thermal conductivity.

The fact that there is scarcity of experimental data that addresses the thickness and thermal conductivity of these nanolayers is an important drawback of the proposed

mechanism. Some researchers developed a theoretical model, as shown in Fig. 2.2, by considering liquid layering around nanoparticles, and illustrated the predictions of their model by assuming preliminary values for the thermal conductivity and thickness of the nanolayer [149]. In certain other models the thermal conductivity of the nanolayer is assumed to linearly vary along the radial direction [135], and there are models where the effect of the temperature dependence of the thermal conductivity of these layers is also taken into account [108]. By choosing the parameters of the nanolayer accordingly, it is possible to produce results which are consistent with experimental data; however this does not prove the validity of the proposed mechanism.

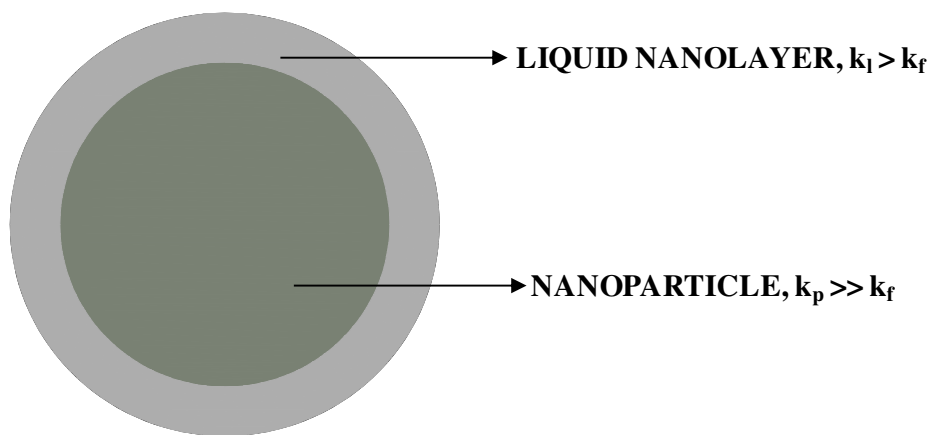


**Figure 2.2:** Presence of liquid layer around nanoparticle in nanofluid

Keblinski et al. [66] calculated the thermal conductivity enhancement induced by the particle-layered-liquid structure. To estimate the upper limit for this effect, the thermal conductivity of the interfacial liquid layer is set to be the same as that of the solid particle. Based on simple calculations, it is observed that 2.5 nm thickness of liquid layer required doubling the effective volume of a particle with 10 nm diameter. However, results from experiments and simulations done by Henderson et al. [124] have shown that a typical

interfacial layer thickness is only of the order of 1nm. Thus, although the liquid layer at the interface may influence thermal transport, it is not significant enough to account for the increase in thermal conductivity of nanofluids. Xue et al. [135] examined the effect of nanolayer by molecular dynamics simulations and reported the ineffectiveness of nanolayers on thermal transport. For performing the simulations, a simple monoatomic liquid is considered and the authors noted the results might be different in the case of water and other base fluid.

#### **2.7.4 Ballistic heat transport in nanoparticles**

In crystalline solids such as nanoparticles used in nanofluids, heat transfer occurs through phonons; that is, by the propagation of lattice vibrations. Such phonons are created at random, propagate in random directions, and are scattered by each other or by defects and thus justify the use of the macroscopic description of thermal transport. In solids, diffusive heat transport is valid if the mean-free path of phonons is smaller than the characteristic size of the particle in consideration.

Kebllinski et al. [66] estimated the phonon mean-free path of alumina nanoparticles at room temperature according to the theory developed by Debye [39]. In a particle with a diameter smaller than 35 nm, the heat transport is not diffusive, but heat is transported ballistically. Although this fact prevents the application of conventional theories for the modelling of thermal conductivity of nanofluids, Kebllinski et al. [66] noted that ballistic heat transport still cannot explain the anomalous thermal conductivity enhancements, because the temperature inside the nanoparticles is nearly constant and is also independent of the mode of heat transport, whether by diffusion or ballistic. Therefore the boundary conditions for the base fluid are the same in both cases, and the result is identical thermal conductivity values

for the nanofluid. Alternately they indicated the significant effect of ballistic heat transport on thermal conductivity of nanofluids, provided it enables efficient heat transport between nanoparticles. This is only possible if the nanoparticles are very close to each other (a few nanometers separated) and they opined that this could be the case for nanofluids with very small nanoparticles. Furthermore, the authors stress on the fact that the particles may become closer to each other due to the Brownian motion and ballistic heat transport can happen in the nanofluid.

Nie et al. [93] theoretically investigated the possibility of a change in the phonon mean-free path of the liquid phase of nanofluids due to the presence of nanoparticles. The authors found that the layering structure, in which there is significant change in phonon mean-free path, is confined to a distance of around 1.0 nm. As a result, it is concluded that the highly localized effect may be responsible for the anomalous thermal conductivity enhancement of nanofluids. Furthermore, change of phonon transport speed in the liquid phase due to the presence of nanoparticles is also investigated and the associated effect is also found to be negligible.

Keblinski et al. [66] and Eastman et al. [30] discussed the nature of thermal transport in nanoparticles. Although it is difficult to envision how ballistic phonon transport could be more effective than very-fast-diffusion phonon transport, particularly to the extent of explaining the order of magnitude larger increase of thermal conductivity in Cu nanofluids, the other ballistic phonon effects could lead to significant increase in thermal conductivity. As can be shown, the nanoparticles in a nanofluid are surprisingly close to each other even at very low volume fractions. For example, the surfaces of 10 nm particles are only separated by 5nm at 5% volume fraction. Therefore the ballistic phonons initiated in one particle can persist in the liquid and reach a nearby particle even though the phonon mean free path in

liquid is very short (~1-2 nm). This process continues to propagate even further due to the increased agitation of the random Brownian motion of nanoparticles. Therefore this particular thermal transport process in nanofluids is expected to be responsible for the major increase in effective thermal conductivity.

## 2.8 Summary of the Literature Survey

Nanofluid, with fuel as a base fluid could make significant contribution in enhancing the cooling capacity of the rocket nozzles. It is notable however that many of the nanofluid enhanced heat transfer rates reported in the literature are beyond the effect of increased thermal conductivity alone. Heat transfer is a surface phenomenon and the increased surface area also enhances the heat conduction in nanofluids. The effect of particle size and fluid temperature on the thermal conductivity of nanofluids is determined by many researchers. Literature reviews [8,109,122,126,138,148] indicate large disparity among the researchers on the percentage enhancement in thermal conductivity with respect to its temperature dependency even for the same nanofluid. The disagreement between these reported values may be attributed to the different techniques used for the production of nanoparticles and the method of preparing the nanofluid itself. Heat transfer performance at turbulent flow regime is also well documented in the literature for oxide, carbide and carbon nanotube in water and EG based nanofluids. While some of the studies show very high convective heat transfer performance of nanofluids that could not be predicted using the pure fluid correlation with incorporation of modified thermo-physical properties of nanofluids, the others indicate that the conventional correlation can accurately predict the heat transfer behavior of nanofluids.

Due to ultra-high thermal conductivity of graphene sheets compared to other type of nanoparticles, researchers have started investigating graphene based nanofluid for heat

transfer application. Though many experimental studies on thermal conductivity of graphene based nanofluids are available in the literature, the studies on convective heat transfer performance are limited.

It is also evident from the collection of literatures, that very few studies are available on kerosene-alumina nanofluid. No study has been carried out so far for kerosene-graphene nanofluid. A study close to the kerosene based nanofluid is carried out by Sonawane et al. [111], where the authors have used ATF based nanofluid and determined the heat transfer properties. Thus a systematic study with the standardization of experimental method starting from nanofluid preparation till measurement to assess heat transfer augmentation is essential to evaluate the true potential of nanofluids in heat transfer applications.

## **2.9 Scope and Objective of the Present Study**

Prior to exploring the potential use of kerosene based nanofluid for rocket nozzle cooling application, significant knowledge of the thermo-physical properties along with the convective heat transfer properties of the fuel based nanofluid is essential. The present study aims for the preparation and characterization of stable kerosene based nanofluids for heat transfer applications. Following are the major goals of current work

1. Synthesis of stable kerosene-alumina and kerosene-GNP nanofluids at low particle concentration.
2. Identification of suitable surfactant and ultrasonication method for greater stability of kerosene- alumina and kerosene-GNP nanofluid.
3. Determination of nanofluids stability using particle size measurement and distribution in nanofluid along with the thermal conductivity measurements with time.

4. To determine the effect of particle size, particle concentration and fluid temperature on thermal conductivity and viscosity of nanofluids and to identify the reason for the observed trends.
5. Detailed convective heat transfer experiments to evaluate the heat transfer performance of nanofluids at turbulent flow regime.
6. Study of pressure drop characteristics of nanofluids at turbulent flow regime and determination of effective heat transfer performance for the utility of these nanofluids as a heat transfer fluid.
7. Develop correlations for convective heat transfer and friction factor of kerosene based nanofluids.

## CHAPTER 3

### 3 EXPERIMENTAL METHOD

In the present work, kerosene based nanofluids are prepared and characterized for its thermal performance. In this chapter details of the instruments, test setups and test procedure used for the synthesis and characterization of kerosene-alumina and kerosene-graphene nanofluids are briefly discussed.

#### 3.1 Materials

Current study deals with the preparation of kerosene based nanofluids using two-step techniques. Rocket grade kerosene is used as a base fluid. Alumina and Graphene Nano Platelets (GNPs) are used as nanoparticles and are purchased from M/s Sigma Aldrich and M/s XG Sciences respectively.

##### 3.1.1 Base fluid

Base fluid used in the present study is Rocket grade kerosene, a highly refined form of kerosene that is used as a fuel in semi cryogenic engine. Kerosene is burnt inside the combustion chamber with oxygen and produces high temperature combustion gas to propel the launch vehicle. Kerosene is a mixture of various long chain hydrocarbons with paraffins, olefins, naphthenes and aromatics as major constituents. Long chain aromatic hydrocarbons present in the kerosene forms complex carbon structure (coke), if heated to a particular temperature (coking temperature~ 570K). In the regenerative channel, when kerosene temperature reaches its coking temperature, coke starts depositing on the heat transfer surface and the heat transfer resistance of the wall increases significantly. The increased heat

resistance on the surface further enhances the surface temperature and leads to additional coke deposition on wall to occur. Due to the adverse thermal effect of coking in the regenerative cooling passage, the metal wall burns out and thereby leading to puncturing of hot gas-coolant surface. Rocket grade kerosene contains very low sulphur (<10ppm) and aromatic contents (<5%) to reduce tendency of coking during its flow in hot regenerative coolant channel. Thermodynamic properties of the kerosene used in the present study are detailed in Table 3.1

**Table 3.1:** Thermodynamic properties of rocket grade kerosene

Density	809 kg/m <sup>3</sup>
Viscosity	1.39 cP
Specific heat	2093 kJ/kg.K
Thermal conductivity	0.104 W/m.K

### 3.1.2 Nanoparticle

Nanoparticles used in the current study are procured from commercial vendor. Alumina nanopowders with part no 71475 and part no 544833 are procured from M/s Sigma Aldrich, USA. The surface area and size is of the alumina powder by the manufacturer is provided in Table 3.2.

**Table 3.2:** Size and surface area of alumina powder

Part no	718475	544833
Average particle size	13nm	50nm
Average particle surface area	85-115 m <sup>2</sup> /g	>40 m <sup>2</sup> /g

Graphene Nano Platelets (GNPs) are procured from M/s XG Sciences, USA. Three “C-grade” materials with different surface areas of 300 m<sup>2</sup>/g, 500 m<sup>2</sup>/g and 750 m<sup>2</sup>/g are used in the study. As defined in the catalogue, all these GNPs have “small flake” morphology, with particle sizes that are larger in the lower surface area GNPs and smaller in the highest surface area GNPs. The size of a typical Grade C sample has a distribution that ranges from very small flakes (below 10 nm) up to relatively large flakes (1-2 μm). Grade C-750 has the smallest average size, followed by C-500 while C- 300 has the largest average size. Thermal properties of alumina and GNP used in the current study are provided in Table 3.3.

**Table 3.3:** Nano material properties

	$\rho$ (kg/m <sup>3</sup> )	$C_p$ (J/kgK)	k(W/mK)
Alumina	3920	773	40
GNP	2300	420	2000

## 3.2 Synthesis

As mentioned earlier, the present study used two-step technique to prepare the kerosene-based nanofluids. Nanoparticles procured from the vender are dispersed into the kerosene using different ultrasonication techniques. Out of the various stabilization techniques that are tried, steric stabilization technique is found suitable.

### 3.2.1 Ultrasonication method:

Ultrasonication process plays a major role in breaking down the agglomerates in nanofluids. The sound waves propagate into the fluid with alternating high pressure and low pressure cycles, creating small bubbles or voids during the low pressure cycles. During the

high pressure cycle, the bubbles attain a threshold volume at which no more absorption of energy is possible, they collapse violently and create mixing of nanoparticle in the base fluid. Particle dispersion occurs by the action of a collapsing cavitation bubble at the agglomerate interface. At the collapsing bubble interface, high energy is released in a localized region that overcomes the interparticle attractive forces in agglomerate structures. In the current study various ultrasonication methods with bath and disruptors of varying frequency and power are used, as shown in Table 3.4.

**Table 3.4:** Type of ultrasonication methods

<b>Type</b>	<b>Frequency</b>	<b>Power</b>	<b>Make</b>
Bath	25 kHz	500W	CREST
Bath	68kHz	500W	CREST
Bath	1 MHz	500W	CREST
Dual frequency bath	58 kHz, 132 kHz	500W	CREST
Bath	470 kHz	250W	CREST
Disruptor	20 kHz	750W	COLE PARMER
Disruptor with flow cell type	20 kHz	100W	COLE PARMER

Figures 3.1 and 3.2 show bath type and disruptor flow cell type ultrasonication system used in the present study. In bath type ultrasonicator, ultrasonic transducers are placed at the bottom of the tank, which converts electrical energy into ultrasound waves. Nanofluid of required quantity is filled and the ultrasonication of complete nanofluid takes place. In disruptor type ultrasonic process, an electronic generator transforms AC power to 20 kHz signal that drives a piezoelectric convertor and produces mechanical vibrations. Here, the required quantity of nanofluid is filled inside a container and with the help of peristaltic

pump, in a closed loop circuit, fluid is passed through the horn where ultrasonic mixing of nanoparticles with the fluid takes place.



**Figure 3.1:** Ultrasonic disruptor and bath (25KHz 500W)



**Figure 3.2:** Ultrasonic disruptor with flow cell

### 3.2.2 Stabilization method:

Kerosene based nanofluids are stabilized using steric stabilization technique. Various surfactants as shown in Table 3.5, procured from M/s Sigma Aldrich, are used based on their affinity towards kerosene to stabilize the nanofluid. Suitable surfactant is selected for each combination depending upon the stability of the nanofluids. Anionic surfactants with lower Hydrophilic - Lipophilic Balance (HLB) number are found to be suitable for the preparation of stable kerosene based nanofluid.

**Table 3.5:** Surfactants used for preparation of kerosene based nanofluids

Sl no	Surfactant	HLB	Charge type
1	Oleic acid	1	Anionic
2	TritonX100	13.51	Anionic
3	Tween20	16	Non-ionic
4	MERPOL	6	Non-ionic
5	Hexadecyltrimethyl ammonium bromide	10	Cationic
6	Cetylpyridinium chloride	26.0	Cationic
7	Kolliphor	14	Non-ionic
8	Oleylamine	4.7	Anionic

## 3.3 Characterization

### 3.3.1 Particle surface area measurement

In the current study nanoparticles are purchased from commercial vendors. Before using the nanoparticles for the preparation of nanofluids, specific surface area of dry

nanopowder is measured using Quantachrome Nova 1200e surface area analyzer using Brunauer–Emmett–Teller (BET) theory [12] of gas adsorption on solids.

Figure 3.3 shows the Quantachrome Nova 1200e equipment used for the present study. In this method, prior to the gas adsorption experiments, solid surfaces are freed from contaminants such as water and oils. The surface cleaning (degassing) of solid samples is carried out by placing the solid in a glass cell and heating it under vacuum conditions. Then the sample is brought to a constant temperature by means of an external bath. A small amount of nitrogen gas (the adsorbate) is admitted in steps into the chamber. Gas molecules that stick to the surface of the solid (adsorbent) are considered to be adsorbed and tend to form a thin layer that covers the entire adsorbent surface. Subsequently, BET expression as in Eq. (3.1) is used to determine the specific surface area of the particle.

$$\frac{1}{v\left[\frac{p_0}{p} - 1\right]} = \frac{c-1}{v_m c} \left(\frac{p}{p_0}\right) + \frac{1}{c v_m} \quad (3.1)$$

where  $p$  and  $p_0$  are the equilibrium and the saturation pressure of the adsorbents at the temperature of adsorption respectively,  $v$  is the adsorbed gas quantity, and  $v_m$  is the monolayer adsorbed gas quantity and ‘ $c$ ’ is the BET constant.

$$c = \exp\left(\frac{E_1 - E_L}{RT}\right) \quad (3.2)$$

here,  $E_1$  is the heat of adsorption for the first layer and correspondingly,  $E_L$  is for the second and higher layers and is equal to the heat of liquefaction.

Equation (3.1) is an adsorption isotherm and is plotted as a straight line (BET plot) with  $\frac{1}{v\left[\frac{p_0}{p} - 1\right]}$  on the y-axis and  $\frac{p}{p_0}$  on the x-axis in accordance with the experimental results.

The linear relationship of this equation is maintained for the range of pressure values of following  $0.05 < \frac{p}{p_0} < 0.35$ .

$$\text{Specific surface area (SSA), } SSA = \frac{N S v_m}{V a} \quad (3.3)$$

where, N is Avogadro's number; 'S' the adsorption cross section of the adsorbing species.



**Figure 3.3:** Instrument for particle specific surface area measurement

### 3.3.2 Particle size measurement

The particle size of the nanofluids is measured using Malvern Zetasizer. Many researchers [107,153,155] have successfully used this instrument in their studies for measuring the particle size distribution in nanofluids. Dynamic Light Scattering (DLS)

method is used to measure the particle size distribution in nanofluid. Figure 3.4 presents the schematic of backscatter DLS technique used in the current study. A laser beam is illuminated through a liquid medium with suspended nanoparticle, the beam scatters off those particles in all directions (Rayleigh scattering), thereby resulting in a scattering-angle-dependent intensity pattern. Especially when the particles are experiencing Brownian motion, the intensity pattern fluctuates randomly. Constructive and destructive interference occurs as the illuminated light is scattered by the presence of nanoparticles. As a result, the photon detector measures an average intensity pattern that fluctuates as a function in time. The time required for these fluctuations to decay down to the average intensity depends on the Brownian motion of the particles and the size of the particles. Smaller sized particles experience highly rapid Brownian motion and results in faster decaying fluctuations than larger sized particles.

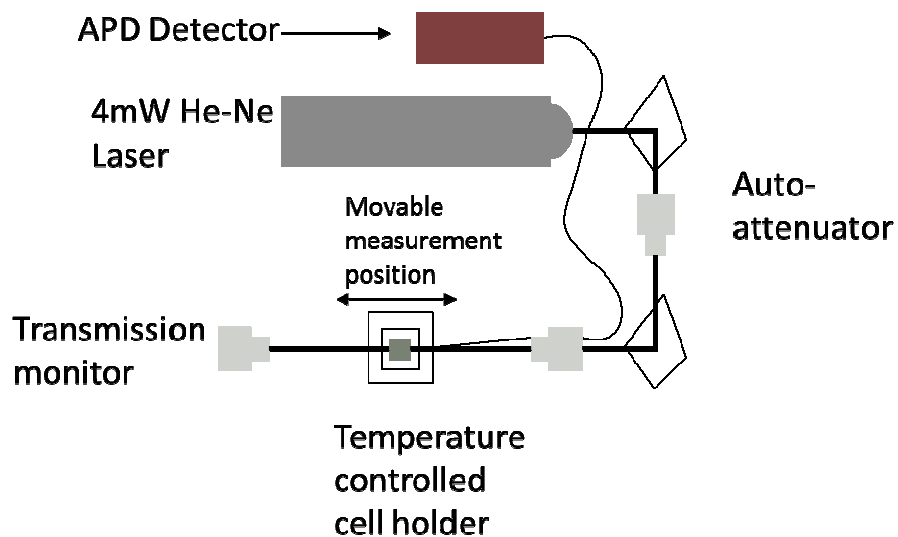


**Figure 3.4:** Schematic of backscatter DLS measurement techniques

Analysis of the intensity fluctuations allows for the determination of diffusion coefficient of the particles in the liquid and the particle size distribution can be further calculated using the Stokes-Einstein equation.

In a DLS experiment, to quantify the intensity decay time, an auto-correlation function is used to measure the intensity at time  $t$ , and at a time  $t + \tau$ , thereby yielding the correlation as a function of  $\tau$ . For the case of mono-disperse, non-interacting spherical particles, the correlation is given by,

$$G(\tau) = A \exp(-2\Gamma\tau) + B \quad (3.4)$$

where 'A' and 'B' are instrument constants,  $\Gamma = D_f q^2$  is the intensity decay rate where ' $D_f$ ' is the diffusion coefficient which can be determined from Stokes – Einstein equation and ' $q$ ' is the scattering vector. The diffusion coefficient is represented as follows [135]:

$$D_f = \frac{k_b T}{3\pi\eta D} \quad (3.5)$$

where  $k_b$  is the Boltzmann constant, T is the temperature of the fluid,  $\eta$  is the fluid viscosity and D is the diameter of the particle. The scattering vector  $q$  is expressed as:

$$q = \frac{4\pi n}{\lambda} \sin\left(\frac{\theta}{2}\right) \quad (3.6)$$

where, 'n' is the refractive index of the fluid,  $\lambda$  is the wavelength of the light and  $\theta$  is the angle at which the scattered light is measured. The size distribution of nanoparticles in this work is determined by using a Zetasizer-Nano (Malvern Instruments) as shown in Fig 3.5. It uses a He-Ne laser (4 mW,  $\lambda = 633$  nm) and avalanche photodiode detector.



**Figure 3.5:** Zetasizer-Nano for particle size measurement using DLS technique

### 3.3.3 Thermal conductivity measurements

Researchers have used various techniques to measure the thermal conductivity of nanofluids viz: transient hot wire method [2,86,110,111,115,130,133,153], transient plane source method [81,128], steady-state parallel plate method [97] oscillation method [17] and the  $3-\omega$  method [16]. Some research groups make use of nonintrusive optical measurement techniques such as forced Rayleigh scattering [122] and infrared microscopy [41] for thermal measurements. A recent benchmark study [13] carried out by 32 research groups worldwide concluded that the measurement technique have insignificant impact in the enhancement of thermal conductivity of nanofluids reported in the literature and any method can be chosen for the comparative study of nanofluid to the base fluid. In the present work, thermal conductivity of nanofluids is measured in static condition using transient hot wire method and confirmatory study for few cases is made using transient plane source method.

### 3.3.3.1 Transient Hot Wire method (THW)

The aforementioned methods utilized in the current study are also used by various other researchers [2,86,110,111,115,130,133,153] for measurement of the thermal conductivity of nanofluids. Many of them [86,115,130,1453] have employed the commercial apparatus KD2 Pro, which works based on the principle of THW method.

In the present work, thermal conductivity of nanofluid samples is measured using the commercial apparatus KD2 Pro. In the benchmark exercise [13] conducted by INPBE in 2009, as many as 8 out of 32 researchers have used KD2 Pro for thermal conductivity measurement. The study clearly concludes that eventhough the absolute values of thermal conductivity depends upon the methods and device used, the relative comparison in thermal conductivity carried out between the base fluid and nanofluids is not affected, and percentage enhancement in thermal conductivity of nanofluids can be accurately predicted using KD2-Pro as long as the same technique and environment conditions are maintained.

Figure 3.6 shows the details of the experimental setup with KD2 probe inside a constant temperature bath. In this method, a probe made up of thin platinum wire is used as a line heat source, as well as a temperature sensor. This method is based on the principle of measurement of temperature and time response of the wire subjected to an abrupt electrical pulse. The probe is placed in the fluid for which thermal conductivity needs to be determined. A pulse mode of electrical current is supplied to the wire for its heating. The heat dissipated in the wire increases the temperature of the wire as well as that of the fluid. The rate of temperature rise depends on the thermal conductivity of the surrounding fluid.

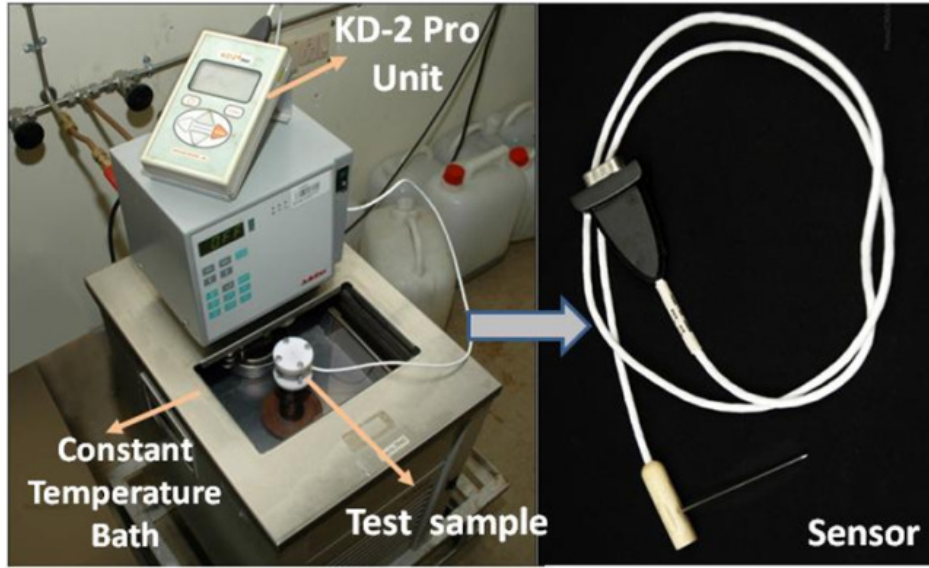


**Figure 3.6:** THW Setup for nanofluid thermal conductivity measurements

Carslaw and Jaeger [14] modelled the rise in temperature surrounding an infinite line heat source with zero mass in an infinite medium. According to them, the temperature response of an infinite thin and infinite long heater, for a constant heat input can be computed by the equation

$$\Delta T = \frac{q}{4\pi k} Ei \left[ \frac{-r^2}{4D_f t} \right] \quad 0 < t \leq t_1 \quad (3.7)$$

where 'q' is the heat rate, 'k' is the thermal conductivity of the medium, 'D<sub>f</sub>' is the diffusivity of the medium, 'r' is the distance from the line at which temperature is measured, 't<sub>1</sub>' is the heating time and 'Ei' is the exponential integral.

Temperature rise after the heat input is turned off is represented by

$$\Delta T = \frac{q}{4\pi k} \left[ -Ei \left( \frac{-r^2}{4D_f t} \right) + \left( \frac{-r^2}{4D_f (t-t_1)} \right) \right] \quad t \geq t_1 \quad (3.8)$$

Equations 3.7 and 3.8 are solved to determine the diffusivity and thermal conductivity of the fluid. Initially, it must be ensured that fluid, probe, and the surroundings are in equilibrium. A full measurement cycle includes a 15 minutes time period for attaining temperature equilibrium, and a subsequent time period of 60s for measurement. Fluid sample is heated for 30s using the probe through electrical power, and the same probe is also utilized to monitor the cooling rate. In order to eliminate errors that could arise due to temperature induced fluid convection, temperature rise is restricted to around 0.5°C. To avoid convection due to outer vibrations, a special holding stand is made with heavy copper slab. Due to small temperature gradients, the probe is found to be very sensitive to minor fluctuation of  $\pm 0.1$  °C, at the room temperature. The probe temperature during heating and cooling cycle is used to compute thermal conductivity of the fluid with an accuracy of 5%.

### 3.3.3.2 Transient Plane Source (TPS) Method:

Hot Disk Thermal Constant Analyser, which works on the principle of TPS method, is also used in the current study for thermal conductivity measurement of nanofluids. This apparatus is used by many researchers [81,128] for nanofluid thermal conductivity measurements. In this method, TPS element behaves both as the temperature sensor and the heat source. This method uses the Fourier law of heat conduction as its fundamental principle for measuring the thermal conductivity. The TPS element is made up of a 10  $\mu\text{m}$  thick Nickel-metal double spiral that is embedded in an insulating layer made of Kapton or Mica (70  $\mu\text{m}$ ). A constant electric power is supplied to the sensor which is dipped into the fluid, and the increase in temperature  $\Delta T(\tau)$  is calculated from the variation in the sensor resistance with time  $R(t)$  by using the equation:

$$\Delta T(\tau) = \frac{1}{\alpha} \left( \frac{R(t)}{R_0} - 1 \right) \quad (3.9)$$

where  $R_0$  is the resistance of the disk before heating (initial resistance),  $\alpha$  is the temperature coefficient of resistance of the nickel foil, and  $\Delta T(\tau)$  is the temperature increase of the sensor that is expressed in terms of the variable  $\tau$ , defined as

$$\tau = \sqrt{\frac{tD_d}{a^2}} \quad (3.10)$$

here 't' is the measurement time, 'D<sub>d</sub>' is the thermal diffusivity of the sample and 'a' is the sensor radius.

According to the Fourier Law of heat conduction, the temperature rise in absence of convection in the fluid can be expressed as

$$\Delta T(\tau) = \frac{W}{\pi^{1.5}ak} J(\tau) \quad (3.11)$$

where,  $J(\tau)$  is the geometrical function and 'W' is the electric power to the probe. By fitting the experimental data to the straight line as in Eq. 3.11, the thermal conductivity of the fluid can be obtained from the slope of the line ( $W/\pi^{1.5}ak$ ).

The experimental setup is represented in Fig. 3.7. The setup comprises of Hot disk unit, a constant temperature bath, and a sample holder with TPS sensor. To avoid natural convection during the measurement, a special sample holder is used for the measurement as shown in Fig.3.5. The sample holder is made of high thermal conductivity Al metal and TPS sensor is placed in between the two halves of the holder. Small quantity of nanofluid (<5 ml) is filled in the sample holder. The sample holder is placed in the constant temperature bath. During a pre-set time, 200 recordings are acquired and the thermal conductivity of the nanofluid is determined with an accuracy of  $\pm 5\%$ .

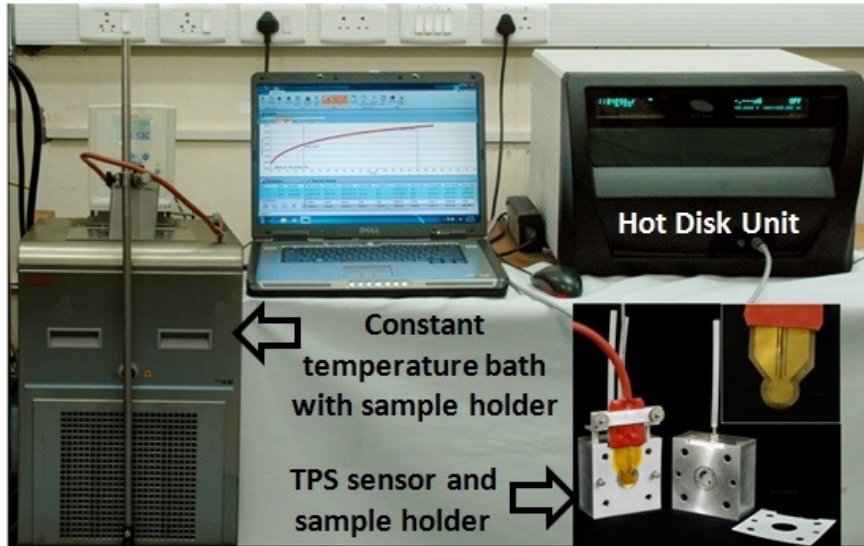


**Figure 3.7:** TPS System used for thermal conductivity measurement

Before using both the apparatus for nanofluids, thermal conductivity of water and glycerin are measured and compared with the reference values at different temperature for accurately calibrating the setup. The measured thermal conductivity data varies only by  $\pm 2.6\%$  and  $2.2\%$  for KD2 Pro and Hot Disk TPS measurement system respectively. These values are well within the instrument accuracy limits as specified by the respective manufacturers.

### 3.3.4 Dynamic viscosity measurement

The dynamic viscosity of the nanofluids is measured using Brookfield LVDV-II digital viscometer (shown in Fig. 3.8), and is used by many researchers [1,72,81] for carrying out viscosity measurements in nanofluids. The operation of this viscometer involves the driving of a spindle, which is immersed in the test fluid through a calibrated spring and the corresponding torque on the rotating cylinder in the sample is determined to calculate the viscosity. The viscous resistance of the sample against the cylinder is measured by the spring deflection and the same is converted to the measurement using a rotary transducer. The

viscometer consists of two concentric cylinders, namely a bob (spindle) and a crucible (cylinder). At constant rotational speed the viscosity of fluid is obtained using the expression given in Eq. 3.12:

$$\mu = \left( \frac{1}{r_1^2} - \frac{1}{r_0^2} \right) \frac{M}{8\pi r^4 n h_e} \quad (3.12)$$

where 'M' is the torque, 'n' is the number of revolutions per second, 'r<sub>1</sub>' is the radius of spindle, 'r<sub>0</sub>' is the radius of spindle crucible, and 'h<sub>e</sub>' is the height of spindle.



**Figure 3.8:** Brookfield LVDV-II for viscosity measurements

The Brookfield viscometer with cone type spindle is capable of measuring viscosity as low as 0.1 cP. The sample volume used in this apparatus is 0.5 ml. Water from constant temperature bath is used in the apparatus for the measurement of viscosity at constant temperature. The rotation of the spindle is maintained at 100rpm and it corresponds to the maximum viscosity measurement range of 3.04 Cp. Instrument accuracy specified by the manufacturer is  $\pm 1\%$  of the maximum value. Thus the error associated with all the measurements is less than 0.03 cP. Apparatus is calibrated using silicone oil with viscosity of 5 cP at 60 rpm and the  $\pm 1\%$  accuracy in the measurement of the maximum value is also verified.

### **3.4 Convective Heat Transfer Setup**

#### **3.4.1 Experimental setup description**

The schematic of the closed loop convective heat transfer experimental setup is shown in Fig. 3.9. The experimental setup consists of a test section, which is resistively heated by a DC power source, flow cell type nanofluid ultrasonication unit with peristaltic pump, variable flow gear pump, turbine flow meter, heat exchanger, a differential pressure gauge, data acquisition system and heat exchanger. Turbine type flow meter used in the experiments measures the flow rate with an accuracy of  $\pm 0.25\%$ . A variable high current DC power source of 20 KW (1000A, 20W) is used for resistive heating of test section. Water cooled heat exchanger with cooling capacity upto 25 kW is used to cool the fluid after it passes through the test section. The differential pressure indicator with a range of 200/700 mbar is connected to the test section for pressure drop measurement. A 30 channel data acquisition system is used to record the surface temperatures as well as the inlet and outlet fluid temperature during the test. Test section is made up of 1.2 m long stainless steel tube

with 9.5 mm outer diameter and 0.9 mm thickness. Twelve T-type thermocouples are welded on to the test section for measuring the surface temperatures and two T-type thermocouples, each of which are positioned at the inlet and outlet of the test section respectively are utilized for measuring the corresponding fluid temperatures. The accuracy of T-type thermocouple used in the setup is  $\pm 0.5^{\circ}\text{C}$ . Accuracy of various instruments used in the closed test setup is provided in Table 3.6.

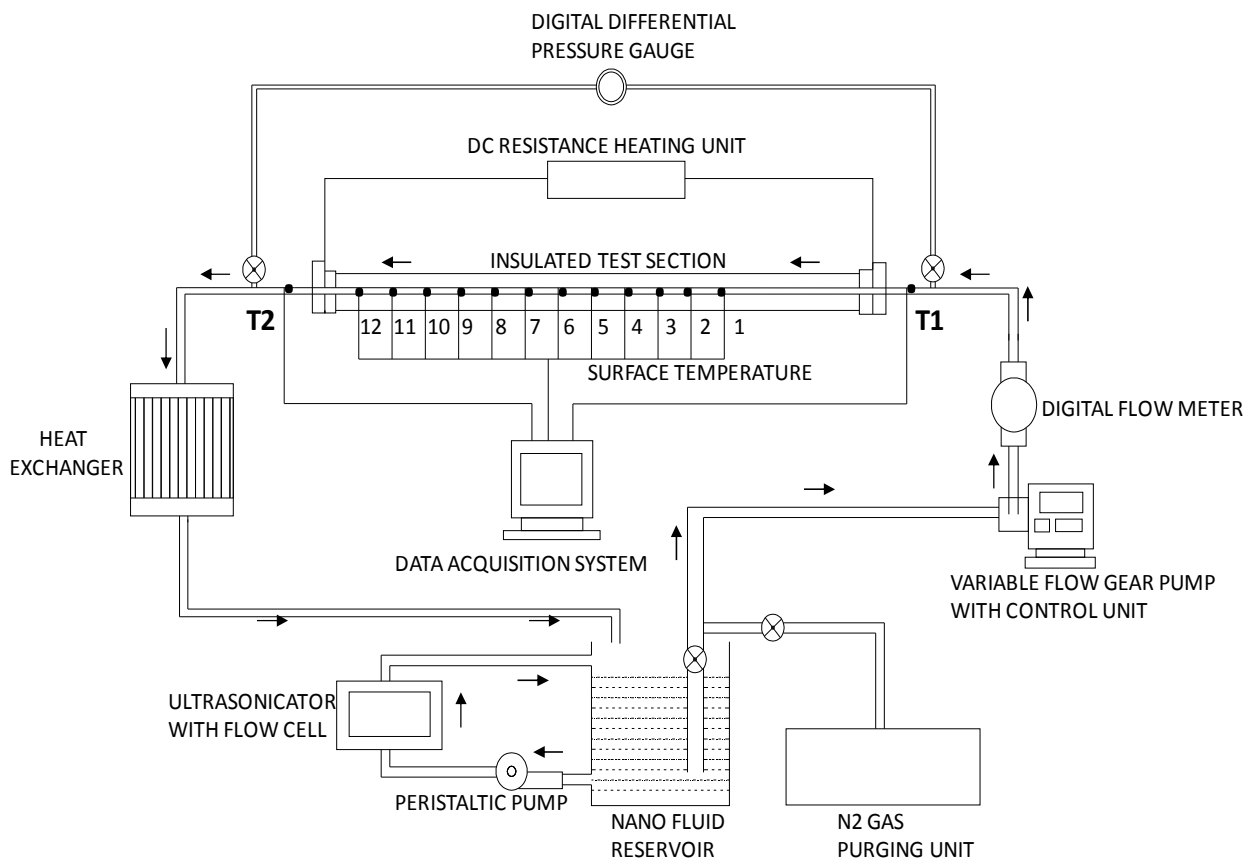


**Figure 3.9:** Schematic of closed loop setup for convective heat transfer experiments

**Table 3.6:** Accuracy of various instruments used in the study

<b>Parameter</b>	<b>Instrument</b>	<b>Accuracy</b>
Temperature	T type thermocouple	0.5 % +0.5 (°C)
Pressure	Druck DPI (Strain Gauge type)	0.3% (FS)
Flow Rate	Turbine Flow meter	0.25%
Current	DC power source (20KW)	0.5%
Voltage		0.1%
k	THW method (TKD2 Pro)	5%
$\mu$	Cup and Cone Viscometer (Brookfield Viscometer)	1% (FS)

In the current study convective heat transfer experiments are carried out in turbulent flow regime. In a pipe flow, transition from laminar to turbulent occurs at  $Re$  2300-3600 [59]. Various researchers [110,111,112] have carried out the experiments in turbulent flow regime with  $Re > 5000$ . In the present work the convective heat transfer experiments are carried out for  $Re > 6000$ . The entrance length ( $X$ ) for fully developed flow [59] in turbulent regime is defined as:

$$X \geq 10D_i \quad (3.13)$$

where ' $D_i$ ' is the inner diameter of the test section.

The minimum entrance length for a fully developed flow is estimated for the current setup as 0.077 m. The tube diameter in the setup is constant throughout and also remains same upstream of the test section; hence a length of 0.2 m is provided for the flow to become

hydrodynamically fully developed. The test section is insulated with glass wool to ensure negligible heat loss to the ambient.

### 3.4.2 Experimental procedure

Figure 3.10 presents the realised test setup for carrying out the convective heat transfer study. Nanofluid of desired particle mass concentration and quantity is prepared using the suitable surfactant. Thermal conductivity and viscosity of nanofluid is measured using KD2 pro and Brookfield viscometer respectively. Thermo-physical properties are determined at various temperatures from 20<sup>0</sup>C to 70<sup>0</sup>C for each weight percentage and particle size. Samples are kept at constant temperature during the measurement using a constant temperature bath.

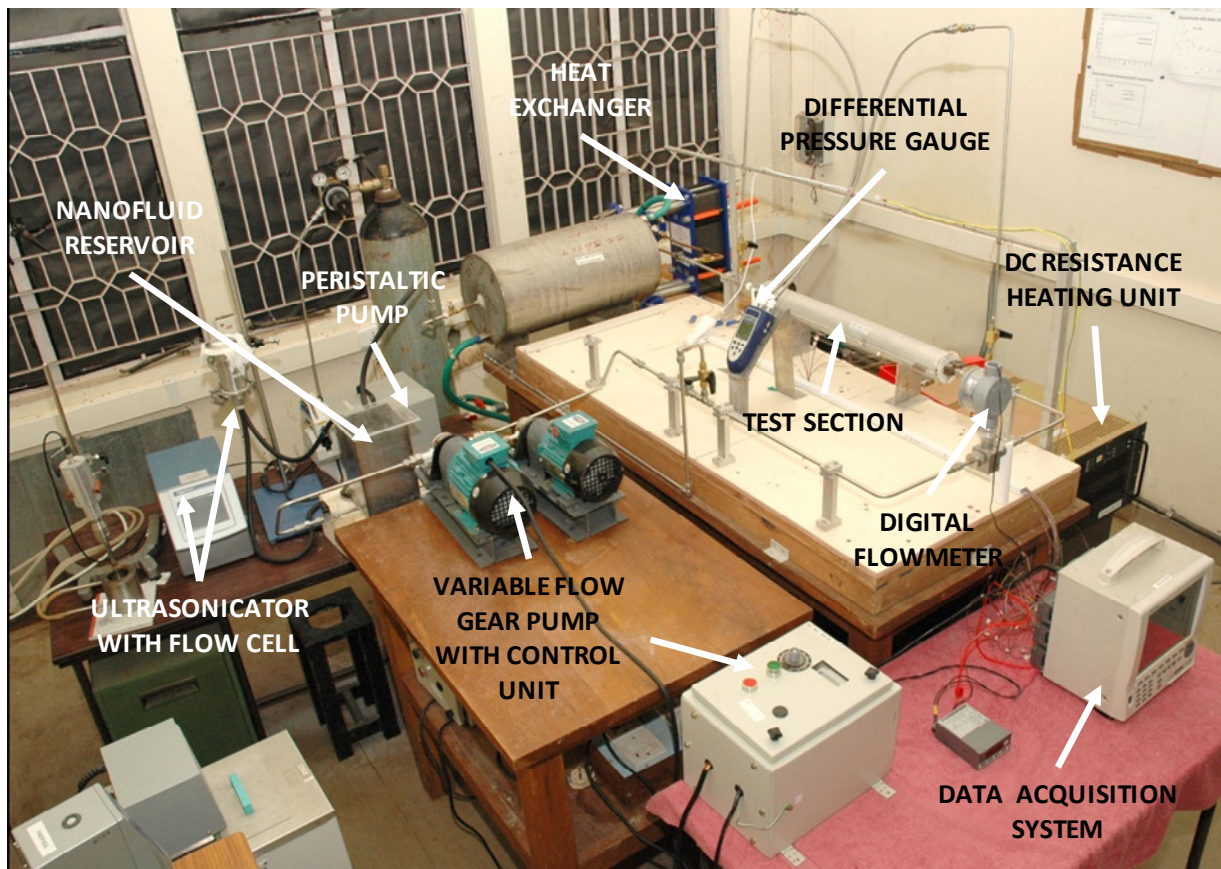


**Figure 3.10:** Convective heat transfer setup

Nanofluid is filled in the reservoir and is continuously ultrasonicated with the help of ultrasonic probe, flow cell and peristaltic pump. A variable speed gear pump delivers the desired volume flow of nanofluid to the test section. The test section is resistively heated with DC power source. The heated nanofluid after its passes through the test section is cooled to near room temperature using water cooled heat exchanger and is emptied into the reservoir. The process is continued till the flow reaches the steady state condition. The inlet fluid temperature to the test section is maintained constant during the test. The experiments are carried out for different Reynolds number by varying the flow rate, and each test is repeated for four times to ensure repeatability.

After each test the fluid lines are purged initially with nitrogen gas to clear nanofluid in the test section. Subsequently purging is also carried out with isopropyl alcohol to remove traces of kerosene on the walls.

### 3.5 Data Reduction

A series of convective heat transfer experiments are carried out to investigate the heat transfer characteristics of nanofluid in turbulent flow regime. Steady state fluid temperature, surface temperature, current (I) and voltage (V) from DC power source and flow rate are measured during the experiment for determining the heat transfer coefficient and Nusselt number at various particle mass concentrations and Reynolds numbers. Measured thermal conductivity and viscosity at various temperatures are curve-fitted to estimate the values at any intermediate temperature point. The effective density and specific heat of nanofluid are estimated based on the physical principle of the mixture rules as follows;

$$\rho_{nf} = \phi \rho_{np} + (1 - \phi) \rho_{bf} \quad (3.14)$$

where,  $\rho_{nf}$ ,  $\rho_{np}$  and  $\rho_{bf}$  is the density of nanofluid, nanoparticle and base fluid respectively and  $\phi$  is the volume fraction of nanoparticle.

$$Cp_{nf} = (\phi \rho_{np} Cp_{np} + (1 - \phi) \rho_{bf} Cp_{bf}) / \rho_{nf} \quad (3.15)$$

where,  $Cp_{nf}$ ,  $Cp_{np}$  and  $Cp_{bf}$  is the specific heat of nanofluid, nanoparticle and base fluid respectively.

Heat absorbed by the nanofluid in test section is calculated by

$$Q_f = m Cp_{nf} (T_{out} - T_{in}) \quad (3.16)$$

where,  $m$ ,  $T_{in}$ ,  $T_{out}$  are fluid mass flow rate, temperature at inlet and outlet of the test section respectively

Electrical heat supplied to the test section  $Q_e$  is given as,

$$Q_e = V I \quad (3.17)$$

where,  $V$  is the input voltage and  $I$  is input current to the test section.

As the value of specific heat of nanofluid is calculated by mixing rule, the correctness of specific heat is ensured by comparing the heat absorbed by the nanofluid,  $Q_f$  in test section to the electrical heat supplied to the test section,  $Q_e$ . In all the experiments  $(Q_e - Q_f)$  is found to be positive and the value is less than 5.9% and this also indicated the effectiveness of the insulation provided on the test section. Reynolds number ( $Re$ ) and Prandtl number ( $Pr$ ) of nanofluid is determined using the expressions

$$Re_{nf} = 4m_{nf} / \pi D_i \mu_{nf} \quad (3.18)$$

$$\text{Pr}_{\text{nf}} = \mu_{\text{nf}} \text{Cp}_{\text{nf}} / k_{\text{nf}} \quad (3.19)$$

Where,  $m_{\text{nf}}$ ,  $k_{\text{n}}$ ,  $\mu_{\text{nf}}$  is the mass flow rate and measured thermal conductivity and dynamic viscosity of the nanofluid.

The outside tube wall temperature ( $T_{\text{so}}$ ) is measured by means of thermocouples. Furthermore, the inside tube wall temperature ( $T_{\text{s}}$ ) is calculated from the measured outside tube wall temperature, by using the Fourier's heat conduction equation with internal heat generation (electrical resistance heating,  $Q_e$ ). As the outer test section is perfectly insulated, the assumptions of no heat loss to the ambient from the outer surface ( $(dT/dr)_{D_0} = 0$ ) is considered. The solution of Fourier's heat conduction equation is determined using convective boundary at the inner surface of the tube as given below.

$$\mathbf{T_s} = \mathbf{T_{so}} + \frac{Q_e}{4\pi L k_t} \left[ \frac{\xi(1-\ln\xi)-1}{\xi-1} \right]$$

(3.20)

here  $k_t$  is thermal conductivity of the material used for test section (steel) and  $\xi = \left(\frac{D_o}{D_i}\right)^2$

Local heat transfer coefficient is estimated using, electrical heat supplied to the test section ( $Q_e$ ), tube inner wall temperature ( $T_{\text{s}}$ ) and the local fluid temperature ( $T_{\text{f}}$ ). Local heat transfer coefficient is estimated as,

$$h_{\text{xnf}} = Q_e / (\pi D_i L (T_{\text{s}} - T_{\text{f}})) \quad (3.21)$$

where,

$$T_{\text{f}} = T_{\text{in}} + x/L(T_{\text{out}} - T_{\text{in}}) \quad (3.22)$$

The average heat transfer coefficient ( $h_{nf}$ ) is calculated as the length-weighted averages of the local heat transfer coefficients ( $h_{x,nf}$ ). Similarly, the average Nusselt numbers (Nu) are calculated from the average heat transfer coefficient.

$$\text{Nusselt Number } Nu_{nf} = h_{nf}Di/k_{nf} \quad (3.23)$$

The Peclet number (Pe) and the friction factor (f) are obtained as follows;

$$Pe_{nf} = Re_{nf}Pr_{nf} \quad (3.24)$$

$$\text{Friction factor, } f = 2\Delta pDi/(\rho_{nf}Lu_{nf}^2) \quad (3.25)$$

where,  $\Delta p$  is the measured pressure drop and  $u_{nf} = m_{nf}/(\pi Di^2 \rho_{nf})$  is the nanofluid velocity at test section.

The merit number is calculated using estimated heat transfer coefficient and measured pressure drop for nanofluid and pure kerosene and is defined as

$$\text{Merit Number} = (h_{nf}/h_{bf})/(\Delta P_{nf}/\Delta P_{bf}) \quad (3.26)$$

Blasius and McAdams correlation [59] for the friction factor in turbulent flow is used for the validation of test setup using pure kerosene and is given in Eq 3.27 and 3.28 respectively.

$$f = 0.316Re^{-\frac{1}{4}} \quad (3.27)$$

$$f = 0.184Re^{-\frac{1}{5}} \quad (3.28)$$

The Dittus–Boelter equation [59] is used for test setup validation using pure kerosene in turbulent flow regime with constant heat flux boundary condition ( $0.7 \leq Pr \leq 160$ , and  $L/d \geq 10$ ) and is shown in Eq 3.29.

$$Nu = 0.023 Re^{4/5} Pr^{2/5} \quad (3.29)$$

### 3.6 Uncertainty Analysis

Detailed uncertainty analysis is carried out prior to analysing the result and outcome of the study. Overall uncertainty is determined using Root sum square (RSS) method (absolute & random error).

#### 3.6.1 Absolute error

Analysis is carried out to estimate errors in both measured and derived quantities. Basic equations are used for deriving absolute error during the experiments due to test setup. Uncertainties in derived parameters are calculated as given below.

Let  $A = f(x, y, z)$ , then uncertainty in A can be determined using uncertainty in x, y, z as

$$U_A = \pm \sqrt{\left(\frac{\partial A}{\partial x} U_x\right)^2 + \left(\frac{\partial A}{\partial y} U_y\right)^2 + \left(\frac{\partial A}{\partial z} U_z\right)^2} \quad (3.30)$$

Error in length and diameter is considered to be 0.5%. Accuracy of various instruments as given in table 3.6 is used for error estimation.

### 3.6.1.1 Temperature measurement

In the current study maximum surface temperature is limited to 100°C and the minimum surface temperature measured in all the experiments is 70°C. The error in measurement of temperature due to thermocouple (T type) and data acquisition system is within 0.5%+0.5°C. Hence maximum error in surface temperature measurement will be

$$\begin{aligned}\text{Maximum error} &= 0.5\% + \frac{0.5}{70} \times 100\% \\ &= 1.2\%\end{aligned}$$

Similarly fluid temperature measured is between 29-46°C. Hence maximum error in fluid temperature measurement is

$$\begin{aligned}\text{Maximum error} &= 0.5\% + \frac{0.5}{29} \times 100\% \\ &= 2.2\%\end{aligned}$$

### 3.6.1.2 Pressure measurement

The pressure drop across the test section is measured using Druck DPI 800 instrument. The accuracy of differential pressure measurement system is 0.1% of full scale. Pressure drop measured during the test range from 20 mbar to 300 mbar. Two different maximum measurement setting is used in the study. Maximum pressure setting upto 200 mbar is used for the experiment whereas the measured pressure drop is 20 to 90 mbar and pressure transducer capable of measuring 700 mbar is also used for high flow rate experiments. Hence, maximum error in pressure measurement is

$$\begin{aligned}
\text{Maximum error} &= \text{Max} \left( \frac{0.1 \times 200}{20} \%, \frac{0.1 \times 700}{90} \% \right) \\
&= \text{Max} (1\%, 0.8\%) \\
&= 1.0\%
\end{aligned}$$

Table 3.7 lists the maximum uncertainty in various measured parameters. The maximum uncertainty in density and specific heat of the nanofluid is taken as 2%. Equation 3.16-3.26 in conjunction with the aforementioned values are used for determining the uncertainty in various derived parameters like those in, heat transfer coefficient, Nusselt number, friction factor, merit number etc, and the details are provided in Table 3.8.

**Table 3.7:** Maximum uncertainty in various measured parameters

<b>Parameter</b>	<b>Accuracy</b>
Length, diameter	0.5%
Fluid Temperature	2.2%
Surface temperature	1.2%
Pressure	1.0%
Flow Rate	0.25%
Current	0.5%
Voltage	0.1%
Thermal Conductivity, k	5%
Dynamic Viscosity, $\mu$	4%

**Table 3.8:** Uncertainty in various derived parameters

Parameter	Uncertainty
Reynolds number, Re	4%
Prandtl Number, Pr	6.7%
Heat Transfer Coefficient, h	4.5%
Nusselt number, Nu	6.8%
Fluid velocity, u	2.1%
Peclet Number, Pe	7.8%
Friction factor, f	3.8%
Merit number	8.3%

### 3.6.2 Random experimental uncertainty

Experiments are repeated four times for a test condition and the mean value is reported. Two times the standard deviation from the mean value is considered as a random experimental error for the analysis assuming 95% confidence level. Total uncertainty ( $U_T$ ) in each parameter is determined by using both fixed uncertainty ( $U_f$ ) and random experimental uncertainty ( $U_r$ ) and shown in Eq. 3.31.

$$U_T = \pm \sqrt{U_f^2 + U_r^2} \quad (3.31)$$

Table 3.9 and Table 3.10 shows the maximum uncertainty in various derived parameters for kerosene-aluminium and kerosene-GNP nanofluid respectively.

**Table 3.9:** Maximum uncertainty in various derived parameters for kerosene-aluminium nanofluid

<b>Parameter</b>	<b>% Standard deviation (<math>\sigma</math>)</b>	<b>Total uncertainty (<math>U_T</math>) %</b>
Thermal Conductivity, k	2.3%	6.0%
Dynamic Viscosity, $\mu$	0.8%	4.2%
Heat Transfer Coefficient, h	4.9%	8.2%
Nusselt number, Nu	5.2%	9.9%
Friction factor, f	4.1%	6.9%
Merit number	9.0%	15.2%

**Table 3.10:** Maximum uncertainty in various derived parameters for kerosene-GNP nanofluid

<b>Parameter</b>	<b>% Standard deviation (<math>\sigma</math>)</b>	<b>Total uncertainty (<math>U_T</math>) %</b>
Thermal Conductivity, k	1.8%	5.6%
Dynamic Viscosity, $\mu$	1.1%	4.3%
Heat Transfer Coefficient, h	4.3%	7.5%
Nusselt number, Nu	4.9%	9.7%
Friction factor, f	4.3%	7.1%
Merit number	8.6%	14.7%

# CHAPTER 4

## 4 RESULTS AND DISCUSSION

Kerosene-alumina and kerosene-GNP nanofluids are prepared using the two-step technique as explained earlier. The thermo physical properties and the heat transfer performance of the nanofluids in the turbulent flow regime are experimentally investigated. The effect of particle size, particle concentration and fluid temperature on the thermal conductivity and the viscosity of the nanofluids is also evaluated. In this chapter, the analysis pertinent to the synthesis and characterization, and those associated with the performance of convective heat transfer in the turbulent flow regime is discussed in details for kerosene-alumina and kerosene-GNP nanofluids respectively. The matrix of experiments carried out in the present study describing the parametric variations is shown in Table 4. 1.

### 4.1 Kerosene-Alumina Nanofluid

The experimental investigation involved the preparation of kerosene-alumina nanofluids at different particle volume fraction followed by stabilization using various ultrasonic techniques. Different surfactants are employed to enhance the stability of the nanofluids and subsequently, the detailed characterization of the nanofluids is carried out. Thermo-physical properties of kerosene-alumina nanofluids are determined for two particle sizes at various volume fractions. Detailed discussion related to synthesis, characterization and the heat transfer performance of kerosene-alumina nanofluid is presented in this section.

**Table 4.1:** Matrix of Experimental study

Nanofluid	Parameters	Particle concentration	Sample Particle size	Temperature range (°C)	Re number
Kerosene-Alumina	k	0.05, 0.1, 0.2,0.3,0.5, 1vol%	13nm, 50 nm	25 - 70	---
	$\mu$				
	h	0.05, 0.1, 0.2, 0.3, 0.5vol%		---	6700-28000
	f				
Kerosene-GNP	k	0.005, 0.02,0.05,0.1,0.2wt%	750, 500, 300 m <sup>2</sup> /g (SSA)	20 -70	----
	$\mu$				
	h	0.005, 0.05, 0.2wt%		----	6700-28000
	f				

#### 4.1.1 Synthesis

##### 4.1.1.1 Nanofluid preparation

A colloidal solution of uniformly dispersed nanoparticle in the base fluid is an important requirement for any nanofluid to be effectively used for potential heat transfer application. This has been analyzed in detail in the present work wherein nanofluids are prepared using a two-step technique. Alumina nanoparticles of two catalogue specified average particle sizes, 50 nm and 13 nm are used in the current investigation. Two different ultrasonication methods, namely bath type and disruptor type with different power and frequency levels, are employed in the preparation of nanofluid. Initially, water and kerosene based nanofluids with alumina nanoparticles are prepared with different ultrasonication time. The stability of nanofluids is visually inspected with time and it is observed that, irrespective of ultrasonication time and method, alumina nanoparticles are found to settle immediately

(within few minutes) in kerosene. However, water based nanofluids are visually stable for few hours after ultrasonication. Based on visual observation, it is found that the disruptor type ultrasonication is more efficient in the preparation of stable water based nanofluids. However, these experimental investigations also revealed that the stability of the nanofluids depends on other factors, and the different methods of ultrasonication are necessary but not sufficient.

#### **4.1.1.2 Nanofluid stabilization**

The stability of any colloidal system depends on the balance of repulsive and attractive forces existing between the particles. The repulsive force must be larger as compared to the attractive force between the particles for obtaining stable nanofluids. The forces between the particles depends upon the ionic concentration near the particle, and it can be varied by either electrostatic or steric stabilization techniques as used by many researchers [57,101,110,111,130,134,136] to stabilize nanofluids.

Initially, the electrostatic stabilization technique is employed for 0.05% volume fraction kerosene-alumina nanofluid. The pH of the nanofluid thus prepared is 5.6 and it is progressively reduced to 3 by adding few drops of Hydrochloric acid (HCl), and increased upto 8 using NaOH. On visual inspection, it is found that a stable solution is not achievable for any value of pH ranging from 3 up to 8. Kerosene being a non-polar fluid is less responsive to charged particles and thus electrostatic stabilization is not found to be effective in kerosene based nanofluids. In the case of steric stabilization the method is effective in non-polar medium like kerosene, where the surfactant effectively separates the nanoparticles due to the higher osmotic pressure build-up between the hydrocarbon chains of surfactant.

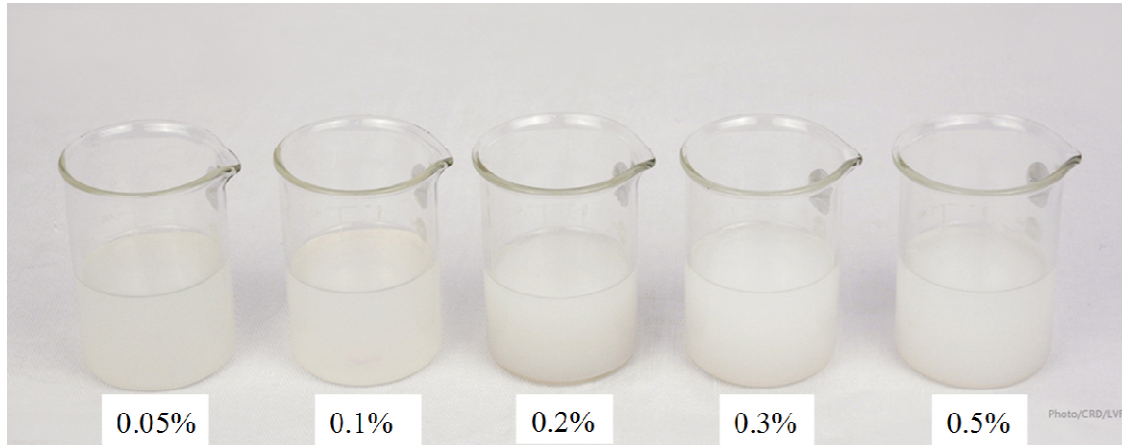


**Figure 4.1:** Kerosene-alumina nanofluid prepared using various particle concentrations

Subsequently, detailed studies for steric stabilization with different types of surfactants were carried out using 20 kHz disrupter type ultrasonicator of 100 W power. Oleic acid and Tween-20 LR are selected for the preparation of 0.05% volume fraction kerosene-alumina nanofluid. Surfactants are introduced through a syringe and the nanofluid is continuously ultrasonicated during the addition process. Sonawane et al. [110,111] studied the stability of ATF-alumina nanofluid with the addition of these two surfactants together. However, in the current study the maximum stability is observed for the case that involved the addition of oleic acid alone as the surfactant. The reason is attributed to the nanofluid combination being used in the current set of experiments and the difference in purity level of surfactant. The surfactant to particle volume ratio is varied from 0.1 to 1.0 in steps. Nanoparticles are found to settle immediately after preparation for the case corresponding to surfactant to particle volume ratio of less than 0.2 and greater than 0.7. An optimum quantity of oleic acid of 0.15 ml in 1 lit of kerosene for 0.05% volume concentration with surfactant to particle volume ratio of 0.3 (mass ratio of 0.07) is found to yield the maximum visual stability. The nanofluid thus prepared is visually inspected for more than 10 days and no

major particle settling is noted. The kerosene-alumina nanofluid prepared at various particle concentrations is presented in Fig. 4.1.

Nanofluids of different particle concentration at constant oleic acid to particle volume ratio of 0.3 are prepared. Different ultrasonication time of 30 minutes for 0.05 % to 3 hrs for 1% is used. The stability of the nanofluids is found to be directly related to the concentration of the nanoparticles. Nanofluids at lower volume fraction of less than 0.2% are very stable (more than 10 days) as compared to those at higher particle concentration. As the ultrasonication time is increased beyond 2 hours, the change in color of the nanofluids from white to gray is observed for nanofluid of 0.2% volume concentration (as shown in Fig. 4.2).

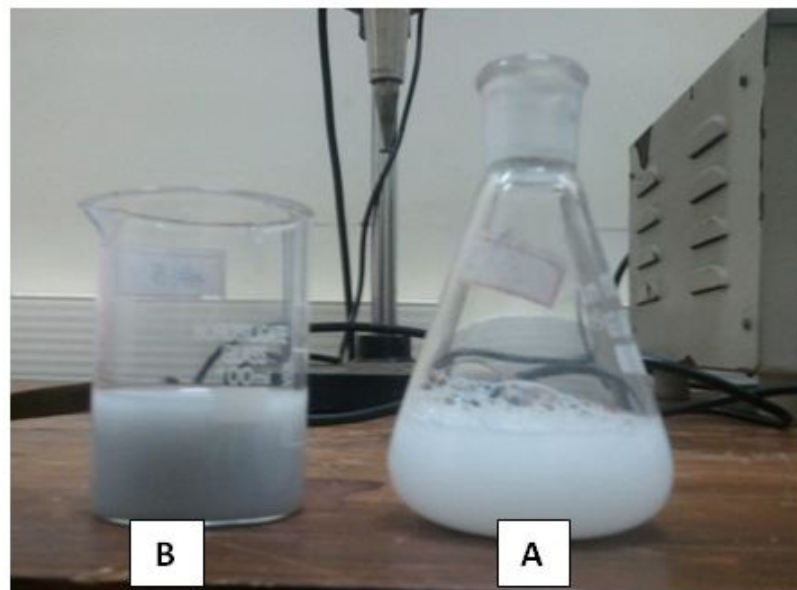


**Figure 4.2:** Kerosene-alumina nanofluid sample - A) after 1 hour of ultrasonication B) after 2 hours of ultrasonication

Similar observation is noted for all the cases that involved ultrasonication for a time period in excess of 2 hours. The nanofluids subjected to ultrasonication for larger duration is found to undergo thermal heating and the temperature of nanofluid was found to increase

above 70°C. Similar observation is reported by Hosseini et al. [55]. They have observed the change in color of water-alumina nanofluid from white to grey during the ultrasonication and the temperature of the nanofluid is also found to increase beyond 70°C due to ultrasonication. Subsequently, in all the further studies carried out the nanofluids are prepared in a special vessel with provision for circulation of water to maintain the nanofluid temperature at  $30\pm 2^\circ\text{C}$ .

#### **4.1.2 Particle size measurement**

Prior to the measurement of surface area of kerosene alumina nanofluid, the particle size of dry alumina particles are determined. Surface area is measured by Quantachrome Nova 1200e surface area analyzer. First, the sample is heated under vacuum for three hours to remove any adsorbed gas or volatiles and this is referred to as degassing. After degassing, BET isotherm is recorded at LN2 temp and the  $P/P_0$  range is 0.05 to 0.3. Surface area is calculated from the slope and intercept of the BET isotherm. The surface area is found to be  $58\text{ m}^2/\text{g}$  and  $98\text{ m}^2/\text{g}$  for 50 nm and 13 nm alumina sample size particles respectively. The measured values are in good agreement with the values specified by the manufacturer as given in section 3.1.2.

Nanofluids with 0.1vol%, 0.2vol% and 0.3vol% of nanoparticles are prepared with 50 nm particle size, and with a surfactant to particle volume ratio of 0.3. All the samples are prepared in 100 ml kerosene with the addition of oleic acid as the surfactant. The particle size distribution in the samples is measured using Zetasizer. All the size measurements are performed at 25°C with a scattering angle of  $173^\circ$ . Each sample is tested three times and the mean value is reported here.

Figure 4.3 represents the particle size distribution with percentage particle count as measured using DLS technique for the nanofluid of 50nm particle size sample. The peak count of the particle size is found to shift towards the higher particle size as the volume concentration of the nanoparticle increases indicating slight agglomeration of particles at higher concentrations. The size of most of the particles in the nanofluids is 78nm for the 0.1vol% as compared to 95 nm for 0.2vol% and 0.3vol% nanofluid. The results clearly indicate to marginal increase in agglomeration of nanoparticles with increase in particle volume concentration in nanofluid.

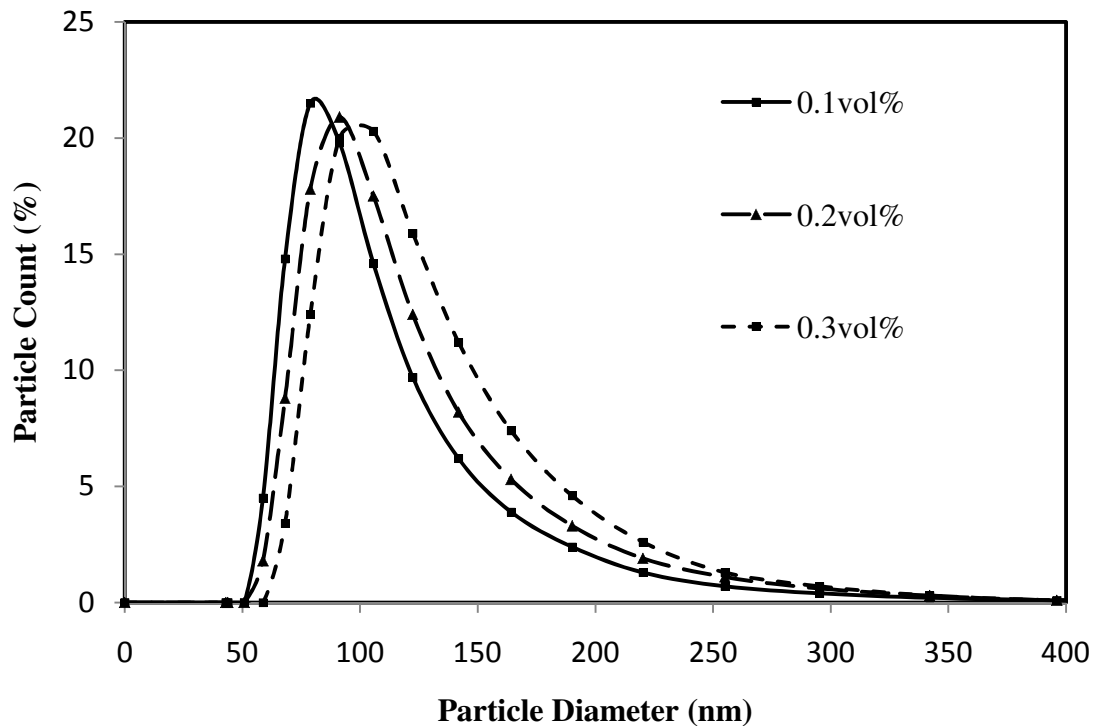


**Figure 4.3.:** Particle size distribution of the kerosene-alumina nanofluid at different particle volume concentration for 50 nm nanofluid sample

Particle size distribution for the two different sizes of nanopowder at 0.2vol% particle concentration is shown in Fig. 4.4. The average particle diameter in 13 nm sample particle nanofluid is found to be 59 nm as compared to 110 nm for 50 nm sample particle nanofluid.

During the measurements, it is noted that the minimum particle size measured for 13 nm and 50 nm sample particles is 21 nm and 44 nm respectively. Table 4.2 presents the mean of minimum and average size measured by DLS with standard deviation ( $\sigma$ ) from 4 sets of readings.

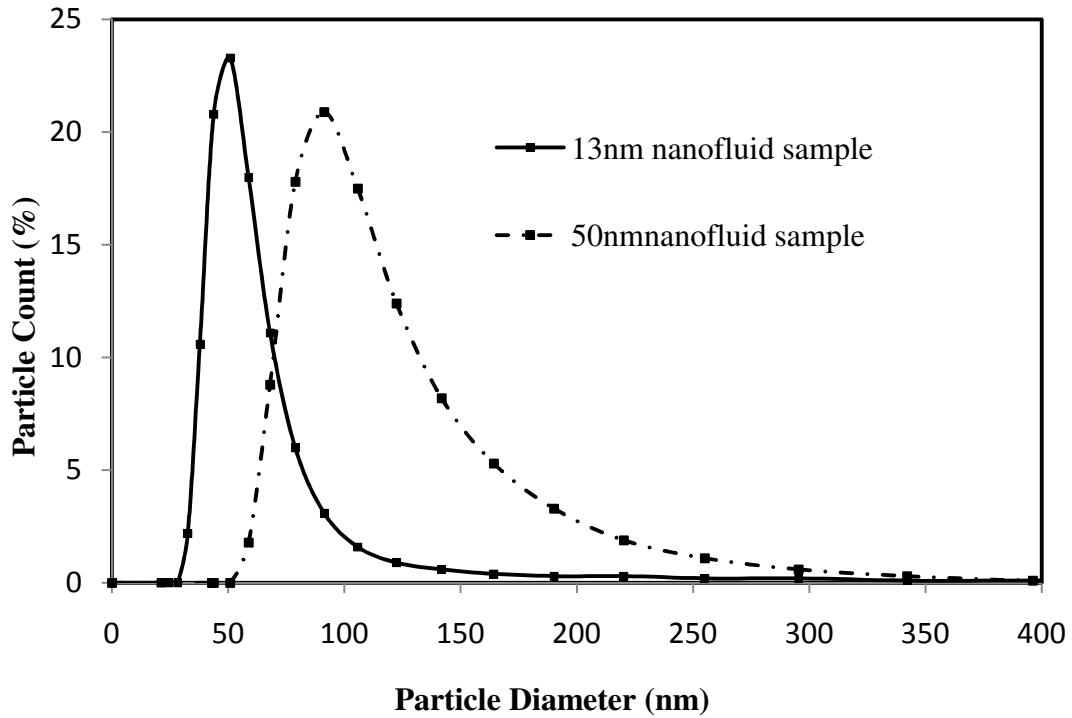


**Figure 4.4:** Particle size distribution for two sample sizes of alumina nanoparticle at 0.2vol%

**Table 4.2:** Minimum and average particle size measured for kerosene-alumina nanofluid

Sample particle size	Minimum size	Average size (mean $\pm$ $\sigma$ )
13 nm	21.5	59 $\pm$ 2.5nm
50 nm	44	110 $\pm$ 4.25 nm

It is to be noted that though the measured values of particle size are marginally higher than the nominal particle size reported by the manufacturer, the increase is lower than the value reported by Ju et al. [63], wherein the authors used the colloids of alumina with nominal particle diameter of <20 nm and correlated the measured particle size against the corresponding ultrasonication time. The minimum average particle diameter reported by them is around 120 nm. The lower value of particle diameter obtained in the present investigation indicates that the alumina nanoparticles are well dispersed in kerosene.

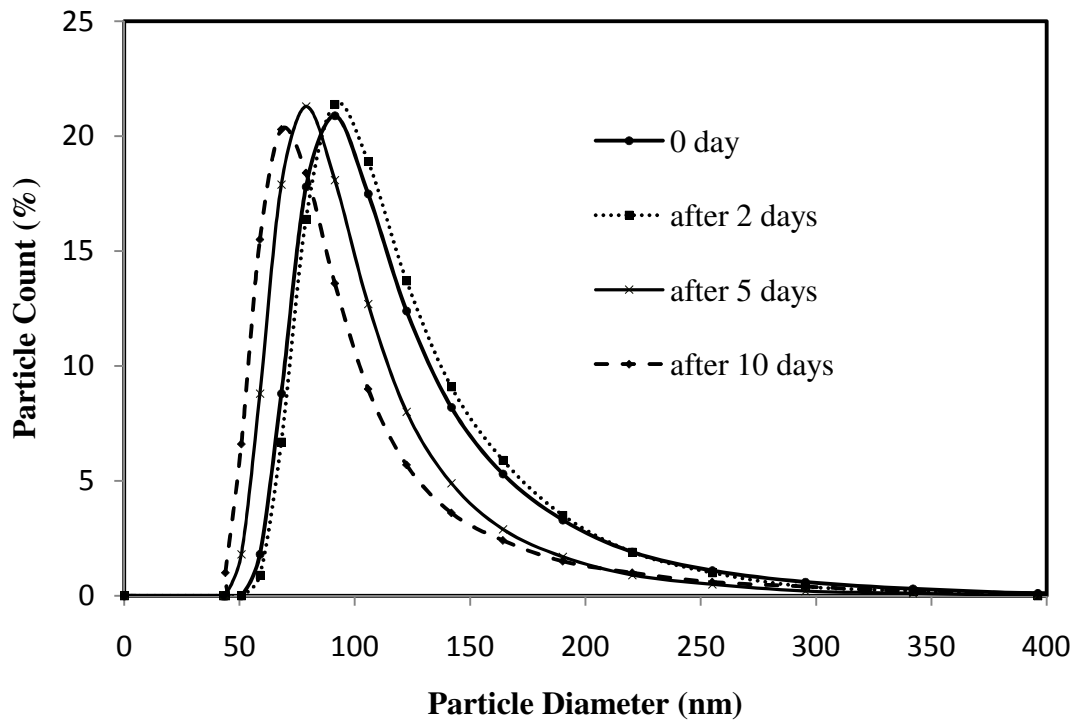


**Figure 4.5:** Particle size distribution of 50 nm nanofluid sample with time for 0.2vol% particle concentration

The stability of 0.2vol%, 50 nm kerosene-alumina nanofluid sample, prepared using oleic acid as a surfactant is determined with time (described in days) using particle size measurement. Nanofluid sampled from the top layers in the bottle after 2, 5 and 10 days are analyzed, and their particle size is measured. Figure 4.5 shows the particle size distribution at

different intervals for 50nm nanofluid sample, 0.2vol% nanofluid. It is observed from the figure that after 2 days of nanofluid preparation, the peak value of average particle diameter marginally increased from 95 nm to 102 nm. The slight increase in the particle diameter could be due to the clustering of nanoparticles with time. Subsequently, with time, the bigger particle would start settling at the bottom and the average diameter of nanoparticles in fluid in the top layers start decreasing. It may however be noted that the nanofluid is significantly stable as the average peak of the particle size is not varying much with time.

### **4.1.3 Thermal conductivity**

The major factors that influence thermal conductivity of nanofluid are the particle loading, particle size and the temperature. Kerosene-alumina nanofluid at 0.01vol%, 0.05vol%, 0.1vol%, 0.2vol%, 0.3vol%, 0.5vol% and 1.0vol% particle loadings are prepared for the catalogue specified 13nm and 50nm sample particle size using oleic acid to particle volume ratio of 0.3, and subjected to ultrasonication to de-agglomerate the nanoparticles. As mentioned earlier, the current study uses THW technique for the measurement of thermal conductivity of the nanofluids. The samples prepared for measurements are maintained at constant temperature using a constant temperature bath. For each volume fraction, particle size and temperature, the measurements are repeated six times, and the values are found to lie within  $\pm 0.003$  W/mK. Mean value of these measurements is presented in the results and is further utilized in the subsequent analysis carried out.

#### **4.1.3.1 Effect of particle loading**

Thermal conductivity of kerosene-alumina nanofluid is determined at various particle loading conditions. Measurements are repeated six times for each concentration. Figure 4.6

presents the value of thermal conductivity obtained for each measurement for 13 nm sample kerosene-alumina nanofluid.

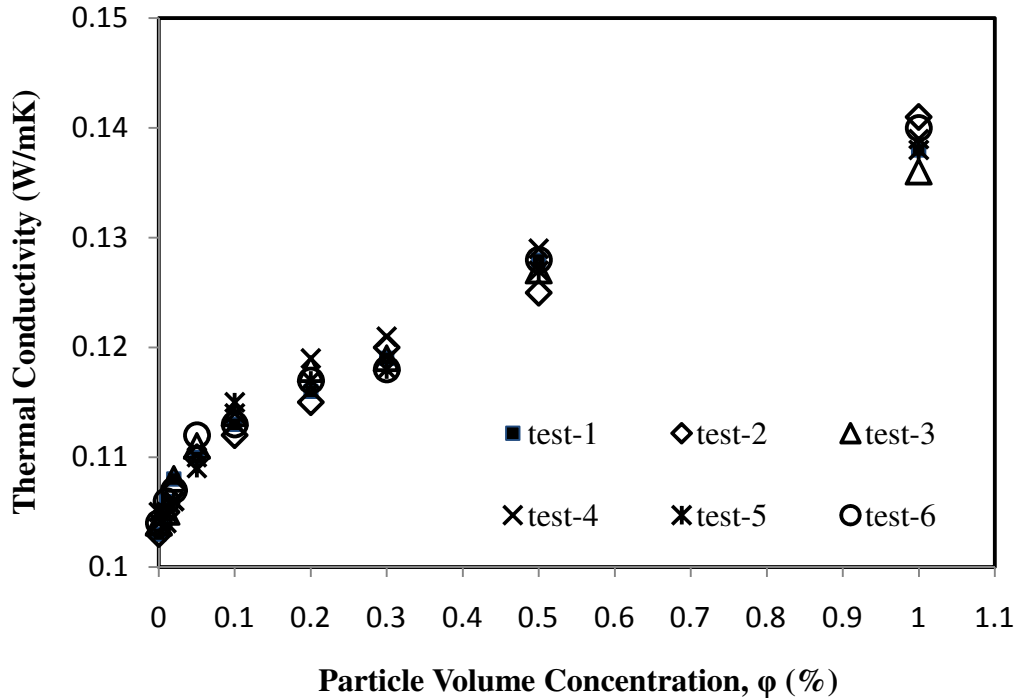


**Figure 4.6:** Thermal conductivity of 13nm kerosene-alumina nanofluid sample at various particle volume concentrations at 25 °C

It can be noted that the measured thermal conductivity of nanofluid for a particular particle loading condition is nearly the same for all the measurements. Mean and standard deviation of thermal conductivity values are estimated from the test data and the mean thermal conductivity thus arrived at is used in the heat transfer analysis carried out as part of the current study. The maximum standard deviation associated with the data presented in Fig. 4.6 is 0.00175 W/mK. The maximum percentage standard deviation obtained for this data set is 1.26%. Similar data analysis is carried out for each measured parameter and their mean value is utilized for subsequent heat transfer analysis.

The effect of particle loading on the thermal conductivity ratio of 13nm and 50 nm nanofluid samples is presented in Fig. 4.7. Figure 4.8 shows the relative change in thermal conductivity ratio with volume concentration ( $\Delta(k_{nf}/k_{bf}) / \Delta\phi$ ).

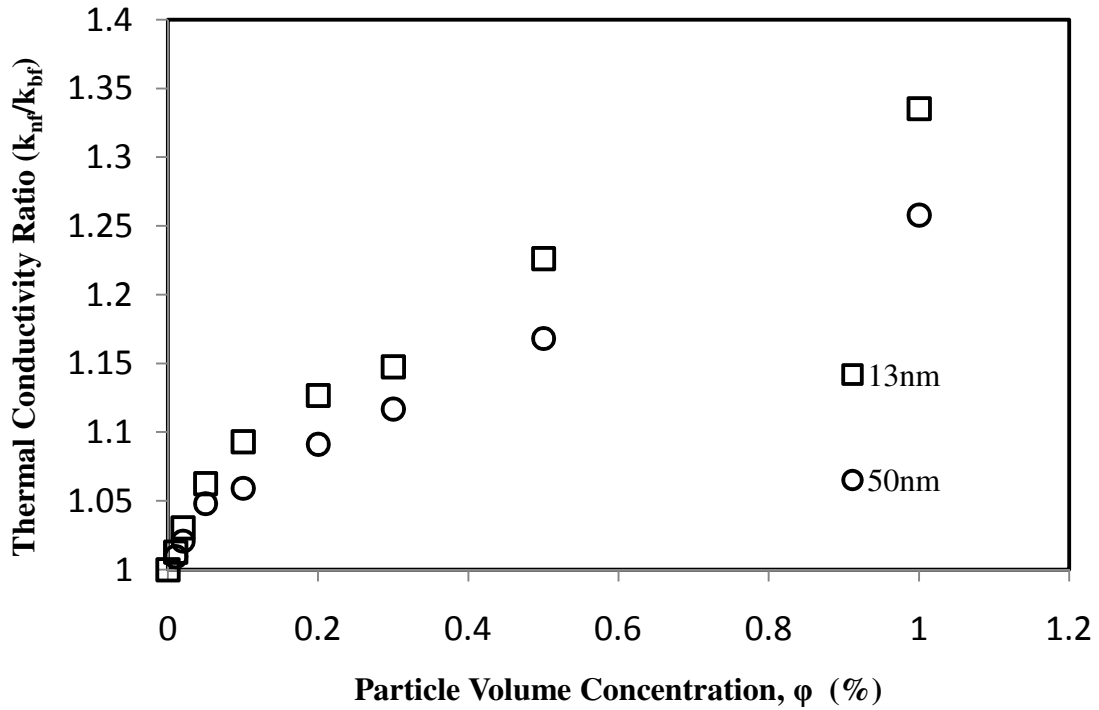


**Figure 4.7:** Effect of particle size on thermal conductivity of kerosene-alumina nanofluid at various particle volume concentrations at 25 °C

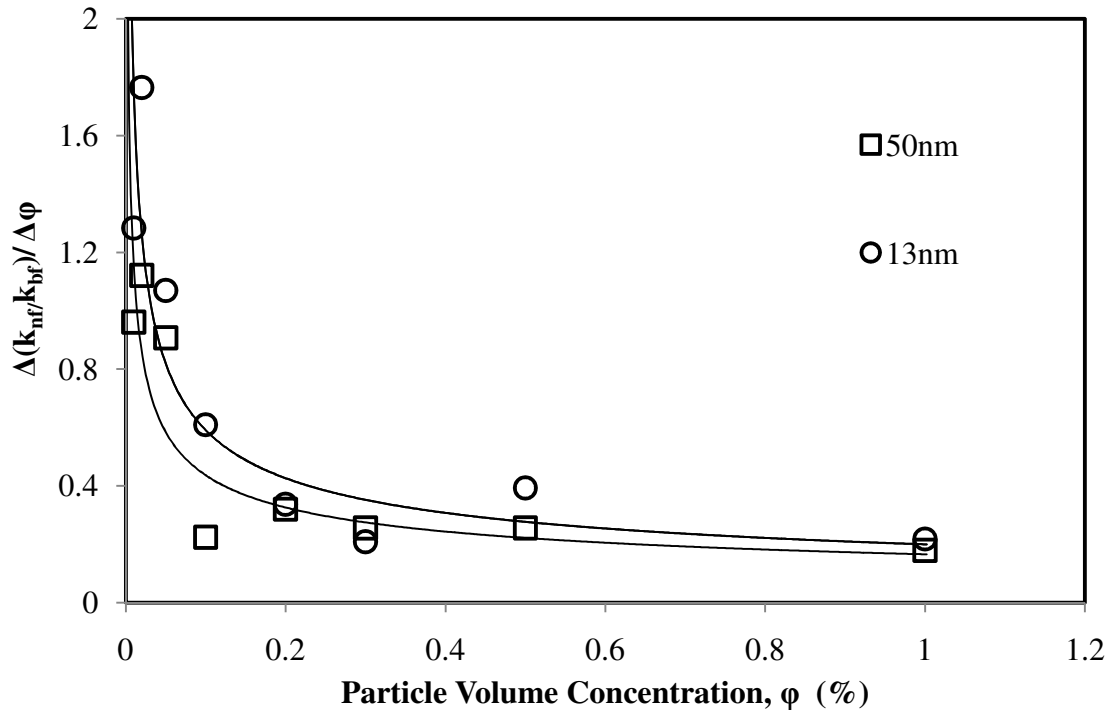


**Figure 4.8:** Relative increase in thermal conductivity ratio with particle concentration

It can be clearly seen from the above figures that the rate of increase in thermal conductivity of nanofluids is significant at lower particle loading of up to 0.1% for both the samples and the enhancement is observed to be sluggish beyond this point. Similar behavior at very low particle concentration is also reported by Lee et al. [76]. They have reported a linear increase in the thermal conductivity of water-alumina nanofluids up to 0.1vol% particle concentration. The linear behavior of nanofluid thermal conductivity at lower particle concentration could be attributed to the various factors like improved homogeneity and stability of the nanofluid and partially due to the increased number of agglomeration sites that are beneficial till an optimum concentration is attained. The sluggish behavior beyond 0.1% particle concentration could be attributed to the higher number of agglomeration sites beyond the optimum which results in a less homogenized nanofluid at higher concentration.

#### 4.1.3.2 Effect of particle size

The effect of particle size on the thermal conductivity is determined for two different catalogue specified particle sizes of 13 nm and 50 nm is shown in Fig.4.7. The enhancement in thermal conductivity of nanofluid is found to be higher for smaller sized particle as compared to bigger size at identical volume concentration. This observation is in line with those reported by many other researchers [2,70,111]. The higher enhancement is observed for smaller particle size nanofluid due to higher specific surface area per unit mass in the case of smaller size. The enhancement ratio in thermal conductivity for 50 nm nanofluid sample is only 1.05 as compared to 1.06 for the case of 13 nm nanofluid sample at 0.05vol% particle concentration. At 1.0vol% particle concentration, the enhancement ratio is found to be 1.33 and 1.26 for 50 nm and 13 nm nanofluid samples respectively.

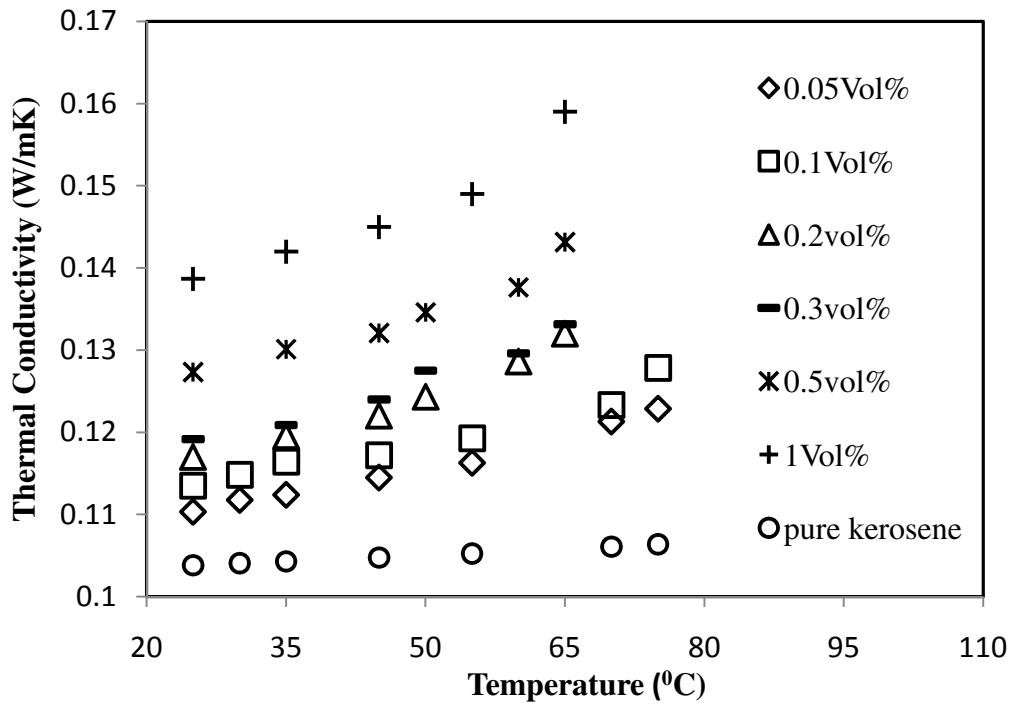
#### 4.1.3.3 Effect of temperature

The temperature dependency on the thermal conductivity of nanofluid is investigated for the two sample particle sizes of 13 nm and 50 nm at 0.2% particle volume concentration. Thermal conductivity of pure kerosene and nanofluids are measured in the temperature range of 25°C to 65°C. The measured value of thermal conductivity of pure kerosene increases linearly with the temperature as in Eq 4.1.

$$k = 2 \times 10^{-8} * T^2 + 0.00003 * T + 0.103 \quad (4.1)$$

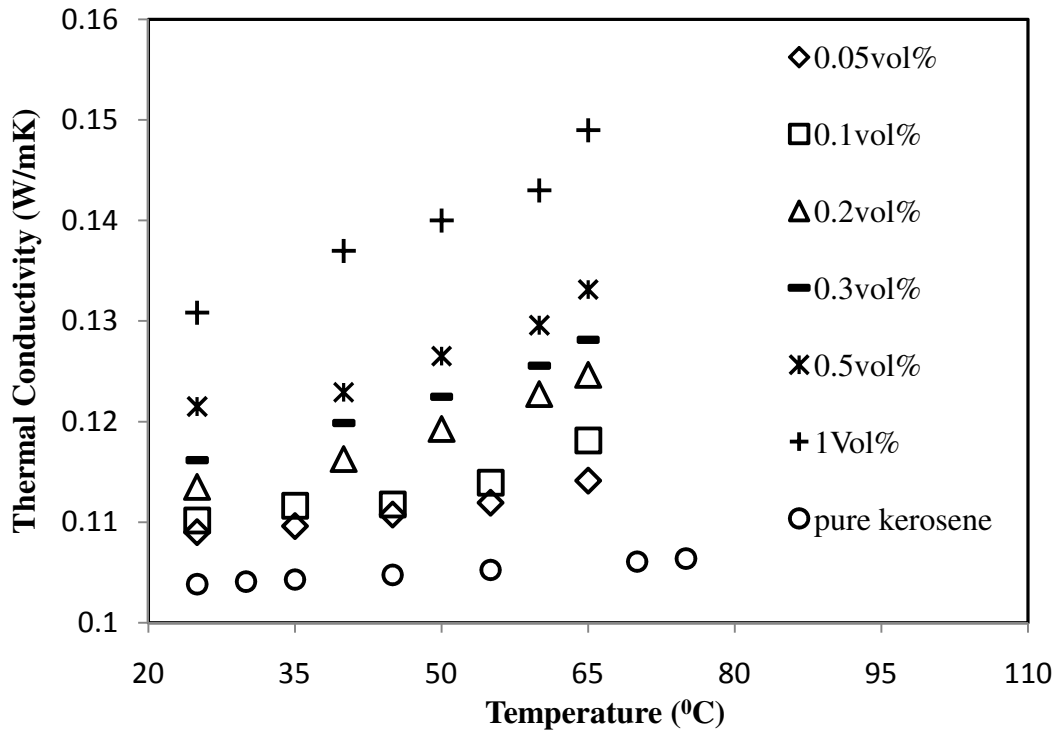
with  $R^2 = 0.986$

here, 'k' is the thermal conductivity of pure kerosene in W/mK and 'T' is the temperature in °C.



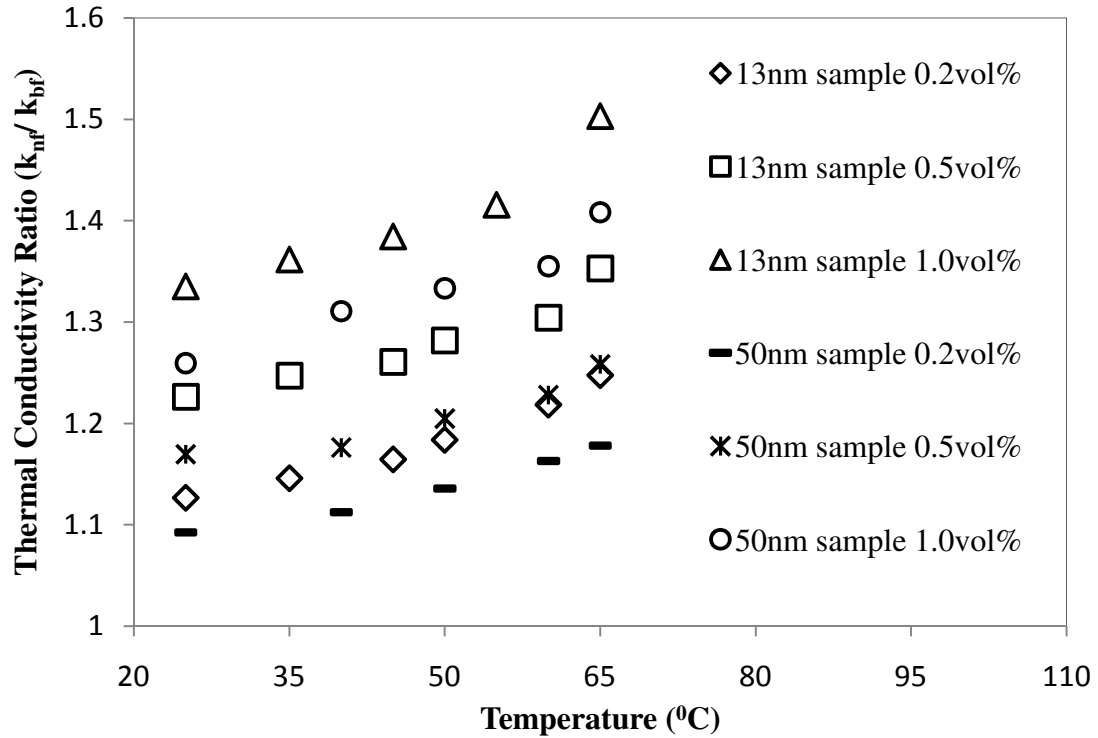
**Figure 4.9:** Thermal conductivity of 13 nm kerosene- alumina nanofluid sample at various temperatures

Figures 4.9 and 4.10 represents the thermal conductivity of various particle concentrations of kerosene-alumina nanofluids for 13nm and 50 nm sample particle size respectively. It is evident from the figures that thermal conductivity of nanofluid increases with temperature for both the particle sizes and it can be attributed to the higher Brownian motion induced particle interaction at elevated temperature. It can also be seen that the increase in the thermal conductivity of nanofluid with temperature is non linear and higher increase in thermal conductivity is noticed at elevated temperature.



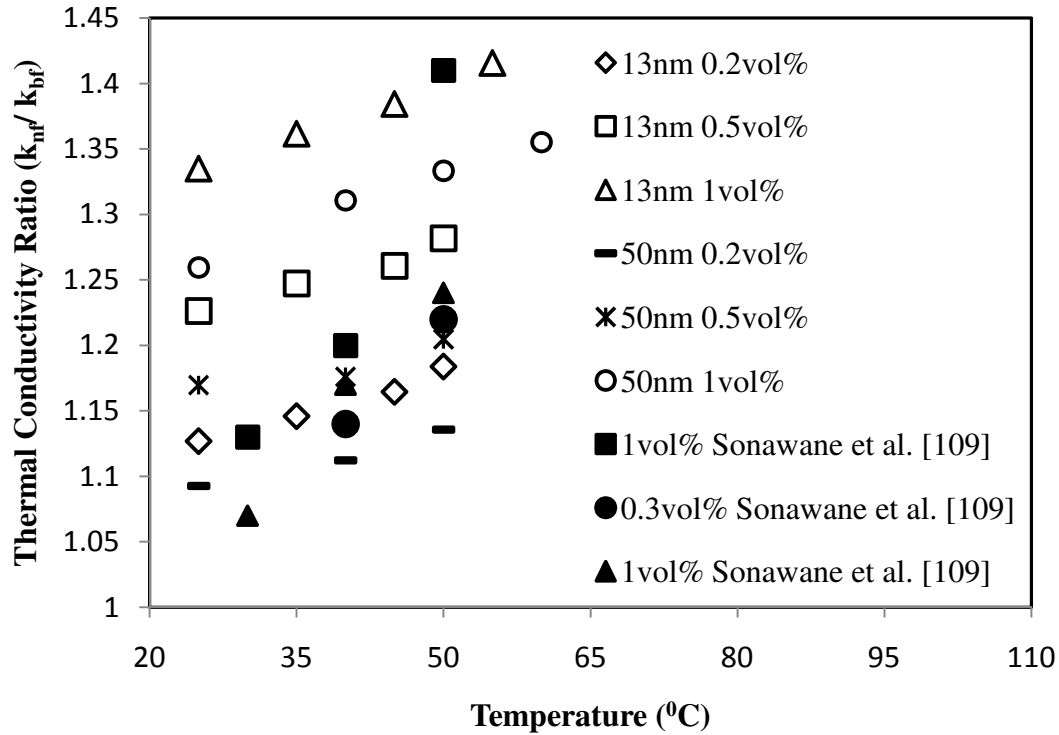
**Figure 4.10:** Thermal conductivity of 50 nm kerosene- alumina nanofluid sample at various temperatures

Figure 4.11 presents the enhancement ratio in thermal conductivity of the nanofluid to pure kerosene across a temperature range of 25°C to 65°C for both the particle sizes at 0.2vol%, 0.5vol% and 1vol% particle concentration. The thermal conductivity ratio increases from 1.12 to 1.25 for 13 nm sample size, and 1.09 to 1.18 for 50 nm sample size in the 25 °C to 65 °C temperature range for 0.2 vol% kerosene-alumina nanofluid. For 1 vol% concentration, thermal conductivity ratio increases from 1.26 to 1.41 for 50 nm sample size and 1.33 to 1.50 for 13nm sample size kerosene-alumina nanofluid respectively. The strong dependency of temperature on thermal conductivity as observed in the present work is in good agreement with those observed in other reported works [77,86,111,130] and is attributed to the enhanced Brownian motion of nanoparticles in base fluid at higher temperature.



**Figure 4.11:** Effect of temperature on thermal conductivity ratio of 13 nm and 50 nm kerosene-alumina nanofluid samples

In the current work, the increase in thermal conductivity with temperature is around 1.5 to 2 times for both the particle size. The studies on ATF-alumina nanofluids carried out by Sonawane et al. [111] also indicate considerable effect of temperature on the nanofluid thermal conductivity, and reported a three-fold increase in thermal conductivity for ATF based nanofluid in the temperature range of 30°C to 50°C. The current experimental results also indicate higher percentage enhancement in thermal conductivity for lower particle size nanofluids at higher temperatures as compared to bigger particle size nanofluid. This is further attributed to the relatively high degree of Brownian motion at lower particle size as compared to the larger particle size nanofluid.



**Figure 4.12:** Comparison of measured thermal conductivity of kerosene-alumina nanofluid with literature data

It may be noted that the nanoparticle-base fluid combination used in the present investigation is not investigated till date. The only study that investigated a similar nanofluid-base fluid combination is by Sonawane et al. [111] where the authors have used 30 nm sample alumina particles in ATF base fluid. As aforementioned, they reported thermal conductivity augmentation in the range of 5% to 41% for various conditions. Figure 4.12 shows comparison of the present measurements with the experimental results of Sonawane et al. [111] for ATF-alumina nanofluid. Though at few data points the thermal conductivity measured by Sonawane et al. [111] is in good agreement with the present results, the observed trends deviated at various concentration and temperature conditions. This may be attributed to the improved stability of the nanofluids, difference in the base fluid, nanoparticle

size, method of preparation of nanofluid and measurement techniques adopted in the respective investigations.

#### **4.1.4 Dynamic viscosity**

Dynamic viscosity of nanofluids is measured for two sizes of alumina particles in kerosene at various volume fractions and temperature ranges. Prior to the measurement of the viscosity of nanofluids, viscosity of pure kerosene is measured at different temperatures. As expected, the decrease in viscosity is noticed for pure kerosene with an increase in temperature and is expressed as

$$\mu = 0.000146*T^2 - 0.0296*T + 2.06 \quad (4.2)$$

with  $R^2 = 0.979$

where,  $\mu$  is the dynamic viscosity in cP and 'T' is the fluid temperature in °C.

##### **4.1.4.1 Effect of particle loading**

Nanofluids of particle concentrations of 0.05vol%, 0.1vol%, 0.2vol%, 0.3vol%, 0.5vol% and 1.0vol% are prepared and their dynamic viscosity at 25°C temperature is measured. Figure 4.13 represents the ratio of dynamic viscosity of nanofluids to the pure kerosene at various particle concentrations for 13 nm and 50 nm catalogue particle sizes. An enhancement in dynamic viscosity is observed for the 13 nm sample particle nanofluid from 1.015 to 1.223 over a particle loading range of 0.05vol% to 1.0vol%. The non-linear dependency of particle loading on dynamic viscosity indicates the presence of particle-particle interaction as observed by Lee et al. [76] with water-alumina nanofluid at low particle volume concentrations.

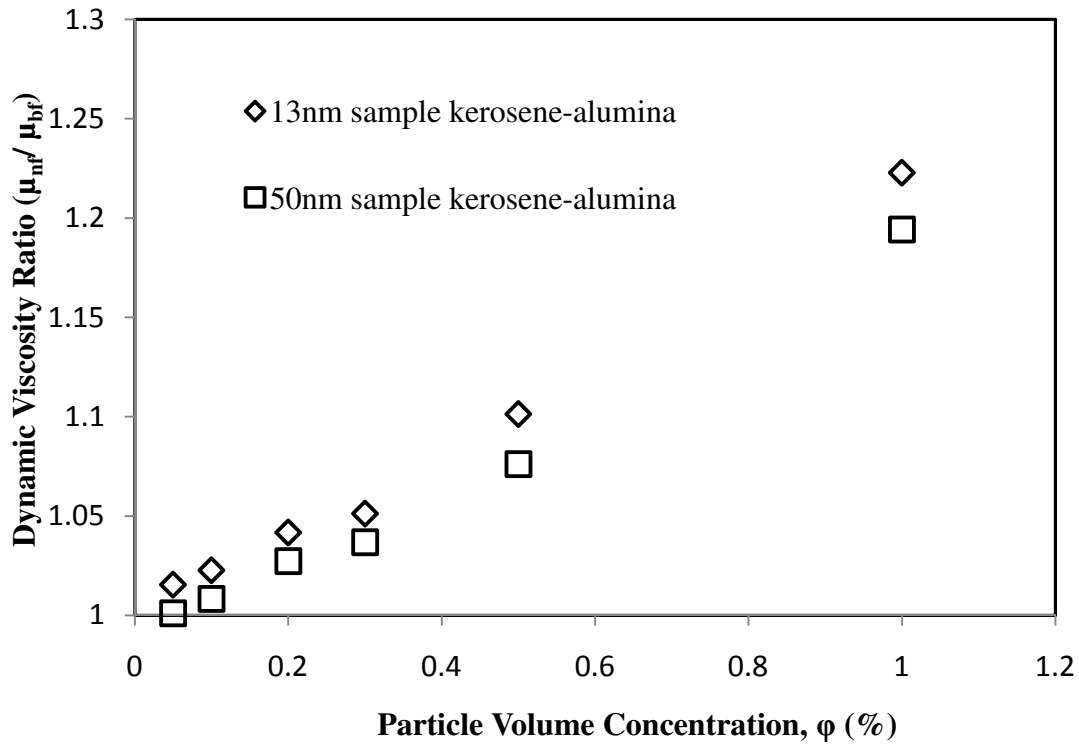
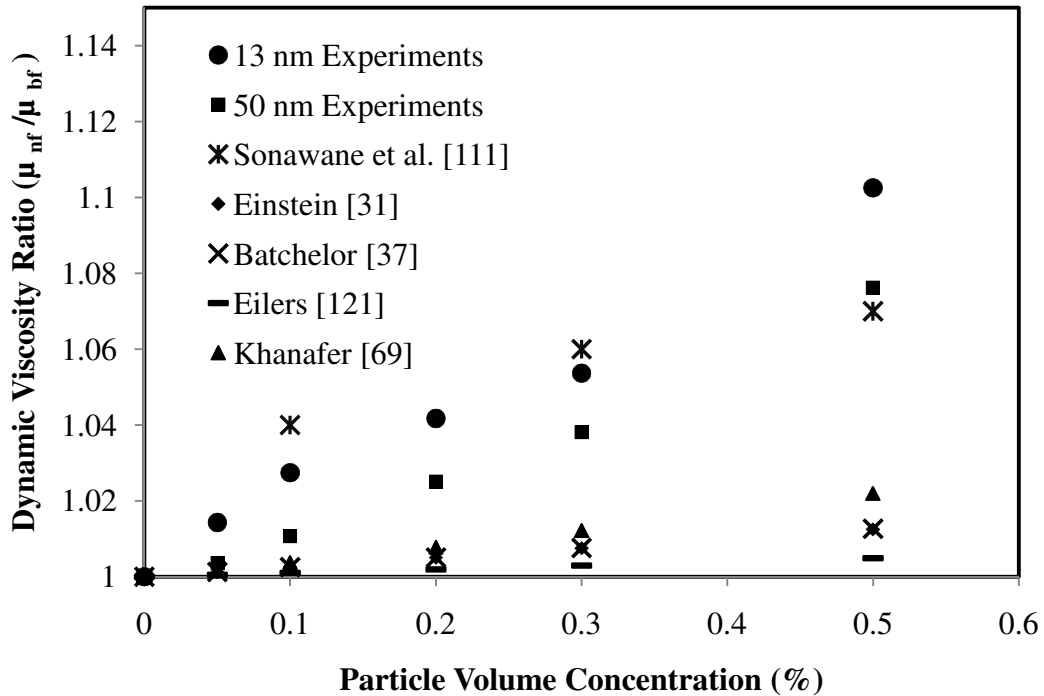


**Figure 4.13:** Effect of particle size on dynamic viscosity of kerosene-alumina nanofluid samples at various particle volume concentrations at 25 °C

#### 4.1.4.2 Effect of particle size

The effect of particle size on viscosity is also ascertained by measuring the viscosity of nanofluids for two different sizes of nanoparticles. It is observed from Fig. 4.13 that the increase in dynamic viscosity for smaller particle size nanofluid is larger as compared to the case with bigger sized particles. This is due to the increased surface area available in the case of the smaller particle as compared to the case with bigger particle size at same volume concentration. The increased surface area leads to higher interface resistance, with the fluid layer causing increased viscosity for smaller nanoparticle size fluid. The ratio of dynamic viscosity of nanofluid to the base fluid at 0.05vol% at 50 nm catalogue particle sizes is found to be 1.007% as compared to 1.015% for 13 nm catalogue particle size. Similarly at higher

particle concentration of 1vol%, the percentage ratio of dynamic viscosity of nanofluid to base fluid is 1.194 and 1.223 for 50 nm and 13 nm catalogue particle sizes respectively.



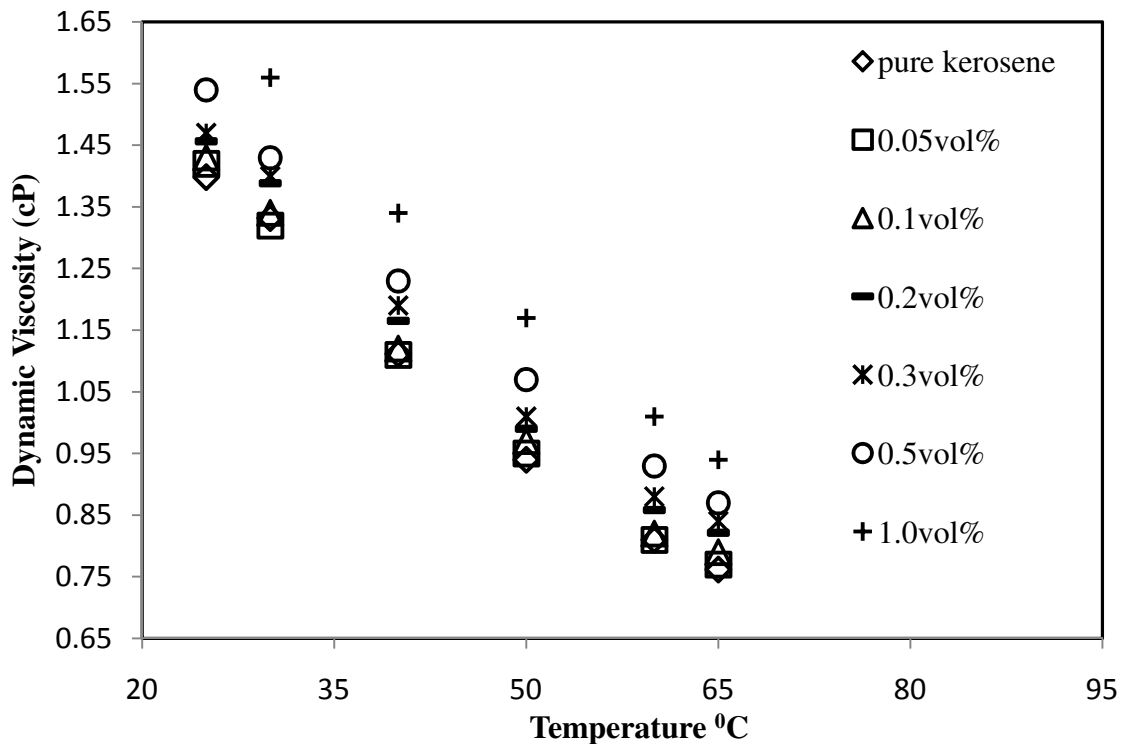
**Figure 4.14:** Comparison of measured dynamic viscosity of kerosene-alumina nanofluid with literature data and various theoretical models

Figure 4.14 presents the comparison of current results with the experimental data obtained by Sonawane et al. [111] and those obtained through other theoretical models. It is to be noted that the theoretical models of Einstein [31] and Batchelor [37] include the hydrodynamic contribution while the correlation factor applied by Khanafer [69] and Eilers [121] is derived based on the experimental study using water-alumina nanofluid. Though none of the theoretical models predict the enhancement of dynamic viscosity as observed in the current study, the measurements by Sonawane et al. [111] for ATF-alumina nanofluid indicate good agreement with the current results. The under-prediction of dynamic viscosity of nanofluid by theoretical models may be attributed to: (i) theoretical models [31,37] do not

account for the particle size and particle-particle interactions (ii) the correlation factors are derived for water-alumina [69,121] nanofluid and (iii) the difference in the particle size and base fluid combination used by Sonawane et al [111] as compared to the current nanofluid under investigation. It is to be however noted that the nanoparticle-base fluid combination used in the present investigation is not investigated till date.

#### 4.1.4.3 Effect of temperature

The effect of temperature on the viscosity of nanofluids is investigated by measuring the dynamic viscosity of nanofluid at various temperatures ranging from 25°C to 65°C. Figures 4.15 and 4.16 depict the effect of temperature on dynamic viscosity at various concentrations of kerosene-alumina nanofluid for 13 and 50 nm sample size nanofluids respectively.



**Figure 4.15:** Dynamic Viscosity of 13 nm kerosene- alumina nanofluid sample at various fluid temperatures

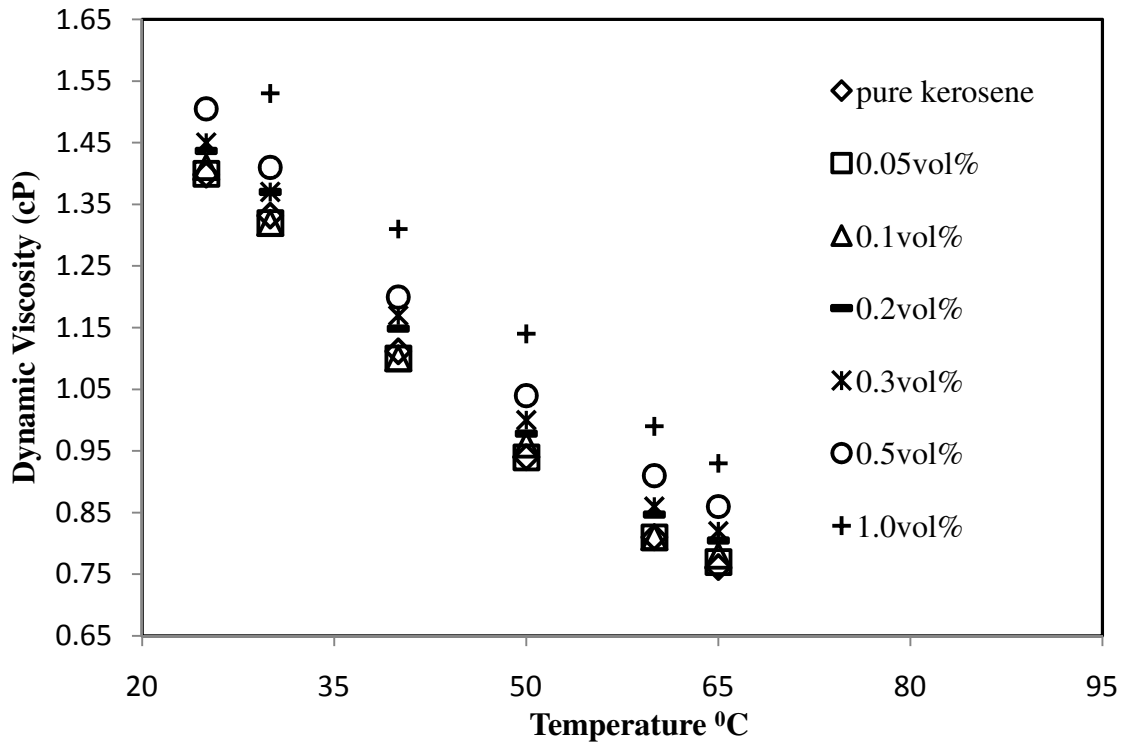


**Figure 4.16:** Dynamic Viscosity of 50 nm kerosene- alumina nanofluid at various temperatures

The dynamic viscosity of nanofluid decreases with temperature as expected and as observed by Nguyen et al. [91]. It can be noted that the similar to the base fluid, nanofluids also show significant reduction in viscosity at elevated temperature. Nguyen et al. [91] have reported similar behavior for water-alumina nanofluid. However they reported hysteresis in their measurements at high temperature. Such phenomenon is not observed in current nanofluid and temperature range.

Ratio of dynamic viscosity of nanofluid to pure kerosene for two particle sizes at 0.2vol% particle concentration is presented in Fig.4.17. The viscosity ratio increases from 1.04 at 25°C to 1.08 at 65°C for 13 nm and 1.03 at 25°C to 1.06 at 65°C for 50 nm particle size nanofluid sample. In the case of pure base fluid, as temperature increases, viscous shear stress decreases due to thermal expansion of the fluid, thereby leading to lower viscosity at

high temperature. In nanofluids, thermal expansion of base fluid at high temperature results in higher Brownian motion of nanoparticles and this could result in the increase of internal resistance and leads to higher percentage enhancement in viscosity at high temperatures.

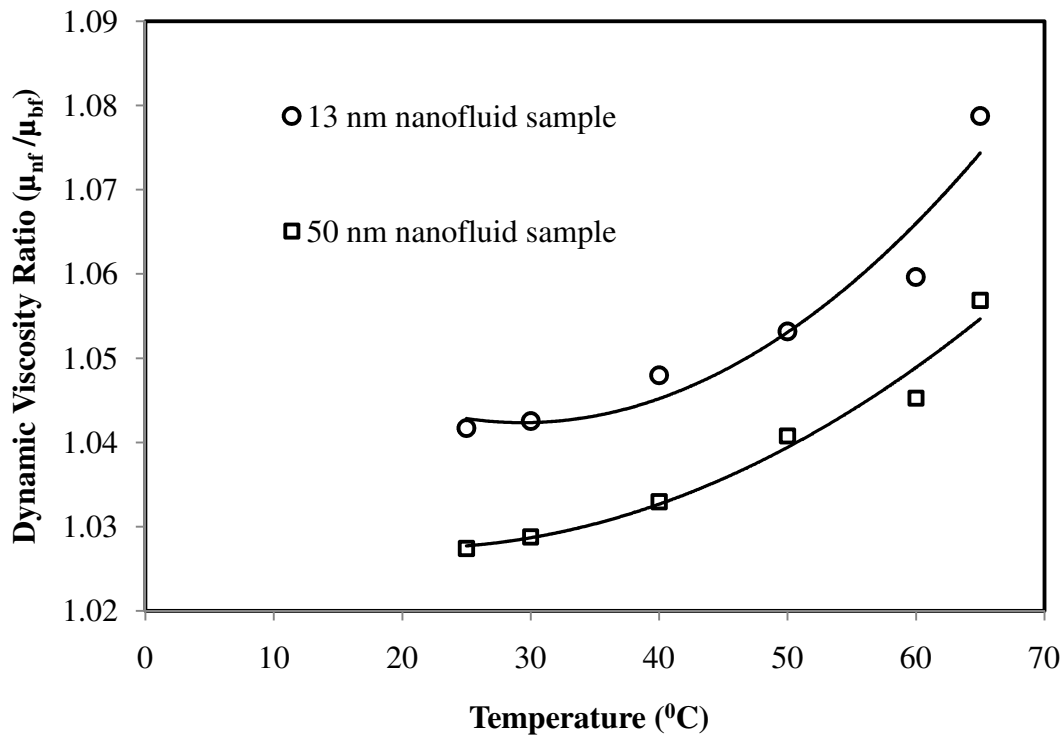


**Figure 4.17:** Effect of temperature on viscosity ratio for 13 and 50 nm nanofluid samples at  $\phi = 0.2\text{vol}\%$

#### 4.1.5 Measurement for stability

A simple but effective approach to assess the stability of the nanofluid is adopted in the present study. Nanofluids are binary mixtures of nanoparticles in base fluid, and due to the various stabilization techniques and ultrasonication energy, the colloids remain stable for certain period of time. However with the passage of time the nanoparticles get agglomerated; this not only results in particle settlement but also affects the thermo-physical properties of

nanofluids. Measurement of thermal conductivity of nanofluids with time is an effective indication for assessing the degree of settlement.

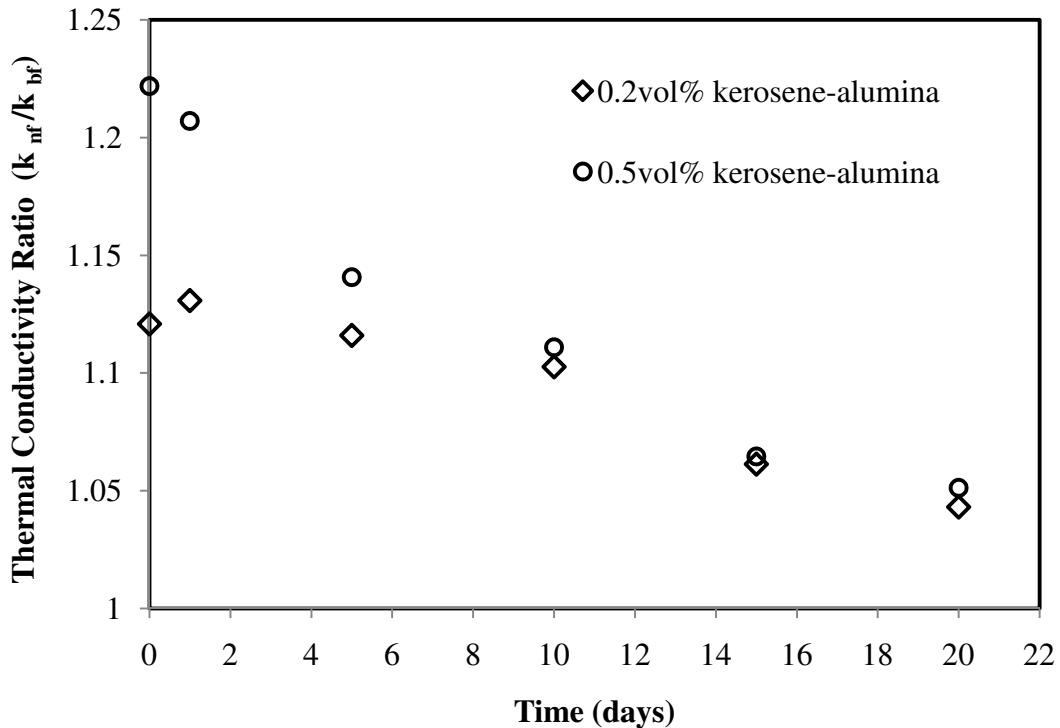


**Figure 4.18:** Variation in thermal conductivity of kerosene-alumina nanofluid with time at  $\phi = 0.2\text{vol}\%, 0.5\text{vol}\%$

Thermal conductivity of 0.2vol% and 0.5vol% particle concentration nanofluids prepared with 13nm catalogue particle size is measured with time. Thermal conductivity of the nanofluids is measured after 1, 5, 10, 15, 20 days of preparation. Figure 4.18 represents the variation in the ratio of thermal conductivity of nanofluid to pure kerosene with time for 0.2vol% and 0.5vol% particle concentration nanofluids. Thermal conductivity measured after one day of preparation (after 22-24 hrs) indicates marginal increase in the thermal conductivity for the 0.2vol% particle concentration nanofluid and it is due to the possible formation of clustered structures of nanoparticles in the fluid. In general thermal conductivity of both the samples decreases with time, thereby indicating an unstable nanofluid.

As expected, the nanofluid prepared with lower particle concentration exhibits improved stability with time. Visual inspection also revealed significant settling of nanoparticles at the bottom of the sample tube with time for higher concentration nanofluid as compared to that at lower concentration. Nanofluid of 0.2vol% particle concentration is stable for almost 10 days and the value of thermal conductivity is only slightly decreased during this time period. Marginal amount of settling is noticed after the first day in the case of the nanofluid with 0.5vol% particle concentration and the settling of particles is found to increase with time.

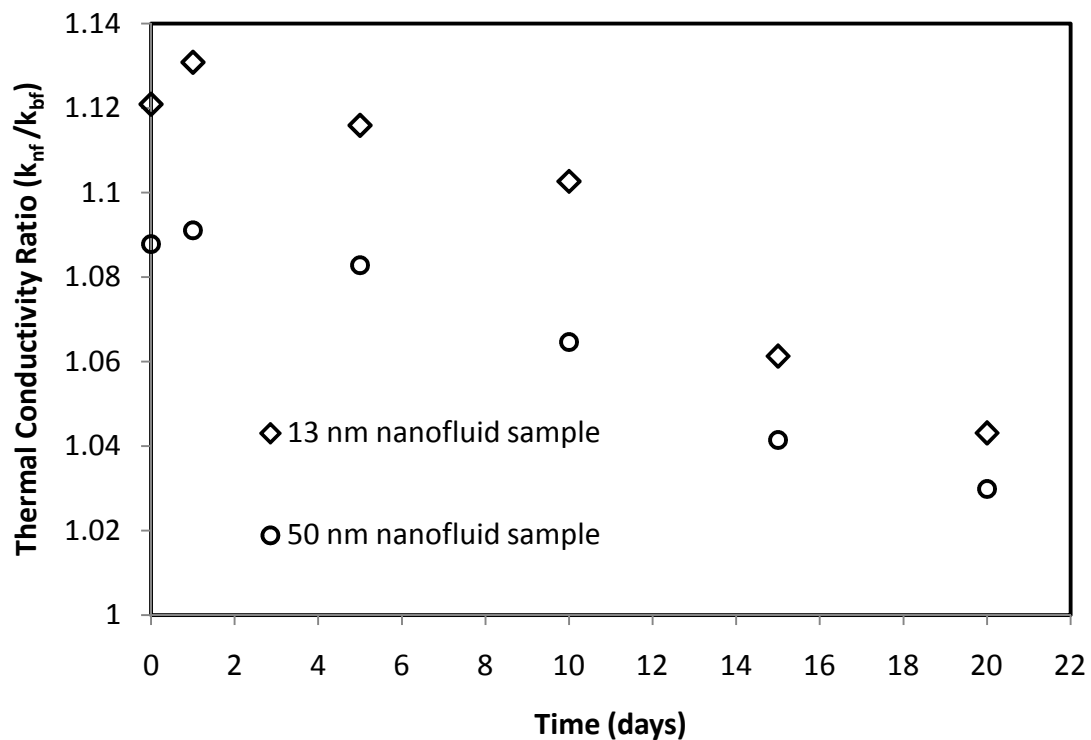


**Figure 4.19:** Thermal conductivity of 13 nm and 50 nm kerosene-alumina nanofluid samples with time at  $\phi = 0.2\text{vol}\%$

Measurements are repeated for nanofluid prepared using 50 nm catalogue particle size. Figure 4.19 shows change in thermal conductivity as a ratio of the two samples with time. Slight increase in thermal conductivity of both nanofluids is observed after 1 day of

preparation and this could be attributed to the possible particle agglomeration and clustering in the nanofluid. Figure 4.5 also confirms this argument as the number average particle diameter increased from 95 nm to 102 nm after two days of preparation, and similar behavior is noticed in thermal conductivity as well.

The percentage settling is inferred by comparing the value of thermal conductivity that is determined with time to the thermal conductivity obtained at different particle volume concentration as in Fig.4.6. The piecewise linear curve fitting is carried out on thermal conductivity data at different volume concentrations. The percentage settling is defined as:

$$\% \text{ settling} = (\varphi_i - \varphi_c) / \varphi_i \times 100 \quad (4.3)$$

where,  $\varphi_i$  is the initial volume concentration and  $\varphi_c$  is the current volume concentration.

$\varphi_c$  is determined by comparing the current thermal conductivity with the thermal conductivity values plotted in Fig. 4.7 and identifying the equivalent volume fraction. The linear interpolation is carried out to determine the volume fraction that lies in between the measured thermal conductivity data points.

Figure 4.20 represents the percentage settling of nanoparticle based on Eq. (4.3) with time for the 0.2vol% and 0.5vol% particle concentration case. The percentage settling is very fast for higher concentration nanofluid as compared to the lower concentration case. After 5 days of nanofluid preparation, more than 38% nanoparticles are found to settle in the case of 0.5vol% particle concentration whereas for 0.2vol% particle concentration, the percentage settlement is only 8%.

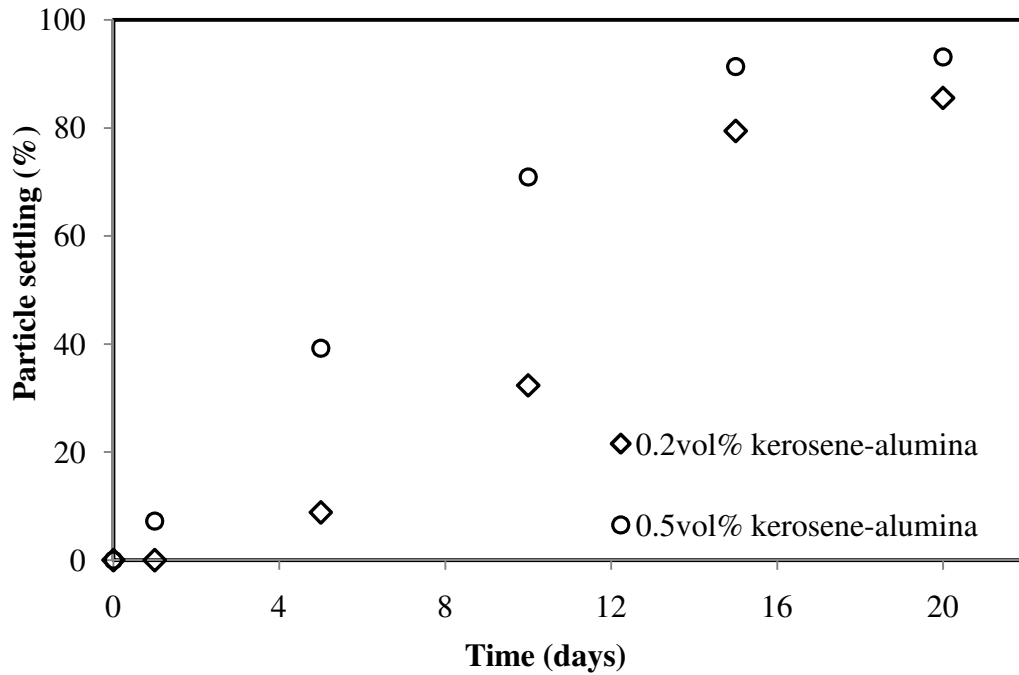


**Figure 4.20:** Estimated percentage particle settling of kerosene-alumina nanofluid with time

Although, the current methodology used for assessing the nanoparticle settlement is not an explicit method, it gives an indication of the nature of settlement of nanoparticles with time, and ascertains the relatively low stability of nanofluids with higher concentration of nanoparticles as compared to fluids at lower particle concentrations.

#### 4.1.6 Convective heat transfer

The convective heat transfer performance of any fluid depends on various physical and thermo-physical properties. Though the enhanced thermal conductivity of nanofluid will result in reduced resistance to thermal diffusion in the laminar sub layer, increased viscosity of nanofluid could increase the thickness of the sub layer and in turn increase the thermal resistance to heat transfer.

In the current work, detailed experimental study is carried out to determine the convective heat transfer performance of kerosene-alumina nanofluid under turbulent flow regime. The effect of particle size is also determined for two sizes of alumina particles. The results obtained in the study are discussed below.

#### 4.1.6.1 Test setup validation

Prior to carrying out the convective heat transfer experiments with nanofluid, the experimental test setup and the operational procedure is validated by experimentally evaluating the convective heat transfer data and comparing it with the available correlations from the literature for pure kerosene. Figure 4.21 shows the comparison of heat transfer coefficient determined from the current experiments and those calculated based on the Dittus-Boelter correlation [59] as given in Eq. 3.29.

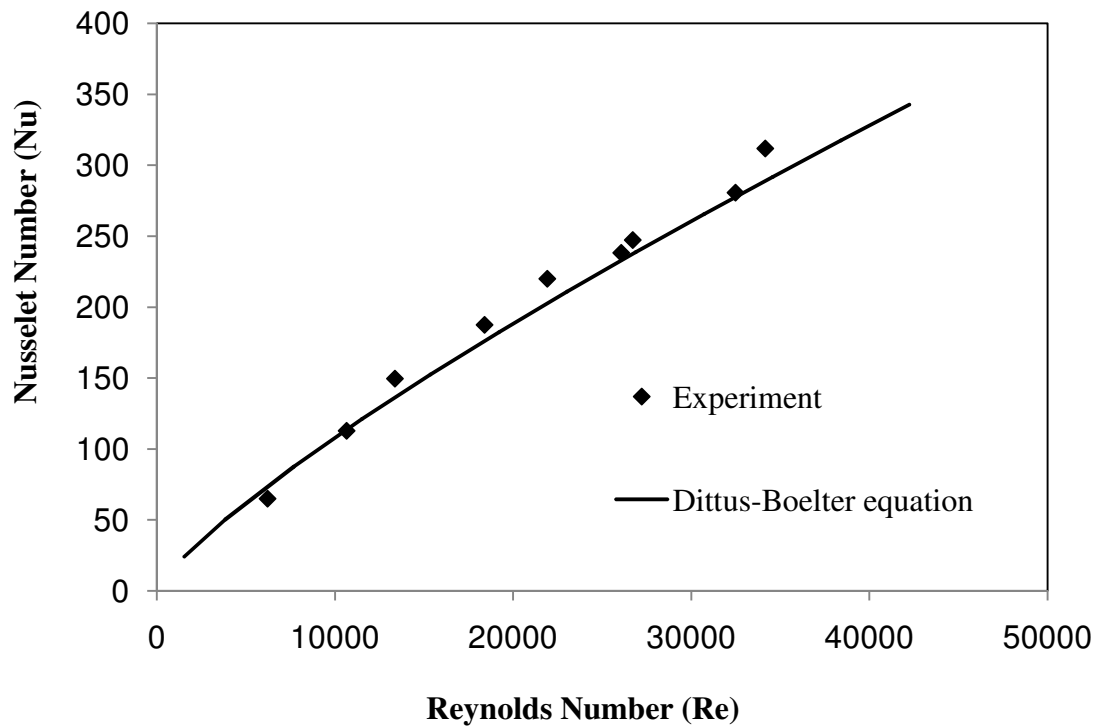


**Figure 4.21:** Nusselt numbers vrs Reynolds numbers for pure kerosene

#### 4.1.6.2 Validation of pressure drop characteristics

Though the current investigation on thermal conductivity indicates enhanced thermal performance of the kerosene-alumina nanofluid, it is expected that the system of flowing nanofluid will have higher pressure drop due to the increased viscosity of nanofluids. Higher pressure drop may limit nanofluid applicability in thrust chamber cooling as it will necessitate increased pump power to push the fluid through the regenerative passage in thrust chamber.

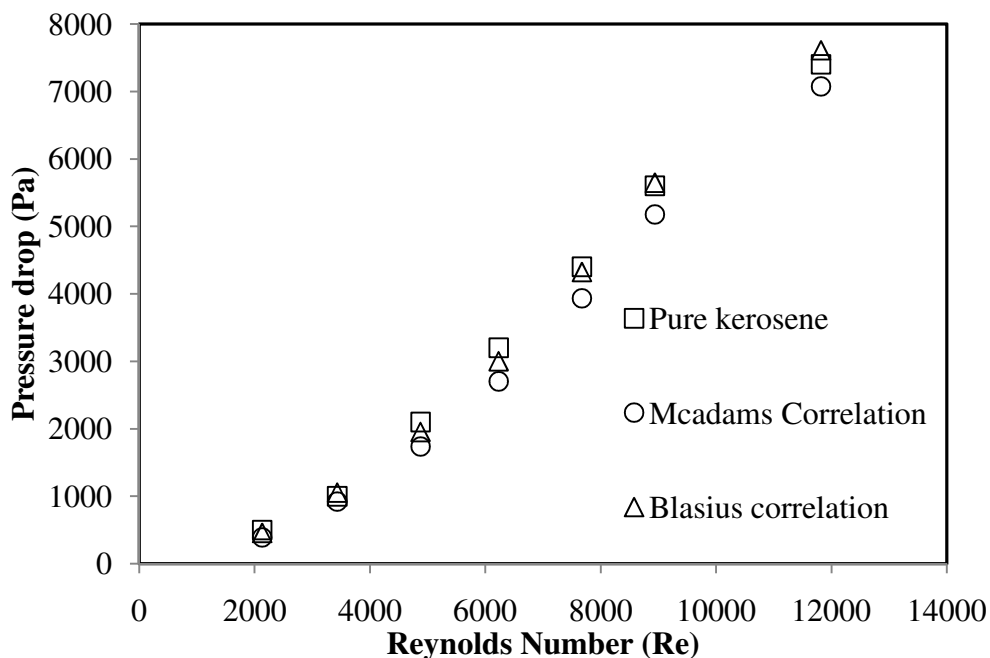


**Figure 4.22:** Pressure drop characteristic of pure kerosene

The pressure drop in the flow of pure kerosene in the test section is measured using differential pressure gauge (Druck DPI-800). The comparison of measured pressure drop of pure kerosene at various Reynolds number to the pressure drop computed using Blasius and McAdams correlation [59] is presented in Fig. 4.22. The experimental results obtained in the

current study are in good agreement with the values determined using the correlation [59]. This confirms the reliability of the experimental data obtained from the current test setup.

#### 4.1.6.3 Mouromtseff number (Mo)

To compare the fluid property related to heat transfer performance of the nanofluid to that of the base fluid for the given geometry at fixed velocity, Mouromtseff number (Mo) is used. It is a figure of merit and the fluid with larger value of Mo is considered to exhibit improved performance as a coolant than the others [115,149,150]. The estimation of Mo number with the thermo physical properties can indicate the expected relative heat transfer performance of the two fluids without actually conducting the heat transfer experiments.

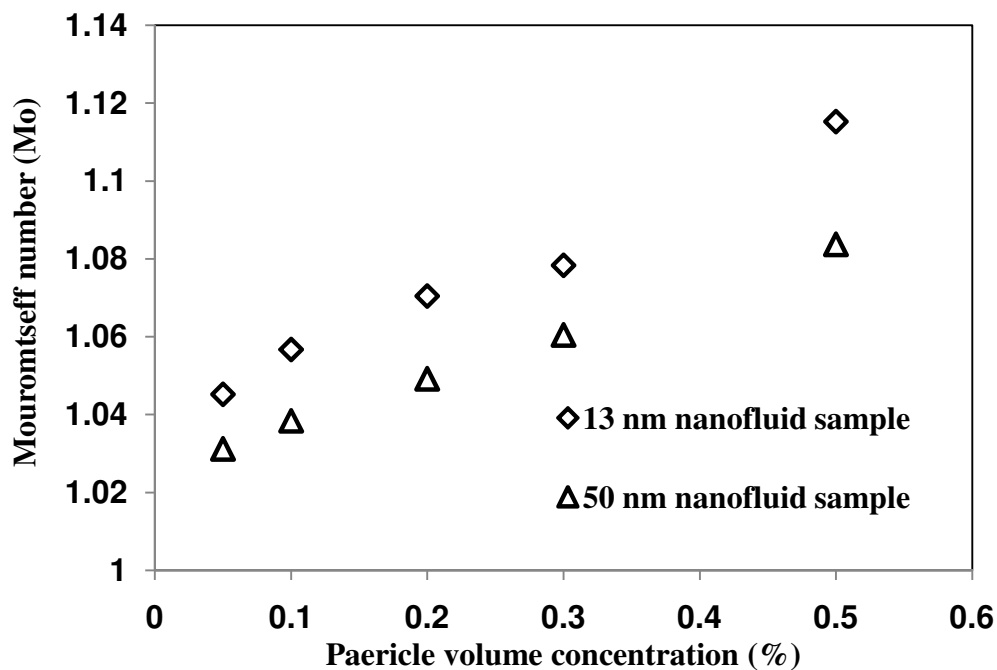


**Figure 4.23:** Mouromtseff number for kerosene- alumina nanofluid

The Mouromtseff number can be estimated using heat transfer coefficient determined from Dittus-Boelter equation for constant velocity comparison, and expressed as

$$Mo = (h_{nf}/h_{bf}) = (\rho_{nf}/\rho_{bf})^{4/5} (Cp_{nf}/Cp_{bf})^{2/5} (\mu_{nf}/\mu_{bf})^{-2/5} (k_{nf}/k_{bf})^{3/5} \quad (4.4)$$

Figure 4.23 represents the Mouromtseff number calculated for 13 nm and 50 nm kerosene-alumina nanofluid samples at various particle concentrations. It can be observed that at all particle concentrations and for both particle size nanofluids, the Mo number is greater than unity and this clearly indicates the higher heat transfer performance expected for the current kerosene- alumina nanofluids over pure kerosene.

#### 4.1.6.4 Convective heat transfer coefficient (h)

Subsequent to the validation of the experimental setup, detailed convective heat transfer study of nanofluid is carried out for 0.05vol%, 0.2vol%, 0.3vol% and 0.5vol% particle concentrations of the nanofluid. Effect of particle size on heat transfer is also studied experimentally for 13nm and 50nm catalogue particle size nanofluids.

Figure 4.24 represents the steady state surface temperature measured along the pipe length for 13nm 0.5vol% kerosene-alumina nanofluid for two Reynolds number conditions. The inlet fluid temperature is kept constant at 30°C during the test. The heating power in this experiment is 5.9 kW. Subsequently, Heat transfer coefficient is obtained from the measured fluid and surface temperature data using Eq. 3.21. Thermo-physical properties at average film temperature  $((T_s+T_f)/2)$  is used for the computation of heat transfer coefficient from the experimental data.

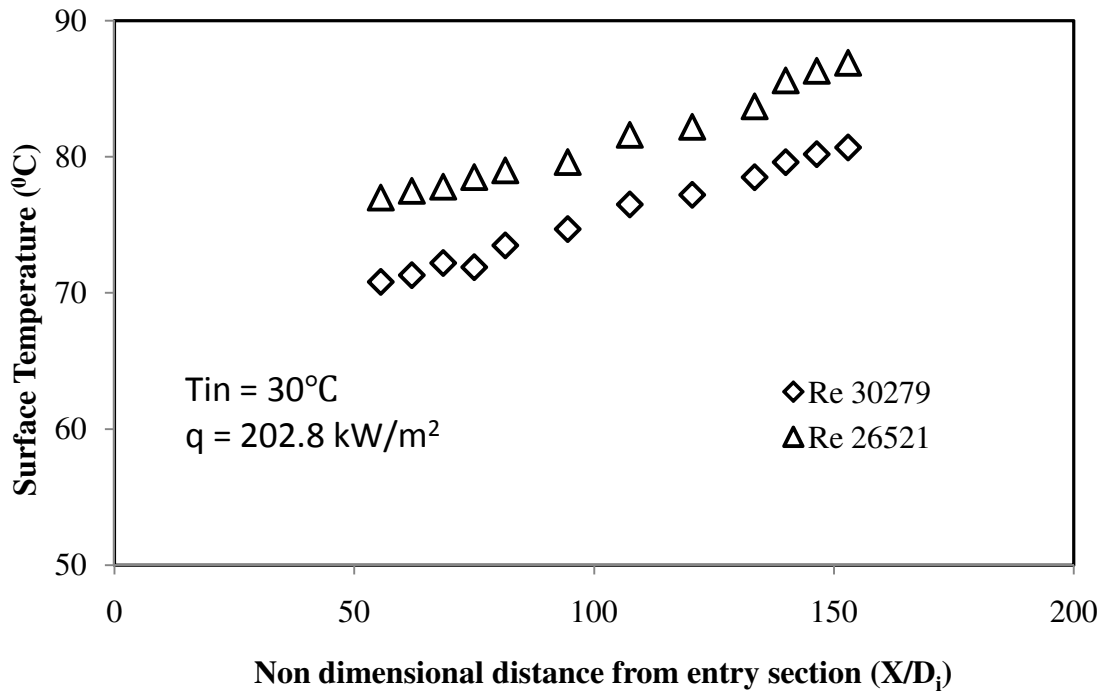


Figure 4.24: Surface temperature along the test section at various  $X/D$  locations

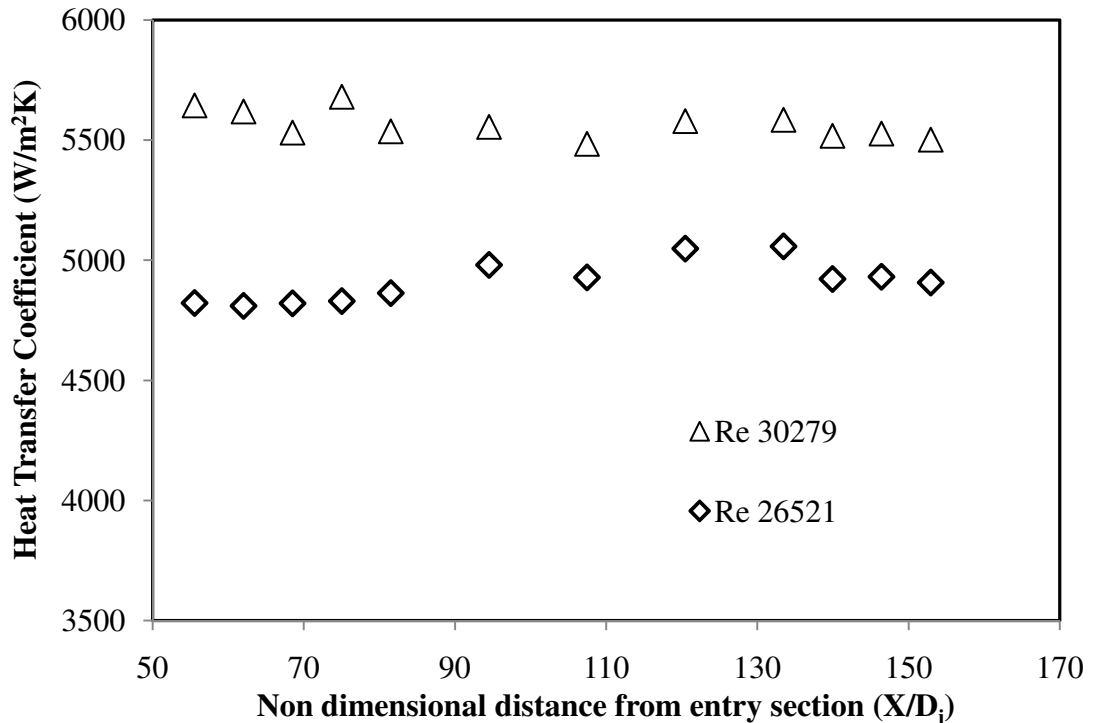
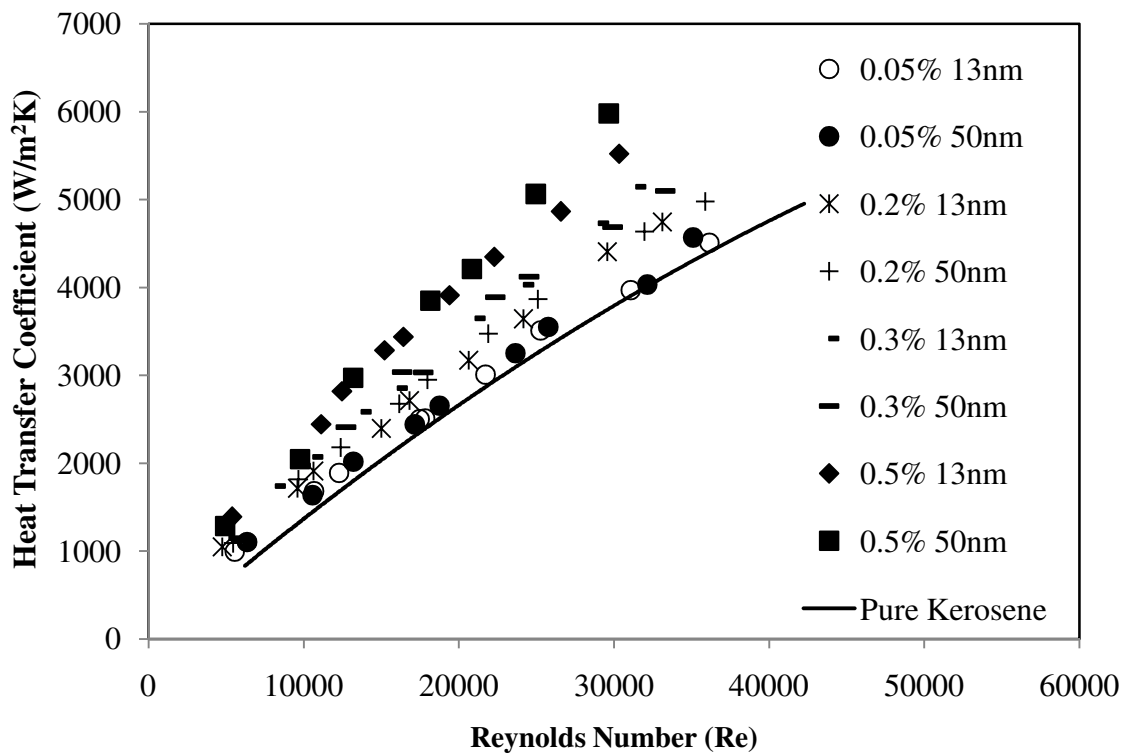


Figure 4.25: Heat transfer coefficient for 13nm, 0.5vol% kerosene-alumina nanofluid sample at various  $X/D$  locations.

Figure 4.25 shows the heat transfer coefficients obtained for the measurement data (shown in Fig. 4.24) for 13 nm-0.5vol% kerosene-alumina nanofluid sample at Reynolds number of 30279 and 26521 respectively. The average heat transfer coefficient determined for 0.5vol% kerosene-alumina nanofluid at Reynolds number of 30279 and 26521 is 5562 W/m<sup>2</sup>K and 4899 W/m<sup>2</sup>K, respectively. The percentage maximum standard deviation from the average value for the above data is 2.03%. It is to be noted that as the flow is in turbulent regime, the heat transfer coefficient is nearly constant along X/D = 55 to 152.



**Figure 4.26:** Heat transfer coefficient vrs Reynolds number for kerosene-alumina nanofluid

Each experiment is repeated four times and the similar data analysis is carried out for all the measured temperature, heat flux and flow rate data to obtain the heat transfer coefficient from the tests. The maximum dispersion in the calculated heat transfer coefficients obtained from various experiments for any particular case is within 3.1%. Heat

transfer coefficient for 13 nm and 50 nm particle nanofluids derived from the experimental data at various particle concentrations and Reynolds number is presented in Fig. 4.26.

It is evident from the figure that kerosene-alumina nanofluid exhibits enhanced heat transfer characteristics as compared to pure kerosene at complete Reynolds number range. As expected, the heat transfer coefficient of kerosene- alumina nanofluid is found to increase with Reynolds number and particle volume concentrations. In contrast to lower value of thermal conductivity of bigger size particle nanofluid, the measured heat transfer coefficient is observed to be higher for bigger sized particle nanofluid as compared to the smaller sized particle nanofluids. As already discussed, higher thermal conductivity observed for smaller sized particle nanofluid could be attributed to the higher Brownian motion as compared to the bigger particle in a stagnant fluid; however this need not be true for the nanofluid in a turbulent flow regime. In the turbulent flow regime, the effect of Brownian motion will be dominated by the effect caused due to the very high flow velocity of the fluid. One of the possible reasons for the enhanced thermal conductivity of nanofluid due to mechanisms other than Brownian motion can be attributed to the reduction in the resistance of thermal diffusion in the laminar sub layer of the boundary layer and can result in higher heat transfer performance of the nanofluid as compared to the base fluid. The higher viscosity observed for smaller sized particle nanofluid leads to increased thickness of laminar sub layer of the momentum boundary layer, and in turn increases its resistance to heat transfer. This combined effect of thermo physical properties along with the effect of higher disruption in the sub layer by bigger sized particles can result in higher heat transfer performance. Heat transfer coefficient at 0.3vol%, 50nm nanofluid sample is compared with those reported by Sonawane et al. [111], as shown in Fig. 4.27 because of the surrogate nature of ATF to kerosene. Figure 4.27 shows good agreement between the results obtained from the current

experiments and those due to Sonawane et al. [111] both indicating enhanced convective property of kerosene based nanofluid compared to kerosene alone.

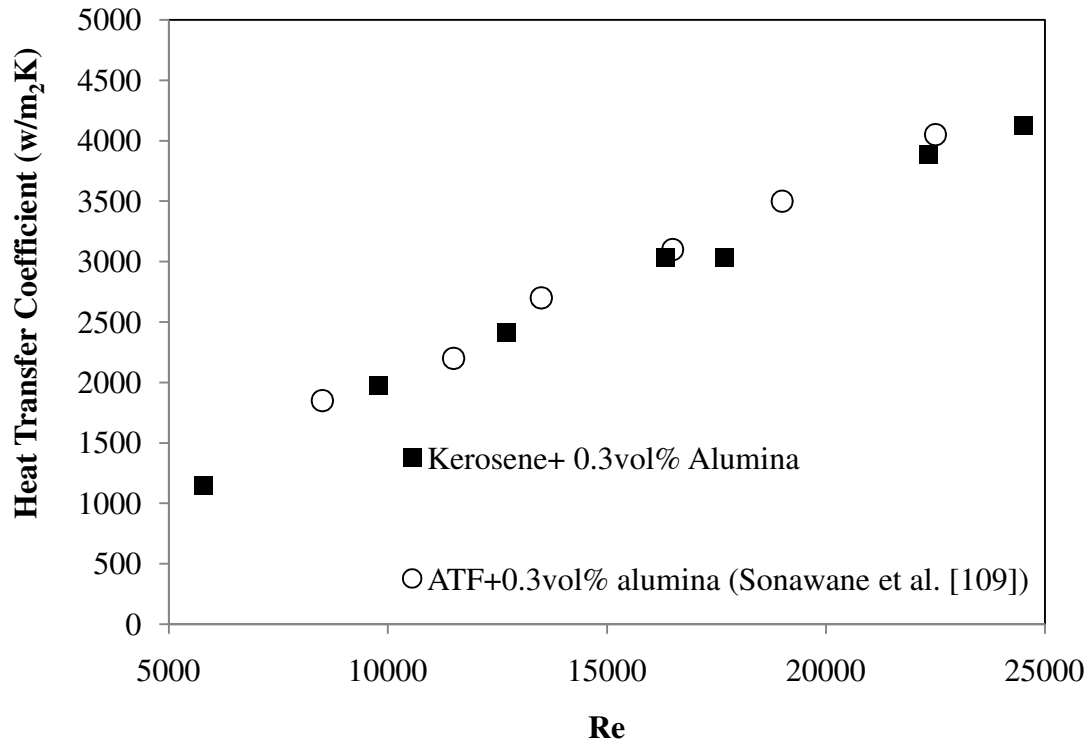


**Figure 4.27:** Comparison of convective heat transfer coefficient with Sonawane et al. [111]

As discussed by the Pak and Cho [96], comparing the heat transfer performance of nanofluid to its base fluid at identical Reynolds number is not the best approach. Higher viscosity of nanofluids requires higher velocity to maintain the same Reynolds number. An identical velocity based comparison rather than identical Reynolds number based assessment is proposed to be more appropriate for determining the heat transfer performance of nanofluids. Keeping this in mind, the heat transfer performance comparison of various kerosene- alumina nanofluids at different flow velocities is also carried out and the results are presented in Fig. 4.28. As expected the measured heat transfer coefficient increases with flow velocities. The heat transfer performance of current nanofluids are significantly higher as compared to the base fluid for identical velocity conditions and is similar to those observed

with Reynolds number based comparison. However, the magnitude of the enhancement in heat transfer coefficient is found to be lower in the case of velocity based analysis as compared to those based on identical Reynolds number.

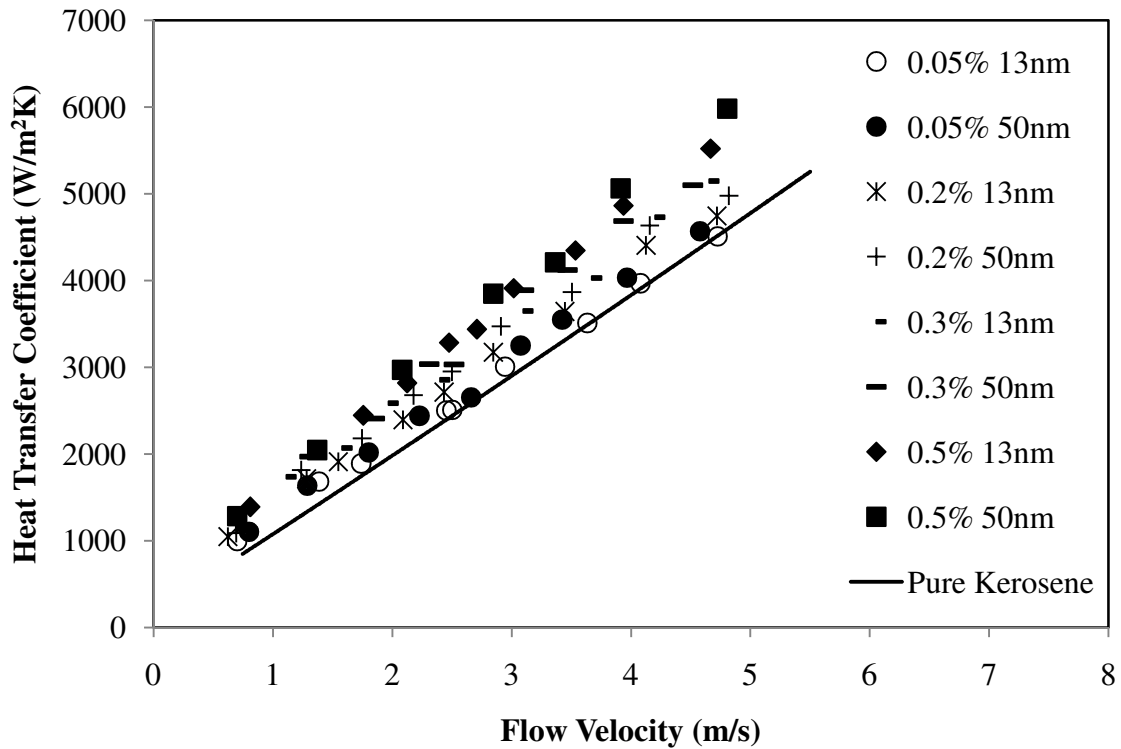


**Figure 4.28:** Heat transfer coefficient vrs fluid velocity for kerosene-alumina nanofluid

Peclet number based criterion has been used by many researchers [52,90,138] for the comparison of heat transfer performance of nanofluids. Peclet number describes the effect of thermal dispersion induced by micro-convection and micro-diffusion of nanoparticles. Figure 4.29 shows the heat transfer coefficient of various nanofluids based on the Peclet number. The higher heat transfer coefficient of nanofluid as compared to the base fluid indicates significant effect of micro convection and micro diffusion along with particle migration and clustering effects.

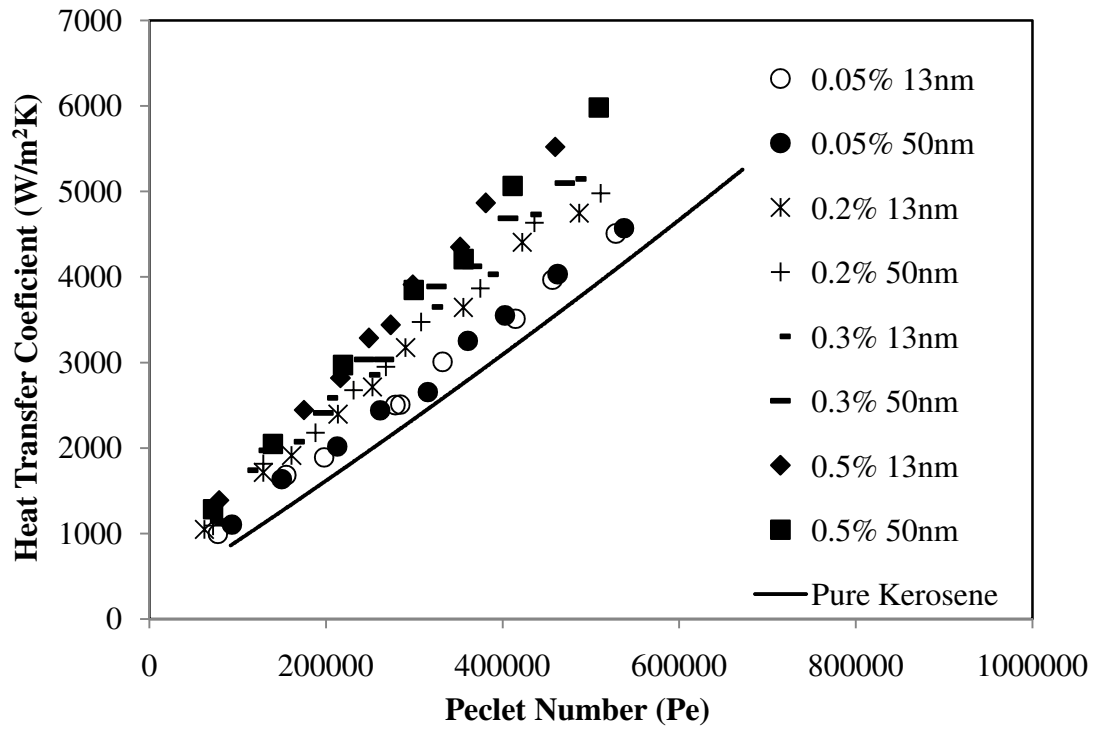
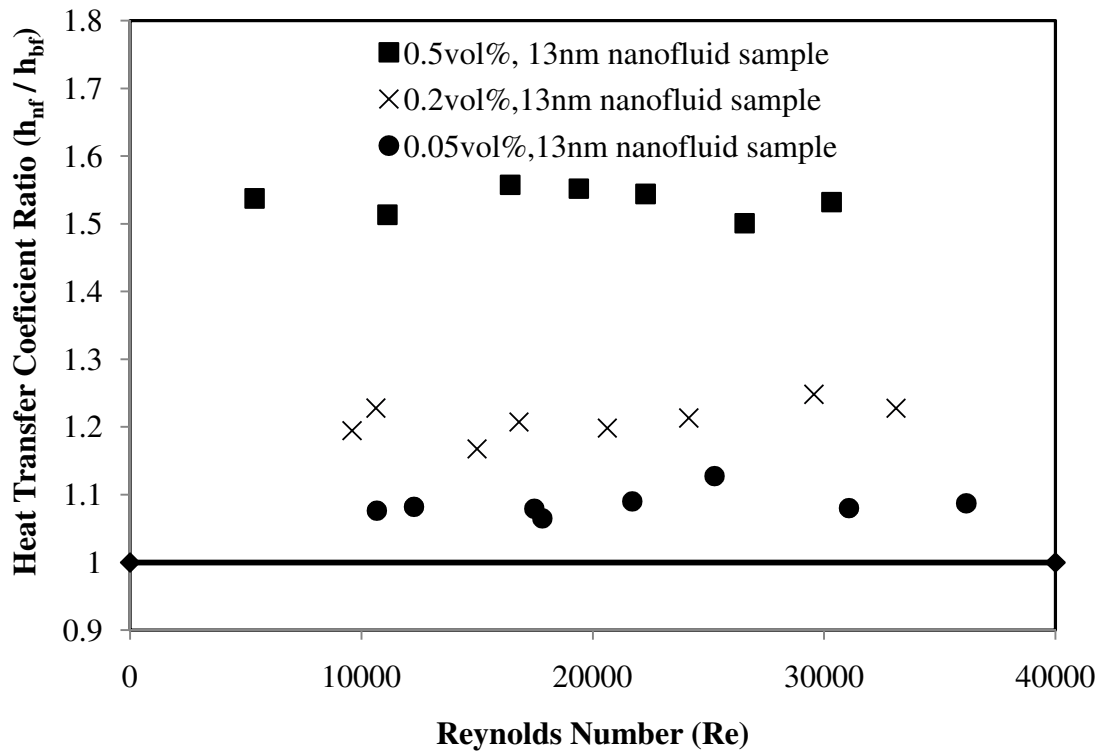
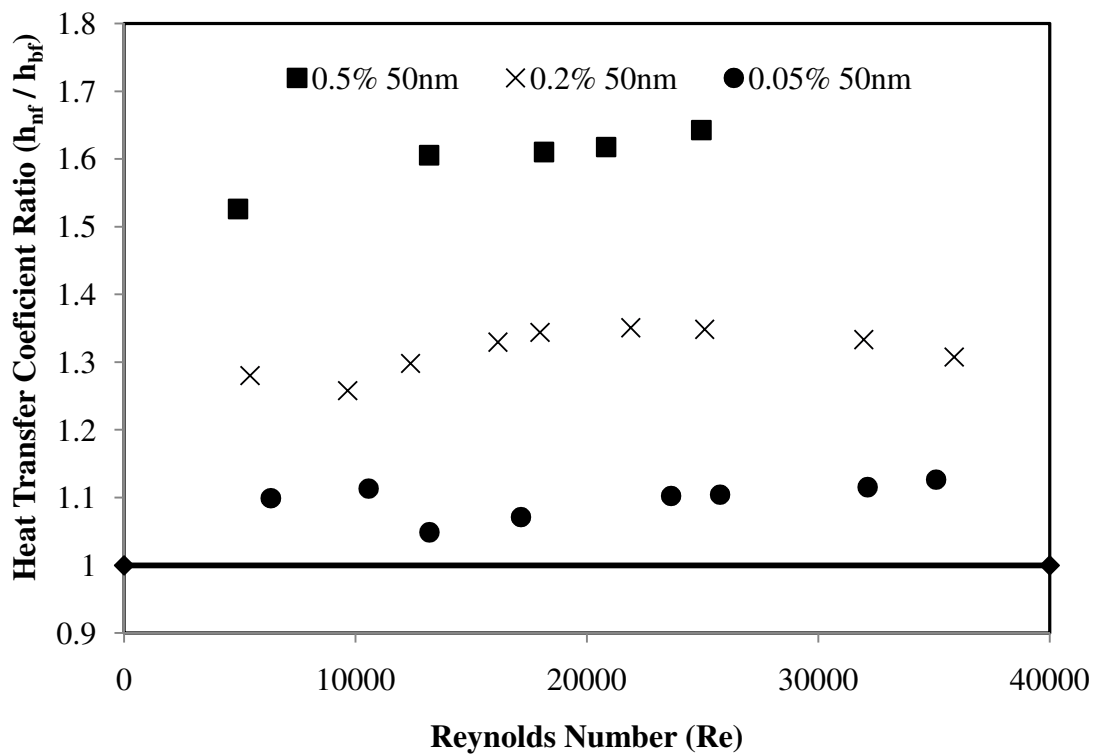


**Figure 4.29:** Heat transfer coefficient vrs Peclet number for kerosene-alumina nanofluid

Figures 4.30 to 4.32 represent the ratio of heat transfer coefficient of nanofluid to its base fluid at various particle concentrations and sizes showing variation based on change in Reynolds number, flow velocity and Peclet number respectively. The maximum enhancement observed in the present investigation is 1.64, 1.41 and 1.56 respectively based on identical Reynolds number, velocity and Peclet number based criteria for 50 nm, 0.5% volume concentration nanofluid, respectively.

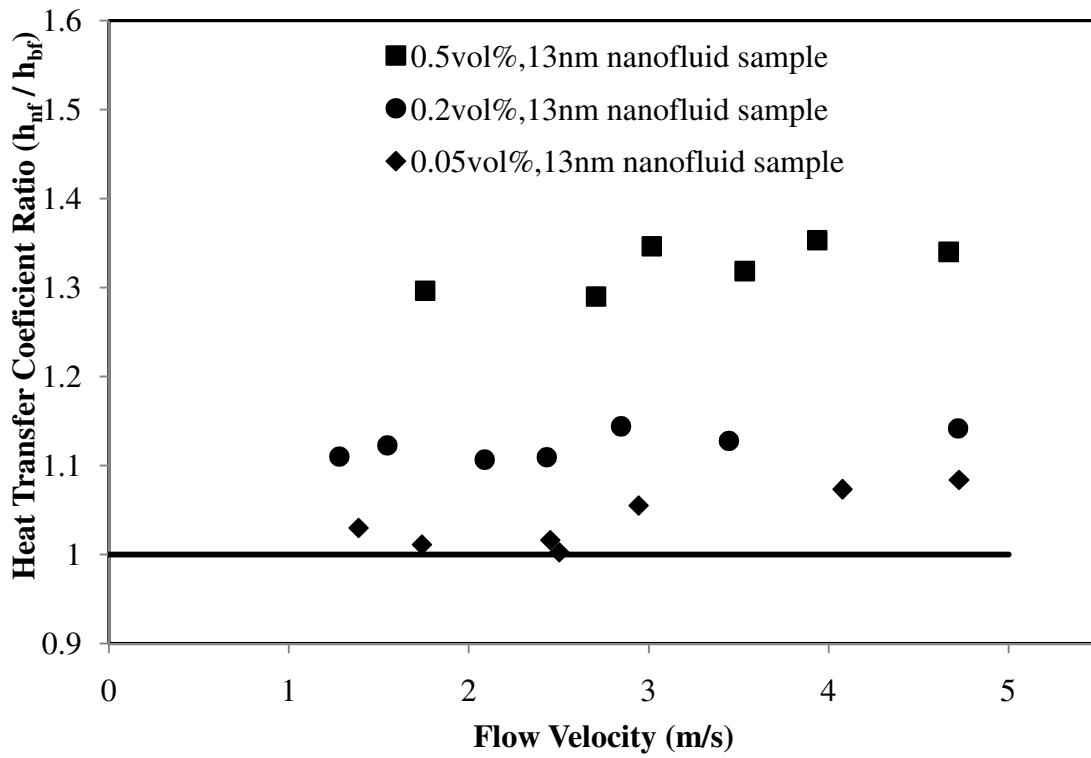


(a)

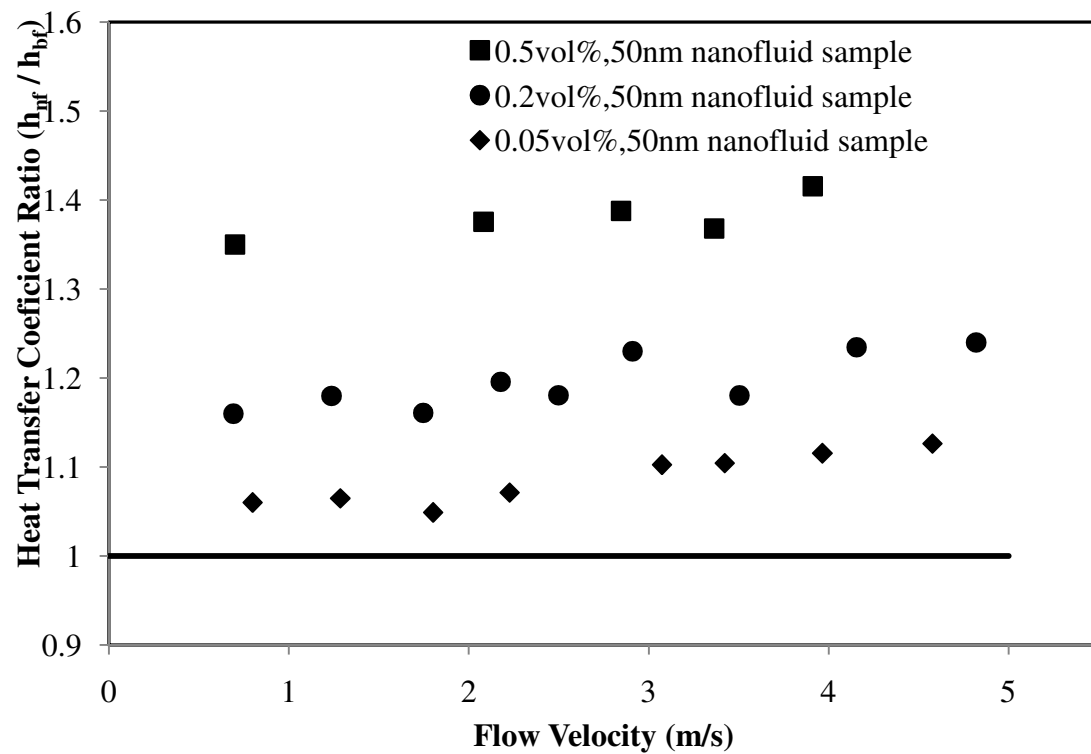


(b)

**Figure 4.30:** Ratio of heat transfer coefficient of kerosene-alumina nanofluid to base fluid with Reynolds number (A) 13 nm nanofluid sample, (B) 50 nm nanofluid sample

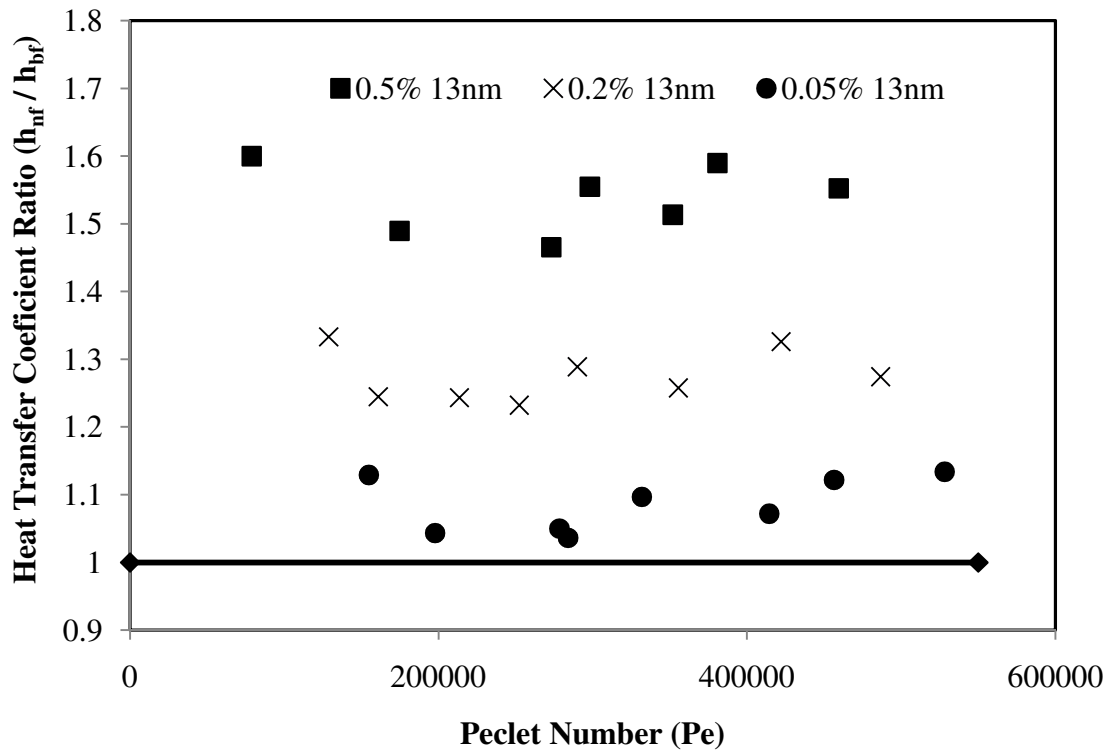


(a)

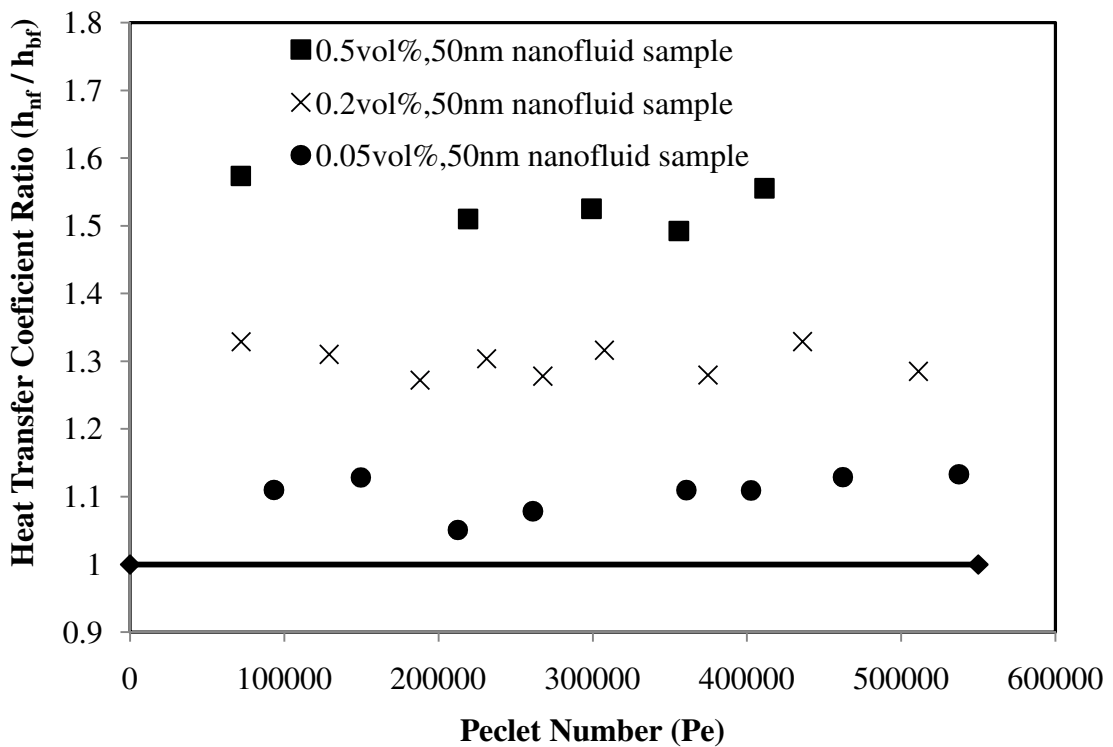


(b)

**Figure 4.31:** Ratio of heat transfer coefficient of kerosene-alumina nanofluid to base fluid with fluid velocity (a) 13 nm nanofluid sample, (b) 50 nm nanofluid sample



(a)



(b)

**Figure 4.32:** Ratio of heat transfer coefficient of kerosene-alumina nanofluid to base fluid with Peclet number (a) 13 nm nanofluid sample, (b) 50 nm nanofluid sample

The maximum convective heat transfer enhancement ratio observed for kerosene-alumina nanofluid based on various criteria is listed in Table 4.3. The enhancement ratio obtained based on the velocity criteria is found to be the lowest as compared to the other criteria. Contrary to the results of Pak and Cho [96] and Yu et al. [150], the current investigation reveals that the enhancement ratio exceeds unity in all the cases employing velocity based criteria. This could be attributed to the very marginal increase in viscosity observed in the current investigation as compared to the significant increase in viscosity observed by Pak and Cho [96] and Yu et al. [150] in their nanofluid wherein the authors observed a decrease in heat transfer coefficient for identical flow velocity magnitudes.

**Table 4.3:** Convective heat transfer enhancement ratio for kerosene-alumina nanofluid

	Particle concentration	Convective heat transfer enhancement ratio		
		Identical Reynolds number based	Identical Peclet number based	Identical flow velocity based
13 nm kerosene-alumina nanofluid sample	0.5vol%	1.54	1.52	1.35
	0.2vol%	1.23	1.21	1.14
	0.05vol%	1.1	1.1	1.08
50 nm kerosene-alumina nanofluid Sample	0.5vol%	1.64	1.56	1.41
	0.2vol%	1.35	1.32	1.23
	0.05vol%	1.15	1.13	1.11

#### 4.1.6.5 Pressure drop and friction factor

The friction factor for kerosene- alumina nanofluid at various particle concentration and sizes is computed from the measured pressure drop. Figure 4.33 shows the variation of

friction factor calculated in the present study, along with the correlation provided by Sonawane et al. [111] for ATF+ alumina nanofluid, from Blasius correlation and the correlation developed using the measured test data.

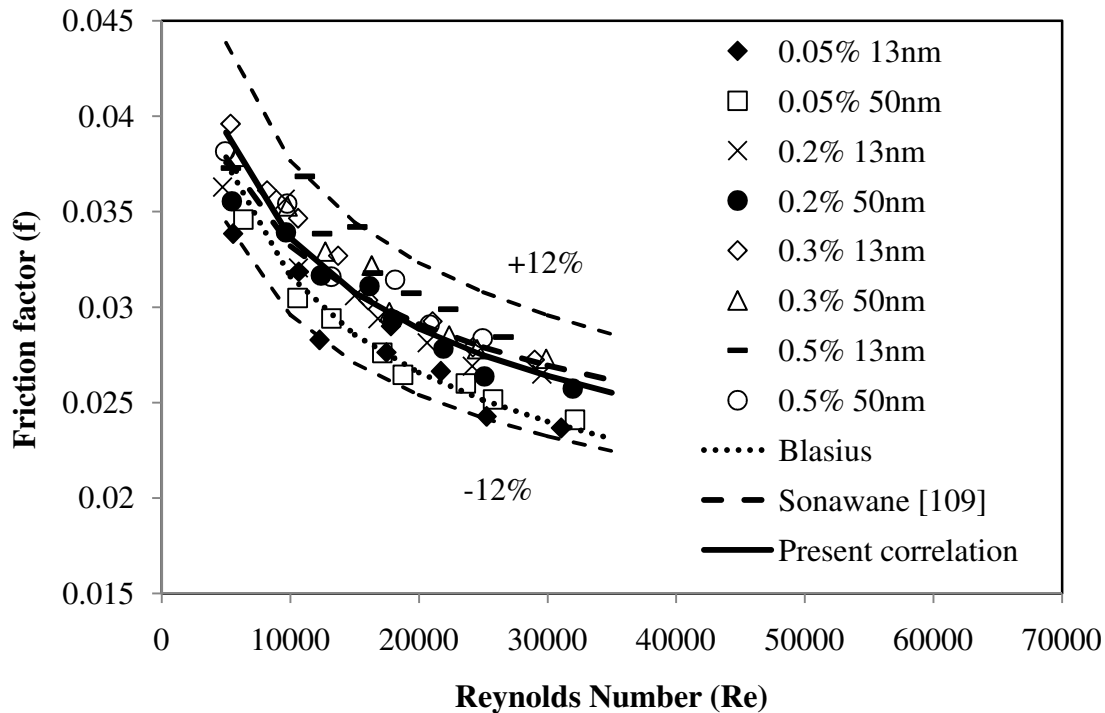


**Figure 4.33:** Friction factor with Reynolds number for kerosene-alumina nanofluid

Correlation for friction factor is obtained in present study by curve fitting all the data points (sample size >70) and is expressed as;

$$f = 0.255Re^{-0.22} \quad (4.5)$$

valid over a range of Reynolds number from 6000 to 30000 and particle size of 13nm and 50nm with  $R^2 = 0.903$  and  $RMSE = 0.00201$ .

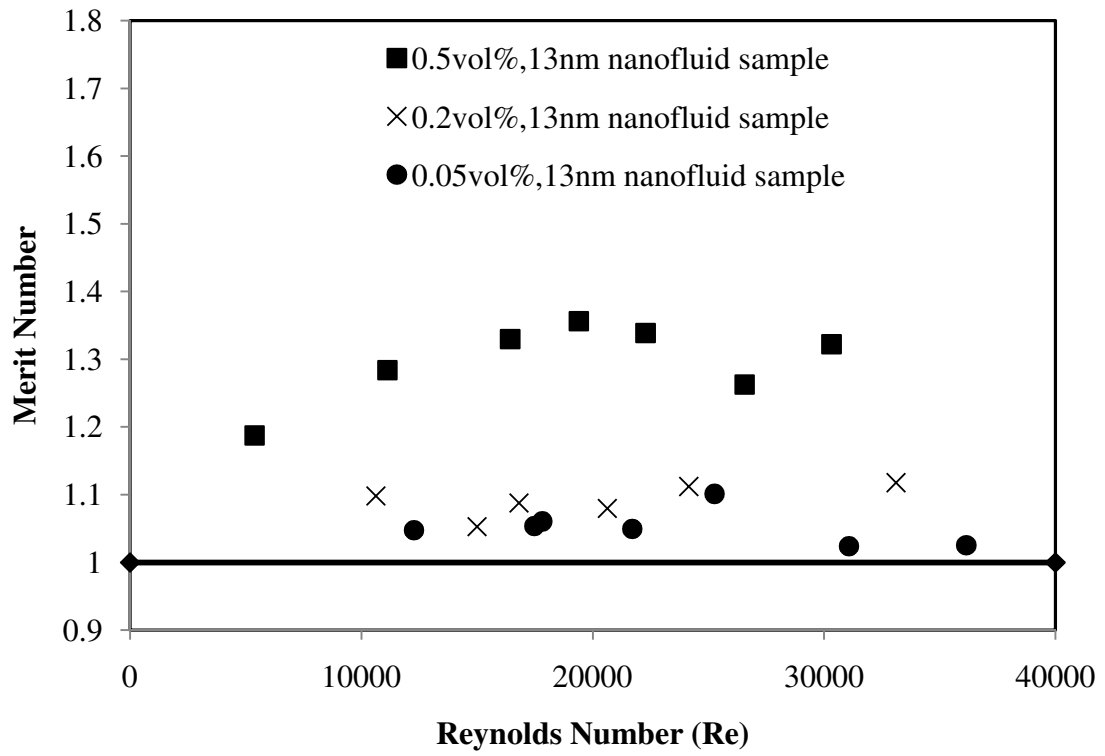
It is observed that a homogeneous fluid correlation is sufficient enough to accurately predict pressure drop characteristics of the nanofluids used in the current study. The

maximum dispersion in the friction factor from the above correlation is found to be within 12% and it can be used for the determination of pressure drop in a flowing system of kerosene- alumina nanofluid in liquid rocket engines.

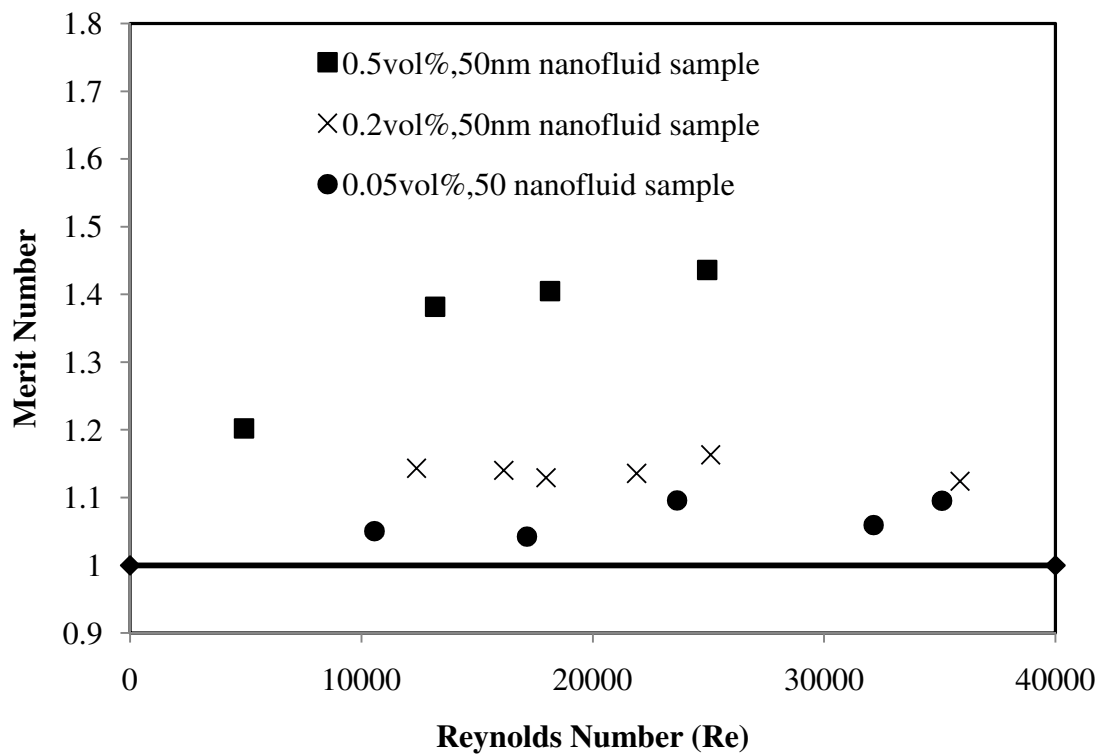
#### **4.1.6.6 Total heat transfer performance**

The total heat transfer performance of kerosene- alumina nanofluid is determined by comparing the heat transfer augmentation of nanofluid against the pressure drop due to increased density and the viscosity of nanofluid. Ratio of heat transfer enhancement to the increase in pressure drop, i.e.  $(h_{nf}/h_{bf})/(\Delta P_{nf}/\Delta P_{bf})$  is used as a parameter to define total heat transfer performance of kerosene- alumina nanofluid. This parameter is named as Merit number and is used by Yu et al. [150] for evaluating the total heat transfer performance of water- SiC and water- alumina nanofluid.

Figures 4.34 and 4.35 indicate the heat transfer performance of 13nm and 50nm kerosene-alumina nanofluid samples based on merit number with respect to Reynolds number and Peclet number respectively. The maximum merit number for 50nm 0.5vol% particle concentration nanofluid is found to be 1.46 and 1.36 respectively for identical Reynolds number and Peclet number. It is also to be seen that in most of the cases the Merit number is found to be higher than unity and this indicates that the nanofluid has the potential to substitute the base fluid as an effective coolant in various heat transfer applications. In very few cases of nanofluid with particle concentration of 0.05vol%, Merit number is found to be lower than one indicating that these nanofluids will not be optimally useful for the heat transfer system.

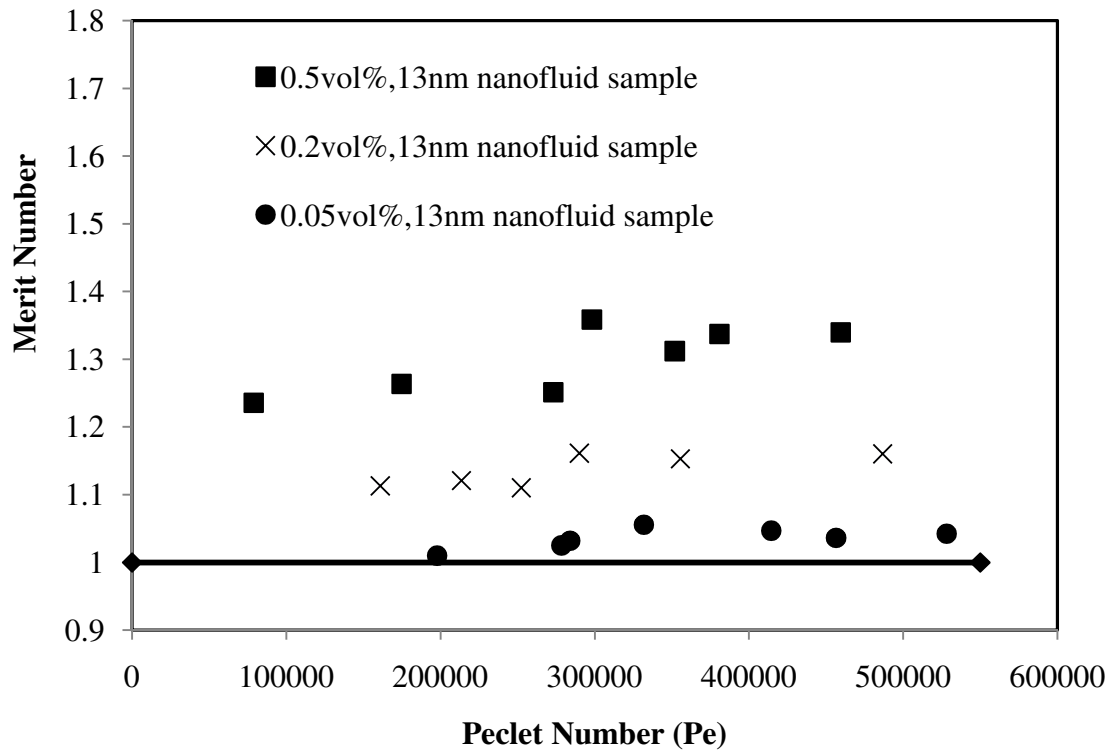


(a)

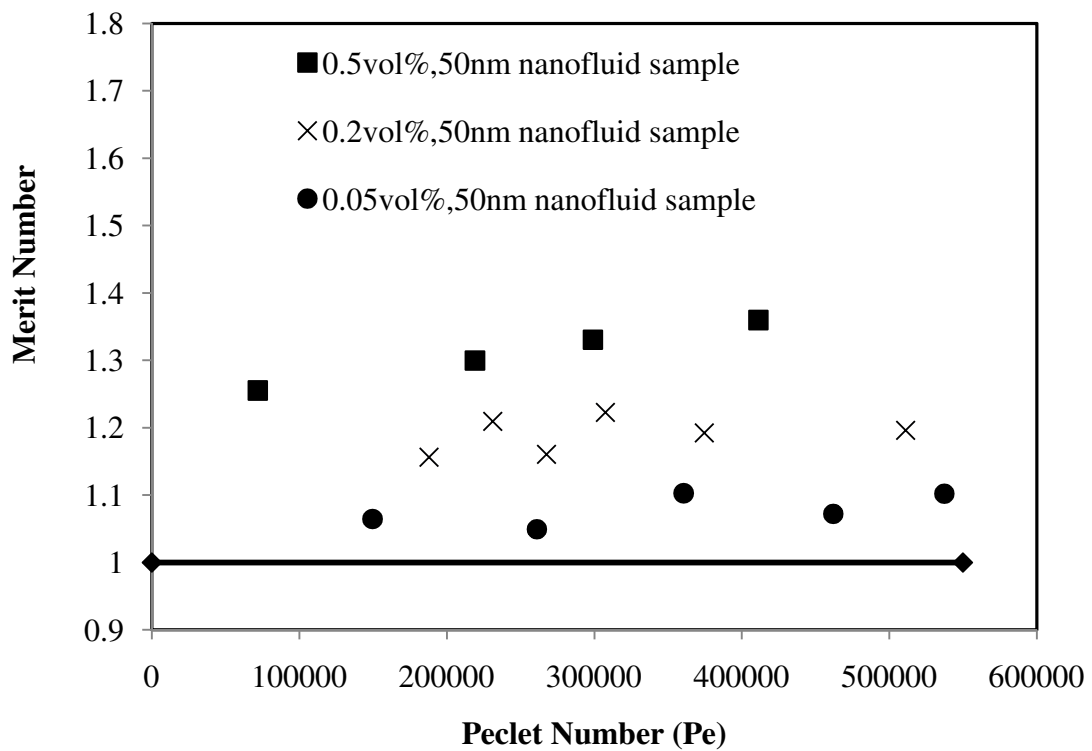


(b)

**Figure 4.34:** Variation in Merit number with Reynolds number for kerosene-alumina nanofluid (a) 13 nm nanofluid sample, (b) 50 nm nanofluid sample



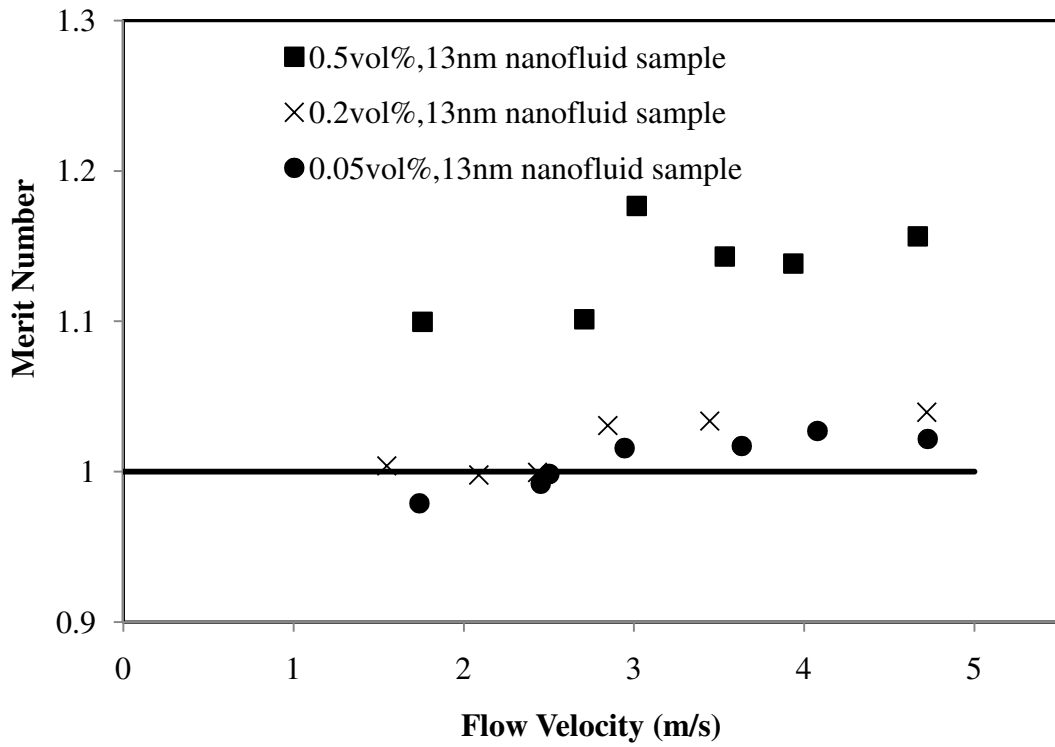
(a)



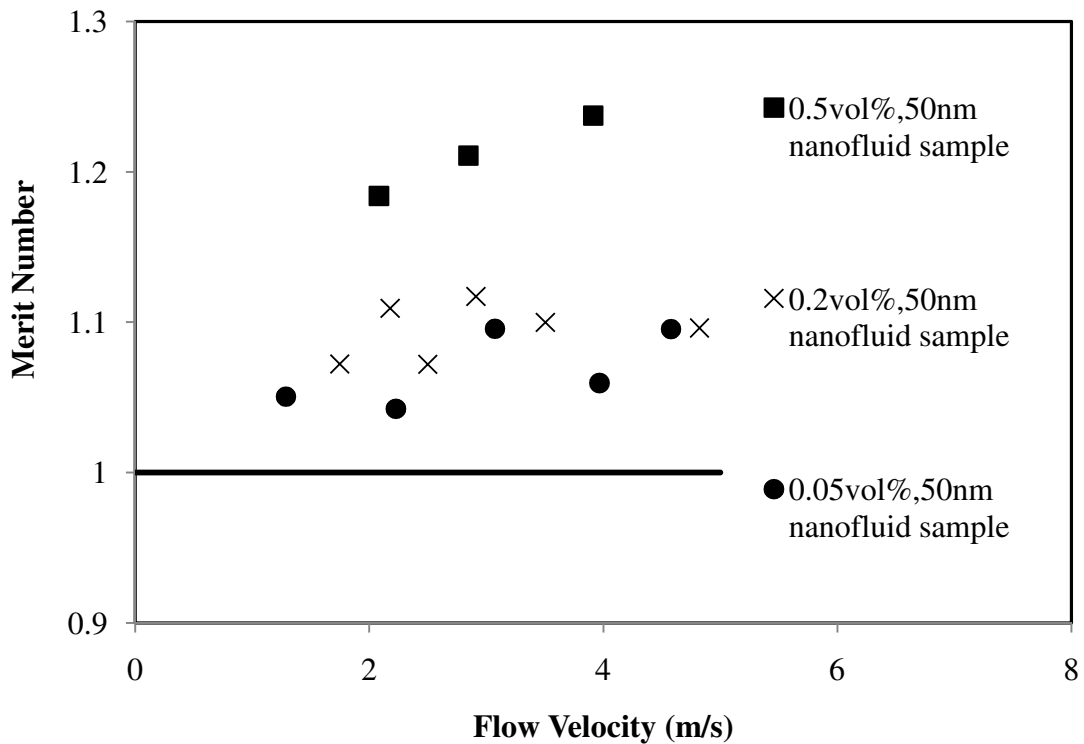
(b)

**Figure 4.35:** Variation in Merit number with Peclet number for kerosene-alumina nanofluid

(a) 13 nm nanofluid sample, (b) 50 nm nanofluid sample



(a)



(b)

**Figure 4.36:** Variation in Merit number with flow velocity for various particle concentrations of kerosene-alumina nanofluids. (a) 13 nm, (b) 50 nm

The merit number distribution for identical velocity conditions is presented for 13nm and 50 nm kerosene-alumina nanofluid samples in Fig.4.36. It can be observed that while using the identical velocity for comparing the total heat transfer performance of nanofluid to the base fluid, the Merit number is lower as compared to the other two criteria. Also the nanofluid with particle concentration of 0.2vol% and above yields Merit number greater than unity, thereby suggesting that the total heat transfer performance of these nanofluids is higher than that of pure kerosene, and can be used as a better coolant in regenerative passage of semi-cryo thrust chamber.

#### 4.1.6.7 Nusselt number

The variation in Nusselt number of kerosene-alumina nanofluid at various particle volume fractions with Reynolds number is shown in Fig. 4.37. The computed Nusselt number is compared with those obtained through single phase correlation of Dittus-Boelter [59], and also with the correlation developed by Sonawane et al. [111] for ATF-alumina nanofluid. It is to be noted that the fluid properties used in Dittus-Boelter correlation are for the nanofluid at 0.5vol% particle concentration and 50nm particle size. A regression analysis of the test data (sample size > 70) is carried out to derive the following modified correlation as:

$$\text{Nu} = 0.005\text{Re}^{0.8}\text{Pr} \quad (4.6)$$

valid over a range of Reynolds number from 6000 to 30000, Prandtl number from 14 to 17 and particle size of 13nm and 50nm with  $R^2 = 0.8707$  and RMSE = 13.56. The equation 4.6 is aimed at predicting the heat transfer performance of a nanofluid, provided all the relevant thermo physical properties are known 'apriori'. The effect of particle concentration and size will be implicitly reflected in the properties. However, in the current study, the aim of

presenting the correlation is to highlight the effectiveness of the homogeneous fluid correlation in determining the heat transfer performance of nanofluid.

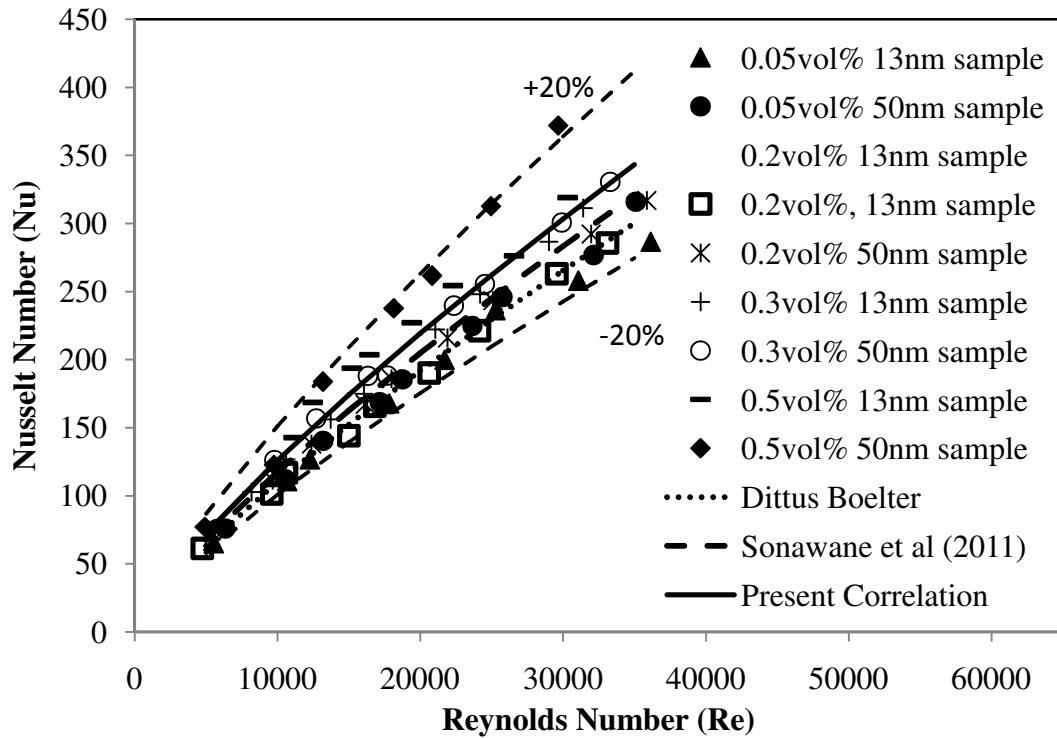


**Figure 4.37:** Nusselt number with Reynolds number for kerosene-alumina nanofluid

It is to be noted that all the experimental data represented in Fig. 4.37 lies within  $\pm 20\%$  of the present correlation. From the correlation presented in Eq (4.7), the exponent of Prandtl number is found to increase from 0.4 as in Dittus- Boelter correlation to 1 in the current study. Correlation developed by Sonawane et al. [111] and Pak and Choi [96] also reported increased exponent value for Prandtl number. This increase in exponent of Prandtl number indicates the significant role of Prandtl number in nanofluid convective heat transfer process. As discussed in section 3.2.3, the enhancement in convective heat transfer properties of nanofluid could be due to the combined effect of change in thermo physical properties, Brownian motion and disturbance in boundary layer thickness. It is true that the effect of nanoparticle concentration and diameter plays an important role in nanofluid convective heat

transfer process. However, the aim of presenting the correlation is to highlight the effectiveness of the homogeneous fluid correlation in determining the heat transfer performance of nanofluid in the current investigation.

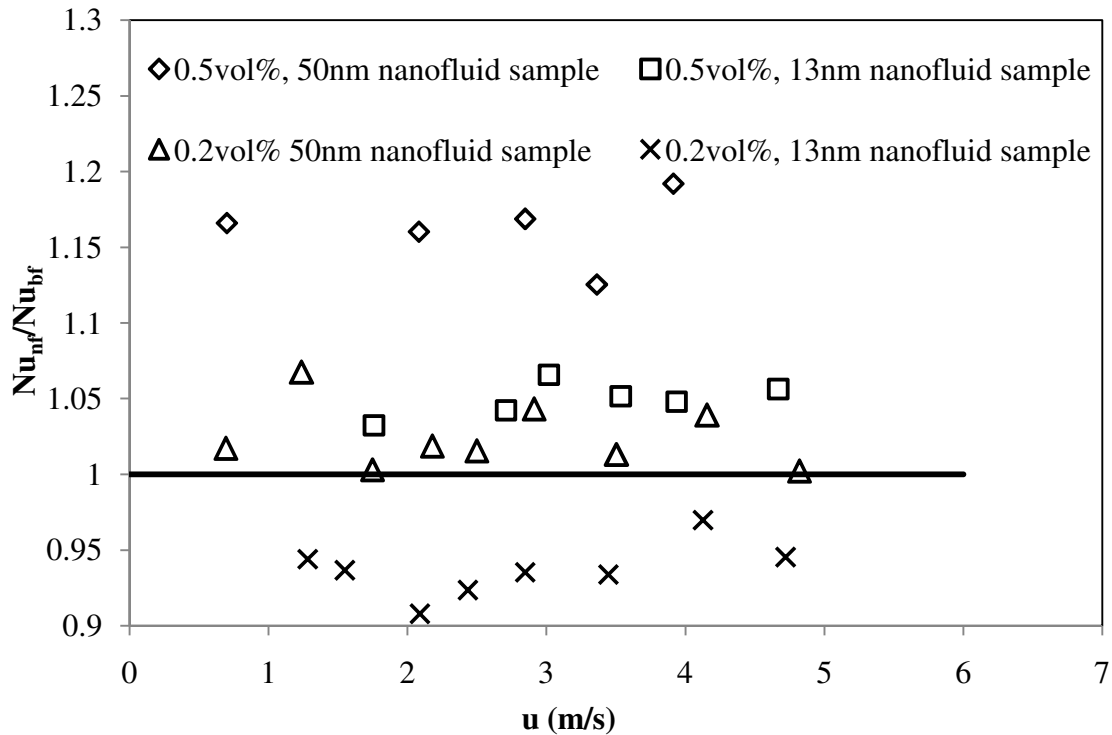


**Figure 4.38:** Ratio of Nusselt number of kerosene-alumina nanofluid to pure kerosene at identical velocity condition

Figure 4.38 shows the ratio of Nusselt number of kerosene-alumina nanofluid to that for pure kerosene at identical velocity condition. It can be clearly seen that the ratio of Nusselt number 0.2vol% 13nm nanofluid sample to pure kerosene is lower than one and for all other cases it is greater than one. The ratio of Nusselt number of nanofluid to the base fluid over unity encourages potential utility of such nanofluids as a heat transfer fluid in cooling system.

## **4.2 Kerosene-GNP Nanofluid**

In this section detailed study carried out for the synthesis and characterization of kerosene-GNP nanofluid are discussed. Kerosene-GNP nanofluids are prepared for three particle size at various particle concentrations. Measurement of thermal conductivity and viscosity is carried out and the effect of fluid temperature is also determined on thermo-physical properties. Detailed convective heat transfer experiments are carried out at turbulent flow regime. Outcome of all these studies are discussed below.

### **4.2.1 Synthesis**

#### **4.2.1.1 Nanofluid preparation**

In the present investigation, kerosene-GNP nanofluids are prepared with three nominal particle sizes 750, 500 and 300 SSA. The disruptor type ultrasonication as used for the preparation of kerosene-alumina nanofluid is used here. As kerosene is a nonpolar solvent, the dispersion of graphene becomes difficult in kerosene as it forms a large bulk in organic solvents. During the initial experiments without surfactant it is ascertained that a stable kerosene-GNP nanofluid cannot be prepared without the addition of surfactant.

In the present work various surfactants are chosen based on their affinity towards the base fluid and are used to stabilize the kerosene-GNP nanofluid. Initially, based on the previous research experience with kerosene-alumina nanofluid, oleic acid is employed for stabilizing 0.05 wt% kerosene-GNP nanofluid. The attempt to stabilize the nanofluid is unsuccessful and GNPs started settling after few hours.

**Table 4.4 :** List of various surfactants used to stabilized kerosene-GNP nanofluids

Surfactant	Observation in stability
Oleic acid	Stable for few hours (4-5 hrs) for lower concentration Poor stability (within 1 hr) for higher concentration
TritonX100, Tween20, MERPOL	Sticks on Probe and Cylinder surfaces Very poor stability
Hexadecyltrimethyl ammonium bromide	Stable for few hours in all concentrations
Cetylpyridinium chloride, Kolliphor	Poor stability even for lower concentrations ( <1 hrs)
Sorbitanmonooleate	Stable for few hours (1-2 hrs) at lower concentration Poor stability (within a 20-30 min) at higher concentration
Oleyamine	Highly stable for more than 2 month for 0.005% solution Stability for few days at higher concentrations.

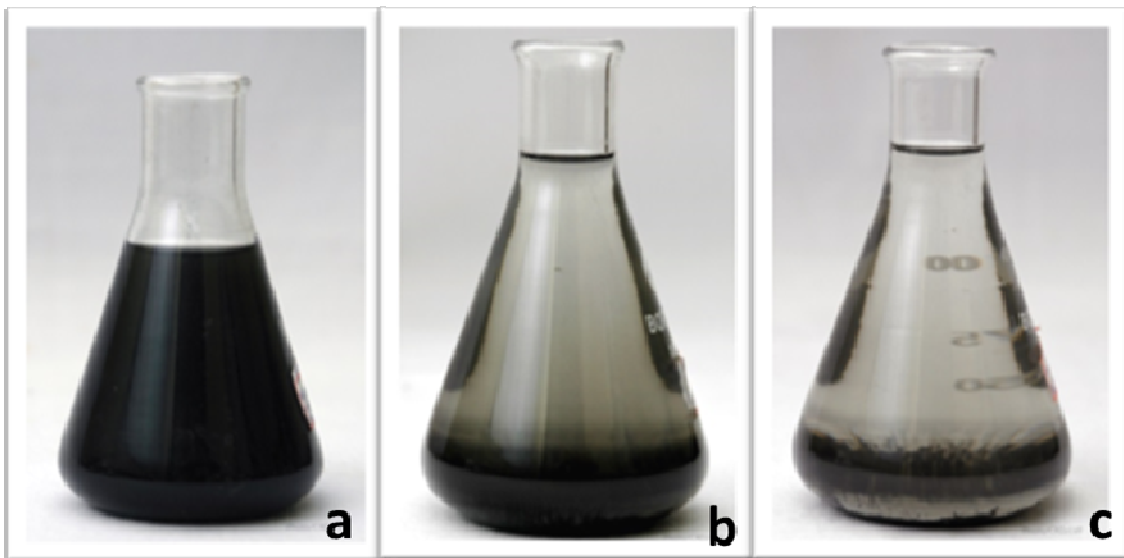


**Figure 4.39:** Kerosene- GNP nanofluid with (a) Oleyamine (b) Oleic acid (c) Tween-20

At higher concentrations above 0.1wt%, settling started even after few minutes itself. Subsequently, many other surfactants are employed, and the behaviour and stability of

nanofluids are visually monitored. Table 4.4 reports the outcome of the stability study using various surfactants. The kerosene-GNP nanofluids prepared using oleylamine, oleic acid and Tween-20 surfactants are shown in Figure 4.39. It is perceived that the nanofluid prepared using oleic acid and Tween-20 is not stable. Oleylamine provides good colloidal stability of GNP in kerosene and is found to be suitable for longer stability of kerosene-GNP nanofluids. Further, oleylamine is added to the nanofluid using a syringe. The nanofluid is continuously ultrasonicated during the addition process. The surfactant to particle mass ratio is varied from 0.3 to 1.2 in small steps. The stability of nanofluid is found to be poor for the mass ratio of less than 0.3. An optimum quantity of oleylamine of 0.1 ml in 1 kg of kerosene for 0.05% mass concentration with surfactant to particle mass ratio of 0.3 is found to yield the maximum visual stability.

Subsequently, nanofluids of different concentration at constant oleylamine to particle mass ratio of 0.3 are prepared. Different ultrasonication time periods of 40 min for 0.005 wt% to 3 hrs for 0.2wt% are employed. The stability of nanofluids is found to be directly related to the concentration of the GNPs. This observation is similar to the kerosene-alumina nanofluid. Nanofluids at lower mass fraction up to 0.05wt% are very stable (> 4 months) as compared to those with higher particle mass concentration of 0.1wt% and 0.2wt% nanofluids for which the stability persists around 20-30 days.

#### **4.2.2 Particle size measurement**

Before carrying out the particle size measurement in kerosene- GNP nanofluid surface area of dry GNPs is determined using Quantachrome Nova 1200e surface area analyser. The values obtained are 638 m<sup>2</sup>/g, 399 m<sup>2</sup>/g and 245 m<sup>2</sup>/g for the manufacturer specified surface area of 750 m<sup>2</sup>/g, 500 m<sup>2</sup>/g and 300 m<sup>2</sup>/g respectively. It can be clearly seen that the measured values are not significantly deviating from the manufacturer specified surface area.

Nanofluids at 0.05 wt % are prepared for 750 and 500 SSA GNPs. Particle sizing of the nanofluid are measured with time (days) to determine the stability of nanofluid. The particle size distribution for the samples is measured using Malvern Zetasizer. All the size measurement is performed at 25<sup>0</sup>C with a scattering angle of 173<sup>0</sup>. Each sample is tested three times and the mean value is reported here.

Nanofluid from the top portion in the bottle is used as the sample for testing at the first day, 30<sup>th</sup> day, and at 60<sup>th</sup> day after preparation, and particle size measurement is conducted. Figures 4.40 and 4.41 represent the particle size distribution based on intensity measurement from DLS technique for 750 and 500 SSA kerosene-GNP nanofluids samples, respectively. It is perceived from the Figures 4.40 and 4.41 that intensity curve of 750 SSA nanofluid remains nearly unchanged even after 60 days of preparation. The Z-average value measured for 750 SSA GNP nanofluid is found to vary only from 184.6 to 192.4 in 60 days. Z-average value is a harmonic intensity averaged particle diameter reported by the measurement system and it is very sensitive to small changes in the colloidal behaviour of sample, viz. particle agglomeration or settling. A constant value of Z-average observed in the present study indicates the very high stability of nanofluid. The particle intensity plot for 500 SSA GNPs nanofluid is slightly varied with time. The Z-average value for 500 SSA nanofluids varies from 442 to 463 in 60 days, and though both the nanofluids are stable up to 60 days, stability of 750 SSA nanofluid is higher as compared to 500 SSA nanofluid.

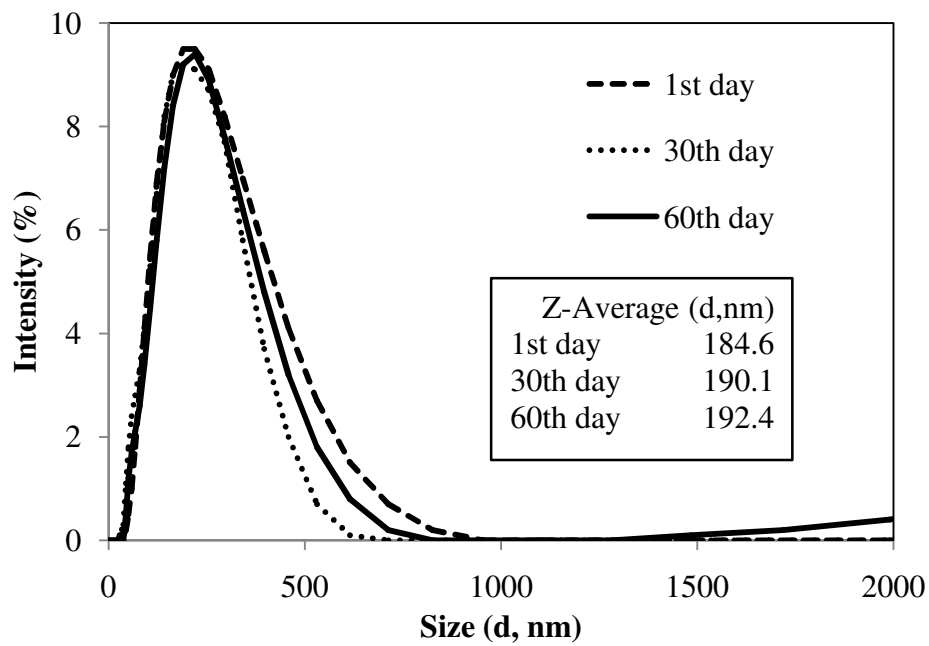


**Figure 4.40:** Particle size distribution of 750 SSA 0.05 wt% kerosene-GNP nanofluid sample with time (days)

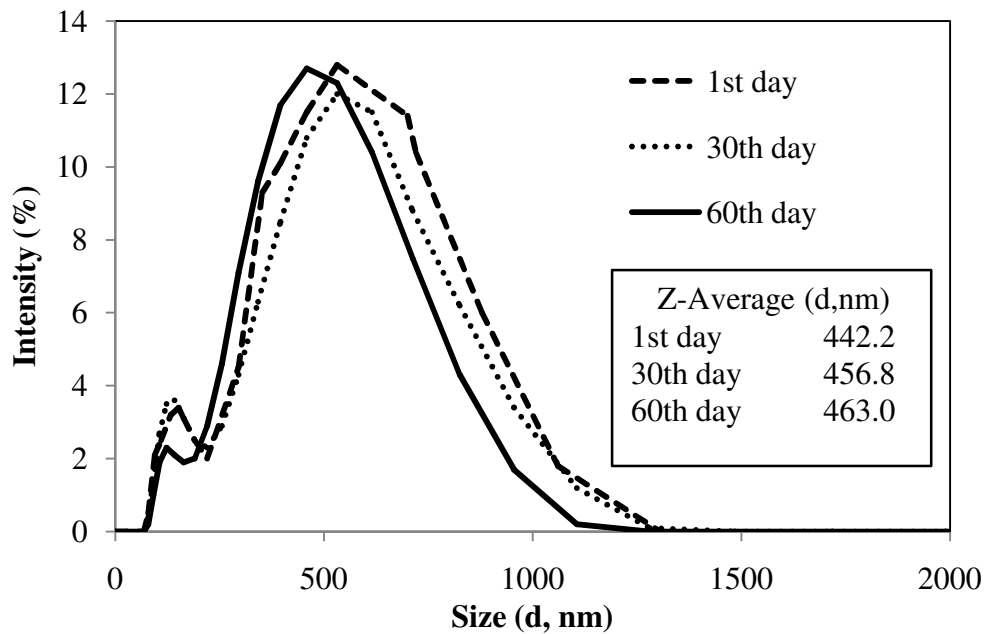


**Figure 4.41:** Particle size distribution of 500 SSA 0.05 wt% kerosene- GNP nanofluid sample with time (days)

### 4.2.3 Thermal conductivity

Thermal conductivity of kerosene-GNP nanofluid is measured using THW technique. Prior to measurements, the instrument is calibrated with DI water and glycerine. During the measurement the sample is kept at a constant temperature of  $30^{\circ}\text{C} \pm 0.25^{\circ}\text{C}$  using a constant temperature bath.

Thermal conductivity of kerosene-GNP nanofluids at particle concentration of 0.005wt%, 0.02wt%, 0.05wt%, 0.1wt% and 0.2wt% is determined for three particle size of 750, 500, 300 SSA. Ratios of thermal conductivity of kerosene-GNP nanofluid to pure kerosene at various particle mass concentrations for three different sizes of 750, 500 and 300 SSA are presented in detail in Fig.4.42. The ratio of thermal conductivity of nanofluid to base fluid increases with particle loading for all sizes of GNPs. The enhancement ratio of thermal conductivity of nanofluid to base fluid is found to be higher for the higher SSA particles as compared to the lower SSA for a range of particle concentrations. The enhancement ratio at 0.2 wt% concentration for 750, 500, 300 SSA GNPs nanofluid is found to be 1.23, 1.17 and 1.13, respectively.

The effect of particle size on thermal conductivity can be attributed to following two main reasons, viz, specific surface area (SSA) and Brownian motion as discussed for kerosene-alumina nanofluid. The higher surface area per unit volume of GNPs will result in increased interaction between the solid particles to the base fluid and will also enhance the possibility of Brownian motion due to lower mass of individual particles. The frequent interactions result in higher thermal conductivity and it also explains the reason for the higher enhancement in thermal conductivity for 750 SSA GNPs nanofluid as compared to the other particle size nanofluid.

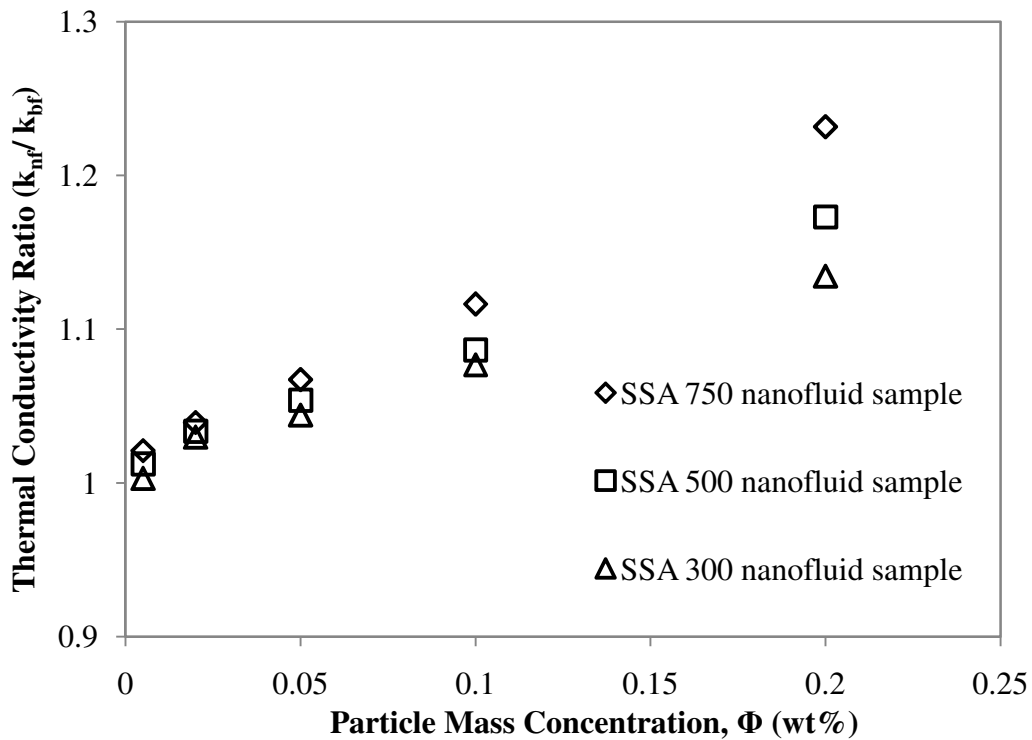


**Figure 4.42:** Effect of particle size (SSA) on thermal conductivity of kerosene- GNP nanofluid at various mass concentrations at 30 °C

To confirm the validity of experimental results on thermal conductivity, same set of measurements are also obtained using transient plane source method (TPS 2500s). It can be inferred from Fig. 4.43 that the results obtained using both the methods are identical, and the maximum dispersion noted in the measurement using two techniques is 2.9%, which is well within the uncertainty limit defined by the manufacturer for both the equipment (uncertainty= 5%).

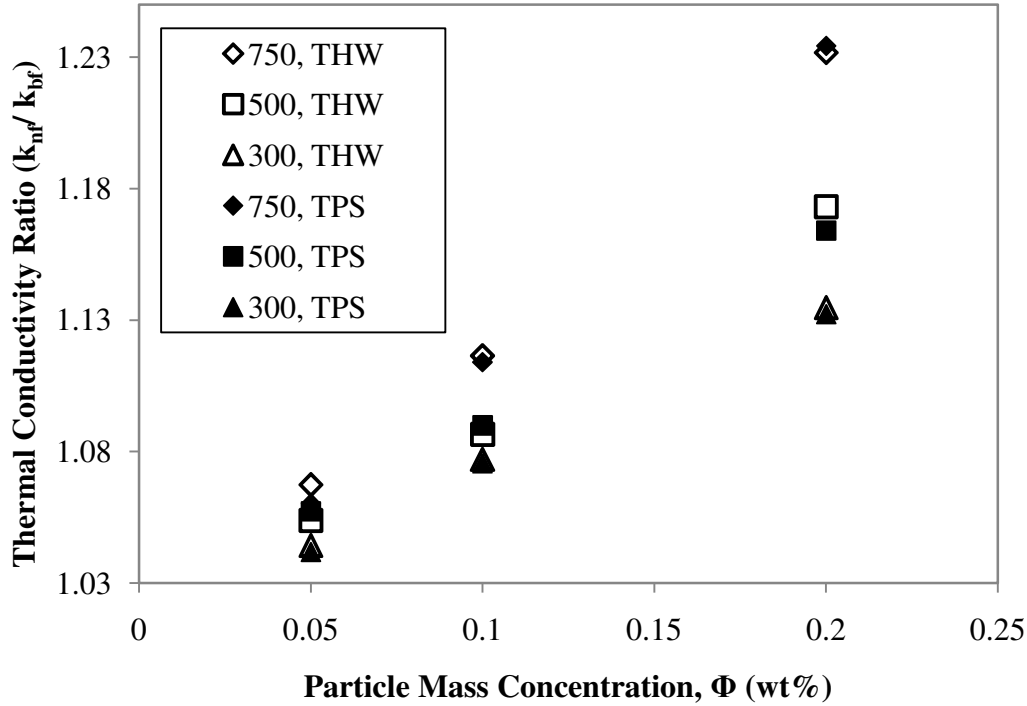


**Figure 4.43:** Effect of measurement techniques on thermal conductivity of kerosene- GNP nanofluids

In the current investigation thermal conductivity enhancement is found to be 23.2% for 0.2 wt%, 750 SSA kerosene-GNP nanofluids. It is to be noted that, similar enhancement in thermal conductivity was noticed for kerosene-alumina nanofluid at particle concentration of 0.5vol% (2.5wt%). The significantly higher enhancement in thermal conductivity noticed for kerosene-GNP nanofluid as compared to kerosene-alumina nanofluid, can be explained based on percolation model [23]. According to the percolation model, long chain present in CNT based nanofluid works as interconnecting thermal network acting as heat conducting path. Gupta et al. [44] reported similar networks for GNPs. Moreover, the thermal conductivity of GNP is higher as compared to CNT and is expected to have the enhanced thermal conductivity for GNP based nanofluids. Graphene, a two-dimensional structure with very high aspect ratio has largest surface area as compared to CNT or other spherical

nanoparticles. Due to the large interface area between the particle and fluid, it has lowest contact resistance that result in increased thermal conductivity for kerosene-GNP nanofluid. In addition, due to the shape of the GNPs as discussed by Hamilton and Crosser [47], higher effective thermal conductivity of nanofluids is expected.

A benchmark study carried out by the researchers [13], of various organizations have used Nan's model [89] to compare their findings and reported a good agreement in the measured thermal conductivity to the model. According to Nan's model,

$$k_{nf} / k_{bf} = (3 + \varphi [2\beta_{11} (1-L_{11}) + \beta_{33} (1-L_{33})]) / (3 - \varphi (2\beta_{11} L_{11} + 2\beta_{33} L_{33})) \quad (4.7)$$

where,  $L_{ii}$  and  $\varphi$  are the geometrical factor and the volume fraction of particles respectively.

$\beta_{ii}$  is determined as

$$\beta_{ii} = (k_p - k_{bf}) / (k_{bf} + L_{ii} (k_p - k_{bf})) \quad (4.8)$$

where,  $k_p$  is in-plane thermal conductivity [72] of nanoparticle. As the aspect ratio of GNPs is very high, the values considered are  $L_{11}=0$  and  $L_{33}=1$ .

Subsequently, Zheng and Hong [154] reported a model by modifying the original Yamada-Ota model [141] with the inclusion of the effect of thermal boundary layer (TBR). The model is represented as;

$$k_{nf} / k_{bf} = ((k_x / k_{bf}) + \alpha - \alpha \varphi [1 - (k_x / k_{bf})]) / ((k_x / k_{bf}) + \alpha + \varphi [1 - (k_x / k_{bf})]) \quad (4.9)$$

where,

$$k_x = k_{np} / (1 + ((2k_{np} \text{TBR}) / Le)) \quad (4.10)$$

$$\text{and, } \alpha = \varphi^{0.2} Le / d. \quad (4.11)$$

In Fig. 4.44 the comparison of thermal conductivity measurements from the current study with those calculated based on models by Nan et al. [89] and those due to Zheng and Hong [154] for three sizes of GNPs nanofluid are presented in detail. It is to be noted that the TBR value play significant role in the modified Yamda and Ota model [141] which is unknown for the current nanofluid under investigation. Therefore, TBR value for the present nanofluids are estimated using the measured thermal conductivity and is found to be  $10^{-7} \text{ m}^2\text{KW}^{-1}$  for 750 and 500 SSA nanofluid, and  $0.7 \times 10^{-7} \text{ m}^2\text{KW}^{-1}$  for 300SSA nanofluid. The value of TBR estimated is comparable to the value used by other researchers [48,49]. In the current work, Le is taken as 1000 nm for 750 GNP nanofluids. In the case of 500 and 300 GNP, Le is calculated in proportionate to its specific surface area per unit volume. Le/d is considered as 400 for all GNP sizes nanofluids.

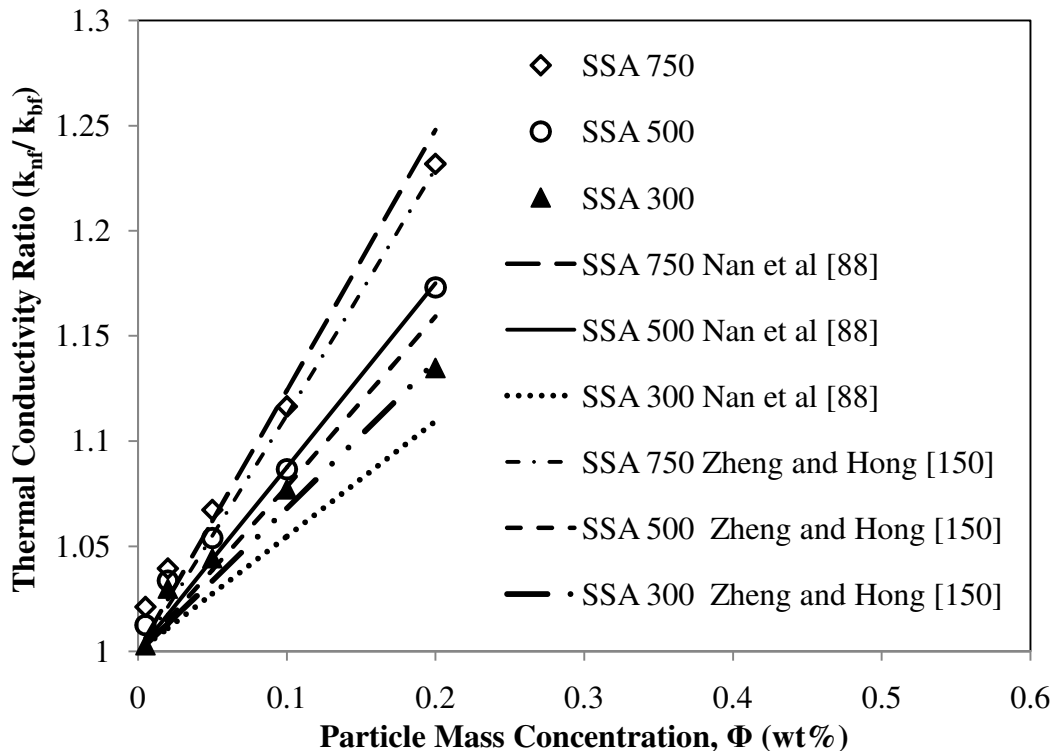


**Figure 4.44:** Comparison of measured thermal conductivity of kerosene-GNP nanofluid with theoretical models

Figure 4.45 shows the ratio of thermal conductivity of nanofluid to the base fluid with change in temperature for various GNP sizes and particle concentrations. The ratio of thermal conductivity for 750 GNPs particle size increases from 1.23 to 1.30 over 20<sup>0</sup>C to 70<sup>0</sup>C temperature range. It can be noted that for kerosene-alumina nanofluid thermal conductivity ratio increases from 1.12 to 1.25 (> 2 times) for 13nm, 0.2vol% particle size in the 25 <sup>0</sup>C to 65<sup>0</sup>C temperature range. Such large enhancement in thermal conductivity with temperature is not observed in the case of kerosene-GNP nanofluids and the lesser dependence of thermal conductivity on temperature for kerosene-GNP nanofluid is very similar to the observation made by other researchers [81,125,148] for CNT and GNP based nanofluids. It is to be noted that the significant effect of temperature on thermal conductivity reported by previous researchers is mainly for metallic and ceramic nanofluids, and is mainly attributed to the micro convection caused by Brownian motion of particles in nanofluids at higher temperature. It is expected that at high temperature, the random motion of nanoparticles along with the decrease in base fluid viscosity causes increased micro convection and results in enhanced thermal conductivity. The CNT based nanofluid does not show temperature dependency [106] due to the network structure as discussed earlier. GNPs used in the current study have minimum 2.5 nm thickness sheet with varying length from 100nm to 2000nm. The smaller GNPs would participate in Brownian motion, and result in enhanced thermal conductivity with temperature. However, the longer GNPs do not cause Brownian motion and the thermal conductivity increase in such case is mainly due to percolation theory [44,104]. It is to be noted that the percolation mechanism is independent of temperature and hence, thermal conductivity of these GNPs is not dependant on temperature.

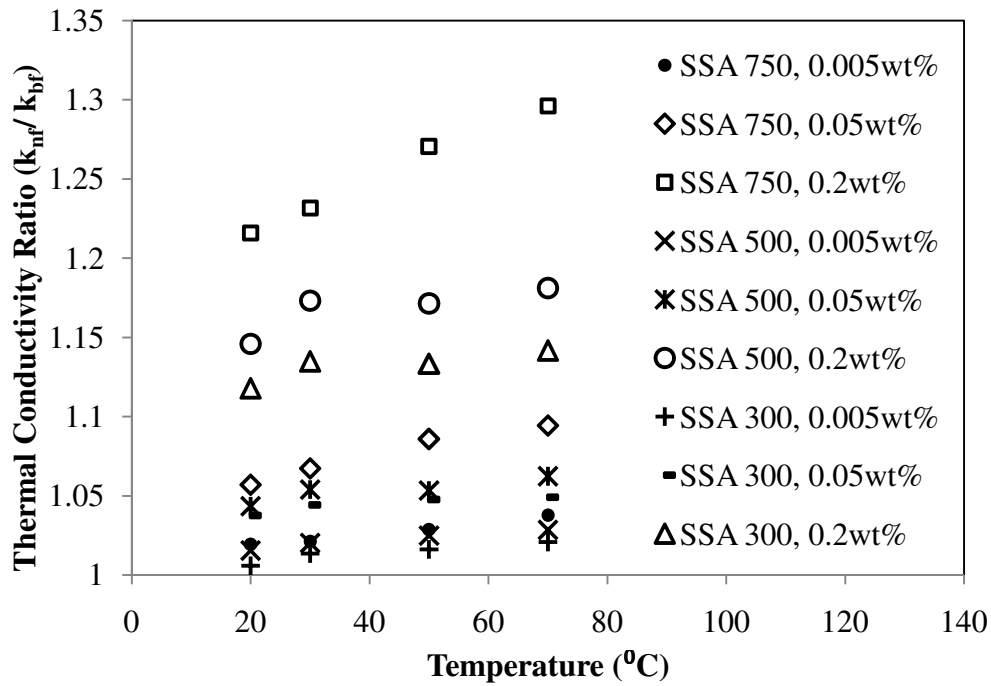


**Figure 4.45:** Effect of temperature on thermal conductivity ratio of kerosene-GNP nanofluids to pure kerosene at various particle concentration and sizes

In the present study the ratio of thermal conductivity of kerosene-GNP nanofluids increases from 1.23 to 1.30 for 750 GNPs, 1.15 to 1.18 for 500 GNPs and 1.15 to 1.14 for 300 GNPs particle size over the 20<sup>0</sup>C to 70<sup>0</sup>C temperature range respectively. The effect of temperature on thermal conductivity of nanofluids is higher for the 750 GNPs nanofluid as compared to the others. This can be attributed to the different sized GNP particles present in the kerosene-GNP nanofluid. The smaller sized particle undergo random movement and thereby contribute to the Brownian motion, whereas in the bigger sized particle the network like chain structure as postulated in percolation model could be dominant. Gupta et al. [44] also observed the similar hybrid behaviour of GNPs nanofluid and reported that the thermal conductivity of Graphene nanofluids lies in between CNT and metallic nanofluids.

Though the detailed measurement of thermal conductivity of kerosene-GNP nanofluids indicates similar trend as observed with kerosene-alumina nanofluids, the

observed thermal conductivity for kerosene-GNP nanofluid are much higher as compared to kerosene-alumina nanofluid at same particle concentration. Thermal conductivity of kerosene-GNP nanofluid is compared with kerosene-alumina nanofluid for similar mass concentration. Figure 4.46 presents the comparison of thermal conductivity ratio of 0.2wt% kerosene-GNP nanofluid with the case of 0.25wt% kerosene-alumina nanofluid, for all the particle sizes at various fluid temperature conditions. It can be clearly noted that thermal conductivity ratio of kerosene-GNP nanofluid to the base fluid is much higher as compared to kerosene-alumina nanofluid at all particle sizes and fluid temperatures. Thermal conductivity ratio is found to be 1.12, 1.15 and 1.22 for 0.2wt% 300SSA, 500SSA and 750 SSA kerosene-GNP nanofluids, respectively, at 20°C. For similar mass concentration of 13 nm and 50nm nanofluid samples, the thermal conductivity ratio is found to be only 1.04 and 1.02 at 25°C.

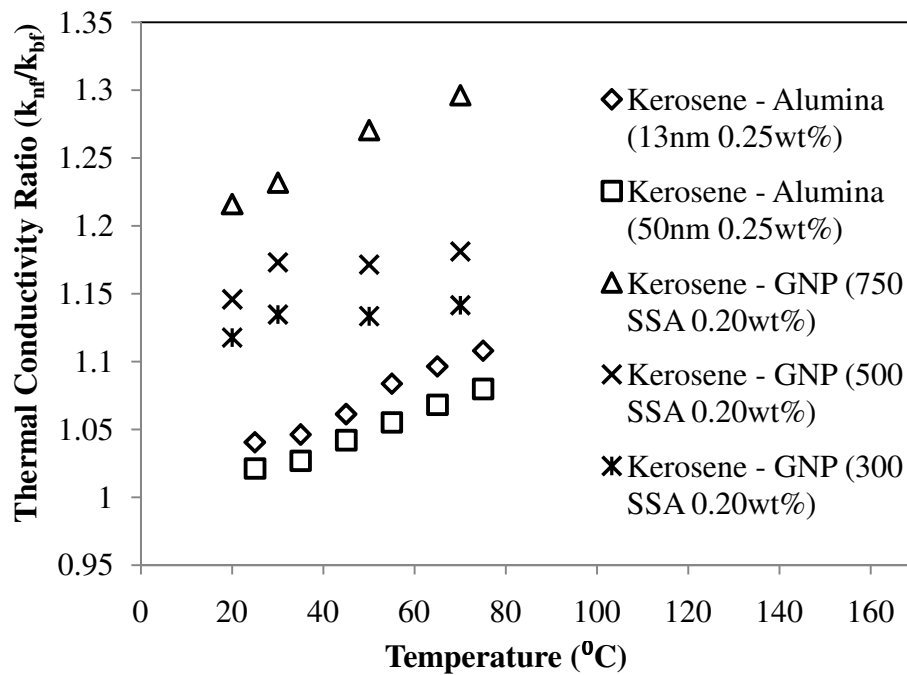


**Figure 4.46:** Effect of temperature on thermal conductivity of kerosene based nanofluids

The effect of temperature on the thermal conductivity of nanofluid is found to be significant for kerosene-alumina nanofluid compared to kerosene-GNP nanofluid. The

thermal conductivity ratio is found to increase from 1.22 to 1.30 for 750SSA kerosene-GNP nanofluid for a temperature range of 20°C to 70°C. Figure 4.47 presents the ratio of relative thermal conductivity of nanofluid to the base fluid at elevated temperature to the value at 20°C for both the type of nanofluids at similar particle concentration. It is to be noted that the thermal conductivity ratio increases by more than 2.5 times for kerosene-alumina nanofluid compared to only 1.3 times for kerosene-GNP nanofluid over a temperature range of 20°C to 70°C. It can be clearly seen from the figure that the rate of thermal conductivity enhancement with temperature is much higher for kerosene-alumina nanofluid as compared to kerosene-GNP nanofluid. The lesser effect of temperature observed in the thermal conductivity of kerosene-GNP nanofluid is similar to those observed by various previous researchers. As already explained, this observation is due to the combined mechanism of Brownian motion and percolation in kerosene-GNP nanofluid compared to Brownian motion in kerosene-alumina nanofluid.

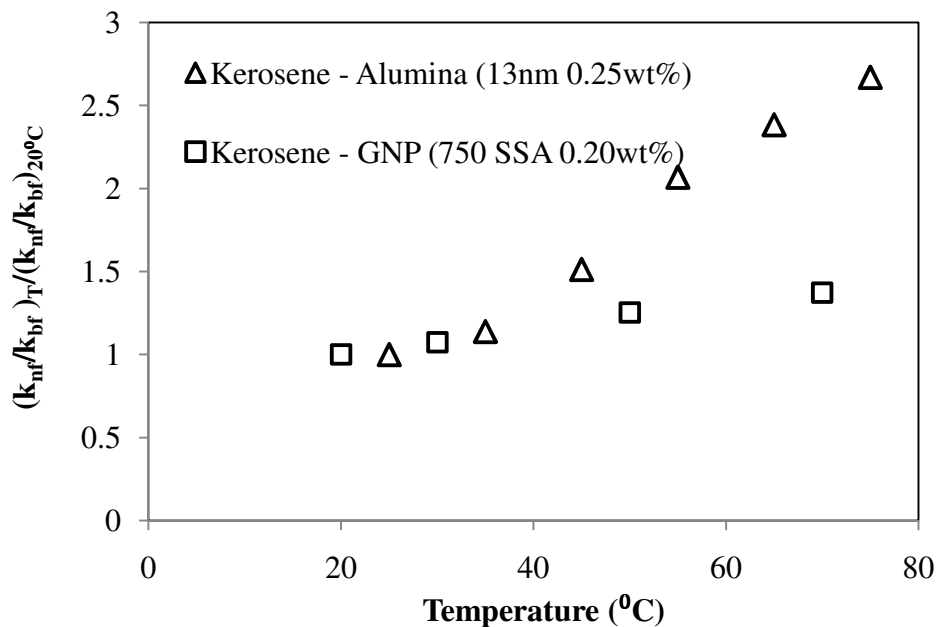


**Figure 4.47:** Relative increase in thermal conductivity of kerosene-GNP nanofluid to kerosene-Alumina nanofluid over various temperature ranges.

#### 4.2.4 Dynamic viscosity

Though the increased particle loading enhances the thermal conductivity of the nanofluid, the increased viscosity due to addition of nanoparticles in the base fluid increases the pressure head requirement of the heat transfer system and thus, poses a constraint in using nanofluids in heat transfer systems.

Nanofluids of particle mass fraction 0.005%, 0.02%, 0.05%, 0.1% and 0.2% are subjected to the measurement of dynamic viscosity for three particle sizes along with pure kerosene. Ratio of dynamic viscosity of nanofluids to the base fluid at various fluid temperatures and particle concentrations for 300, 500 and 750 SSA particle size is presented in Fig. 4.48. It is observed that the dynamic viscosity of nanofluid is higher as compared to the base fluid and the enhancement in viscosity increases with particle loading and specific surface area (SSA).

The increase in viscosity with particle concentration is due to the formation of agglomeration and clustered structure at higher concentration and could result in increased internal shear stress for the nanofluid. The increase in dynamic viscosity for higher SSA GNPs is large as compared to the lower SSA GNPs nanofluids. Higher surface area leads to higher interfacial resistance in the fluid layer and results in increased viscosity for 750 SSA GNPs nanofluid as compared to others. The ratio of dynamic viscosity of nanofluid to the base fluid is 1.076, 1.068 and 1.06 for 750, 500 and 300 GNP nanofluids respectively at 0.2wt % at 30 °C.

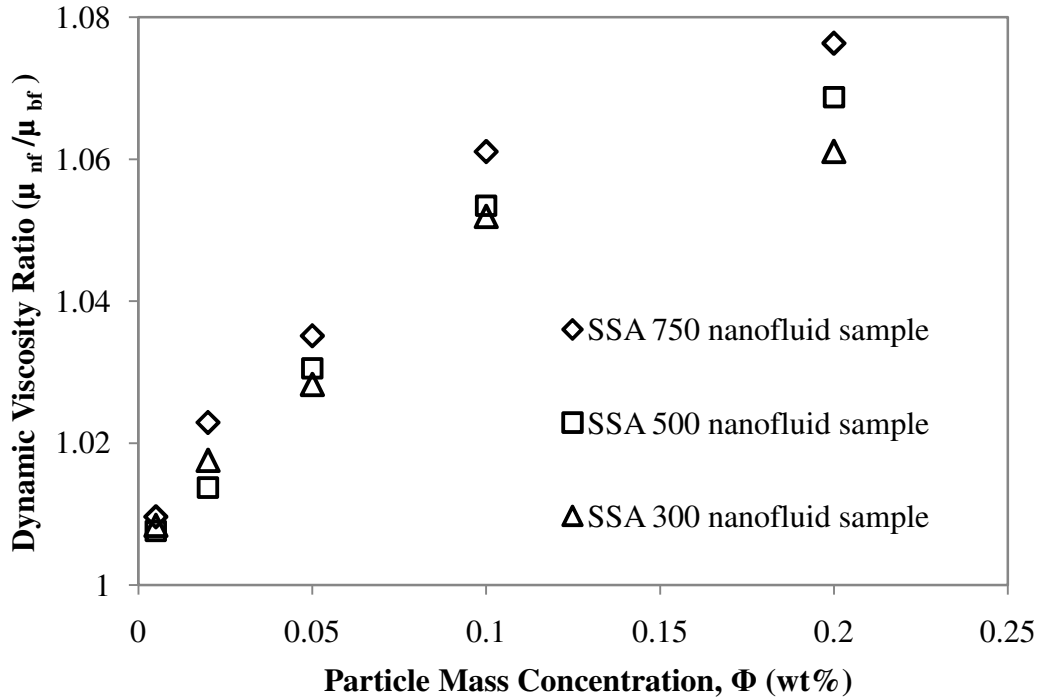


**Figure 4.48:** Effect of particle size on dynamic viscosity of kerosene-GNP nanofluid at various particle mass concentrations at 30<sup>0</sup>C

The effect of temperature on the viscosity of nanofluids is investigated by measuring the dynamic viscosity of 0.2 wt% nanofluid at various temperatures ranging from 20<sup>0</sup>C to 70<sup>0</sup>C. Dynamic viscosity of nanofluid for three sizes of GNP nanofluids along with pure kerosene is plotted in Fig. 4.49. The viscosity of nanofluid decreases rapidly with rise in temperature and exhibits an asymptotic behaviour. This behaviour is similar to the one observed for kerosene-alumina nanofluid. For the base fluid, as the temperature increases, the viscous shear stress decreases due to thermal expansion, thereby resulting in lower viscosity at high temperature. The decrease in nanofluid viscosity with increase in temperature is expected due to the weakening of the interparticle and intermolecular adhesion forces and similar trends have also been observed in almost all type of nanofluids by other researchers [91] and well as the study carried out for kerosene-alumina nanofluid.

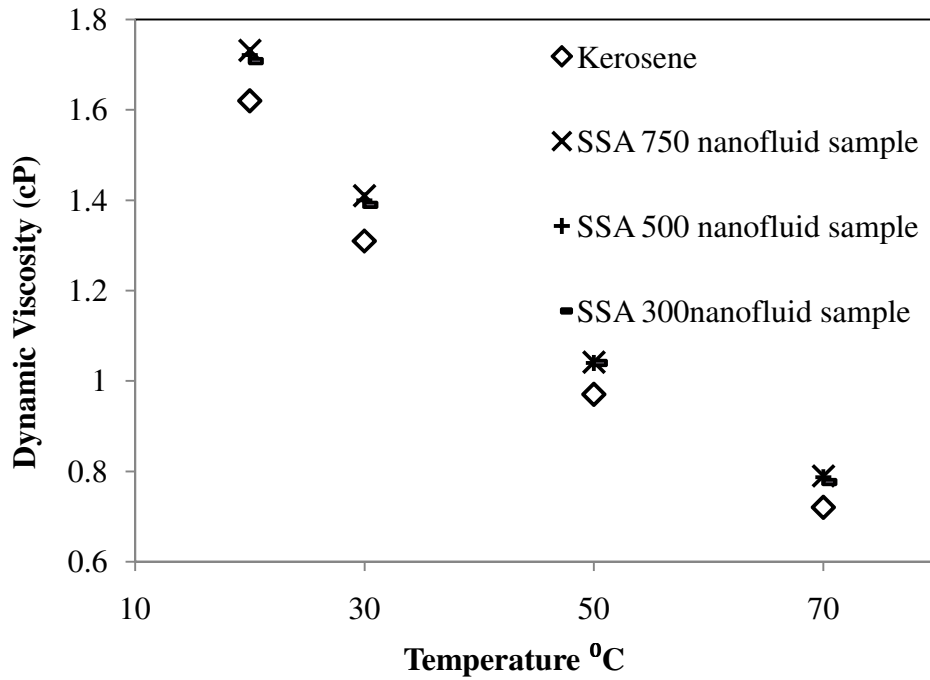


**Figure 4.49:** Effect of temperature on viscosity of kerosene-GNP nanofluid at 0.2wt%

#### 4.2.5 Stability of nanofluids

The consistency in the measured thermal conductivity and viscosity of the nanofluid with time indicates the stability of nanofluids. Thermal conductivity and viscosity of nanofluids are measured periodically and presented in Fig. 5.50 and 5.5,1 respectively as done in the case of kerosene-alumina nanofluid. It is observed that the thermal conductivity of 0.1wt% and 0.2wt% nanofluids indicates marginal drop over time for initial 20 days, and remain nearly constant afterwards. It is to be noted that the thermal conductivity of nanofluids at lower concentrations of 0.005 wt%, 0.02 wt% and 0.05wt% never indicates decreasing trend with time, and remains almost constant. This trend of thermo-physical property highlights significantly high stability for the current kerosene- GNP nanofluids and which is considered to be one of the prime requirements of such a fluid to be used for heat transfer application in rocket engines. This observation is in line with the observation

described in section 3.1.1 for particle size distribution for 0.05 wt% kerosene- GNP nanofluid.

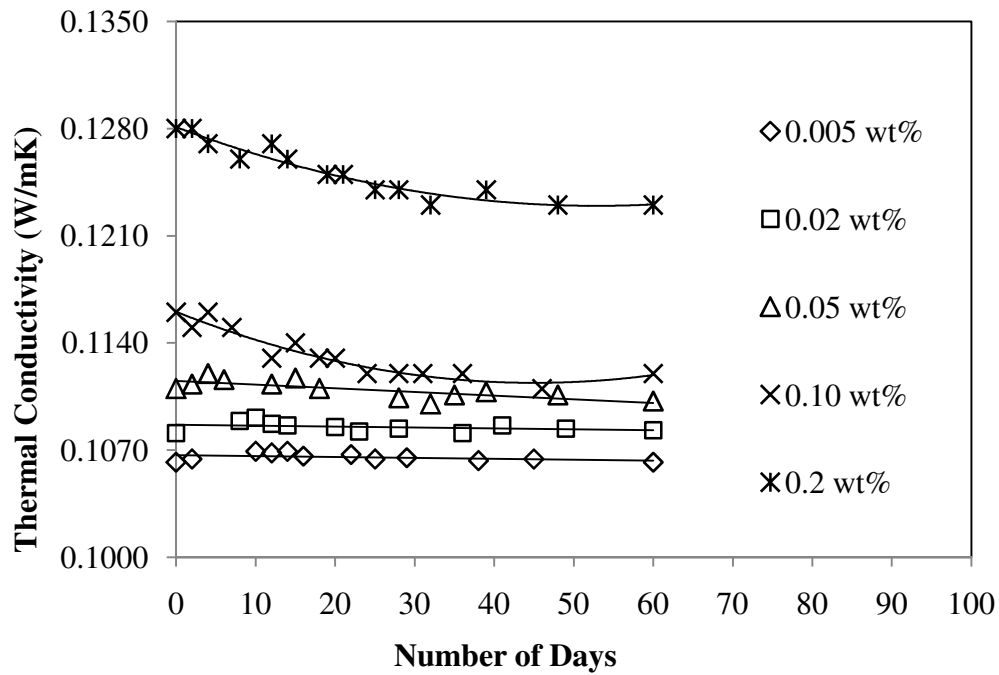


Figure 4.50: Thermal conductivity of 750 SSA kerosene- GNP nanofluid with time (days)

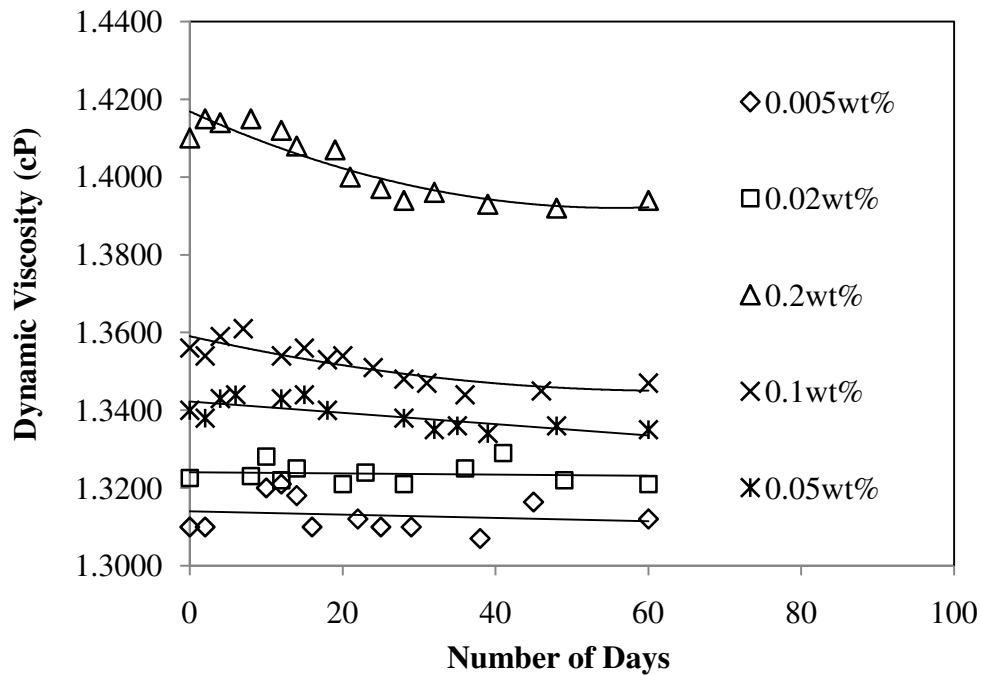


Figure 4.51: Dynamic Viscosity of 750 SSA kerosene- GNP nanofluid with time (days)

## **4.2.6 Convective heat transfer performance**

While an increase in effective thermal conductivity is an indication of improved heat-transfer behaviour of nanofluids, the effectiveness of nanofluid as heat transfer fluids is evaluated through the heat transfer coefficient. The convective heat transfer performance of any fluid depends upon various physical and thermo-physical properties. Though, the enhanced thermal conductivity of nanofluid will result in reduced resistance to thermal diffusion in the laminar sub layer, the increased viscosity of nanofluid could increase the thickness of sub layer and in turn, increase the thermal resistance to heat transfer.

### **4.2.6.1 Mouromtseff number ( $Mo$ )**

Before carrying out the heat transfer experiments using kerosene-GNP nanofluid, Mouromtseff number ( $Mo$ ) is employed to compare the fluid property related to heat transfer performance of a kerosene-GNP nanofluid to that of the pure kerosene. Figure 4.52 shows the Mouromtseff number estimated for 750, 500 and 300 SSA kerosene- GNP nanofluids at various particle concentrations. It can be observed that at all particle concentrations and for all particle sizes, the  $Mo$  number is greater than unity and this clearly indicates higher heat transfer performance of kerosene- GNP nanofluids over pure kerosene.

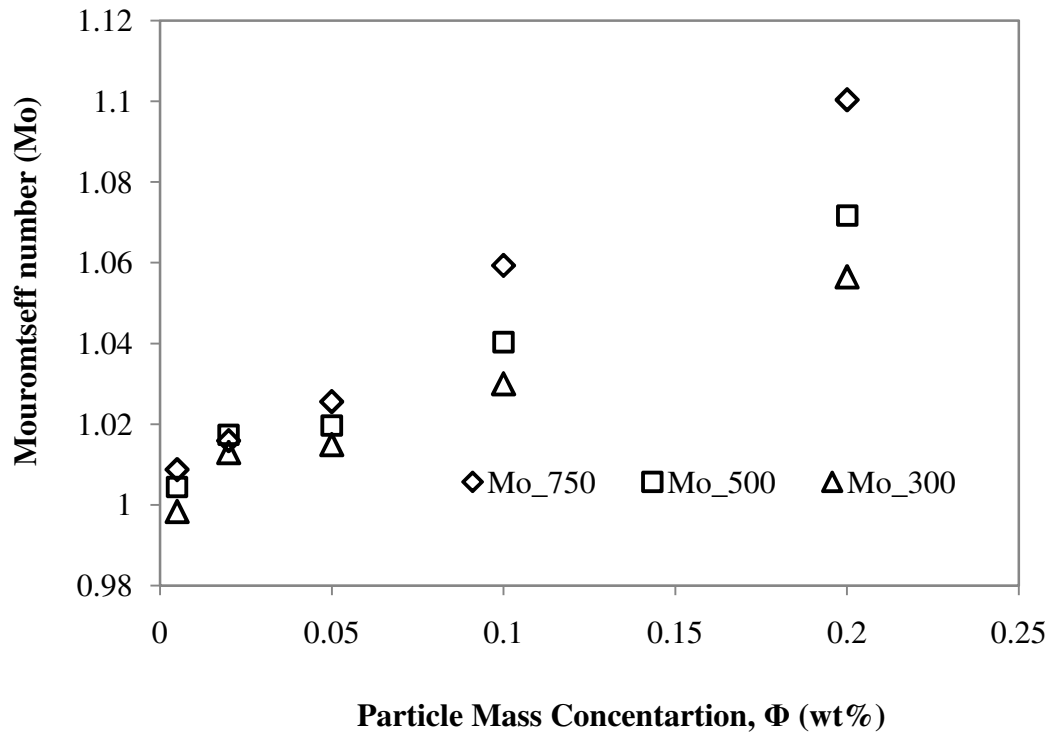


**Figure 4.52:** Mouromtseff number for kerosene-GNP nanofluid

#### 4.2.6.2 Convective heat transfer coefficient

Detailed investigation on convective heat transfer characteristics of nanofluids using the closed loop experimental test rig illustrated in Figs. 3.9 and 3.10, is carried out for 0.005wt%, 0.05wt% and 0.2wt% particle concentration kerosene-GNP nanofluids. Effect of particle specific surface area on heat transfer is experimentally studied for 750, 500 and 300 SSA GNPs nanofluids. As discussed earlier, thermo-physical properties at average film temperature  $((T_s+T_f)/2)$  is used for the estimation of heat transfer coefficient from the experimental data. Each experiment is repeated four times and the mean values are used for the subsequent analysis. The maximum dispersion in the calculated heat transfer coefficients among the experiments for any particular case is within  $\pm 2.7\%$ .

Figure 4.53 represents the heat transfer coefficient for 750, 500 and 300 SSA GNPs nanofluids derived from the experimental data at various particle concentrations and

Reynolds numbers. It is evident that kerosene- GNP nanofluids indicate enhanced heat transfer properties as compared to the pure kerosene at all Reynolds numbers. As expected, the heat transfer coefficient of the kerosene-GNP nanofluid is found to increase with Reynolds number and particle concentrations. Higher increase in heat transfer coefficient is noticed for higher SSA nanofluids at higher concentration. Highest increase in heat transfer coefficient is noticed for 0.2wt% 750 SSA kerosene-GNP nanofluid.

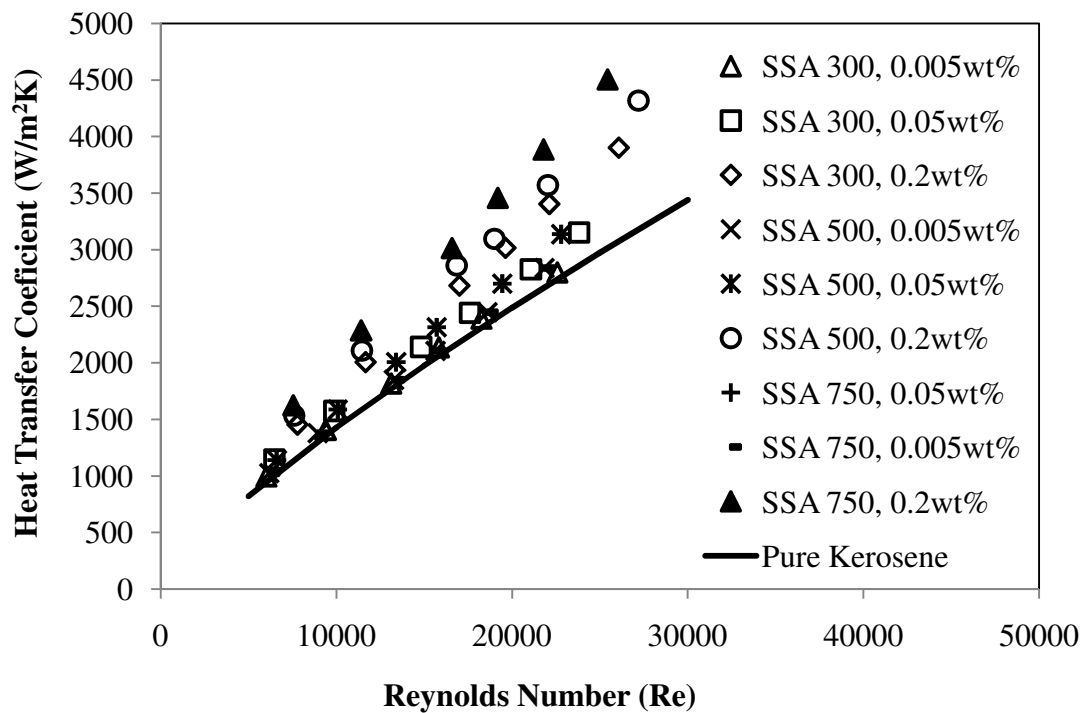


**Figure 4.53:** Heat transfer coefficient vrs Reynolds number for kerosene-GNP nanofluid

Ding et al. [24] proposed that a higher heat transfer coefficient observed using nanofluid is due to the increase in effective thermal conductivity ( $k$ ) of the nanofluid and the decrease in thickness of the thermal boundary layer ( $\delta$ ). The two effects together result in augmentation of heat transfer coefficient ( $h=k/\delta$ ). The hypothesis of thinning of boundary layer is developed based on the assumption of chaotic motion of nanoparticles in the nanofluid, which tends to disturb the boundary layer, resulting in thinning of the same. This

trend represented by Ding et al. [24] is also further discussed by Aravind and Ramaprabhu [3], and it is found to be true in the current investigation too. The large enhancement observed in convective heat transfer is due to increased thermal conductivity, particle re-arrangement; shear induced thermal conduction enhancement and the reduction in boundary layer thickness due to the presence of GNPs as discussed by Aravind and Ramaprabhu [3]. The possible reasons for boundary layer thickness reduction include particle migration in nanofluids due to shear action, viscosity gradient, and Brownian motion as discussed by Phillips et al. [98] and Ding et al. [24]. Further as suggested by Xuan and Li [139], the increase in effective thermal conductivity due to dynamic conditions could be another major factor for significant enhancement in convective heat transfer coefficient. It must be recalled that the thermal conductivity measurements carried out in the present study is at static conditions and significant effect of shear could exist in the flowing condition, which would improve the thermal conductivity of the nanofluid during convective experiments.

Figure 4.54 shows the ratio of convective heat transfer coefficient of nanofluid to base fluid at various values particle concentration and Reynolds numbers. Higher enhancement is noticed for higher SSA nanofluid for all particle mass fractions. The higher performance of lower sized particle (higher specific surface area) nanofluids is observed by many researchers in the past [123,141]. The maximum enhancement noticed is 49% for 750 SSA nanofluid and 37% for 500 SSA nanofluid at 0.2 wt% of GNPs in kerosene at identical Reynolds number criteria.

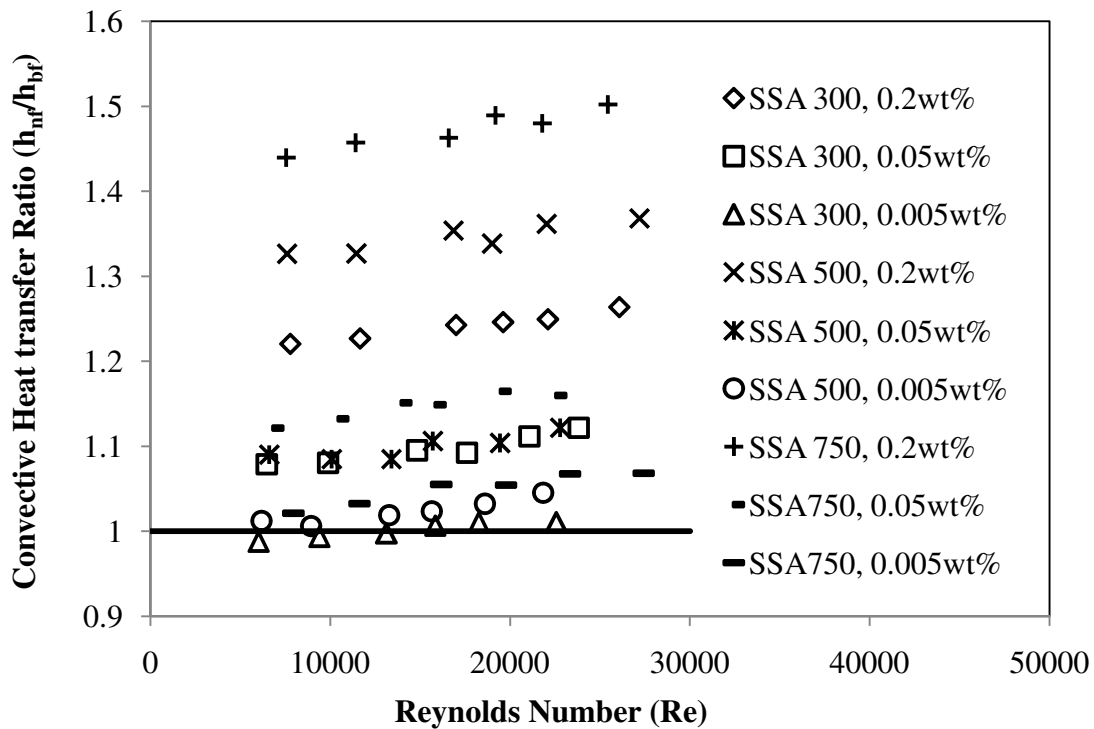


**Figure 4.54:** Ratio of heat transfer coefficient of nanofluid to base fluid with Reynolds number for kerosene-GNP nanofluid

As discussed earlier that the true enhancement in heat transfer of nanofluid to base fluid can be determined only by comparing experimental data for identical velocity conditions. Figure 4.55 presents the ratio of convective heat transfer coefficient of kerosene-GNP nanofluid to kerosene at various particle size and concentration values, for identical fluid velocity cases. It can be clearly seen from the figure that though, the enhancement ratio is found to be lesser for identical velocity based criteria in comparison to the identical Reynolds number based results, the heat transfer enhancement ratio is above unity for almost all the particle size and particle concentrations of kerosene-GNP nanofluids. Which clearly indicates higher thermal performance of these nanofluids as compared to pure kerosene alone. The maximum enhancement ratio for 0.2wt% kerosene-GNP nanofluid is found to be 1.37,

1.28 and 1.18 for 750 SSA, 500 SSA and 300SSA particle sizes respectively for identical flow velocity conditions.

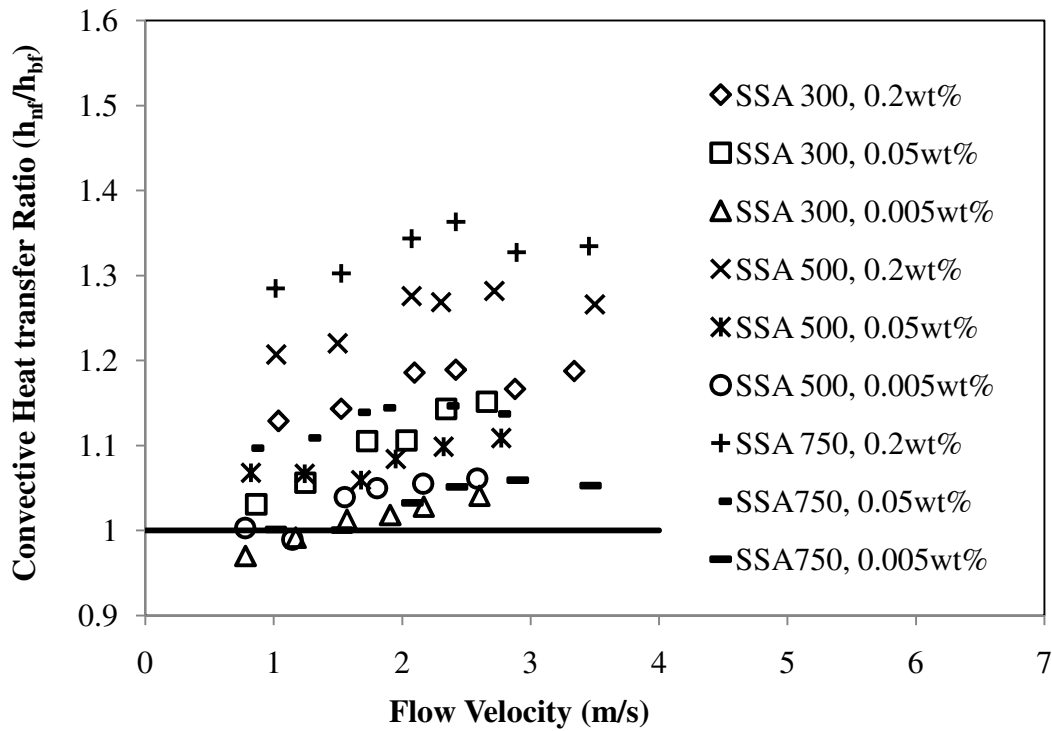


**Figure 4.55:** Ratio of heat transfer coefficient of kerosene-GNP nanofluid to base fluid with flow velocity

Figure 4.56 shows the comparison of convective heat transfer performance of kerosene-alumina and kerosene-GNP nanofluid at nearly identical particle concentrations. It is observed from Fig 4.56 that the ratio of convective heat transfer of 0.2wt% kerosene-GNP nanofluid to the base fluid is much higher as compared to the kerosene-alumina nanofluid. Convective heat transfer enhancement ratio is around 1.3 for kerosene-GNP nanofluid as compared to only 1.1 for kerosene-alumina nanofluid. It can be clearly observed from the figure that the heat transfer performance of kerosene-GNP nanofluid is significantly higher compared to kerosene-alumina nanofluid.

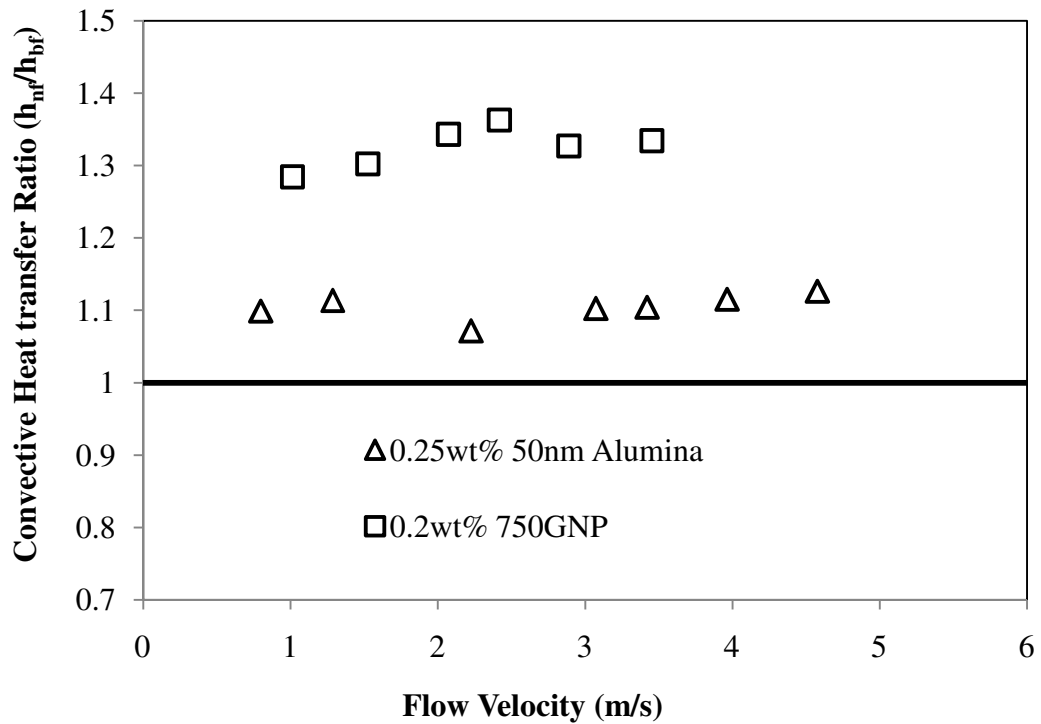


**Figure 4.56:** Comparison of heat transfer coefficient ratio for kerosene-alumina and kerosene-GNP nanofluid.

#### 4.2.6.3 Pressure drop and friction factor

Though the current investigation observed enhanced heat transfer coefficient of kerosene- GNP nanofluid, it is expected that the increased viscosity of nanofluids could also result in higher pressure drop. Higher pressure drop may limit nanofluid applicability in thrust chamber cooling as it may necessitate a bigger sized pump to push the fluid through the regenerative passage in thrust chamber.

The friction factor for kerosene- GNP nanofluid at various particle mass concentration and sizes is computed from the measured pressure drop. Figure 4.57 shows the variation of friction factor calculated in the present study along with the correlation developed using the measurements at various Reynolds number for kerosene-alumina nanofluid as presented in Eq. 4.6.

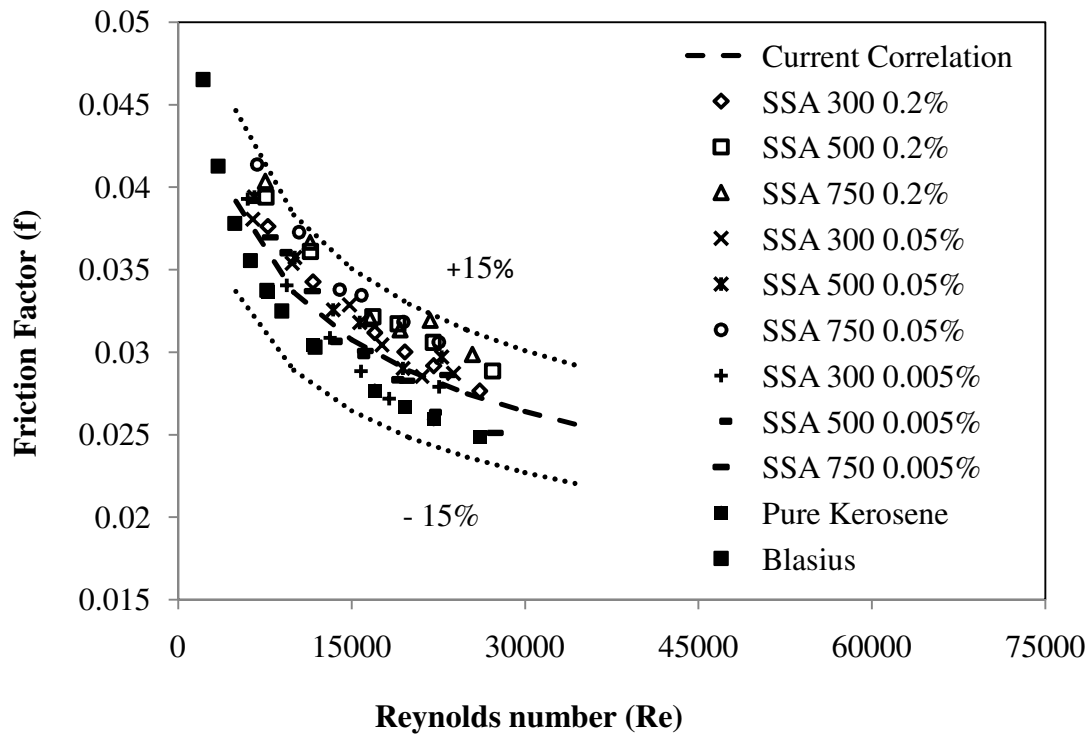


**Figure 4.57:** Friction factor with Reynolds number for kerosene-GNP nanofluid

It can be seen that the maximum dispersion in the friction factor developed for kerosene-alumina nanofluid from the experimental data of kerosene-GNP nanofluid is within 15%. The correlation represented by Eq. (4.6) is very similar to Blasius correlation ( $f = 0.314 \text{ Re}^{-0.25}$ ), and reveals that the homogeneous fluid correlation can be used to accurately predict pressure drop characteristics of the nanofluids as used in the current study. Though, the nanofluid friction factor obtained from the present study does not significantly differ from the pure fluid, the presence of higher friction factor is evident for higher SSA and also for higher concentration kerosene-GNP nanofluids. Maximum increase in friction factor is observed for 0.2wt% 750 SSA kerosene-GNP nanofluid.

The pressure drop and friction factor depend upon the Reynolds number and the GNP concentration. As expected, similar to the pure fluid, the friction factor decreases with

increase in Reynolds number. Table 4.5 shows the increase in friction factor at various GNP sizes and concentrations for Reynolds number range of 6000-30000. It can be noted that the higher enhancement in friction factor is noticed for 750 GNP nanofluids and it increases with particle concentration. At higher particle concentration, the density of fluid changes and results in higher viscous drag thereby increasing the friction factor. The dynamic viscosity of 750 SSA nanofluid is also noticed to be higher as compared to other particle sizes as discussed in section 4.2.4. The maximum enhancement in friction factor noticed in the present study is 21% for 0.2wt%, 750 SSA kerosene-GNP nanofluid.

**Table 4.5:** Increase in friction factor for kerosene-GNP nanofluid at various particle sizes and concentrations

<b>GNP size</b>	<b>Concentration (wt%)</b>	<b>Percentage increment in friction factor</b>
300	0.005	0-8
	0.05	8-12
	0.2	11-13
500	0.005	2-10
	0.05	10-15
	0.2	15-18
750	0.005	3-11
	0.05	14-18
	0.2	16-21

#### 4.2.6.4 Nusselt number

The variation in Nusselt number for kerosene- GNP nanofluid at various particle volume fractions with Reynolds number is shown in Fig. 4.58. The test data is compared with the Nusselt number correlation developed for kerosene-alumina nanofluid as presented in

section 4.1.6.7 ( $Nu = 0.005Re^{0.8}Pr$ ). It is evident that the data points are within  $\pm 12\%$  of the Nu correlation.

It is to be again noted the exponent of Prandtl number is found to increase from 0.4 as in Dittus- Boelter correlation to 1 in the current study, which indicates the significant role of Prandtl number in nanofluid convective heat transfer process.

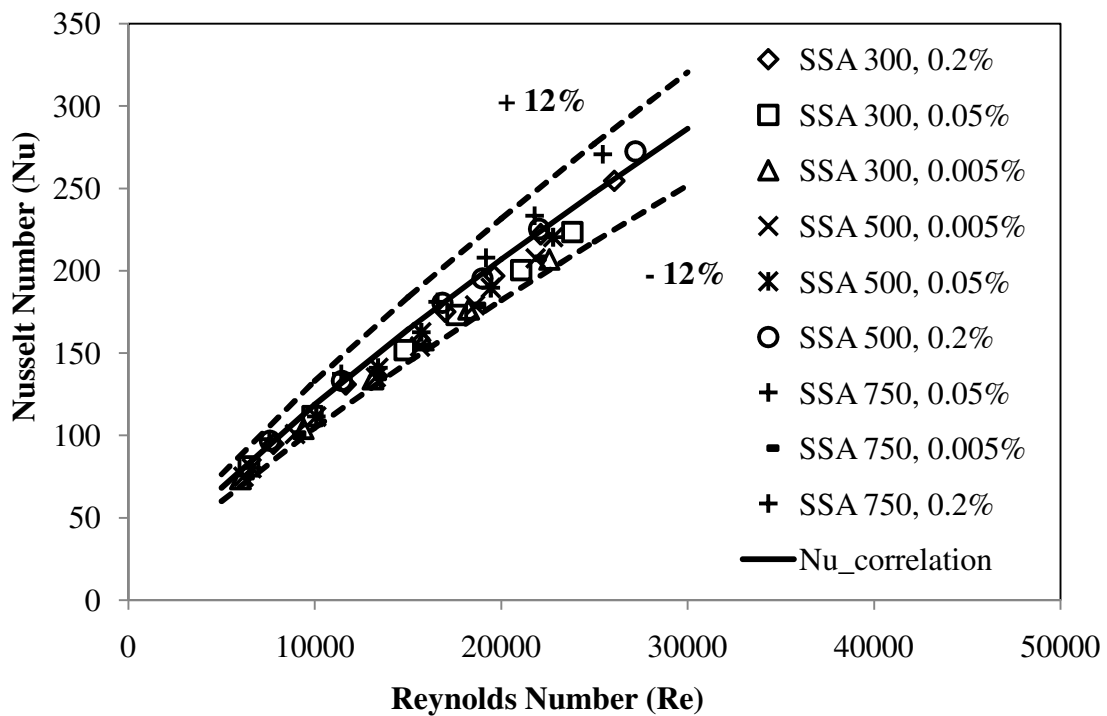


**Figure 4.58:** Nusselt number at various Reynolds number for kerosene-GNP nanofluid

The ratio of Nusselt number of kerosene-GNP nanofluid to pure kerosene at various particle concentrations and sizes are presented in Fig 4.59 and Fig.4.60 for identical Reynolds number and velocity based criteria, respectively. The maximum Nusselt number enhancement ratio obtained in the present study is 1.23 and 1.12 for identical Reynolds number and identical velocity criteria, respectively for 750SSA 0.2wt% kerosene-GNP nanofluid. It can be noted from the figures that the Nusselt number of kerosene-GNP nanofluid is higher than

those for pure kerosene at all Reynolds numbers for the particle concentration above 0.05wt% GNP. These results again indicate utility of these nanofluids for heat transfer applications.

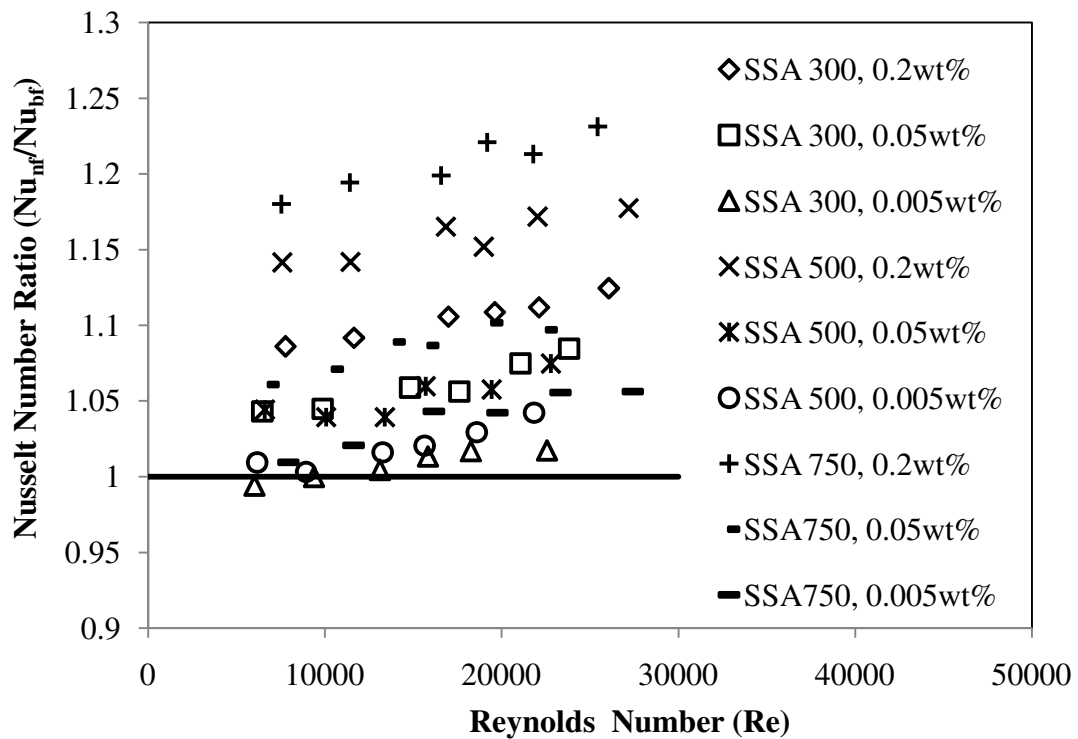


**Figure 4.59:** Ratio of Nusselt number of kerosene-GNP nanofluid to pure kerosene at various Reynolds number

Figure 4.60 show the ratio of Nusselt number of nanofluid to the base fluid at various particle concentrations and sizes for flow identical velocity conditions. It can be noted from the figure that in most of the cases the enhancement ratio is above one. The random experimental uncertainty observed for kerosene-GNP nanofluid in Nusselt number calculation is 4.9% which is lower than the Nusselt enhancement observed in the current study. The fixed error, which is common for both base fluid as well as nanofluid, can be excluded while evaluating the relative advantage of nanofluid over base fluid. Moreover, it can be seen from the figure that almost all the data points lie above 1 indicating a definite enhancement in Nusselt number using kerosene-GNP nanofluid. The study clearly indicates

improved heat transfer performance of 0.2wt% kerosene-GNP nanofluid compared to the pure kerosene even at identical velocity conditions.

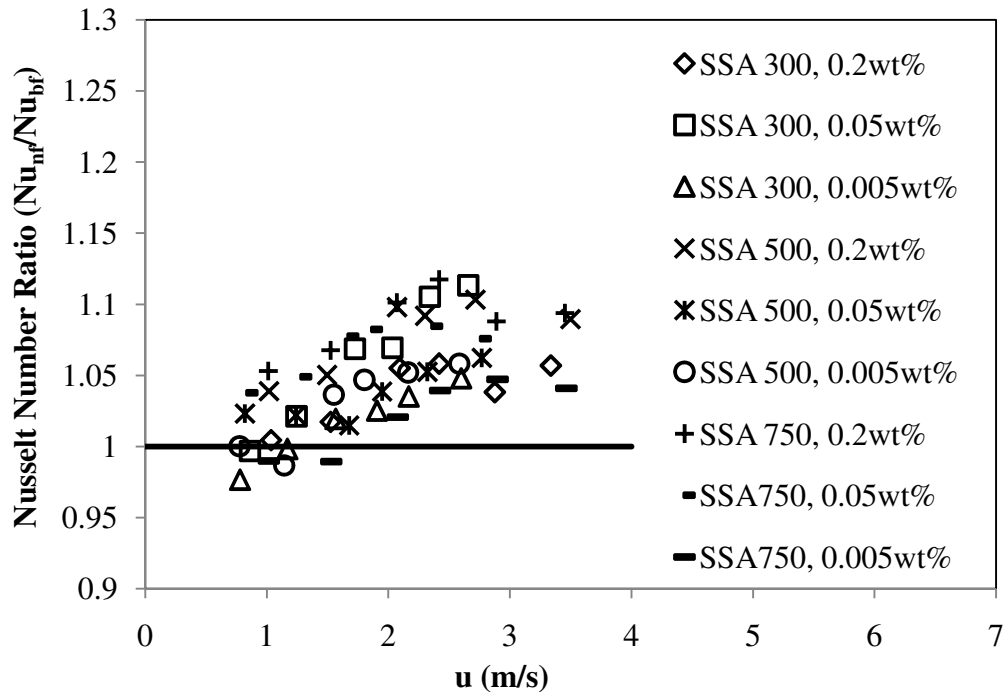


**Figure 4.60:** Ratio of Nusselt number of kerosene-GNP nanofluid to pure kerosene at various flow velocity conditions

#### 4.2.6.5 Total heat transfer performance

The total heat transfer performance of kerosene- GNP nanofluid is determined by Merit number. Merit number is used by Yu et al. [151] for evaluating the total heat transfer performance of kerosene- alumina and water- SiC nanofluid respectively. As explained earlier, it is defined as the ratio of heat transfer enhancement to the increase in pressure drop and the expression is provided in Eq. (3.2.7).

Figure 4.61 highlights the heat transfer performance of 750 and 500 SSA nanofluids based on merit number with respect to Reynolds number for 0.05% and 0.2% GNP mass concentrations. For nanofluid with particle mass fraction of 0.05%, Merit number is found to

be lower than one, and indicates lower performance of these nanofluids as a coolant. Merit Number is found to be above unity for 0.2% mass concentration nanofluid for both sizes of GNPs.

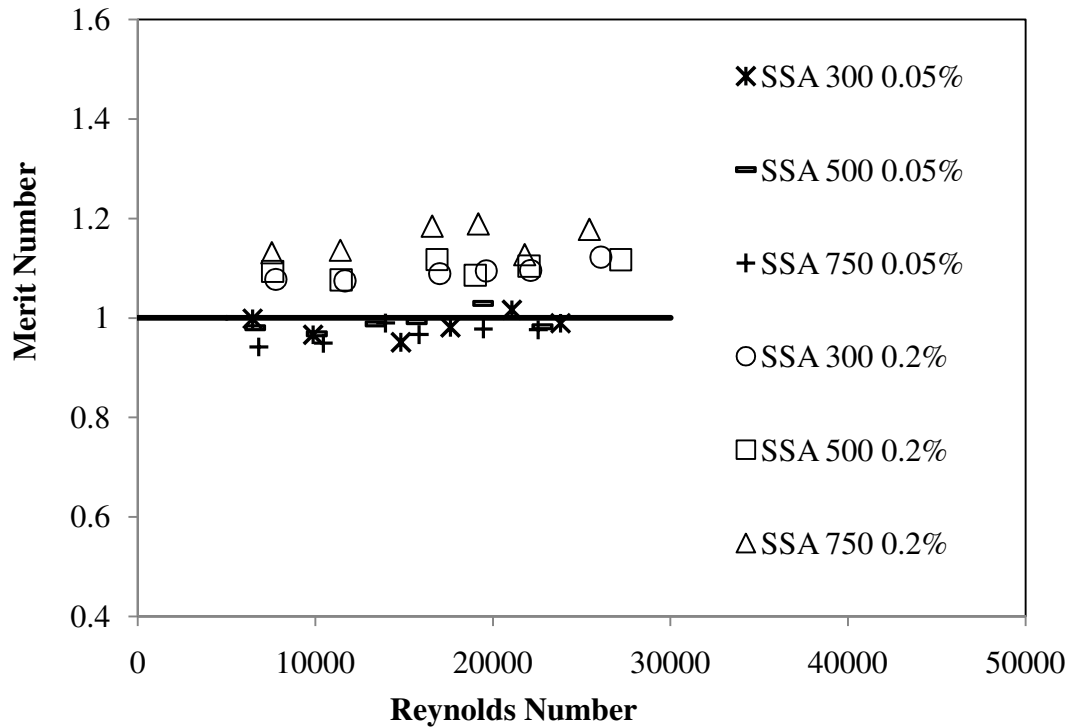


**Figure 4.61:** Variation in Merit number with Reynolds number for various particle size and concentrations of kerosene-GNP nanofluid

Figure 4.62 presents the heat transfer coefficient of nanofluid with respect to the measured pressure drop and the solid line in the figure represents the heat transfer coefficient of pure kerosene with respect to pressure drop. It is to be noted that the data points that occupy the region above the solid line indicate higher heat transfer performance of nanofluid as compared to pure kerosene for an identical value of pressure drop. Higher heat transfer coefficient with minimum pressure drop is observed for 0.2wt% nanofluid for all sizes of GNPs. The study clearly suggests that the total heat transfer performance of 0.2wt%

kerosene-GNP nanofluids is higher than that of pure kerosene and can be used as an effective coolant in regenerative passage of semi-cryo thrust chamber.

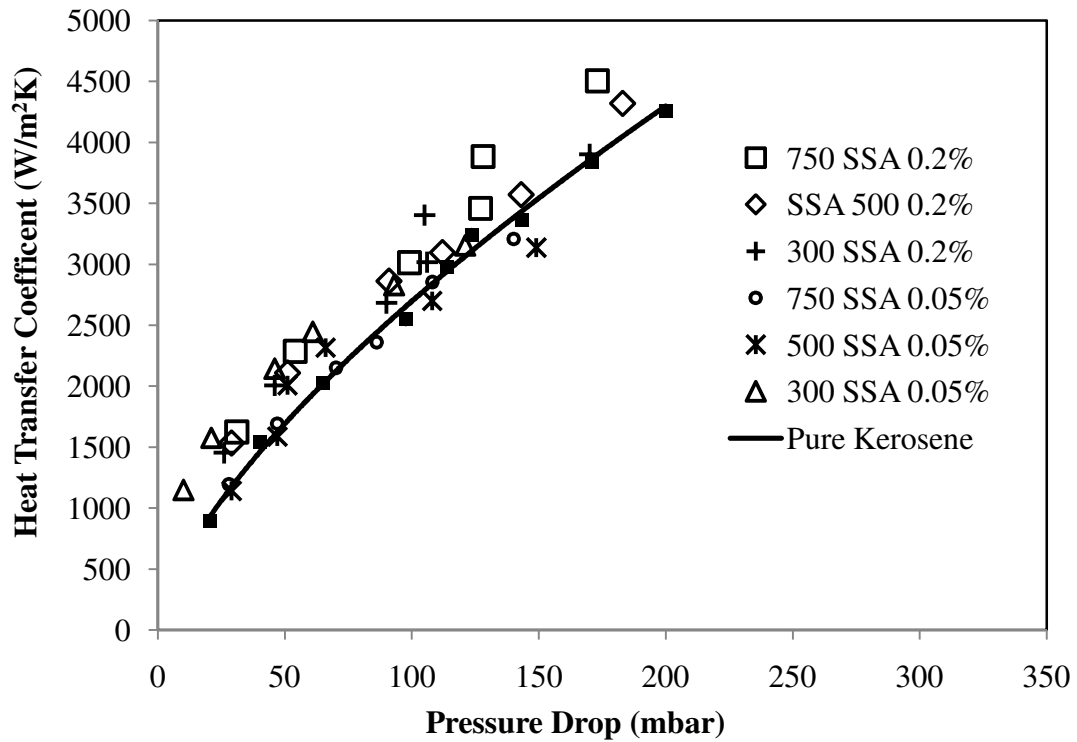


**Figure 4.62:** Heat transfer coefficient vrs pressure drop for kerosene-GNP nanofluid.

The current study carried out for kerosene-alumina and kerosene-GNP nanofluid clearly indicates higher heat transfer performance of kerosene based nanofluid over pure kerosene. The study concluded the potential use of these nanofluids in heat transfer application.

## **CHAPTER 5**

### **5 CONCLUSIONS**

The study aims at characterization and assessing the potential use of kerosene-based nanofluid for thrust chamber cooling in a semi-cryogenic rocket engine. In this regard, a comprehensive experimental study is carried out to prepare stable kerosene-alumina and kerosene-GNP nanofluid. Ultrasonic method, its duration and optimum quantity of surfactant is determined and finalized after series of experimental investigations for both the nanofluids. Precise measurements are made to determine thermal conductivity and viscosity of these nanofluids. Effect of particle loading, particle size and fluid temperature is determined based on the series of measurements performed on these fluids. A closed loop convective heat transfer setup is utilized to carryout convective flow experiments in turbulent flow regime. The heat transfer performance in conjunction with the pressure drop characteristics are used to determine the total heat transfer performance of these nanofluids. Following are the major outcomes of the study.

#### **5.1 Synthesis of Nanofluids**

Extensive studies with various ultrasonication methods are carried out to prepare stable kerosene-alumina and kerosene-GNP nanofluids. After a detailed study with various ultrasonication methods, disruptor flow cell type ultrasonic method is found to be more effective for preparing nanofluid. Various surfactants were investigated for the preparation of stable kerosene based nanofluid. Finally, Oleic acid and Oleylamine is found to be suitable surfactants for the preparation of stable kerosene-alumina and kerosene-GNP nanofluid

respectively. The optimum surfactant to particle mass ratio of 0.07 for kerosene-alumina and 0.3 for kerosene-GNP nanofluid is determined.

Dynamic Light Scattering (DLS) method used for particle size measurements, determines uniformity and stability of the nanofluid. Average alumina particle size in kerosene-alumina nanofluid as measured by DLS is 59 nm and 110 nm for the catalogue specified nanoparticle sizes of 13 nm and 50 nm respectively. The measured particle size in nanofluid is close to the dry particle size reported by the manufacture, indicates well dispersed nanoparticles in nanofluid without much agglomeration. Particle size measurement carried out for kerosene-alumina and kerosene-GNP nanofluid for several days after the nanofluid synthesis, also suggest good stability of current nanofluids with time. However, the stability is found to be significantly higher for kerosene-GNP nanofluid compared to kerosene-alumina nanofluid.

## **5.2 Thermal Conductivity and Dynamic Viscosity**

Stable kerosene-alumina, kerosene- GNP nanofluids are prepared and investigated for thermo-physical properties through detailed measurements. The effect of particle concentration, particle size and fluid temperature on thermo-physical properties of kerosene-alumina and kerosene-GNP nanofluids are determined.

The rate of increase in thermal conductivity of kerosene-alumina nanofluids is found to be significant at lower particle concentrations. For 13 nm kerosene alumina nanofluid sample the enhancement ratio in thermal conductivity of the nanofluid to pure kerosene increases from 1.01 to 1.09 over a particle loading of 0.01vol% to 0.1vol% and thereafter up to 1.33 for 1vol% for 13 nm kerosene-alumina nanofluid sample. Similar behavior of higher increase in thermal conductivity at lower particle concentration is reported in the literature by

Lee et al. [76] and it is attributed to factors like higher stability, homogeneity and the rate of agglomeration in nanofluids.

The thermal conductivity of nanofluid is found to be higher for smaller size particles nanofluids as compared to bigger particle size nanofluids for both the of nanofluids tested. The enhancement ratio observed in the present study is 1.33 and 1.26 for 1vol% kerosene-alumina nanofluid at particle sizes of 13nm and 50nm samples respectively. For kerosene-GNP nanofluid, the enhancement ratio is found to be 1.23, 1.16, 1.12 for 750SSA, 500SSA, 300SSA GNP sheets, respectively, at 0.2wt% particle concentration. The higher enhancement in thermal conductivity observed for lower sized particles is attributed to the larger particle surface area available and higher Brownian motion in smaller particle size nanofluids.

It is to be noted that the higher enhancement in thermal conductivity is noticed for kerosene-GNP nanofluid compared to kerosene-alumina at similar particle concentrations. The observed enhancement ratio of nanofluid to pure kerosene is 1.12 to 1.23 for 300 and 750SSA nanofluids respectively compared to only 1.02 to 1.04 for 50nm and 13nm particle size nanofluid samples, respectively for similar particle concentration. This is due to the thermal conduction in longer chain structure leading to percolation mechanism and higher thermal conductivity of GNPs compared to the alumina particles.

The role of temperature on the enhancement of thermal conductivity is found to be of a great significance for kerosene-alumina nanofluid. Higher increase in thermal conductivity for lower particle size and the existence of temperature dependency supports the hypothesis of Brownian motion/ nanolayer convection in kerosene-alumina nanofluids.

The enhancement in thermal conductivity ratio is found to be significant (1.5-3.0 times) for kerosene-alumina nanofluid as compared to kerosene-GNP nanofluid (1.1-1.4 times) over the temperature range of 20°C -70°C. The lower temperature dependency observed

in kerosene-GNP nanofluids as compared to kerosene-alumina nanofluid, is due to the presence of various size sheets in the GNPs. Brownian motion in smaller size sheets and thermal conduction in longer chain structure plays an important role for enhanced thermal conductivity of kerosene-GNP nanofluids.

Dynamic viscosity of nanofluids is found to be higher as compared to base fluids and exhibits an increasing trend with particle loading. The maximum increase in dynamic viscosity of nanofluid is 22.2% for 1vol% 13 nm kerosene-alumina nanofluid. The corresponding highest increase observed is 7.6% for the 0.2wt% 750 SSA kerosene-GNP nanofluid. Significantly higher viscosity is noticed for kerosene-GNP nanofluid as compared to kerosene-alumina nanofluid at similar particle concentrations. An increase in viscosity of 5.9%-7.6% for kerosene-GNP nanofluid at 0.2wt% particle concentration is noticed as compared to an insignificant increase ( $\mu_{nf}/\mu_{bf} < 1.02$ ) for kerosene-alumina nanofluid at similar particle concentrations. Higher increase in viscosity noticed for smaller sized nanoparticle nanofluid as compared to bigger sized particle nanofluid is due to higher surface area available for the case of smaller sized particles, which creates more resistance to flow and hence increases dynamic viscosity. Though, the absolute value of viscosity of nanofluid is found to be lower at high temperature, relatively higher enhancement in viscosity of nanofluids is noticed at high temperature which is again corroborated to the Brownian motion induced internal resistance in nanofluids.

### **5.3 Convective Heat transfer Performance**

Experimental investigation of convective heat transfer performance of kerosene based nanofluids at turbulent flow regime is carried out to determine its utility as a coolant in

regenerative cooling channel of semi cryogenic engine. Detailed convective heat transfer study is carried out at Reynolds number values from of 6000 to 30000.

In the present study convective heat transfer performance of the nanofluids at identical Reynolds number, velocity and Peclet number are compared. Results indicate enhanced heat transfer performance of nanofluid for all these cases. The maximum enhancement ratio noticed for nanofluid to the base fluid, in convective heat transfer performance noticed is 1.56 and 1.64 for 13 nm and 50 nm kerosene-alumina nanofluid samples at identical Reynolds number values. It is to be noted that though higher enhancement in thermal conductivity is noticed for smaller sized nanoparticle fluid, the convective heat transfer experiments carried out for kerosene-alumina nanofluid indicates lower heat transfer performance for smaller size particle nanofluids compared to bigger particle sized nanofluids. The reason for such behavior could be attributed to the combined effect of enhanced thermo-physical properties and increased disruption in the sub layer by bigger sized particles in kerosene-alumina nanofluid, this results in higher convective heat transfer performance in the kerosene-alumina nanofluid. However, for kerosene-GNP nanofluid, the higher convective heat transfer coefficient is noticed in higher SSA particle nanofluid. The maximum increase in convective heat transfer ratios is 1.49, 1.37 and 1.26 for 750SSA, 500SSA, 300SSA kerosene GNP nanofluids, respectively. The additional disturbance due to bigger sized particles as hypothesized for kerosene-alumina nanofluid will not be present in case of kerosene-GNP nanofluid.

The maximum enhancement ratio observed for 50 nm and 0.5vol% kerosene-alumina nanofluid is 1.64, 1.41 and 1.59 for identical Reynolds number, velocity and Peclet number, respectively. The maximum convective heat transfer enhancement ratio for 0.2wt% kerosene-GNP nanofluid is found to be 1.37, 1.28 and 1.18 for 750, 500 and 300 SSA respectively at

identical flow velocities. Though, the magnitude of increase in convective heat transfer coefficient is found to be lower for identical fluid velocities as compared to identical Reynolds number, the study clearly indicates significant improvement in convective heat transfer property of kerosene based nanofluids irrespective of the comparison method used for all the sizes. The lower heat transfer performance observed at velocity based criteria compared to others is due to increased dynamic viscosity of these nanofluids compared to pure fluids. Higher convective performance for kerosene-GNP nanofluids as compared to kerosene-alumina nanofluids at identical particle concentration is observed. Enhancement ratio for convective heat transfer performance is 1.37 for 750SSA kerosene-GNP nanofluid as compared to 1.1 for 50 nm kerosene-alumina nanofluid at similar particle concentrations.

Correlations for friction factor and Nusselt number is developed using the measured test data for Reynolds number varying from 6000 to 30000. All the measurements lie within  $\pm 20\%$  of the correlations for all the sizes and mass concentration of kerosene based nanofluids. Higher exponent of Prandtl number observed in Nusselt number correlations indicates the significant role of Prandtl number in convective heat transfer process in nanofluids as compared to pure fluids.

Merit number, which is a ratio of heat transfer enhancement to the increase in pressure drop, is used as a parameter to define total heat transfer performance of nanofluid and a value greater than unity indicates higher total heat transfer performance. Detailed analysis of convective heat transfer and measured pressure data shows Merit number to be above unity for nanofluids with particle mass concentration above 0.2wt% for kerosene-GNP nanofluids and above 1wt% for kerosene-alumina nanofluids, thereby encouraging the utility of these nanofluids for regenerative cooling of semi-cryogenic rocket engine.

The present work clearly shows the significant improvement in convective heat transfer performance of kerosene based nanofluids as compared to pure kerosene. Higher heat transfer performance is noticed for the kerosene-GNP nanofluid as compared to the kerosene-alumina nanofluid. The present study suggests the kerosene-GNP nanofluid as a potential candidate for thrust chamber cooling application.

#### 5.4 Future Scope

The experimental study carried out in the present work aims to exploring the potential of kerosene based nanofluids in liquid rocket engines for augmenting regenerative cooling performance in thrust chamber. The present work clearly demonstrated the significant improvement in heat transfer performance of kerosene based nanofluids over pure kerosene, which can improve the thrust chamber regenerative cooling efficiency in semi-cryogenic engine. However, the study in the present work is limited in many aspects and if the kerosene is to be replaced as kerosene based nanofluid in semi cryogenic engine, the following studies need to be carried out.

The effect of nanoparticle flow velocity on metal erosion is not well studied in the literature. Nguyun et al [92] have carried out the heat transfer study using jet impingement configuration for water-alumina nanofluid with 5vol% concentration and reported significant wear due to particle impingement. However it is to be noted that the particle concentration in the current study is much lower (0.5vol%) as compared to Nguyun et al [92] and in the current study the particles will not directly impinge on the tube surface. The erosion may not be significant at lower particle concentrations. However this needs to be further investigated.

Yu et al. [145] studied the tribological effects of copper nanoparticles in lubricating oil. The conclusion drawn from the experiment was that the protective copper film of low

hardness provided both wear and friction reduction. Wang et al. [124] researched a method to suspend copper nanoparticles in oil for testing with regards to tribological performance. They concluded that a reduction of friction at low loadings of copper nanoparticles was possible with a nanofluid of good dispersion and stability characteristics. Moshkovith et al., [87] studied the effects of dispersion process as a precursor to tribological testing using 120 nm diameter, inorganic fullerene, tungsten disulfide particles. This study emphasized on the dispersion of nanofluid prior to experimental testing. Literature review clearly indicates significant reduction in friction for well dispersed and stable nanofluids. This aspect of kerosene based nanofluid must be addressed before employing it for regenerative cooling of LRE.

It is to be noted that any oxide of aluminium particles will not participate in combustion processes in thrust chamber and hence will not improve energy generation resulting in insignificant change in specific impulse ( $I_{SP}$ ) of the rocket engine. Pure aluminium particles are widely used in solid motor rocket engine to improve combustion characteristics. Current study did not deal with pure aluminium nanoparticles due to the nature of sudden exothermic reaction of aluminium particles when it comes in contact with ambient air.

However, as explained earlier graphene can be alternatively used due to its heat release characteristics similar to pure aluminium. The current study clearly demonstrated superior heat transfer performance of kerosene-GNP nanofluid compared to pure kerosene. As GNP participates in combustion phenomenon inside a rocket thrust chamber, the  $I_{SP}$  of the system can also improve along with the cooling performance. However, before actually utilizing this novel nanofluid in rocketry, much more research has to be carried out. Few of the future research activities are listed below.

- As the pressure in the regenerative passage and the combustion chamber is very high (30-40 MPa), stability and thermo-physical properties of these nanofluids at high working pressure is to be assessed.
- Coking temperature of kerosene is around 560K. Experiments need to be performed at elevated temperature (fluid temperature up to 600K) to address its effect on coking temperature.
- High pressure pumps are used in LRE to supply propellant from tank to the thrust chamber. The pump performance with the use of a nanofluid is to be determined. Detailed study needs to be done for the rheological properties of these nanofluids in concern with appropriate operating conditions.
- Detailed study needs to be carried out to understand the behaviour of spray characteristics and the combustion characteristics of these nanofluids.
- The effect of high velocity nanoparticle impingement on a surface needs to be studied in the turbulent flow regime to determine the surface erosion characteristics of coolant channels.
- Tribological behaviour of these nanofluids needs to be determined to understand its behaviour in rotating parts of LRE.
- All above study can also be carried out for kerosene-aluminium nanofluid.

## 6 REFERENCES

- [1] Ahmad A., Sadri R., Shanbedi M., Ahmadi G., Chew B.T., Kazi S.N., Dahari M., Performance dependence of thermo syphon on the functionalization approaches: An experimental study on thermo physical properties of graphene nanoplatelet-based water nanofluids, *Energy Conservation and Management* 92 (2015) 322-330.
- [2] Anoop K. B., Sundararajan T., Das S. K., Effect of particle size on the convective heat transfer in nanofluid in the developing region, *International Journal of Heat and Mass Transfer* 52 (2009) 2189-2195.
- [3] Aravind S S J., Baskar P., Baby T. T., Sabareesh R. K., Das S., and Ramaprabhu S., Investigation of structural stability, dispersion, viscosity, and conductive heat transfer properties of functionalized carbon nanotube based nanofluids, *Journal of Physical Chemistry C* 115, no. 34 (2011): 16737-16744.
- [4] Assael M. J., Chen C. F., Metaxa I., Wakeham W. A., Thermal conductivity of suspensions of carbon nanotubes in water, *International Journal of Thermophysics*. (2004) ;25(4):971-85.
- [5] Baby, T. T., Ramaprabhu S. Investigation of thermal and electrical conductivity of graphene based nanofluids, *Journal of Applied Physics* 108, no. 12 (2010): 124308.
- [6] Baby, T. T., Ramaprabhu S., Enhanced convective heat transfer using graphene dispersed nanofluids, *Nanoscale Research Letters* 6, no. 1 (2011): 1-9.

- [7] Baby, T. T., Ramaprabhu S., Synthesis and nanofluid application of silver nanoparticles decorated graphene, *Journal of Materials Chemistry* 21, no. 26 (2011): 9702-9709.
- [8] Bahrami, M., Yovanovich, M.M. and Culham, J. R., Assessment of relevant physical phenomena controlling thermal performance of nanofluids, *In ASME (2006) International Mechanical Engineering Congress and Exposition (pp. 187-198). American Society of Mechanical Engineers.*
- [9] Balandin, A. A., Ghosh S., Bao W., Calizo I., Teweldebrhan D., Miao F., and Lau C. N., Superior thermal conductivity of single-layer graphene, *Nano Letters* 8, no. 3 (2008): 902-907.
- [10] Beck M. P., Yuan Y., Warriar P., Teja A. S., The effect of particle size on the thermal conductivity of alumina nanofluids, *Journal of Nanoparticle Research* (2009) 11:1129-1136.
- [11] Biercuk M. J., Llaguno M. C., Radosavljevic M., Hyun J. K., Johnson A. T., Fischer J. E., Carbon nanotube composites for thermal management, *Applied Physics Letters*. (2002); 80(15):2767-9.
- [12] Brunauer, S., Emmett, P. H. and Teller E., Adsorption of gases in multimolecular layers, *Journal of the American Chemical Society*, 60(2), (1938) pp.309-319.
- [13] Buongiorno J., Venerus D. C., Prabhat N., Mckrell T., Townsend J., A benchmark study on the thermal conductivity of nanofluids, *Journal of Applied Physics* 106 09312 (2009) 1-14.

- [14] Carslaw, H. S., and Jaeger J. C., Conduction of heat in solids. Vol. 2. Oxford: Clarendon Press, (1959).
- [15] Choi S. U. S, Eastman J. A., Enhancing thermal conductivity of fluids with nanoparticles, *Report submitted to Argonne National Laboratory, Illinois (United States), (1995), ANL/MSD/CP-84938.*
- [16] Choi T. Y., Maneshian M. H., Kang B, Chang W. S., Han C. S., Poulikakos D., Measurement of the thermal conductivity of a water-based single-wall carbon nanotube colloidal suspension with a modified 3-omega method, *Nanotechnology.* (2009) ;20(31).
- [17] Choi, S. U. S., Zhang Z. G., Yu W., Lockwood F. E., Grulke E. A. Anomalous thermal conductivity enhancement in nanotube suspensions. *Applied Physics Letters* 79, no. 14 (2001): 2252-2254.
- [18] Das S. K, Putra N., Thiesen P., Roetzel W., Temperature dependence of thermal conductivity enhancement for nanofluids, *ASME Journal of Heat Transfer*, 125 (2003) 567-574.
- [19] Das S. K., Choi S. U. S, Patel H. E., Heat transfer in nanofluids - a review, *Heat Transfer Engineering* 27 (10) (2006) 3-19.
- [20] Das S. K., Choi S. U. S., Yu W., Pradeep T., Nanofluids-Science and Technology, *John Wiley & Sons, (2008).*
- [21] Davies J. T., , Gas/Liquid and Liquid/Liquid Interface, Proceedings of the International Congress of Surface Activity, (1957), pp. 426–38

- [22] Derjaguin, B. V., A theory of the heterocoagulation, interaction and adhesion of dissimilar particles in solutions of electrolytes, *Discussions of the Faraday Society 18 (1954): 85-98.*
- [23] Dhar P, Gupta S. S., Chakaraborty S., Pattamatta A., Das S. K., The role of percolation and sheet dynamics heat conduction in poly dispersed graphene nanofluids, *Physics Review Letter 163114 (2013).*
- [24] Ding, Y, Alias H., Wen D., Williams R. A., Heat transfer of aqueous suspensions of carbon nanotubes (CNT nanofluids), *International Journal of Heat and Mass Transfer 49, no. 1 (2006): 240-250.L*
- [25] Eapen, J., Williams W. C., Buongiorno J., Hu Lin-wen, Yip S., Rusconi R., Piazza R. Mean-field versus microconvection effects in nanofluid thermal conduction, *Physical Review Letters 99, no. 9 (2007): 095901.*
- [26] Eastman J. A., Choi S. U. S., Li S., Thompson L. J., Lee S., Enhanced thermal conductivity through the development of nanofluids, *Proceeding of the Symposium on Nanophase and Nanocomposite Materials II, 457( 1997) Material Research Society, Boston.*
- [27] Eastman J. A., Phillpot S. R., Choi S. U. S., Keblinski P., *Annual Review of Materials Research. (2004) ;34:6.*
- [28] Eastman, J. A., Choi S. U. S., Soyez G., Thompson L. J., Dimelfi R. J., Novel thermal properties of nanostructured materials, *Materials Science Forum, (Metastable, Mechanically Alloyed and Nanocrystalline Materials): (1999), 312-314 p. 629-634.*

- [29] Eastman, J. A., Choi, S. U. S., Li, S., Yu, W., Thompson, L. J., Anomalously increased effective thermal conductivities of ethylene glycol-based nanofluids containing copper nanoparticles, *Applied Physics Letters*, 78(6), (2001), 718-720.
- [30] Eastman, J. A., Phillpot S. R., Choi S. U. S., Keblinski P. Thermal transport in nanofluids 1. *Annual. Rev. Mater. Res.* 34 (2004): 219-246.
- [31] Einstein, Albert., On the theory of the Brownian movement, *Annalen der physik* 4, no. 19 (1906): 371-381.
- [32] Elias M. M., Miqdad M., Mahbubul I. M., Saidur R., Kamalisarvestani M., Sohel M. R., Hepbasli A., Rahim N. A., Amalina M. A., Effect of nanoparticle shape on the heat transfer and thermodynamic performance of a shell and tube heat exchanger, *International Communications in Heat and Mass Transfer*, 44 (2013) 94-99.
- [33] Evans, W., Fish J., Keblinski P., Role of Brownian motion hydrodynamics on nanofluid thermal conductivity, *Applied Physics Letters* 88, no. 9 (2006): 093116.
- [34] Fan, J. and Wang, L., Review of heat conduction in nanofluids, *Journal of Heat Transfer*, (2011)133(4), p.040801.
- [35] Fedele L., Colla L., Bobbo S., Barison S., Agresti F., Experimental stability analysis of different water based nanofluids, *Nanoscale Research Letters* 6 1 300 (2011) 1-8.
- [36] Feng, Y., Yu, B., Xu, P., and Zou, M., The Effective Thermal conductivity of nanofluids based on the nanolayer and the aggregation of nanoparticles, *Journal of Physics D: Applied Physics*, (2007),40(10), pp. 3164-3171.

- [37] G. Batchelor, The effect of Brownian motion on the bulk stress in a suspension of spherical particles, *Journal of Fluid Mechanics*. 83 (1977) 97–117.
- [38] Gao, J. W., Zheng R. T., Ohtani H., Zhu D. S., and Chen G., Experimental investigation of heat conduction mechanisms in nanofluids: Clue on clustering, *Nano Letters* 9, no. 12 (2009): 4128-4132.
- [39] Geiger, G. H., and Poirier, D. R., Transport phenomena in metallurgy, *Addison-Wesley, Reading, (1973) PA*.
- [40] Ghadimi A., Saidur R., Metselaar H. S. C., A review of nanofluid stability properties and characterization in stationary conditions, *International Journal of Heat and Mass Transfer* 54 (2011) 4051-4068
- [41] Gharagozloo P. E., Eaton J. K., Goodson K. E., Diffusion, aggregation, and the thermal conductivity of nanofluids. *Applied Physics Letters*. (2008);93(10).
- [42] Griffin, William C., Calculation of HLB values of non-ionic surfactants, *Journal of the Society of Cosmetic Chemists (1954) 5 (4): 249-56*.
- [43] Griffin, William C., Classification of Surface-Active Agents by 'HLB, *Journal of the Society of Cosmetic Chemists (1949) 1 (5): 311-26*.
- [44] Gupta, S.S., Siva, V.M., Krishnan, S., Sreeprasad, T.S., Singh, P.K., Pradeep, T. and Das, S.K., Thermal conductivity enhancement of nanofluids containing graphene nanosheets, *Journal of Applied Physics*, (2011) 110(8), p.084302.

- [45] Haghghi, E. B., Mohsin Saleemi, N. N., Ghadamgahi, M., Khodabandeh, R., Palm, B., Toprak, M. S. and Muhammed, M., Measurement of temperature-dependent viscosity of nanofluids and its effect on pumping power in cooling systems. *International Conference on Applied Energy, Pretoria. (2013)*
- [46] Haghghi, E. B., Saleemi, M., Nikkam, N., Anwar, Z., Lumbreras, I., Behi, M., ...& Palm, B. Cooling performance of nanofluids in a small diameter tube. *Experimental Thermal and Fluid Science, (2013) 49, 114-122.*
- [47] Hamilton R. L. and Crosser O. K., Thermal conductivity of heterogeneous two component systems, *Industrial & Engineering Chemistry Fundamentals, 1 3 (1962) 187-191.*
- [48] Harish, S., Ishikawa K., Chiashi S., Shiomi J., and Maruyama S., Anomalous thermal conduction characteristics of phase change composites with single-walled carbon nanotube inclusions. *The Journal of Physical Chemistry C 117, no. 29 (2013): 15409-15413.*
- [49] Harish, S., Ishikawa K., Einarsson E., Aikawa S., Chiashi S., Shiomi J., Maruyama S., Enhanced thermal conductivity of ethylene glycol with single-walled carbon nanotube inclusions. *International Journal of heat and mass transfer 55, no. 13 (2012): 3885-3890.*
- [50] He, Y., Jin, Yi., Chen, H., Ding, Y., Cang, D., Lu, H., Heat transfer and flow behaviour of aqueous suspensions of TiO<sub>2</sub> nanoparticles (nanofluids) flowing upward through a vertical pipe. *International Journal of Heat and Mass Transfer (2007) 50, 2272-2281.*

- [51] Henderson, J. R. and van Swol, F., On the interface between a fluid and a planar wall: theory and simulations of a hard sphere fluid at a hard wall, *Molecular Physics*, (1984) 51(4), pp.991-1010.
- [52] Heris S. Z., Esfahany M. N., Etemad S. G., Experimental investigation of convective heat transfer of Al<sub>2</sub>O<sub>3</sub>/water nanofluid in circular tube, *International Journal of Heat and Fluid Flow* (2007) 28, 203-210.
- [53] Heyhat M. M., Kowsary F., Rashidi A. M., Momenpour M.H., Amrollahi A., Experimental investigation of laminar convective heat transfer and pressure drop of water-based Al<sub>2</sub>O<sub>3</sub> nanofluids in fully developed flow regime, *Experimental Thermal and Fluid Science*, (2013) 44, 483-489.
- [54] Horton, M., Hong H., Li C., Shi B., Peterson G. P., Jin S., Magnetic alignment of Ni-coated single wall carbon nanotubes in heat transfer nanofluids, *Journal of Applied Physics* 107, no. 10 (2010): 104320.
- [55] Hosseini S. Sh., Adam N. M., Goudarzi K., Effect of temperature increasing on nanofluid structure, *Australian Journal of Basic and Applied Sciences* 5 (9) (2011) 979-984.
- [56] Hwang K. S., Jang S. P., Choi S. U. S., Flow and convective heat transfer characteristics of water-based Al<sub>2</sub>O<sub>3</sub> nanofluids in fully developed laminar flow regime, *International Journal of Heat and Mass Transfer* (2009) 52, 193-199.

- [57] Hwang Y., Lee Jae-Keun, Lee Jong-Ku, Jeong Young-Man, Cheong Seong-ir, Ahn Young-Chull, Kim S.H., Production and dispersion stability of nanoparticles in nanofluids. *Powder Technology* 186 (2008) 145-153.
- [58] Ijam A, Golsheikh A. Moradi, Saidur R., and Ganesan P. A glycerol–water-based nanofluid containing graphene oxide nanosheets, *Journal of Materials Science* 49, no. 17 (2014): 5934-5944.
- [59] Incropera Frank P., DeWitt David P., Fundamental of heat and mass transfer, USA, *John Wiley & Sons. Ed 7, (2011)*.
- [60] Jagannathan, R., and Irvin G. C.. Nanofluids: A new class of materials produced from nanoparticle assemblies, *Advanced Functional Materials* 15, no. 9 (2005): 1501-1510.
- [61] Jana, S., A. Salehi-Khojin, and W. H. Zhong, Enhancement of fluid thermal conductivity by the addition of single and hybrid nano-additives. *Thermochimica Acta*, 2007. 462(1-2): p. 45-55.
- [62] Jang, S.P. and Choi, S.U., Role of Brownian motion in the enhanced thermal conductivity of nanofluids, *Applied Physics Letters*, (2004) 84(21), pp.4316-4318.
- [63] Ju Y. S., Kim J., Hung Ming-Tsung, Experimental study of heat conduction in aqueous suspensions of aluminum oxide nanoparticles, *ASME Journal of Heat Transfer* 130 (2008) 092403 1-6.
- [64] Kakaç, S., Pramuanjaroenkij, A., Review of convective heat transfer enhancement with nanofluids, *International Journal of Heat and Mass Transfer*, (2009) 52(13), 3187-3196.

- [65] Keblinski P. , Cahill D.G. Comment on model for heat conduction in nanofluids, *Physical Review Letters*. 2005; 95, 209401.
- [66] Keblinski P., Phillpot S. R., Choi S. U. S., Eastman J. A., Mechanism of heat flow in suspension of nano-sized Particles, *International Journal of Heat and Mass Transfer* 45 (2002) 855-863.
- [67] Keblinski, P., Eastman J. A., and Cahill D. G., Nanofluids for thermal transport, *Materials Today* 8, no. 6 (2005): 36-44.
- [68] Keblinski, P., Phillpot S. R., Choi S. U. S., Eastman J. A., Mechanisms of heat flow in suspensions of nano-sized particles (nanofluids), *International Journal of Heat and Mass Transfer* 45, no. 4 (2002): 855-863.
- [69] Khanafer K., Vafai K., A critical synthesis of thermophysical characteristics of nanofluids, *International Journal of Heat and Mass Transfer*, 54 (2011) 4410-4428.
- [70] Kim S. H., Choi. S R., Kim D., Thermal conductivity of metal oxide nanofluids: Particle size dependence and effect of laser irradiation, *Transactions of the ASME*, 129 (2007) 298-307.
- [71] Ko G. H., Heo K., Lee K., Kim D. S., Kim C., Sohn Y., Choi M., An experimental study on the pressure drop of nanofluids containing carbon nanotube in a horizontal tube, *International Journal of Heat and Mass Transfer* (2007) 50, 4749-4753.
- [72] Kole, M., and Dey T. K., Investigation of thermal conductivity, viscosity, and electrical conductivity of graphene based nanofluids, *Journal of Applied Physics* 113, no. 8 (2013): 084307.

- [73] Koo, J. and Kleinstreuer C., A new thermal conductivity model for nanofluids, *Journal of Nanoparticle Research*, (2004) 6(6): p. 577-588.
- [74] Lee D, Kim JW, Kim BG. A new parameter to control heat transport in nanofluids: Surface charge state of the particle in suspension *Journal of Physical Chemistry B*. (2006) 110 (9):4323-8.
- [75] Lee, J. H., Hwang, K. S., Jang, S. P., Lee, B. H., Kim, J. H., Choi, S. U. S and Choi, C. J., Effective viscosities and thermal conductivities of aqueous nanofluids containing low volume concentrations of Al<sub>2</sub>O<sub>3</sub> nanoparticles *International Journal of Heat and Mass Transfer*, (2008) 51(11), pp.2651-2656.
- [76] Lee, S., Choi S.U .S., and Eastman J. A., Measuring thermal conductivity of fluids containing oxide nanoparticles, *Journal of Heat Transfer* 121, no. 2 (1999): 280-289.
- [77] Li C. H., Peterson G. P., Experimental investigation of temperature and volume fraction variations on the effective thermal conductivity of nanoparticle suspensions (nanofluids), *Journal of Applied Physics* 99 (2006) 084314 1-8.
- [78] Li D., Xie W., Fang W., Preparation and properties of copper-oil-based nanofluids, *Nanoscale Research Letters* , 6 1 373 (2011) 1-7.
- [79] Li, Q., Xuan, Y. M., Jiang, J., Xu, J. W., Experimental investigation on flow and convective heat transfer feature of a nanofluid for aerospace thermal management, *Journal of Astronautics(China)*, (2005) 26(4), 391-394.

- [80] Li. C. H., Peterson G. P., The effect of particle size on the effective thermal conductivity of  $\text{Al}_2\text{O}_3$ -water nanofluids, *Journal of Applied Physics* 101, 044312 (2007) 1-5.
- [81] Liu, J, Wang F., Zhang L., Fang X., Zhang Z., Thermodynamic properties and thermal stability of ionic liquid-based nanofluids containing graphene as advanced heat transfer fluids for medium-to-high-temperature applications, *Renewable Energy* 63 (2014): 519-523.
- [82] Liu, M.S., Lin, M.C.C., Huang, I.T. and Wang, C. C., Enhancement of thermal conductivity with carbon nanotube for nanofluids, *International Communications in Heat and Mass Transfer*, (2005) 32(9), pp.1202-1210.
- [83] Maxwell, J. Clerk., On double refraction in a viscous fluid in motion, *Proceedings of the Royal Society of London* 22, no. 148-155 (1873): 46-47.
- [84] Mazer N. A., Carey M. C., Kwasnick R. F., Benedek G. B., Quasielastic light scattering studies of aqueous biliary lipid systems. Size, shape, and thermodynamics of bile saltmicelles. *Biochemistry*. (1979) 18(14):3064-75.
- [85] Mehrali, M., Sadeghinezhad E., Latibari S. T., Kaz S. N., Mehrali M., MohdZubir Mohd N. Bin, and Metselaar H. S. C., Investigation of thermal conductivity and rheological properties of nanofluids containing graphene nanoplatelets, *Nanoscale Research Letters* 9, no. 1 (2014): 1-12.

- [86] Mintsu H. A, Roy G, Nguyen C. T., Doucet D., New temperature dependent thermal conductivity data for water-based nanofluids, *International Journal of Thermal Sciences* 48 (2009) 363-371.
- [87] Moshkovith A., Perfiliev V., Verdyan A., Lapsker I., Popovitz-Biro R, Tenne R., and Rapoport L., Sedimentation of IF-WS2 aggregates and a reproducibility of the tribological data, *Tribology International*, vol. 40, no. 1, pp. 117–124, 2007.
- [88] Murshed, S. M. S., K. C. Leong, and C. Yang., Enhanced thermal conductivity of TiO<sub>2</sub>—water based nanofluids, *International Journal of Thermal Sciences* 44, no. 4 (2005): 367-373.
- [89] Nan C. W., Shi Z., Lin Y., A simple model for thermal conductivity of carbon nanotube-based composites, *Chemical Physics Letters* 375, (2003): 666-669.
- [90] Nasiri, M., Etemad, S. G., Bagheri, R., Turbulent convective heat transfer of nanofluids through a square channel, *Korean Journal of Chemical Engineering*, (2011) 28(12), 2230-2235.
- [91] Nguyen C. T., Desgranges F., Galanis N., Mare T., Boucher S., Mintsu H. A., Viscosity data for Al<sub>2</sub>O<sub>3</sub>-water nanofluid-hysteresis: is heat transfer enhancement using nanofluids reliable?, *International Journal of Thermal Sciences* 47 (2008) 103-111.
- [92] Nguyen C. T., Laplante G., Cury M., Simon G., Experimental investigation of impinging jet heat transfer and erosion effect using al<sub>2</sub>o<sub>3</sub>-water nanofluid, *6th*

- [93] Nie, C., Marlow, W., and Hassan, Y., Discussion of proposed mechanisms of Thermal conductivity enhancement in nanofluids, *International Journal Heat Mass Transfer*, (2008) *51*(5-6), pp. 1342-1348.
- [94] Novoselov, K. S., Geim A. K., Morozov S. V., Jiang D., Zhang Y., Dubonos S. V., Grigorieva I. V., and Firsov A. A., Electric field effect in atomically thin carbon films, *Science* 306, no. 5696 (2004): 666-669
- [95] Ohshima, K. I., Yatsuya S., Harada J., Characterization of Ultra Fine Palladium Particles with the Mean Size of 20 Å by X-Ray Diffraction, *Journal of the Physical Society of Japan* 50, no. 9 (1981): 3071-3074.
- [96] Pak, B. C., Cho, Y. I., Hydrodynamic and heat transfer study of dispersed fluids with submicron metallic oxide particles, *Experimental Heat Transfer an International Journal*, (1998) *11*(2), 151-170.
- [97] Pettes MT, Shi L., Thermal and structural characterizations of individual single-double and multi-walled carbon nanotubes, *Advanced Functional Materials*.(2009) *19*(24):3918-25.
- [98] Phillips R. J., Armstrong R. C., Brown R. A., Graham A. L., and Abbott J. R., A constitutive equation for concentrated suspensions that accounts for shear-induced particle migration, *Physics of Fluids A: Fluid Dynamics (1989-1993)* 4, no. 1 (1992): 30-40.

- [99] Prasher, R., Phelan, P. E., and Bhattacharya, P., Effect of aggregation kinetics on the thermal conductivity of nanoscale colloidal solutions (Nanofluid), *Nano Letters*, (2006) 6(7), pp. 1529-1534.
- [100] Prasher, R., William E., Paul M., Jacob F., Phelan P., and Keblinski P. Effect of aggregation on thermal conduction in colloidal nanofluids, *Applied Physics Letters* 89, no. 14 (2006): 143119.
- [101] Raghu, G., Hongwei, S., Pengtao, W., Majid, C., Fan, G., Zhiyong, G. and Bridgette, B., 2010. Effects of particle surface charge, species, concentration, and dispersion method on the thermal conductivity of nanofluids, *Advances in Mechanical Engineering*, (2010).
- [102] Rea U., McKrellt., Hu Lin-wen, Buongiorno J., Laminar convective heat transfer and viscous pressure loss of alumina-water and zirconia-water nanofluids, *International Journal of Heat and Mass Transfer* (2009) 52, 2442-2448.
- [103] S. S. J. Aravind, S. Ramaprabhu, Graphene- multiwalled carbon nanotube-based nanofluids for improved heat dissipation, *Royal Society of Chemistry Advances*, 3, (2013): 4199-4106.
- [104] S. S. J. Aravind, S. Ramaprabhu, Graphene weapper multiwalled carbon nanotubes dispersed nanofluids for heat transfer applications, *Journal of Applied Physics* 112, (2012): 124304.
- [105] Sabourin J. L., Dabbs D. M., Yetter R. A., Dryer F. L., Aksay I. A., Functionalized graphene sheet colloids for enhanced fuel/ propellant combustion, *ACS Nano*, (2009) 3 (12), pp 3945–3954, DOI: 10.1021/nn901006w

- [106] Sastry, NN Venkata, Bhunia Avijit, Sundararajan T., and Das Sarit K., Predicting the effective thermal conductivity of carbon nanotube based nanofluids, *Nanotechnology* 19, no. 5 (2008): 055704.
- [107] Shukla, R.K. and Dhir, V.K., Effect of Brownian motion on thermal conductivity of nanofluids, *Journal of Heat Transfer*, (2008) 130(4), p.042406.
- [108] Sitprasert, C., Dechaumphai, P., and Juntasaro, V., A thermal conductivity model for nanofluids including effect of the temperature-dependent interfacial layer, *Journal of Nanoparticle. Research.* (2009) 11(6), pp. 1465-1476.
- [109] Solangi, K.H., Kazi, S.N., Luhur, M.R., Badarudin, A., Amiri, A., Sadri, R., Zubir, M.N.M., Gharekhani, S. and Teng, K.H., A comprehensive review of thermo-physical properties and convective heat transfer to nanofluids. *Energy*, (2015) 89, pp.1065-1086.
- [110] Sonawane, S., Bhandarkar, U., Puranik, B., Kumar, S. Sunil, convective heat transfer characterization of aviation turbine fuel-metal oxide nanofluids, *Journal of Thermophysics and Heat Transfer* (2012) Vol.26, No.4.
- [111] Sonawane, S., Patankar K., Fogla A., B. Puranik, B., Bhandarkar, U., Kumar S. Sunil, An experimental investigation of thermo-physical properties and heat transfer performance of Al<sub>2</sub>O<sub>3</sub>-Aviation Turbine Fuel nanofluids, *Applied Thermal Engineering* 31 (2011) 2841-2849.
- [112] Sutton, George P., and Oscar Biblarz. Rocket propulsion elements, *John Wiley & Sons*, (2010).

- [113] Tillman, P., and Hill, J. M., , “determination of nanolayer thickness for a nanofluid,” *International Communications in Heat and Mass Transfer*, (2007) **34**(4), pp. 399-407.
- [114] Timofeeva E. V., Gavrilov A. N., McCloskey J. M., Tolmachev Y. Y., Thermal conductivity and particle agglomeration in alumina nanofluids: Experiments and theory, *Physics Review Letter E76 061203-1- 16* (2007).
- [115] Timofeeva E. V., Smith D. S., Yu W., France D. M., Singh D., Routbort J. L, Particle size and interfacial effects on thermo-physical and heat transfer characteristics of water-based  $\alpha$ -SiC nanofluids, *Nanotechnology 21* (2010) 215703 1-10.
- [116] Timofeeva, E. V., Moravek, M. R., Singh, D. Improving the heat transfer efficiency of synthetic oil with silica nanoparticles. *Journal of Colloid and Interface Science*, (2011) 364(1), 71-79.
- [117] Timofeeva, E. V., Smith, David S., Yu, W., France, D. M., Singh, D., Routbort, J. L., Particle size and interfacial effects on thermo-physical and heat transfer characteristics of water-based  $\alpha$ -SiC nanofluids, *Nanotechnology* (2010) 21, 215-703.
- [118] Timofeeva, E. V., Yu, W., France, D. M., Singh, D., & Routbort, J. L. Nanofluids for heat transfer: an engineering approach, *Nanoscale Research Letters*, (2011) 6(1), 1-7.
- [119] Tsai T. H, Kuo L. S., Chen P. H., Yang C. T., Effect of viscosity of base fluid on thermal conductivity of nanofluids, *Applied Physics Letters 93*, no. 23 (2008): 233121.
- [120] Tsai T. H., Kuo L. S., Chen P.H., Yang C.T., Thermal conductivity of nanofluid with magnetic nanoparticles, *Piers Online 5*, no. 3 (2009): 231-234.

- [121] V.H. Eilers, Die viskosität von emulsionen hochviskoser stoffe als function der konzentration, *Kolloid-Zeitschrift* 97 (1941) 313–321.
- [122] Venerus DC, Kabadi MS, Lee S, Perez-Luna V. Study of thermal transport in nanoparticle suspensions using forced Rayleigh scattering, *Journal of Applied Physics*. (2006) 100(9).
- [123] Venerus et al., Viscosity measurement on colloidal dispersions (nanofluids) for heat transfer applications, *Applied Rheology*, 20 (2010) 44582 1-7.
- [124] Wang X. L., Xu B. S., Xu Y., Yu H. L., Shi P. J., and Liu Q., Preparation of nano-copper as lubrication oil additive, *Journal of Central South University of Technology*, vol. 12, pp. 203–206, Oct. 2005.
- [125] Wang X., Xu X. , Choi S. U. S., Thermal conductivity of nanoparticle- fluid mixture, *Journal of Thermophysics and Heat Transfer*, 13 (4) (1999) 474-480.
- [126] Wang Xiang-Qi, Mujumdar A. S., A review on nanofluids - part II: experiments and applications, *Brazilian Journal of Chemical Engineering* 25 (4) (2008).
- [127] Wang, B.X., Zhou, L.P. and Peng, X.F., A fractal model for predicting the effective thermal conductivity of liquid with suspension of nanoparticles, *International Journal of Heat and Mass Transfer*, (2003) 46(14), pp.2665-2672.
- [128] Wang, F., Han L., Zhang Z., Fang X., Shi J., Ma W., Surfactant-free ionic liquid-based nanofluids with remarkable thermal conductivity enhancement at very low loading of graphene, *Nanoscale Research Letters* 7, no. 1 (2012): 1-7.

- [129] Wang, X.Q. and Mujumdar, A.S., A review on nanofluids-part I: theoretical and numerical investigations, *Brazilian Journal of Chemical Engineering*, (2008) 25(4), pp.613-630.
- [130] Wen D., Ding Y., Effective thermal conductivity of aqueous suspensions of carbon nanotubes, *Journal of Thermophysics and Heat Transfer* 18 (4) (2004) 481-485.
- [131] Williams, W., Buongiorno, J., Hu, Lin-Wen, Experimental investigation of turbulent convective heat transfer and pressure loss of alumina/water and zirconia/water nanoparticle colloids (nanofluids) in horizontal tubes, *Journal of Heat Transfer* (2008) Vol.130, 042412-1.
- [132] Wilson, O. M., Hu X., Cahill D. G., Braun P. V., Colloidal metal particles as probes of nanoscale thermal transport in fluids. *Physical Review B* 66, no. 22 (2002): 224301.
- [133] Xie H., Lee H., Youn W., Choi M., Nanofluids containing multiwalled carbon nanotubes and their enhanced thermal conductivities, *Journal of Applied Physics* 94 (2003) 4967-4971.
- [134] Xie H., Yu W., Li Y., Chen L., Discussion on the thermal conductivity enhancement of nanofluids, *Nanoscale Research Letters* , 6 1 124 (2011) 1-12.
- [135] Xie, H., Fujii, M., and Zhang, X., Effect of interfacial nanolayer on the effective thermal conductivity of nanoparticle-fluid mixture, *International Journal of Heat Mass Transfer*, (2005) 48(14), pp. 2926-2932.

- [136] Xie, H., Lee H., Youn W., and Choi M., Nanofluids containing multiwalled carbon nanotubes and their enhanced thermal conductivities, *Journal of Applied Physics* 94, no. 8 (2003): 4967-4971.
- [137] Xie, H.Q., Wang J.C., Xi T.G., Liu Y., Ai F., and Wu Q. R., Thermal conductivity enhancement of suspensions containing nanosized alumina particles, *Journal of Applied Physics*, (2002) **91**(7): p. 4568-4572.
- [138] Xuan Y., Li Q., Heat transfer enhancement of nanofluids, *International Journal of Heat and Fluid Flow* 21 (2000) 58-64.
- [139] Xuan, Y., Li Q., Investigation on convective heat transfer and flow features of nanofluids, *ASME Journal of Heat transfer* 125, no. 1 (2003): 151-155.
- [140] Xue, L., Keblinski, P., Phillpot, S. R., Choi, S. U. S., and Eastman, J. A., Effect of liquid layering at the liquid-solid interface on thermal transport, *International Journal of Heat Mass Transfer.*, (2004) **47**(19-20), pp. 4277-4284.
- [141] Yamada, E., and Ota T., Effective thermal conductivity of dispersed materials, *Wärme-und Stoffübertragung* 13, no. 1-2 (1980): 27-37.
- [142] Yang, X.F., Liu, Z.H. and Zhao, J., Heat transfer performance of a horizontal micro-grooved heat pipe using CuO nanofluid, *Journal of Micromechanics and Microengineering*, (2008) 18(3), p.035038.
- [143] Yang, Y., Grulke E. A., Zhang Z. G., and Wu G. F., Thermal and rheological properties of carbon nanotube-in-oil dispersions, *Journal of Applied Physics*, (2006) 99(11).

- [144] Yatsuya, S., Tsukasaki Y., Mihama K., Uyeda R., Preparation of extremely fine particles by vacuum evaporation onto a running oil substrate, *Journal of Crystal Growth* 45 (1978) 490-494.
- [145] Yu H., Xu Y., Shi P., Xu B., Wang X., and Q. Liu, Tribological properties and lubricating mechanisms of Cu nanoparticles in lubricant, *Transactions of Nonferrous Metals Society of China (English Edition)*, vol. 18, no. 3, pp. 636–641, 2008.
- [146] Yu, C., Richter, A. G., Datta, A., Durbin, M. K., and Dutta, P., Observation of molecular layering in thin liquid films using x-ray reflectivity, *Physics. Review. Letters*, (1999) 82(11), pp. 2326-2329.
- [147] Yu, L., Liu, D., Botz, F., Laminar convective heat transfer of alumina-polyalphaolefin nanofluids containing spherical and non-spherical nanoparticles, *Experimental Thermal and Fluid Science*, (2012) 37, 72-83.
- [148] Yu, W. and Xie, H., A review on nanofluids: preparation, stability mechanisms, and applications, *Journal of Nanomaterials*, (2012). p.1.
- [149] Yu, W., and Choi, S. U. S., “The role of interfacial layers in the enhanced thermal conductivity of nanofluids: a renovated maxwell model, *Journal of Nanoparticle. Research.*, (2003) 5(1), pp. 167-171.
- [150] Yu, W., France, D. M., Timofeeva, E. V., Singh, D., Routbort, J. L., Thermophysical property-related comparison criteria for nanofluid heat transfer enhancement in turbulent flow, *Applied Physics Letters*, (2010) 96(21), 213109.

- [151] Yu, W., France, David M., Smith, David S., Singh, D., Timofeeva, Elena V., Routbort, Jules L., Heat transfer to a silicon carbide/water nanofluid, *International Journal of Heat and Mass Transfer* (2009) 52, 3606-3612.
- [152] Yu, Wei, Xie H., and Chen W., Experimental investigation on thermal conductivity of nanofluids containing graphene oxide nanosheets, *Journal of Applied Physics* 107, no. 9 (2010): 094317.
- [153] Zhang X., Gu H., Fujii M., Experimental study on the effective thermal conductivity and thermal diffusivity of Nanofluids, *International Journal of Thermophysics* 27 (2) (2006) 569-580.
- [154] Zheng, Yingsong, and Haiping Hong., Modified model for effective thermal conductivity of nanofluids containing carbon nanotubes, *Journal of Thermophysics and Heat Transfer* 21, no. 3 (2007): 658-660.
- [155] Zhu D., Li X., Wang N., Wang X., Gao J., Li H., Dispersion behavior and thermal conductivity characteristics of Al<sub>2</sub>O<sub>3</sub>-H<sub>2</sub>O nanofluids, *Current Applied Physics* 9 (2009) 131-139.
- [156] Zhu, H. T., Zhang, C. Y., Tang, Y. M., and Wang, J. X., Novel Synthesis and thermal conductivity of cuo nanofluid, *Journal of Physical Chemistry. C*, (2007) **III**(4), pp. 1646-1650.
- [157] Zhu, H., Zhang C., Liu S., Tang Y., and Yin Y., Effects of nanoparticle clustering and alignment on thermal conductivities of Fe<sub>3</sub>O<sub>4</sub> aqueous nanofluids, *Applied Physics Letters* 89, no. 2 (2006): 3123.

## CHAPTER 7

### 7 LIST OF PUBLICATIONS

#### Papers in refereed international journals

1. Agarwal D. K, Vaidyanathan A., Kumar S. S., Synthesis and Characterization of Kerosene-Alumina Nanofluids, *Applied Thermal Engineering*, 60 (2013) 275-284.
2. Agarwal D. K, Vaidyanathan A., Kumar S. S., Investigation on Convective Heat Transfer Behavior of Kerosene- Al<sub>2</sub>O<sub>3</sub> Nanofluid, *Applied Thermal Engineering*, 84 (2015) 64-73.
3. Agarwal D. K, Vaidyanathan A., Kumar S. S., Experimental Investigation on Thermal Performance of Kerosene-Graphene Nanofluid, *Experimental Fluid and Thermal Science* 71 (2016) 126-137.

#### Papers in refereed international conferences

1. Agarwal D. K, Peter J., Vaidyanathan A., Kumar S. S., Experimental investigation of kerosene-alumina nanofluid for heat transfer application, *Proceedings of 22<sup>nd</sup> National and 11<sup>th</sup> International ISHMT-ASME Heat and Mass Transfer 2013, HMTC 1300316*
2. Agarwal D. K, Peter J., Vaidyanathan A., Kumar S. S., Measurement of Thermal Conductivity of Kerosene- Graphene Nanofluid, *Proceedings of the 23<sup>rd</sup> National Heat and Mass Transfer Conference and 1<sup>st</sup> International ISHMT-ASTFE Heat and Mass Transfer Conference-2015, IHMTC2015-198.*